SENSITIVITY OF THE YOUNGER DRYAS CLIMATE TO CHANGES IN FRESHWATER, ORBITAL, AND GREENHOUSE GAS FORCING IN COMPREHENSIVE CLIMATE MODELS

by

TAYLOR MICHELLE HUGHLETT

Presented to the Faculty of the Graduate School of
The University of Texas Arlington in Partial Fulfillment
of the Requirements
for the Degree of

DOCTOR OF PHILOSOPHY

THE UNIVERSITY OF TEXAS ARLINGTON

April 2016

Acknowledgements

I would like to acknowledge the faculty and staff at the National Center for Atmospheric Research for their countless hours of support and troubleshooting with the climate model, my simulations, and myself. This work could not have been accomplished without the encouragement and support from my PhD research advisor, Dr. Arne Winguth. Without his enthusiasm and guidance, this dissertation would not have been possible. I would also like to thank the members of my committee, Dr. Cornelia Winguth, Dr. Max Hu, Dr. Majie Fan, and Dr. Jim Grover for their time and input on this project.

On a personal note, I would like to thank my parents, Jeffrey and Kimberlee Hughlett, and my sister, Whitney Hughlett, for standing by me in my decisions, and supporting me writing this dissertation. Without their love and encouragement, I would never have considered a higher degree, and certainly would not have had the motivation to continue as far as I have in the program. Additionally, I would like to thank Laura Carpenter for being there with me and putting up with me through this. I would also like to thank Dr. Teresa Beaty and Dr. Angela Osen for being there for me through my entire dissertation, even long after they both graduated.

All simulations and graphic production were done using NCAR computers, which are supported by the National Science Foundation. This research is supported by NSF grants OCE 1536630 and EAR 0903071.

April 22, 2016

Abstract

SENSITIVITY OF THE YOUNGER DRYAS CLIMATE TO CHANGES IN FRESHWATER, ORBITAL, AND GREENHOUSE GAS FORCING IN COMPREHENSIVE CLIMATE MODELS

Taylor Michelle Hughlett, PhD

The University of Texas Arlington, 2016

Supervising Professor: Arne Winguth

The Younger Dryas cooling event (~12,900 years before present) was the most recent abrupt climate change in the geologic record where climate for the Northern Hemisphere returned to a near-glacial state. The cause of this cooling event is widely controversial, and no consensus has been found as to why the onset of the cooling occurred. Of the several hypotheses proposed, the freshening of the North Atlantic Ocean due to meltwater discharge from the retreating Lake Agassiz and subsequent changes in oceanic circulation is the most widely accepted one. Additionally, this abrupt climate change can be attributed to other changes in the forcing boundary conditions, for example changes in orbital forcing, and changes in greenhouse gas concentrations in the atmosphere.

In this study, each of these three potential triggers of rapid climate change was explored by using comprehensive climate models. The Atlantic meridional overturning circulation (AMOC) is slightly more sensitive to the Mackenzie River discharge (a 9 Sv circulation decrease) as opposed to St. Lawrence discharge (a 7 Sv circulation decrease). High-resolution simulations separating the same magnitude of discharge from both locations are needed to evaluate the impact of distinct regional fresh water forcing. The AMOC reduction by freshwater forcing into the Northern Atlantic Ocean during the Younger Dryas causes a decrease in surface air temperature in agreement with surface air temperature reconstructions from Greenland. The climatic effect of freshwater forcing and the effect of the ice sheet during the Younger Dryas exceed the effects of both the greenhouse gas and orbital forcing. The Younger Dryas

climate is more greatly affected by changes in orbital forcing than by changes in greenhouse gas concentration due to the fact that changes in radiative forcing from orbital parameters are stronger than the change due to greenhouse gas forcing. However, the effects of orbital and CO_2 forcing alone are not enough to cause a transition into a Younger Dryas climate state, indicating that freshwater forcing is required.

The intensity of the West African monsoon is more substantially affected by changes in the orbital parameters compared to changes in the atmospheric pCO_2 values. The model simulations suggest that the West African monsoon during the Younger Dryas was colder and drier, which is related to climatic changes in the North Atlantic region. These findings agree with analyses of proxy reconstructions. Thus the freshwater forcing and the ice sheet may be important to the decline in West African monsoon circulation during the Younger Dryas. A simulated southward shift in the ITCZ due to the Northern hemispheric cooling is also in agreement with previous studies.

Table of Contents

List of Illustrations

List of Tables

Chapter 1

Introduction

1.1 The Younger Dryas

The Younger Dryas (YD) interval occurred after the Bølling-Allerød (a rapid warming event) and is the most recent, significant period of brief and abrupt climate change. The time period was named for the fossil pollen of the *Dryas* plant, a tundra flower commonly found during the YD (*Dryas octopetala*; Haynes, 2008). During the YD, at the end of the Pleistocene, the climate transitioned toward glacial conditions; a rapid warming of the climate terminated the YD before the Pre-Boreal stage at the beginning of the Holocene. The YD period is characterized by an intense cooling event of the Northern Hemisphere with decreased storminess, increased dust accumulations, and decreased snow accumulation (Figure 1-1; Van Der Hammen and Van Geel, 2008; Mayewski and Bender, 1995; Haynes, 2008; DeVernal et al., 1996; Alley, 2000). The onset of the YD cooling event ranges from approximately 13.0 kyr to 12.896 kyr depending on the dating method applied (Bakke et al., 2009; Smith et al., 1997; Fairbanks, 1990). The age discrepancy is a result of differences between radiocarbon and Th/U dating methods, where radiocarbon dates appear to be significantly younger than those estimated by Th/U radiometric dating (Bard et al., 1993). This discrepancy has been suggested to be a result of variations of carbon content of the biosphere (Vries et al., 1990) and atmosphere (Berner et al., 1980; Delmas et al., 1980), deep sea ventilation (Shackleton et al., 1988; Broecker et al., 1990), and changes in the geomagnetic field (Barbetti and Flude, 1979; McElhinny and Senanayake, 1982; Mazaud et al., 1991). Consequently, conversions between calendar and radiocarbon dates present a challenge. In this study, the onset of the YD is approximately 11,000 to 10,000 radiocarbon years, or 12.9 – 11.5 ka (Bakke et al., 2009; Lecompte et al., 2012; Broecker, 2006; Bard et al., 1993).

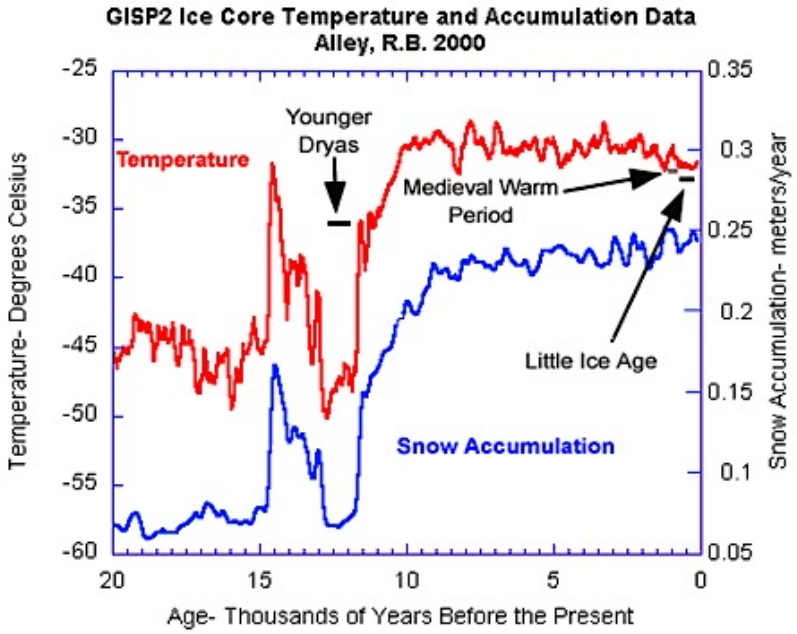

Figure 1-1 Temperature (°C) and snow accumulation in m yr^{-1} from 0-20 ka BP. The YD is shown to occur at approximately 13.0 ka and ends around 11.5 ka. Temperature decreases by approximately 9 °C at the onset of the YD and then increases by approximately 12 °C. Snow accumulation for the same period illustrates a decrease of approximately 0.05 m yr^{-1} and then an increase of approximately 0.075 m yr^{-1} at 13.0 ka and 11.5 ka respectively (Alley, 2000).

Ice cores from the Greenland Ice Sheet Project 2 (GISP2), drilled from Summit, Greenland, as well as climate proxies for areas such as Switzerland, England, Canada, North America, and much of the Northern Hemisphere, contain detailed records of climate change during the YD. Ice core oxygen isotopes ($\delta^{18}O$; δ signifies a change in isotopic ratio relative to a standard multiplied by 1000) from GISP decreased by 3‰ at the onset of the YD, and increased by 3.5‰ by the end of the YD. The decrease and increase at the onset and termination correspond to a 9°C cooling and 11°C warming, respectively (Figure 1-2; Alley, 2000; Figure from Carlson, 2013).

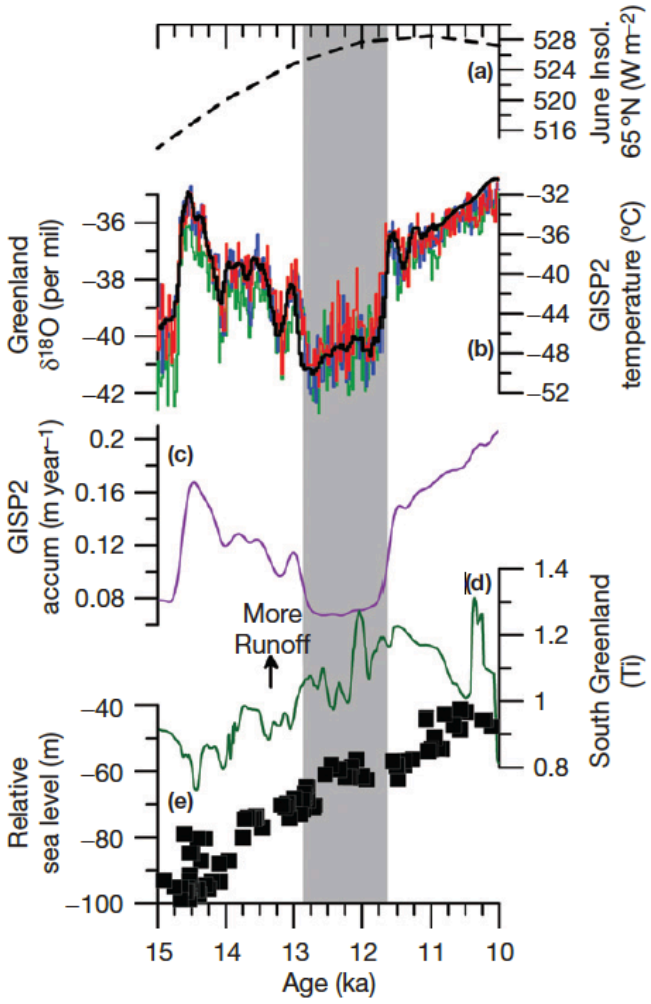

Figure 1-2 Records of oxygen isotopes, snow accumulation, relative sea level, and temperature for the YD (shaded in gray) based on GISP2 data (Carlson, 2013). Oxygen isotope ratios decrease rapidly at the start of the YD and then gradually increase until the termination of the event. This trend is also shown in snow accumulation and temperature. The relative sea level at the start of the YD was approximately 65 m lower than the preindustrial sea level.

Greenland ice core $\delta^{18}O$ measurements can reflect the change in the hydrological cycle (Greenland Ice-core Project (GRIP) Members, 1993). The GISP2 core depicts the YD as a period of increased dust and colder tropical and subtropical wetlands, as shown in increased methane concentrations (Mayewski and Bender, 1995; Mayewski et al., 1993; Severinghaus et al., 1998). Temperature reconstructions from $\delta^{18}O$ values indicate that the temperature decreased anywhere from 15-20 °C at Summit Station, Greenland, and surrounding areas at the onset of the YD and

increased by approximately 7 °C at the end of the YD (Dansgaard et al., 1989; Severinghaus et al., 1998). Freshwater forcing is evident in the Greenland ice sheet cores where $\delta^{18}O$ is substantially depleted on the Southeast Greenland shelf at the onset of the YD (Jennings et al., 2006). The termination of the YD is characterized by a doubling of snow accumulation rates, a 7 °C warming, and an increase in precipitation rate (Dansgaard et al., 1989; Alley et al., 1993).

The YD is also represented in speleothem and travertine samples from a variety of locations, including North America, South America, and Europe. Stalagmites from the European Alps in Italy indicate that the YD was cool and dry owing to heavier $\delta^{18}O$ and increased $\delta^{13}C$ (Frisia et al., 2005). A stalagmite from the Klamath Mountains in Oregon depicts that the YD in the area cools to the same degree as the rest of the Northern Hemisphere (Vacco et al., 2005). Additionally, the biomass increases in the region according to $\delta^{13}C$ values (Vacco et al., 2005). $^{234}U/^{230}Th$ reconstructions from a stalagmite in Onondaga Cave, Missouri indicate decreasing temperatures at the onset of the YD, as well as a decrease in $\delta^{13}C$ values (Denniston et al., 2001). These changes occurred in approximately 200 years, supporting the claim of the abrupt transition between the Bølling-Allerød (BA) and the YD (Denniston et al., 2001). In Brazil, the YD is represented in travertine samples that complement the constructed speleothem records by indicating periods of non-growth of speleothems during arid conditions (Wang et al., 2004).

The YD was first recorded in pollen reconstructions from Europe when the tundra flower, *Dryas octopetala*, reappeared in the pollen record (Meltzer and Holliday, 2010; Seager and Battisti, 2007). Since then, paleoclimate reconstructions via pollen and macrofossil records have been carried out in numerous locations. Pollen reconstructions suggest Northern Europe and Eastern Canada were primarily affected by the YD (Peteet, 1995). Several European cores from Lake Bled (Slovenia), Lake Gerzensee (Switzerland), Lake Lautrey (Eastern France), Lake Accesa (Italy), and Lake Albert (Wales) show that the YD in Europe was cold and dry with summer temperatures around 9-10 °C, that oxygen and tree pollen decreased, and that lake levels were lower, though water was still well oxygenated (Andrič et al., 2009; Schwander et al., 2000; Von Grafenstein et al., 2000; Lotter et al., 2000, 2012; Heiri and Millet, 2005; Peyron et al., 2005; Vescovi et al., 2007; Magny et al., 2006; Talbot et al., 2007). Cores from the Norwegian

Krakenes Project and the Gerzensee-Leysin Project in Switzerland indicate an increase of 1 °C in July temperatures, as well as an overall 2 °C decrease in annual temperature at the YD (Bakke et al., 2009; Birks and Ammann, 2000). Lower than present atmospheric CO_2 concentration and cooler July temperatures of 4-5 °C, as inferred from the extent of the Scandinavian ice sheet and from pollen records, contributed to the extent of mountain forests during the YD (Denton et al., 2005; Gasse, 2000; Jolly, 1997; Street-Perrott et al., 1997). Pollen records from Ohio indicate a temperature increase in the eastern North American region, and it has been suggested that temperature gradients near ice sheets were substantial (3.3 °C km^{-1}) (Hostetler et al., 2000; Ma et al., 2004; Shane and Anderson, 1993). Pollen records obtained from lake environments in Southern Greenland indicate an arid climate during the YD, and that the ocean surrounding the area was glaciated (Björck et al., 1996).

The climate variability of the North Atlantic Ocean during the YD interval has been inferred from stable carbon isotopes ($\delta^{13}C$) and $\delta^{18}O$, cadmium/calcium isotopes (Cd/Ca), and protactinium/thorium isotopes (Pa/Th) of marine sediment cores (Carlson, 2013). $\delta^{18}O$ measured from benthic foraminifera in the marine sediments (Shackleton et al., 1973) is used predominantly as an indicator of ice volume as well as temperature and salinity, whereas $\delta^{18}O$ measured from planktonic foraminifera primarily indicates temperature (Siddall et al., 2003; Rohling et al., 2009).

$\delta^{13}C$ distribution in the ocean depends on the air-sea gas exchange and solubility (Mook et al., 1974), the uptake up CO_2 by photosynthesis and downward flux of carbon into the deep sea (the biological pump; Volk and Hoffert, 1985; Broecker et al., 1982; Berger et al., 1989), and the ocean circulation. Plankton preferentially uptake the lighter ^{12}C as opposed to ^{13}C; therefore, higher $\delta^{13}C$ values indicate an increase in primary production (Broecker et al., 1982; Fischer, 1991). For the YD, Bermuda rise benthic marine sediment records indicate that carbonate $\delta^{13}C$ decreased from 0.2‰ to approximately -0.8‰ at the onset. At the termination of the YD, carbonate $\delta^{13}C$ increased from -0.8‰ to -0.3‰ (Figure 1-3; Carlson, 2013). These rises in carbonate $\delta^{13}C$ suggest a substantial decrease in net primary productivity at the onset of the YD and a recovery when the YD terminated. The recovery of net primary productivity was most likely due to the increase in sea surface temperature.

Export production in the ocean depends on light, temperature, and nutrients; changes in production have been linked to the sources of the nutrient-depleted North Atlantic Bottom Water and nutrient-rich Antarctic Bottom Waters. This linkage may give insight into the general ocean circulation (Boyle and Keigwin, 1987). North Atlantic Deep Water (NADW) is typically enriched in $\delta^{13}C$ and depleted in cadmium relative to calcium, whereas the opposite is true for the Antarctic Bottom Water (Boyle and Keigwin, 1987). The 1.6‰ decrease in $\delta^{13}C$ at the onset of the YD may indicate a slowdown of the oceanic circulation, while the increase to -0.3‰ at the termination of the YD suggested the resumption of the oceanic circulation to pre-YD levels.

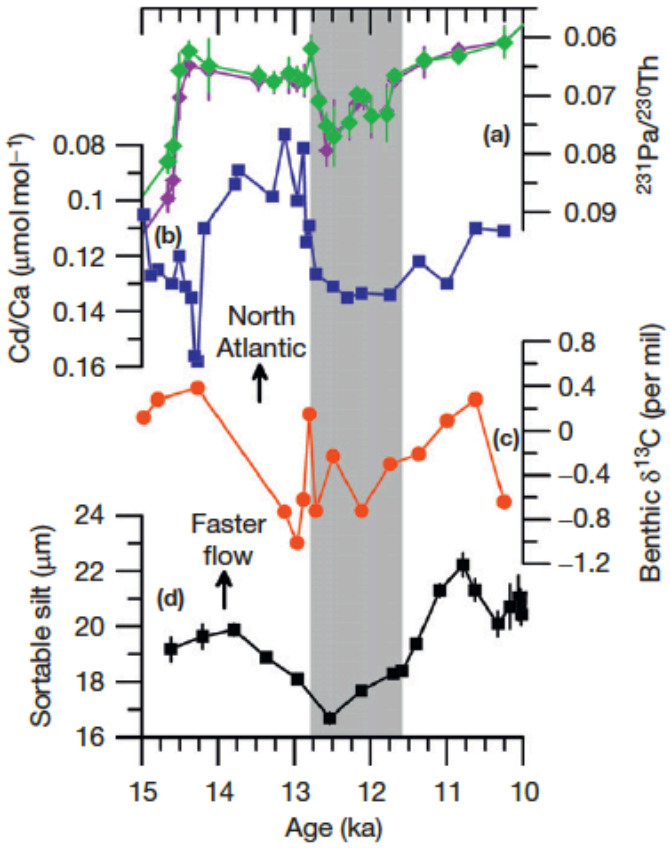

Figure 1-3 Records of Cd/Ca, Pa/Th, and carbon isotope for the YD (shaded in gray) using GISP2 data (Carlson, 2013). All records show a rapid decline at the onset of the YD. Both Pa/Th and carbon isotopes undergo a gradual recovery by the termination of the event, and Cd/Ca continues to decrease until the very end of the YD event.

The uptake of cadmium (Cd) from seawater into planktonic foraminifera is highly correlated to phosphate concentrations in regional ocean waters (Boyle, 1992; Rickaby and Elderfield, 1999) and thus to productivity and circulation. During the YD, the Cd/Ca concentration at the Bermuda Rise was ~0.11 μmol mol^{-1} at the onset and increased to ~0.13 μmol mol^{-1}, implying an increase in nutrient concentration in the deep sea and reduced ventilation of NADW through the cooling event. At the termination of the YD, concentrations rose to ~0.12 μmol mol^{-1} (Figure 1-3; Boyle and Keigwin, 1987) suggesting an increase in the production of NADW (McManus et al., 2004).

The uptake of the magnesium/calcium (Mg/Ca) ratio appears to be temperature-dependent in planktonic foraminifera (Elderfield and Ganssen, 2000; Lea et al., 2000; Barker et al., 2005). Mg/Ca records from low latitude western Atlantic marine cores indicated a rapid decrease from approximately 1.22 μmol mol^{-1} to 1.12 μmol mol^{-1} at the onset of the YD. This indicates a decrease in sea surface temperature at the onset of the YD followed by a warming at the termination (Came et al., 2008). This trend in Mg/Ca in planktonic foraminifera is similar to the one of Cd/Ca, indicating changes in the rate of NADW production.

Protactinium/Thorium (Pa/Th) ratios are also used to indicate ocean productivity as well as circulation and scavenging (Anderson et al., 1983; Yu et al., 1996; Henderson et al., 1999; Guo, 2002). Thorium has a low residence time in the ocean and is deposited to the sea floor quickly. Protactinium has a higher residence time and can be circulated through the water before it is deposited in the sediments (Henderson, 2002). Therefore, when the Pa/Th ratio is high, it suggests a weaker oceanic circulation (Yu et al., 1996). During the YD, the Pa/Th ratio increases from approximately 0.063 to 0.08 at the onset and decreases to 0.066 at the termination (Figure 1-3; Carlson, 2013). These variations in the Pa/Th ratio imply a decrease in the Atlantic meridional oceanic circulation at the onset of the YD, which recovered, leading to the termination of the YD.

1.2 Hypotheses of the Younger Dryas Cooling Event

Several hypotheses exist that address the causes of rapid climate change associated with the ~1,400 year long YD climate event. The following sections summarize commonly discussed hypotheses that serve as motivation for this dissertation's objectives (Chapter 2).

1.2.1 The Freshwater Forcing Hypothesis

This hypothesis, originally proposed by Rooth (1982) and Broecker and Denton (1989), suggested that the flux of freshwater from glacial melting during the Bølling-Allerød event could have triggered the onset of the YD cooling event (Manabe and Stouffer, 1995; Donnelly et al., 2005; Broecker, 2003; Carlson et al., 2007). Discharge of freshwater into the Northern Atlantic could have led to a reduction of NADW and reduction of Atlantic meridional oceanic circulation, which triggered a significant cooling (~4.5 °C) in the Northern Hemisphere, with maximum cooling thought to have occurred at the summit of Greenland (~15 °C-20 °C) (Severinghaus et al., 1998). The magnitude of freshwater discharged has been estimated to be ~9500 km^3 (or approximately 0.3 Sv) before the onset of the YD (Leverington and Teller, 2003; Teller et al., 2005; Broecker, 2003; Huang and Tian, 2008).

Freshwater pulses due to melting of the Laurentide ice sheet could have been entrained at three different locations (the St. Lawrence River, Mississippi River, and Mackenzie River) into the Northern Atlantic during the YD (Figure 1-4; Tarasov and Peltier, 2005; Huang and Tian, 2008; Murton et al., 2010).

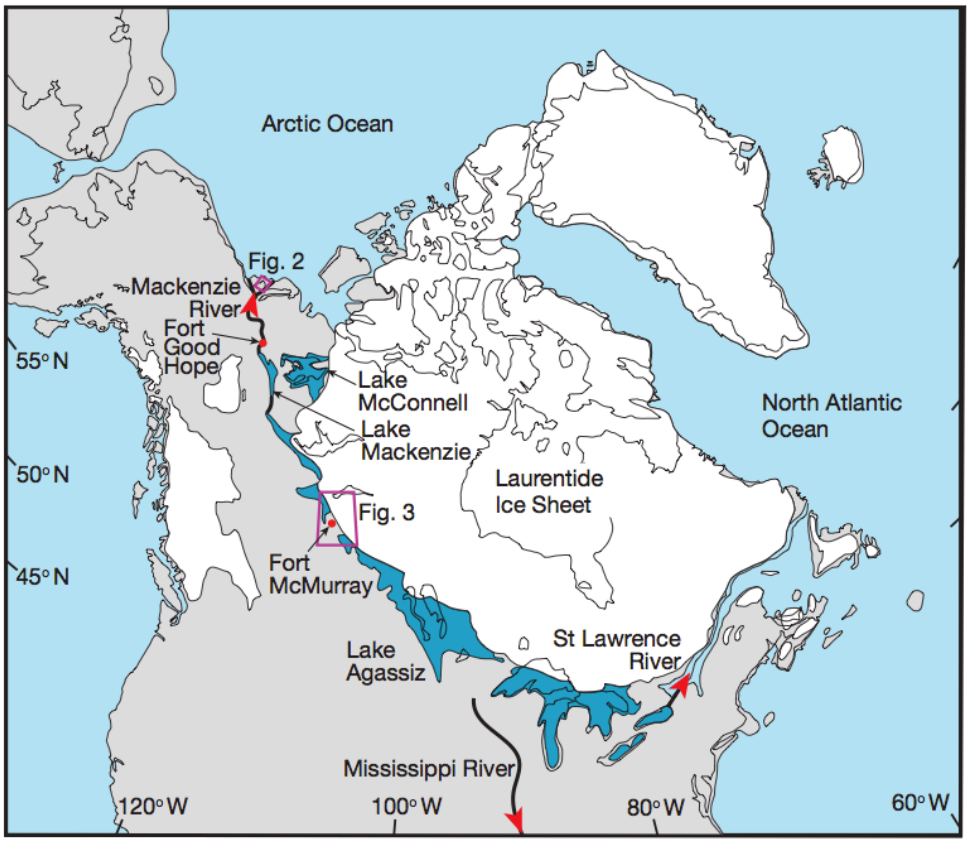

Figure 1-4 Possible routing of freshwater fluxes from the Laurentide Ice Sheet in North America for the last deglaciation (Murton et al., 2010). The northern route consists of movement of freshwater from the Fram Strait directly into the Greenland, Iceland, and Norwegian (GIN) seas. The eastern route involves discharge of freshwater from the St. Lawrence and Hudson rivers. The southern route requires freshwater input from the Mississippi river into the Gulf of Mexico, after which the freshwater is carried to the Northern Atlantic via the Gulf Stream.

Locations of freshwater input are the southern, eastern, and northern routes of drainage. The southern route drains through the Mississippi River into the Gulf of Mexico, and the eastern and northern routes drain through the St. Lawrence and Mackenzie Rivers into the Northern Atlantic Ocean and Arctic Ocean respectively. The discharge into the Arctic Ocean is advected around Greenland and dispersed through the GIN seas (Peltier et al., 2006; Huang and Tian, 2008; Murton et al., 2010). It has been suggested that the southern route would be ineffective at producing a significant reduction in the thermohaline circulation (Manabe and Stouffer, 1997). It

has been proposed that the ice sheet retreated over a period of time during the Bølling-Allerød event, which opened a pathway to the St. Lawrence River (eastern route) for Lake Agassiz, This pathway may have resulted in diverting the drainage from the Mississippi River (southern route), thus making the St. Lawrence River the main pathway for glacial discharge during the YD (Broecker, 2006; Donnelly et al., 2005; Licciardi et al., 1999; Hostetler et al., 2000; Teller et al., 2005).

Drainage of the meltwater and proglacial lakes during the YD could have been rerouted into the Great Lakes and through the St. Lawrence River, or the input of glacial melt may be enough to trigger the YD cooling. However, geologic evidence of an outburst flood from Lake Agassiz into the Arctic Ocean via the Mackenzie River may indicate glacial discharge occurred through the Northern Route (Murton et al., 2010). Additionally, it has been suggested that the St. Lawrence River may not have been deglaciated by the onset of the YD (Teller et al., 2005; Broecker, 2006). Because of this uncertainty, other hypotheses regarding the onset of the YD must be explored.

Climate sensitivity experiments regarding the flux of fresh water into the Northern Atlantic have been performed on a variety of box models (Sima et al., 2004; Stommel, 1961; Abshagen and Timmermann, 2004), models of intermediate complexity (Mikolajewicz, 1996) and fully coupled atmospheric-oceanic general circulation models (AOGCMs; Liu et al., 2009; Peltier, 2007; He, 2011). These climate simulations suggested that a meltwater pulse of 0.1 to 0.3 Sverdrups (1 Sv = 10^6 m^3 s^{-1}) could result in a substantially reduced strength of the AMOC. In addition, the discharge of meltwater could have been augmented by the rafting of land-ice through the Hudson Strait, thus potentially providing a sufficient amount of fresh water to shut down the AMOC and trigger the onset of the YD (Licciardi et al., 1999).

1.2.2 The Ice Sheet Hypothesis

Oceanic and atmospheric circulation, albedo, and ocean surface temperatures can be directly affected by ice sheet dynamics (Clark, 1999). These variables are important when considering feedbacks within the climate system. The reduction or disappearance of glacial ice

sheets can provide meltwater input into the oceans, which affect atmospheric moisture in the form of precipitation (Gildor and Tziperman, 2000; Bard et al., 1996). The reduction of ice sheets can lead to increased net precipitation through an overall positive feedback loop, or a process in which the initial change will amplify a climate response (Figure 1-5; Eisenman et al., 2009). When air temperatures increased, such as during the Bølling-Allerød event, the continental ice sheet size decreased, causing stationary winds to migrate northward and transient winds to be increased in the North Atlantic region. Both factors led to an increased northward vapor transport. Coupled with enhanced freshwater flux, reduced AMOC, and increased sea ice coverage, this scenario conceivably led to a positive feedback loop.

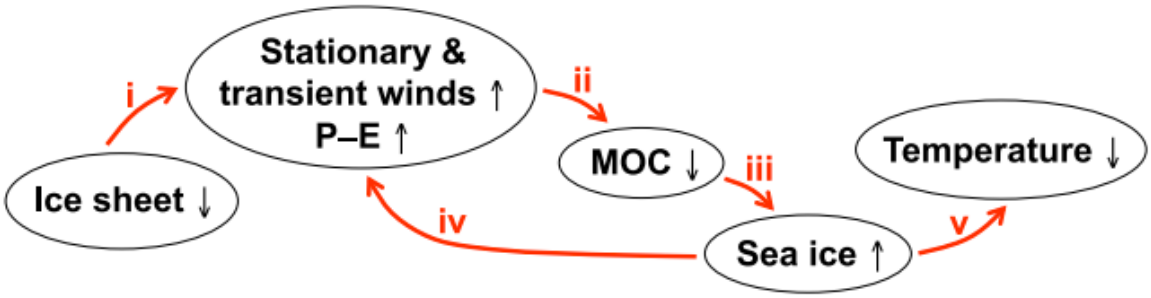

Figure 1-5 Climate feedback loop in response to ice sheet altitude and extent during the YD onset. A decrease in the size of the ice sheet allows for increased precipitation (P-E) as well as stationary and transient winds (i). This resulting input of freshwater caused a reduction of the MOC (ii), which allowed for a cooler climate and a build-up of additional sea ice (iii). The sea ice growth resulted in increased albedo, which can commence in decreased surface temperature (v; Figure from Eisenman et al., 2009).

The estimated increase of net precipitation in the Northern Atlantic could be more than three times as much as estimates proposed by Schmitt et al. (1989). Simulations completed by Eisenman et al. (2009) for present-day climate implied a reduction in ice sheets could produce enough glacial melt to shut down the AMOC, similar to flooding from Lake Agassiz during the YD.

1.2.3 The Extraterrestrial Impact Hypothesis

An extraterrestrial impact has been implied as one potential cause of the YD cooling event (Firestone et al., 2007; Kennett et al., 2009; Israde-Alcantara et al., 2012; Lecompte et al., 2012; Mahaney et al., 2010; Fayek et al., 2012).

The impact theory has been supported by regional extinctions of mammoths, birds, and other smaller mammals that occurred around the same time as the onset of the YD (Firestone, 2009). A carbon-rich layer in North America (black mats), which has been linked to the impact events, has been dated back to approximately 12,900 years before present in areas around the continent including Murray Springs, Arizona, Lake Hind MT in Canada, and Bull Creek, Oklahoma (Figure 1-6; Kennett et al., 2009; Fayek et al., 2012; Haynes, 2008). The layer contains iridium, carbon spherules, magnetic microspherules, and nanodiamonds, all of which are suggestive of an extraterrestrial impact (Kennett et al., 2009; Mahaney et al., 2010; Firestone et al., 2007; Israde-Alcantara et al., 2012; Fayek et al., 2012). Concentrations of nanodiamonds appear to be the highest at the YD boundary in Murray Springs, Lake Hind MT, and Bull Creek (Figure 1-6; (Kennett et al., 2009). These lines of evidence are controversial and may not be entirely related to an extraterrestrial impact; coal beds and black mats are rather linked to terrestrial processes (Surovell et al., 2009; Pinter et al., 2011; Lecompte et al., 2012; Pigati et al., 2012; Van Der Hammen and Van Geel, 2008). Pinter et al. (2011), Pigati et al. (2012) and Surovell et al. (2009) applied microscopy to identify YD Boundary layer microspherules, a methodology that consisted of significant uncertainties (Lecompte et al., 2012). In addition to uncertainties in the methodology, elevated iridium levels could have originated from cosmic rain (Israde-Alcantara et al., 2012). Climatic changes by a bolide impact could have been induced due to freshwater pulses, if the impact melted ice masses, or increase in dust concentration by forest fires. If the cooling event was caused by extraterrestrial influence, knowledge of the size and location of such an impact could help to predict possible abrupt climate changes as a result of extraterrestrial collision in the future.

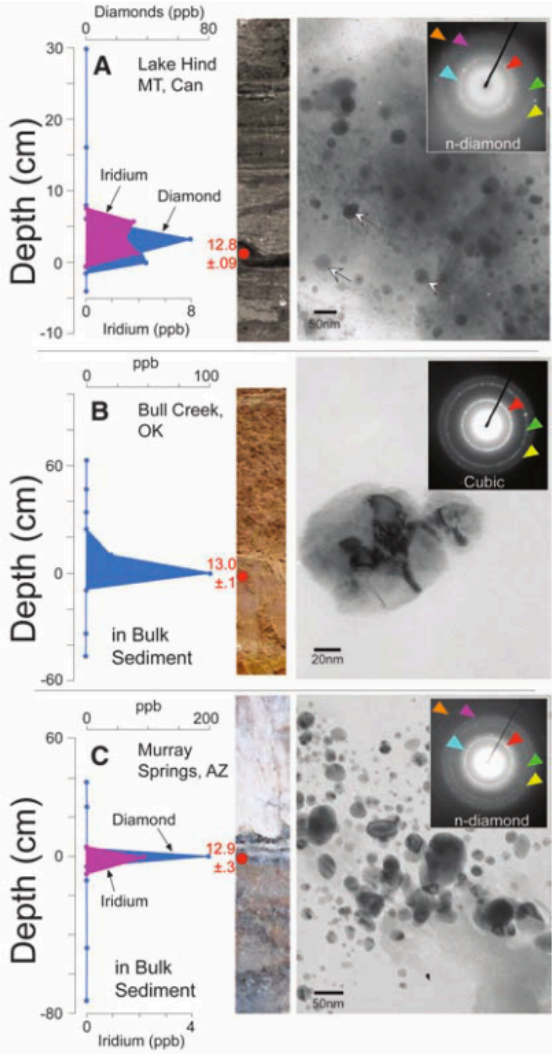

Figure 1-6 Observed extraterrestrial impact proxies from three YD Boundary Layer Sites. Observed amounts of nanodiamonds present at the boundary between the YD and the Bølling-Allerød event for three different locations. Iridium levels were also examined for Murray Springs, AZ and Lake Hind MT in Canada (Kennett et al., 2009).

1.3 The Role of Changes in the Deep Sea Circulation on the Younger Dryas cooling

The strength of the deep sea circulation depends on the formation of water masses that are controlled by the temperature and salinity-dependent density of surface water masses and wind stress (Broecker, 1997; Rahmstorf, 2006). Warmer, less saline water is transferred from the equator to the poles where it cools and becomes more saline by the formation of sea ice (Figure

1-7; Broecker, 1997; Rahmstorf, 2006). Due to the change in temperature and salinity, the water mass overturns, and thus is transported within the core of the North Atlantic Deep Water (NADW) equatorwards (Figure 1-7; Broecker, 1997; Rahmstorf, 2006). The input of glacial discharge (fresh water) into the Northern Atlantic, could reduce the salinity and enhance the vertical density gradient of the water mass as well as increase the vertical stratification and thus reduce the deep-water mass formation. Such a reduction or shut down of NADW formation and strength of the AMOC result in a surface cooling of the climate and reduced poleward heat transport (Broecker and Denton, 1989; Schiller et al., 1997). This process is thought to be the primary mechanism for the onset of the YD cooling event (Rooth, 1982).

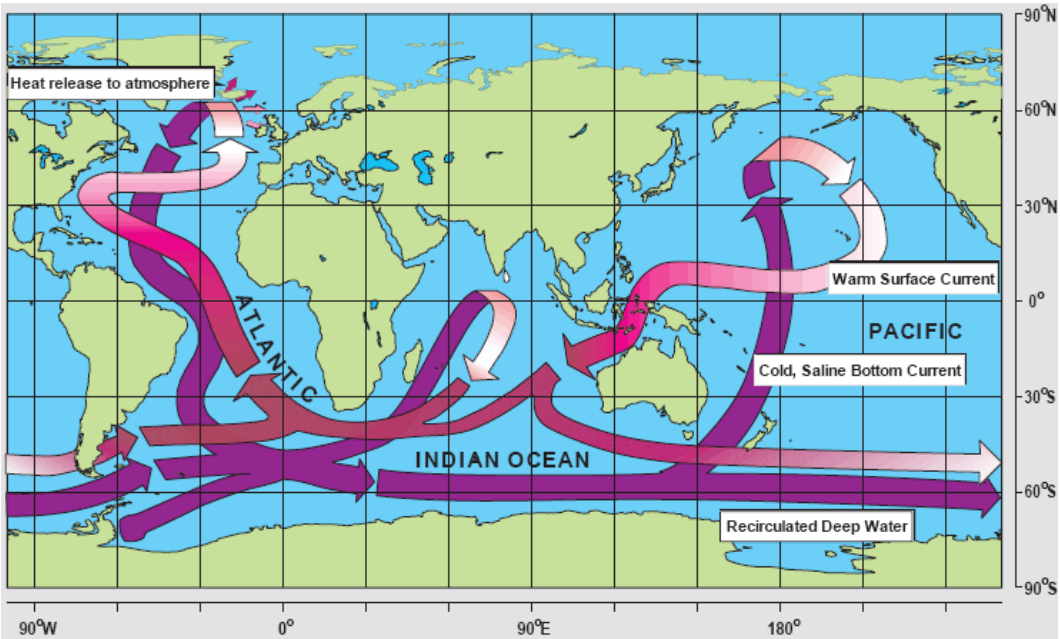

Figure 1-7 Schematic representation of the thermohaline circulation. For the Atlantic Ocean specifically, water masses warmed at the equator is advected toward the North Pole via a series of surface currents. Upon reaching the North Atlantic Ocean, the water mass is cooled and descends through the water column as it becomes denser. This colder and denser water mass moves toward the equator and then further down toward the South Pole. (Source: http://www-pord.ucsd.edu/~ltalley/sio210/nov5/conveyor.jpg)

1.4 Greenhouse Gases and the Global Carbon Cycle

An important factor in climate science involves the biogeochemical cycles (nutrient and gases) through the different reservoirs of the Earth. The carbon cycle is of particular interest and involves the movement of carbon through various reservoirs (Sarmiento and Gruber, 2002). Carbon reservoirs are the atmosphere, ocean, biosphere and land (geosphere). The geosphere is the largest reservoir of carbon (Hönisch et al., 2012). During the Younger Dryas, lower than present greenhouse gas concentrations of CO_2, CH_4, and N_2O due to higher solubility and an altered biological pump led to a tropospheric cooling due to reduced absorption of thermal outgoing long-wave infrared radiation, and back radiation to the Earth's surface (IPCC, 2007).

The natural atmospheric carbon pool contains approximately 590 petagrams of carbon (PgC), and exchanges carbon between the land and the surface ocean waters (Figure 1-8). The flux of CO_2 from the atmosphere into the ocean is approximately 70 PgC yr^{-1} and the flux into the land is 120 PgC yr^{-1} (Figure 1-8). Each is balanced by the fluxes from these reservoirs into the atmosphere. The air-sea gas exchange regulates the transfer of carbon between the atmosphere and the surface ocean and is dependent on wind speed and difference in partial pressure of CO_2 (pCO_2). Approximately 0.8 PgC of the natural carbon flux from the land surface to the ocean is due to riverine runoff (Figure 1-8). The natural carbon cycle has been perturbed significantly since the onset of the industrial revolution (Keeling et al., 2005; Crutzen, 2002). Fossil fuel emission reached a rate of 9.7 PgC yr^{-1} in 2012 and with an uptake ~50% in the atmosphere, and ~25% in the land and ocean (LeQuere et al., 2013;Figure 1-8).

The total surface ocean has a carbon pool of around 900 PgC, and it exchanges carbon with the intermediate and deep ocean layers, as well as the marine biota via the biological pump. The marine biosphere takes up ~50 PgC yr^{-1} due to gross primary production and exchanges approximately 39 PgC yr^{-1} by respiration (Sarmiento and Gruber, 2002; Figure 1-8). The surface water receives approximately 101 PgC yr^{-1} from the intermediate and deep ocean and contributes approximately 90.2 PgC yr^{-1} to the intermediate and deep ocean (Sarmiento and Gruber, 2002; Figure 1-8). The vertical flux of particulate organic carbon from the euphotic zone into intermediate and deep ocean is ~11 PgC yr^{-1} (Sarmiento and Gruber, 2002; Figure 1-8). Only a

small amount of ~0.2 PgC yr^{-1} or 2% of this vertical particulate organic carbon flux is sedimented. The riverine input of particulate organic carbon is in first order in balance with this sedimentation rate.

The solubility pump is driven by how CO_2 solubility changes between warm and cold waters, and determines the dissolved inorganic carbon (DIC) profile of the ocean by itself (Volk and Hoffert, 1985). The DIC profile is determined by the concentrations of CO_2 in the warm mixed layer of the ocean and the mixing of water masses dependent on vertical eddy diffusivity and vertical velocity (Volk and Hoffert, 1985). The biological pump is important in the regulation of vertical carbon gradients in the ocean (Volk and Hoffert, 1985; Gruber and Sarmiento, 2002). Organic matter will sink to the deep sea where it is remineralized by microbial processes utilizing oxygen and releasing CO_2 to the adjacent water column (Volk and Hoffert, 1985; Gruber and Sarmiento, 2002).

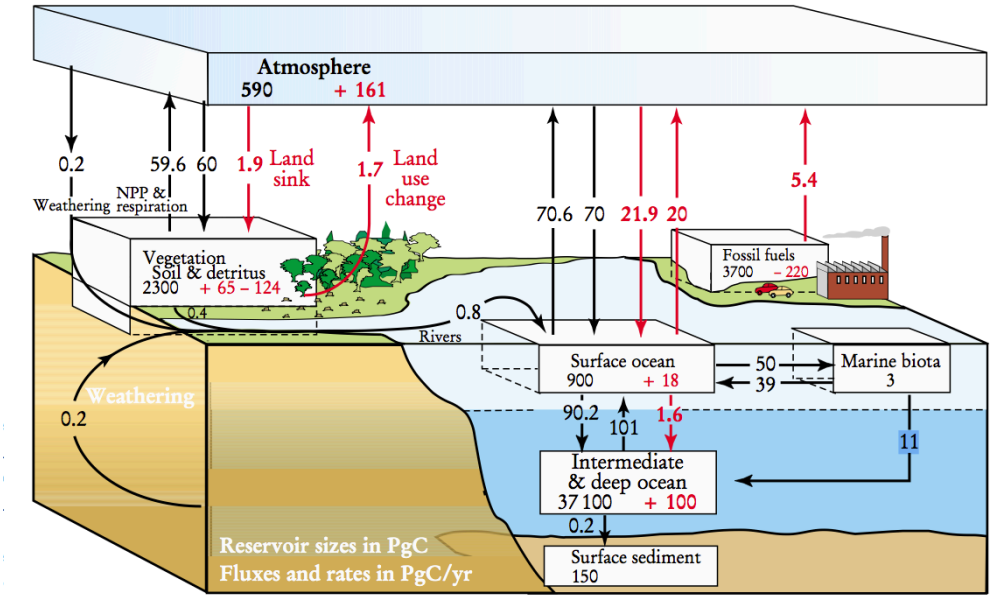

Figure 1-8 Schematic of the global carbon cycle reservoirs and fluxes. Black numbers represent preindustrial values of carbon flux in PgC yr^{-1} between reservoirs, and red values represent fluxes due to anthropogenic industry. For preindustrial settings, the atmospheric reservoir exchanges carbon to both the land and the ocean through precipitation. The ocean exchanges carbon with the atmosphere through evaporation. The land exchanges carbon with

the atmosphere through respiration and the ocean through river runoff. Anthropogenic industrial processes lead to an increase input of carbon from the burning of fossil fuels. (Sarmiento and Gruber, 2002).

References

Abshagen, J., and Timmermann, A., 2004, An organizing center for thermohaline excitability: Journal of Physical Oceanography, v. 34, p. 2756–2760, doi: 10.1175/JPO2642.1.

Alley, R.B., 2000, The Younger Dryas cold interval as viewed from central Greenland: Quaternary Science Reviews, v. 19, p. 213–226, doi: 10.1016/S0277-3791(99)00062-1.

Alley, R., Meese, D., and Shuman, C., 1993, Abrupt increase in Greenland snow accumulation at the end of the Younger Dryas event: Nature, v. 362, p. 527–529, doi: 10.1038/362527a0.

Anderson, R.F., Bacon, M.P., and Brewer, P.G., 1983, Removal of230Th and231Pa from the open ocean: Earth and Planetary Science Letters, v. 62, p. 7–23, doi: 10.1016/0012-821X(83)90067-5.

Andrič, M., Massaferro, J., Eicher, U., Ammann, B., Leuenberger, M.C., Martinčič, A., Marinova, E., and Brancelj, A., 2009, A multi-proxy Late-glacial palaeoenvironmental record from Lake Bled, Slovenia: Hydrobiologia, v. 631, p. 121–141, doi: 10.1007/s10750-009-9806-9.

Bakke, J., Lie, Ø., Heegaard, E., Dokken, T., Haug, G.H., Birks, H.H., Dulski, P., and Nilsen, T., 2009, Rapid oceanic and atmospheric changes during the Younger Dryas cold period: Nature, v. 2, p. 202–205, doi: 10.1038/ngeo439.

Barbetti, M., and Flude, K., 1979, Geomagnetic variation during the late Pleistocene period and changes in the radiocarbon time scale: Nature, v. 279, p. 202–205, doi: 10.1038/279202a0.

Bard, E., Arnold, M., Fairbanks, R.G., and Hamelin, B., 1993, 230Th-234U and 14C ages obtained by mass spectrometry on corals: Radiocarbon, v. 35, p. 191–199.

Bard, E., Hamelin, B., Arnold, M., Montaggioni, L., Cabioch, G., Faure, G., and Rougerie, F., 1996, Deglacial sea-level record from Tahiti corals and the timing of global meltwater discharge: Nature, v. 382, p. 241–244, doi: 10.1038/382241a0.

Barker, S., Cacho, I., Benway, H., and Tachikawa, K., 2005, Planktonic foraminiferal Mg/Ca as a proxy for past oceanic temperatures: a methodological overview and data compilation for

the Last Glacial Maximum: Quaternary Science Reviews, v. 24, p. 821–834, doi: 10.1016/j.quascirev.2004.07.016.

Berger, W.H., Smetacek, V., and Wefer, G., 1989, Ocean Productivity and Paleoproductivity - An Overview, *in* Productivity of the Ocean: Present and Past, p. 1–34.

Berner, W., Oeschger, H., and Stauffer, B., 1980, Information on the CO2 cycle from ice core studies: Radiocarbon, v. 22, p. 227–235.

Birks, H., and Ammann, B., 2000, Two terrestrial records of rapid climatic change during the glacial–Holocene transition (14,000–9,000 calendar years BP) from Europe: Proceedings of the National Academy of Sciences, v. 97, p. 1390–1394, doi: 10.1073/pnas.97.4.1390.

Björck, S., Kromer, B., Johnsen, S., Bennike, O., Hammarlund, D., Lemdahl, G., Possnert, G., Rasmussen, T.L., Wohlfarth, B., Hammer, C.U., and Spurk, M., 1996, Synchronized terrestrial atmospheric deglacial records around the North Atlantic: Science, v. 274, p. 1155–1160, doi: 10.1126/science.274.5290.1155.

Boyle, E., 1992, Cadmium And Delta-13-C Paleochemical Ocean Distributions During The Stage 2 Glacial Maximum: Annual Review of Earth and Planetary Sciences, v. 20, p. 245–287, doi: 10.1146/annurev.earth.20.1.245.

Boyle, E.A., and Keigwin, L., 1987, North Atlantic thermohaline circulation during the past 20,000 years linked to high-latitude surface temperature: Nature, v. 330, p. 35–40, doi: 10.1038/330035a0.

Broecker, W.S., 2003, Does the trigger for abrupt climate change reside in the ocean or in the atmosphere? Science (New York, N.Y.), v. 300, p. 1519–22, doi: 10.1126/science.1083797.

Broecker, W.S., 1997, Thermohaline Circulation, the Achilles Heel of Our Climate System: Will Man-Made CO2 Upset the Current Balance? Science, v. 278, p. 1582–1588, doi: 10.1126/science.278.5343.1582.

Broecker, W.S., 2006, Was the Younger Dryas triggered by a flood? Science, v. 312, p. 1146–1148, doi: 10.1126/science.1123253.

Broecker, W.S., and Denton, G.H., 1989, The role of ocean-atmosphere reorganizations in glacial cycles: Geochimica et Cosmochimica Acta, v. 53, p. 2465–2501, doi: 10.1016/0016-7037(89)90123-3.

Broecker, W.S., Peng, T.-H., and Beng, Z., 1982, Tracers in the sea (Lamont-Doherty Geological Observatory, Ed.): Lamont-Doherty Geological Observatory, Columbia University, Eldigio Press, 690 p.

Broecker, W.S., Peng, T.-H., Trumbore, S., Bonani, G., and Wolfli, W., 1990, The distribution of radiocarbon in the glacial ocean: Global Biogeochemical Cycles, v. 4, p. 103, doi: 10.1029/GB004i001p00103.

Came, R.E., Oppo, D.W., Curry, W.B., and Lynch-Stieglitz, J., 2008, Deglacial variability in the surface return flow of the Atlantic meridional overturning circulation: Paleoceanography, v. 23, p. 1–10, doi: 10.1029/2007PA001450.

Carlson, A.E., 2013, The Younger Dryas Climate Event, *in* Encyclopedia of Quaternary Science, Elsevier, p. 126–134.

Carlson, A.E., Clark, P.U., Haley, B.A., Klinkhammer, G.P., Simmons, K., Brook, E.J., and Meissner, K.J., 2007, Geochemical proxies of North American freshwater routing during the Younger Dryas cold event.: Proceedings of the National Academy of Sciences of the United States of America, v. 104, p. 6556–6561, doi: 10.1073/pnas.0611313104.

Clark, P.U., 1999, Northern Hemisphere Ice-Sheet Influences on Global Climate Change: Science, v. 286, p. 1104–1111, doi: 10.1126/science.286.5442.1104.

Dansgaard, W., White, J.W.C., and Johnsen, S.J., 1989, The abrupt termination of the Younger Dryas climate event: Nature, v. 339, p. 532–539, doi: 10.1038/339532a0.

Delmas, R.J., Ascencio, J.-M., and Legrand, M., 1980, Polar ice evidence that atmospheric CO2 20,000 yr BP was 50% of present: Nature, v. 284, p. 155–157, doi: 10.1038/284155a0.

Denniston, R.F., Gonzalez, L.A., Asmerom, Y., Polyak, V., Reagan, M.K., and Saltzman, M.R., 2001, A high-resolution speleothem record of climatic variability at the Allerød-Younger Dryas transition in Missouri, central United States: Palaeogeography, Palaeoclimatology, Palaeoecology, v. 176, p. 147–155, doi: 10.1016/S0031-0182(01)00334-0.

Denton, G.H., Alley, R.B., Comer, G.C., and Broecker, W.S., 2005, The role of seasonality in abrupt climate change: Quaternary Science Reviews, v. 24, p. 1159–1182, doi: 10.1016/j.quascirev.2004.12.002.

DeVernal, A., Hillaire-Marcel, C., and Bilodeau, G., 1996, Reduced meltwater outflow from the Laurentide ice margin during the Younger Dryas: Nature, v. 381, p. 774–777, doi: 10.1038/381774a0.

Donnelly, J.P., Driscoll, N.W., Uchupi, E., Keigwin, L.D., Schwab, W.C., Thieler, E.R., and Swift, S. a., 2005, Catastrophic meltwater discharge down the Hudson Valley: A potential trigger for the Intra-Allerød cold period: Geology, v. 33, p. 89–92, doi: 10.1130/G21043.1.

Eisenman, I., Bitz, C.M., and Tziperman, E., 2009, Rain driven by receding ice sheets as a cause of past climate change: Paleoceanography, v. 24, p. 12, doi: 10.1029/2009PA001778.

Elderfield, H., and Ganssen, G., 2000, Past temperature and delta18O of surface ocean waters inferred from foraminiferal Mg/Ca ratios.: Nature, v. 405, p. 442–5, doi: 10.1038/35013033.

Fairbanks, R.G., 1990, The Age and Origin of the “Younger Dryas Climate Event” In Greenland Ice Cores: Palaeogeography, v. 5, p. 937–948.

Fayek, M., Anovitz, L.M., Allard, L.F., and Hull, S., 2012, Framboidal iron oxide: Chondrite-like material from the black mat, Murray Springs, Arizona: Earth and Planetary Science Letters, v. 319-320, p. 251–258, doi: 10.1016/j.epsl.2011.11.033.

Firestone, R.B., 2009, The Case for the Younger Dryas Extraterrestrial Impact Event: Mammoth, Megafauna, and Clovis Extinction, 12,900 Years Ago: Journal of Cosmology, v. 2, p. 256–285.

Firestone, R.B., West, A., Kennett, J.P., Becker, L., Bunch, T.E., Revay, Z.S., Schultz, P.H., Belgya, T., Kennett, D.J., Erlandson, J.M., Dickenson, O.J., Goodyear, A.C., Harris, R.S., Howard, G.A., et al., 2007, Evidence for an extraterrestrial impact 12,900 years ago that contributed to the megafaunal extinctions and the Younger Dryas cooling.: Proceedings of the National Academy of Sciences of the United States of America, v. 104, p. 16016–21, doi: 10.1073/pnas.0706977104.

Fischer, G., 1991, Stable carbon isotope ratios of plankton carbon and sinking organic matter from the Atlantic sector of the Southern Ocean: Marine Chemistry, v. 35, p. 581–596, doi: 10.1016/S0304-4203(09)90044-5.

Frisia, S., Borsato, A., Spötl, C., Villa, I.M., and Cucchi, F., 2005, Climate variability in the SE Alps of Italy over the past 17 000 years reconstructed from a stalagmite record: Boreas, v. 34, p. 445–455, doi: 10.1080/03009480500231336.

Gasse, F., 2000, Hydrological changes in the African tropics since the Last Glacial Maximum: Quaternary Science Reviews, v. 19, p. 189–211, doi: 10.1016/S0277-3791(99)00061-X.

Gildor, H., and Tziperman, E., 2000, Sea ice as the glacial cycles' climate switch: Role of seasonal and orbital forcing: Paleoceanography, v. 15, p. 605–615, doi: 10.1029/1999PA000461.

Von Grafenstein, U., Eicher, U., Erlenkeuser, H., Ruch, P., Schwander, J., and Ammann, B., 2000, Isotope signature of the Younger Dryas and two minor oscillations at Gerzensee (Switzerland): palaeoclimatic and palaeolimnologic interpretation based on bulk and biogenic carbonates: Palaeogeography, Palaeoclimatology, Palaeoecology, v. 159, p. 215–229, doi: 10.1016/S0031-0182(00)00086-9.

Greenland Ice-core Project (GRIP), and Members, 1993, Climate instability during the last interglacial period recorded in the GRIP ice core: Nature, v. 364, p. 203–207, doi: 10.1038/364203a0.

Guo, L., 2002, Control of Pa/Th ratio by particulate chemical composition in the ocean: Geophysical Research Letters, v. 29, p. 1961, doi: 10.1029/2002GL015666.

Van Der Hammen, T., and Van Geel, B., 2008, Charcoal in soils of the Allerød-Younger Dryas transition were the result of natural fires and not necessarily the effect of an extra-terrestrial impact: Netherlands Journal of Geosciences, v. 87, p. 359–361.

Haynes, C.V., 2008, Younger Dryas "black mats" and the Rancholabrean termination in North America.: Proceedings of the National Academy of Sciences of the United States of America, v. 105, p. 6520–5, doi: 10.1073/pnas.0800560105.

He, F., 2011, Simulating Transiet Climate Evolution of the Last Deglaciation with CCSM3: University of Wisconsin-Madison, 1-185 p.

Heiri, O., and Millet, L., 2005, Reconstruction of Late Glacial summer temperatures from chironomid assemblages in Lac Lautrey (Jura, France): Journal of Quaternary Science, v. 20, p. 33–44, doi: 10.1002/jqs.895.

Henderson, G.M., 2002, New oceanic proxies for paleoclimate: Earth and Planetary Science Letters, v. 203, p. 1–13, doi: 10.1016/S0012-821X(02)00809-9.

Henderson, G.M., Heinze, C., Anderson, R.F., and Winguth, A.M.E., 1999, Global distribution of the 230Th flux to ocean sediments constrained by GCM modelling: Deep-Sea Research Part I: Oceanographic Research Papers, v. 46, p. 1861–1893, doi: 10.1016/S0967-0637(99)00030-8.

Hostetler, S.W., Bartlein, P.J., Clark, P.U., Small, E.E., and Solomon, A.M., 2000, Simulated influences of Lake Agassiz on the climate of central North America 11 , 000 years ago: Nature, v. 405, p. 334–337, doi: 10.1038/35012581.

Huang, E., and Tian, J., 2008, Melt-Water-Pulse (MWP) events and abrupt climate change of the last deglaciation: Chinese Science Bulletin, v. 53, p. 2867–2878, doi: 10.1007/s11434-008-0206-8.

IPCC, 2007, Climate Change 2007: The Physical Science Basis. Contribution of Working Group I to the Fourth Assessment Report of the Intergovernmental Panel on Climate Change [Solomon, S., D. Qin, M. Mann9ing, Z. Chen, M. Marquis, K.B. Averyt, M. Tignor and H.L. Miller (eds.)]. Cambridge University Press, Cambridge, United Kingdom and New York, NY, USA.

Israde-Alcantara, I., Bischoff, J.L., Dominguez-Vazquez, G., Li, H.-C., DeCarli, P.S., Bunch, T.E., Wittke, J.H., Weaver, J.C., Firestone, R.B., West, A., Kennett, J.P., Mercer, C., Xie, S., Richman, E.K., et al., 2012, PNAS Plus: Evidence from central Mexico supporting the Younger Dryas extraterrestrial impact hypothesis: Proceedings of the National Academy of Sciences, v. 109, p. E738–E747, doi: 10.1073/pnas.1110614109.

Jennings, A.E., Hald, M., Smith, M., and Andrews, J.T., 2006, Freshwater forcing from the Greenland Ice Sheet during the Younger Dryas: evidence from southeastern Greenland shelf cores: Quaternary Science Reviews, v. 25, p. 282–298, doi: 10.1016/j.quascirev.2005.04.006.

Jolly, D., 1997, Effect of Low Glacial Atmospheric CO2 on Tropical African Montane Vegetation: Science, v. 276, p. 786–788, doi: 10.1126/science.276.5313.786.

Keeling, C.D., Piper, S.C., Bacastow, R.B., Wahlen, M., Whorf, T.P., Heimann, M., and Meijer, H.A., 2005, Atmospheric CO2 and 13CO2 Exchange with the Terrestrial Biosphere and Oceans from 1978 to 2000: Observations and Carbon Cycle Implications, *in* Baldwin, I.T., Caldwell, M.M., Heldmaier, G., Jackson, R.B., Lange, O.L., Mooney, H.A., Schulze, E.-D., Sommer, U., Ehleringer, J.R., Denise Dearing, M., and Cerling, T.E. eds., A History of Atmospheric CO2 and Its Effects on Plants, Animals, and Ecosystems, Ecological Studies, New York, NY, Springer New York, p. 83–113.

Kennett, D.J., Kennett, J.P., West, A., Mercer, C., Hee, S.S.Q., Bement, L., Bunch, T.E., Sellers, M., and Wolbach, W.S., 2009, Nanodiamonds in the Younger Dryas boundary sediment layer.: Science, v. 323, p. 94, doi: 10.1126/science.1162819.

Lea, D.W., Pak, D.K., and Spero, H.J., 2000, Climate Impact of Late Quaternary Equatorial Pacific Sea Surface Temperature Variations: Science, v. 289, p. 1719–1724, doi: 10.1126/science.289.5485.1719.

Lecompte, M.A., Goodyear, A.C., Demitroff, M.N., Batchelor, D., Vogel, E.K., Mooney, C., Rock, B.N., and Seidel, A.W., 2012, Independent evaluation of conflicting microspherule results from different investigations of the Younger Dryas impact hypothesis.: Proceedings of the National Academy of Sciences of the United States of America, doi: 10.1073/pnas.1208603109.

Leverington, D.W., and Teller, J.T., 2003, Paleotopographic reconstructions of the eastern outlets of glacial Lake Agassiz: Canadian Journal of Earth Sciences, v. 40, p. 1259–1278, doi: 10.1139/e03-043.

Licciardi, J.M., Teller, J.T., and Clark, P.U., 1999, Freshwater routing by the Laurentide Ice Sheet During the Last Deglaciation: Geophysical Monograph Series, p. 177–201.

Liu, Z., Otto-Bliesner, B.L., He, F., Brady, E.C., Tomas, R., Clark, P.U., Carlson, A.E., Lynch-Stieglitz, J., Curry, W., Brook, E.J., Erickson, D., Jacob, R., Kutzbach, J., and Cheng, J., 2009, Transient simulation of last deglaciation with a new mechanism for Bølling-Allerød warming.: Science, v. 325, p. 310–4, doi: 10.1126/science.1171041.

Lotter, A.F., Birks, H.J.B., Eicher, U., Hofmann, W., Schwander, J., and Wick, L., 2000, Younger Dryas and Allerod summer temperatures at Gerzensee (Switzerland) inferred from fossil pollen and cladoceran assemblages: Palaeogeography, Palaeoclimatology, Palaeoecology, v. 159, p. 349–361, doi: 10.1016/S0031-0182(00)00093-6.

Lotter, A.F., Heiri, O., Brooks, S., van Leeuwen, J.F.N., Eicher, U., and Ammann, B., 2012, Rapid summer temperature changes during Termination 1a: High-resolution multi-proxy climate reconstructions from Gerzensee (Switzerland): Quaternary Science Reviews, v. 36, p. 103–113, doi: 10.1016/j.quascirev.2010.06.022.

Ma, L., Castro, M.C., and Hall, C.M., 2004, A late Pleistocene-Holocene noble gas paleotemperature record in southern Michigan: Geophysical Research Letters, v. 31, p. 4, doi: 10.1029/2004GL021766.

Magny, M., De Beaulieu, J.L., Drescher-Schneider, R., Vannière, B., Walter-Simonnet, A.V., Millet, L., Bossuet, G., and Peyron, O., 2006, Climatic oscillations in central Italy during the Last Glacial-Holocene transition: The record from Lake Accesa: Journal of Quaternary Science, v. 21, p. 311–320, doi: 10.1002/jqs.999.

Mahaney, W.C., Kalm, V., Krinsley, D.H., Tricart, P., Schwartz, S., Dohm, J., Kim, K.J., Kapran, B., Milner, M.W., Beukens, R., Boccia, S., Hancock, R.G. V, Hart, K.M., and Kelleher, B., 2010, Evidence from the northwestern Venezuelan Andes for extraterrestrial impact: The black mat enigma: Geomorphology, v. 116, p. 48–57, doi: 10.1016/j.geomorph.2009.10.007.

Manabe, S., and Stouffer, R.J., 1997, Coupled ocean-atmosphere model response to freshwater input: Comparison to Younger Dryas event: Paleoceanography, v. 12, p. 321–336, doi: 10.1029/96PA03932.

Manabe, S., and Stouffer, R.J., 1995, Simulation of abrupt climate change induced by freshwater input to the North Atlantic Ocean: Nature, v. 378, p. 165–167.

Mayewski, P. a, and Bender, M., 1995, The GISP2 ice core record—Paleoclimate highlights: Reviews of Geophysics, v. 33, p. 1287, doi: 10.1029/95RG00498.

Mayewski, P.A., Meeker, L.D., Whitlow, S., Twickler, M.S., Morrison, M.C., Alley, R.B., Bloomfield, P., and Taylor, K., 1993, The Atmosphere During the Younger Dryas: Science (New York, NY), v. 261, p. 195–197, doi: 10.1126/science.261.5118.195.

Mazaud, A., Laj, C., Bard, E., Arnold, M., and Tric, E., 1991, Geomagnetic field control of 14C production over the last 80ky: Implications for the radiocarbon time-scale: Geophysical Research Letters, v. 18, p. 1885–1888.

McElhinny, M.W., and Senanayake, W.E., 1982, Variations in the geomagnetic dipole. I - The past 50,000 years: Journal of Geomagnetism and Geoelectricity, v. 34, p. 39–51.

McManus, J.F., Francois, R., Gherardi, J.-M., Keigwin, L.D., and Brown-Leger, S., 2004, Collapse and rapid resumption of Atlantic meridional circulation linked to deglacial climate changes.: Nature, v. 428, p. 834–7, doi: 10.1038/nature02494.

Meltzer, D.J., and Holliday, V.T., 2010, Would North American Paleoindians have Noticed Younger Dryas Age Climate Changes? 1-41 p.

Mikolajewicz, U., 1996, A meltwater induced collapse of the `conveyor belt' thermohaline circulation and its influence on the distribution of $\delta^{14}C$ and $\delta^{18}O$ in the oceans: Technical Report, Max Plank Institude for Meteorology, v. 189, p. 125.

Mook, W.G., Bommerson, J.C., and Staverman, W.H., 1974, Carbon isotope fractionation between dissolved bicarbonate and gaseous carbon dioxide: Earth and Planetary Science Letters, v. 22, p. 169–176, doi: 10.1016/0012-821X(74)90078-8.

Murton, J.B., Bateman, M.D., Dallimore, S.R., Teller, J.T., and Yang, Z.-L., 2010, Identification of Younger Dryas outburst flood path from Lake Agassiz to the Arctic Ocean.: Nature, v. 464, p. 740–3, doi: 10.1038/nature08954.

Peltier, W.R., 2007, Rapid climate change and Arctic Ocean freshening: Geology, v. 35, p. 1147, doi: 10.1130/focus122007.1.

Peltier, W.R., Vettoretti, G., and Stastna, M., 2006, Atlantic meridional overturning and climate response to Arctic Ocean freshening: Geophysical Research Letters, v. 33, p. 2–5, doi: 10.1029/2005GL025251.

Peteet, D., 1995, Global Younger Dryas? Quaternary International, v. 28, p. 93–104, doi: 10.1016/1040-6182(95)00049-O.

Peyron, O., Begeot, C., Brewer, S., Heiri, O., Magny, M., Millet, L., Ruffaldi, P., Van Campo, E., and Yu, G., 2005, Late-Glacial climatic changes in Eastern France (Lake Lautrey) from pollen, lake-levels, and chironomids: Quaternary Research, v. 64, p. 197–211, doi: 10.1016/j.yqres.2005.01.006.

Pigati, J.S., Latorre, C., Rech, J. a., Betancourt, J.L., Martinez, K.E., and Budahn, J.R., 2012, Accumulation of impact markers in desert wetlands and implications for the Younger Dryas impact hypothesis: Proceedings of the National Academy of Sciences, v. 109, p. 7208–7212, doi: 10.1073/pnas.1200296109.

Pinter, N., Scott, A.C., Daulton, T.L., Podoll, A., Koeberl, C., Anderson, R.S., and Ishman, S.E., 2011, The Younger Dryas impact hypothesis: A requiem: Earth-Science Reviews, v. 106, p. 247–264, doi: 10.1016/j.earscirev.2011.02.005.

Rahmstorf, S., 2006, Thermohaline Ocean Circulation, *in* Encyclopedia of Quaternary Sciences, p. 1–10.

Rickaby, R.E.M., and Elderfield, H., 1999, Planktonic foraminiferal Cd/Ca: Paleonutrients or paleotemperature? Paleoceanography, v. 14, p. 293–303, doi: 10.1029/1999PA900007.

Rohling, E.J., Grant, K., Bolshaw, M., Roberts, a. P., Siddall, M., Hemleben, C., and Kucera, M., 2009, Antarctic temperature and global sea level closely coupled over the past five glacial cycles: Nature Geoscience, v. 2, p. 500–504, doi: 10.1038/ngeo557.

Rooth, C., 1982, Hydrology and ocean circulation: Progress in Oceanography, v. 11, p. 131–149, doi: 10.1016/0079-6611(82)90006-4.

Schiller, A., Mikolajewicz, U., Voss, R., 1997, The stability of the North Atlantic Thermohaline circulation in a coupled ocean-atmosphere general circulation model: Climate Dynamics, v. 13, p. 325-347.

Schmitt, R.W., Bogden, P.S., and Dorman, C.E., 1989, Evaporation Minus Precipitation and Density Fluxes for the North Atlantic: Journal of Physical Oceanography, v. 19, p. 1208–1221, doi: 10.1175/1520-0485(1989)019<1208:EMPADF>2.0.CO;2.

Schwander, J., Eicher, U., and Ammann, B., 2000, Oxygen isotopes of lake marl at Gerzensee and Leysin (Switzerland), covering the Younger Dryas and two minor oscillations, and their correlation to the GRIP ice core: Palaeogeography, Palaeoclimatology, Palaeoecology, v. 159, p. 203–214, doi: 10.1016/S0031-0182(00)00085-7.

Seager, R., and Battisti, D.S., 2007, Challenges to our understanding of the general circulation: abrupt climate change, *in* Global Circulation of the Atmosphere, p. 332–372.

Severinghaus, J.P., Sowers, T., Brook, E.J., Alley, R.B., and Bender, M.L., 1998, Timing of abrupt climate change at the end of the Younger Dryas interval from thermally fractionated gases in polar ice: Nature, v. 391, p. 141–146.

Shackleton, N.J., Duplessy, J.C., Arnold, M., Maurice, P., Hall, M.A., and Cartlidge, J., 1988, Radiocarbon age of last glacial Pacific deep water: Nature, v. 335, p. 708–711, doi: 10.1038/335708a0.

Shackleton, N.J., Wiseman, J.D.H., and Buckley, H.A., 1973, Non-equilibrium Isotopic Fractionation between Seawater and Planktonic Foraminiferal Tests: Nature, v. 242, p. 177–179, doi: 10.1038/242177a0.

Shane, L.C.K., and Anderson, K.H., 1993, Intensity, gradients and reversals in late glacial environmental change in east-central north America: Quaternary Science Reviews, v. 12, doi: 10.1016/0277-3791(93)90039-O.

Siddall, M., Rohling, E., Almogi-Labin, A., Hemleben, C., Meischner, D., Schmelzer, I., and Smeed, D.A., 2003, Sea-level fluctuations during the last glacial cycle: Nature, v. 423, p. 853–858, doi: 10.1038/nature01687.1.

Sima, A., Paul, A., and Schulz, M., 2004, The Younger Dryas—an intrinsic feature of late Pleistocene climate change at millennial timescales: Earth and Planetary Science Letters, v. 222, p. 741–750, doi: 10.1016/j.epsl.2004.03.026.

Smith, J.E., Risk, M.J., Schwarcz, H.P., and McConnaughey, T. a, 1997, Rapid climate change in the North Atlantic during the Younger Dryas recorded by deep-sea corals: Nature, v. 386, p. 818–820.

Stommel, H.M., 1961, Thermohaline Convection with Two Stable Regimes of Flow: Tellus, v. 13, p. 224–230, doi: 10.1111/j.2153-3490.1961.tb00079.x.

Street-Perrott, F., Huang, Y., Perrott, R., Eglinton, G., Barker, P., Khelifa, L., Harkness, D., and Olago, D., 1997, Impact of lower atmospheric carbon dioxide on tropical mountain ecosystems: Science (New York, N.Y.), v. 278, p. 1422–6, doi: 10.1126/science.278.5342.1422.

Surovell, T.A., Holliday, V.T., Gingerich, J.A.M., Ketron, C., Haynes, C. V., Hilman, I., Wagner, D.P., Johnson, E., and Claeys, P., 2009, An independent evaluation of the Younger Dryas extraterrestrial impact hypothesis.: Proceedings of the National Academy of Sciences of the United States of America, v. 106, p. 18155–8, doi: 10.1073/pnas.0907857106.

Talbot, M.R., Filippi, M.L., Jensen, N.B., and Tiercelin, J.-J., 2007, An abrupt change in the African monsoon at the end of the Younger Dryas: Geochemistry, Geophysics, Geosystems, v. 8, p. 16, doi: 10.1029/2006GC001465.

Tarasov, L., and Peltier, W.R., 2005, Arctic freshwater forcing of the Younger Dryas cold reversal.: Nature, v. 435, p. 662–5, doi: 10.1038/nature03617.

Teller, J.T., Boyd, M., Yang, Z.-L., Kor, P.S.G., and Fard, A.M., 2005, Alternative routing of Lake Agassiz overflow during the Younger Dryas: new dates, paleotopography, and a re-

evaluation: Quaternary Science Reviews, v. 24, p. 1890–1905, doi: 10.1016/j.quascirev.2005.01.008.

Vacco, D.A., Clark, P.U., Mix, A.C., Cheng, H., and Edwards, R.L., 2005, A speleothem record of Younger Dryas cooling, Klamath Mountains, Oregon, USA: Quaternary Research, v. 64, p. 249–256, doi: 10.1016/j.yqres.2005.06.008.

Vescovi, E., Ravazzi, C., Arpenti, E., Finsinger, W., Pini, R., Valsecchi, V., Wick, L., Ammann, B., and Tinner, W., 2007, Interactions between climate and vegetation during the Lateglacial period as recorded by lake and mire sediment archives in Northern Italy and Southern Switzerland: Quaternary Science Reviews, v. 26, p. 1650–1669, doi: 10.1016/j.quascirev.2007.03.005.

Volk, T., and Hoffert, M.I., 1985, Ocean Carbon Pumps: Analysis of Relative Strengths and Efficiencies in Ocean-Driven Atmospheric CO2 Changes, *in* The Carbon Cycle and Atmospheric CO2: Natural Variations Archean to Present, p. 99–110.

Vries, D., Analytic, B., Pecos, L., Adams, J.M., Faure, H., Faure-Denard, L., McGlade, J.M., and Woodward, F.I., 1990, Increases in terrestrial carbon storage from the Last Glacial Maximum to the present: Nature, v. 348, p. 711–714, doi: 10.1038/348711a0.

Wang, X., Auler, A.S., Edwards, R.L., Cheng, H., Cristalli, P.S., Smart, P.L., Richards, D.A., and Shen, C.-C., 2004, Wet periods in northeastern Brazil over the past 210 kyr linked to distant climate anomalies.: Nature, v. 432, p. 740–3, doi: 10.1038/nature03067.

Yu, E.-F., Francois, R., and Bacon, M.P., 1996, Similar rates of modern and last-glacial ocean thermohaline circulation inferred from radiochemical data: Nature, v. 379, p. 689–694, doi: 10.1038/379689a0.

Chapter 2

Objectives and Hypotheses

In this study, the causes of the Younger Dryas cooling were reexamined utilizing comprehensive three-dimensional low- and moderate-resolution Earth system models. Focus is primarily on the response of the AMOC and changes in the marine carbon cycle to various perturbations in the climate system. The goal of this study was to examine the following with a fully coupled climate system model:

- To what extent do greenhouse gas fluctuations (glacial/interglacial) affect the Younger Dryas climate and AMOC?

  Understanding of the response of the AMOC to changes in the atmospheric carbon dioxide concentration is important in examining the causes of the glacial-interglacial climate changes. Changing atmospheric pCO_2 affects the AMOC by influencing the amount of precipitation that can form in the troposphere (Manabe and Stouffer, 1994; Voss and Mikolajewicz, 2001). The warming of the atmosphere due to increased pCO_2 through the greenhouse effect can potentially increase the amount of precipitation, and thus increase freshwater input. These atmospheric changes can lead to stratification of the water column (Manabe and Stouffer, 1980) which can significantly reduce or shut down AMOC (Manabe and Stouffer, 1994; Voss and Mikolajewicz, 2001). A decreased atmospheric CO_2 radiative forcing could cause a decrease in the amount of precipitation over the Northern Atlantic region, which in turn could cause a decrease in vertical density gradients and increase in the AMOC (Manabe and Stouffer, 1980). Atmospheric pCO_2 values were significantly lower during the Younger Dryas as compared to preindustrial times (Joos and Spahni, 2008), and thus precipitation would be expected to be diminished resulting in the strengthening of the AMOC (Manabe and Stouffer, 1980).

- How sensitive is strength of the AMOC to orbital parameters during the onset of the Younger Dryas?

Changes in orbital parameters (precession of the equinoxes, eccentricity, and obliquity) would affect the regional and seasonal incoming solar radiation of the Earth's surface. Precession, eccentricity and obliquity during the preindustrial time in 1850 were approximately 0.01690, 0.017236, and 23.446° respectively (Berger and Loutre, 1991) whereas at 13 ka (the onset of the Younger Dryas), the precession, eccentricity and obliquity were -0.01824, 0.020175, and 24.093° respectively (Berger and Loutre, 1991). Increased seasonality during the Younger Dryas is expected compared to the preindustrial simulation. For example, at 60°N, incoming solar radiation in summer was higher during the YD than during 1850 (~+21.3 W m^{-2} for June) and lower during the winter (~-2.4 W m^{-2} for January; Berger and Loutre, 1991). The higher than present seasonality during the Younger Dryas is evident in sediment cores from the Loess Plateau of China (Zhisheng et al., 1993). The warmer than present summer temperatures and associated increase in net precipitation could have strengthened the vertical density gradient and weakened the AMOC compared to the preindustrial state. The trade winds are expected to be weaker, allowing for weaker monsoonal seasons as well as upwelling. The jet stream should not be affected by orbital variations

The strength of the monsoons are primarily regulated by eccentricity-modulated precessional cycles (Prell and Kutzbach, 1987) which may have resulted in changes in monsoonal patterns during the YD. Evidence from sedimentary records indicate the African and Asian Monsoons during the Younger Dryas were weakened (deMenocal et al., 2000; Yancheva et al., 2007; Garcin et al., 2007; Talbot et al., 2007; Gasse et al., 1991) due to the northern hemisphere cooling. However, these records account for other parameters such as freshwater forcing and a 13 ka ice sheet. Without this effect, the increase in radiative forcing would lead to a strengthening of the monsoonal circulation due to the increased seasonality.

- How does the AMOC respond to freshwater input from the Laurentide ice sheet?

Freshwater hosing experiments with climate models (He, 2011; Liu et al., 2009; Weijer et al., 2012; Peltier, 2007; Rind et al., 2001; Schiller et al., 1997; Mikolajewicz,

1996) provide insights to the sensitivity of the AMOC and associated climate change. In contrast to previous studies, the response of the North Atlantic climate to freshwater pulse and various other changes in the forcing boundary conditions at the Younger Dryas with an improved climate model (Gent et al., 2014) and higher spatial resolution is evaluated in this study. A freshwater input of 0.3 Sv into the northern North Atlantic Ocean (Peltier, 2007) would predict a climate state similar to the YD. Additionally, the strength of the West African monsoon circulation is expected to weaken with the addition of the 13 ka ice sheet and freshwater forcing to the model experiments, which supports paleoproxy reconstructions (deMenocal et al., 2000; Yancheva et al., 2007; Garcin et al., 2007; Talbot et al., 2007; Gasse et al., 1991) and will be in contrast to the findings of the second objective.

- How does the Younger Dryas climate respond to scenarios of freshwater discharge and no freshwater discharge in CCSM3?

  As discussed in the previous objective and chapter 1, freshwater discharge is proposed to be an important mechanism by which the Younger Dryas cold event occurred (Rooth, 1982; Broecker and Denton, 1989; Manabe and Stouffer, 1995; Donnelly et al., 2005; Broecker, 2003; Carlson et al., 2007). Without the influence of freshwater discharge on the Younger Dryas climate, it is anticipated that the AMOC will increase circulation strength because of an increase in convective overturning. Moreover, lower greenhouse gas radiative forcing will lead to cooler temperatures and less precipitation as inferred from Last Glacial Maximum (LGM) climate simulations (e.g. Brady et al., 2013). It is expected that the scenario with freshwater forcing would predict an AMOC that is more consistent to stable isotope $\delta^{13}C$ observations. A freshwater input of 0.3 Sv into the northern North Atlantic Ocean through the St. Lawrence River as suggested by Peltier (2007) can weaken the AMOC and produce subsequent cooling similar to that of the Younger Dryas event. However, a more plausible northern route, through the Mackenzie River (Figure 1-1; Murton et al., 2010), could also produce a slow down of the AMOC with the same amount of freshwater input. While both fresh water

routes are plausible it has been suggested that the northern route via the Mackenzie River is the more effective freshwater pathway for reducing the strength of the AMOC (He, 2011).

Recent climate change due to near-exponentially increasing greenhouse gas concentration in the troposphere due to fossil fuel emissions and land use changes since the industrial revolution (IPCC, 2013) will likely contribute to increased freshwater input from Antarctic and Greenland ice sheets and mountain glaciers. CO_2 radiative forcing has increased to more than 1x glacial-interglacial change (~400 ppmv), and is expected to increase to approximately 4x glacial-interglacial by 2100 (Mikolajewicz et al., 2007). Warming and freshening of surface water by increased rainfall and meltwater input entering the Northern Atlantic Ocean could lead to a decline of the AMOC comparable to that of the Younger Dryas (Mikolajewicz et al., 2007; Weijer et al., 2012). Investigating the causes of rapid climate change at the Younger Dryas cooling event and associated decline of the AMOC will contribute to a better understanding of feedbacks associated with climate change.

References

Berger, A., and Loutre, M.F., 1991, Insolation values for the climate of the last 10 million years: Quaternary Science Reviews, v. 10, p. 297–317, doi: 10.1016/0277-3791(91)90033-Q.

Broecker, W.S., 2003, Does the trigger for abrupt climate change reside in the ocean or in the atmosphere? Science (New York, N.Y.), v. 300, p. 1519–22, doi: 10.1126/science.1083797.

Broecker, W.S., and Denton, G.H., 1989, The role of ocean-atmosphere reorganizations in glacial cycles: Geochimica et Cosmochimica Acta, v. 53, p. 2465–2501, doi: 10.1016/0016-7037(89)90123-3.

Carlson, A.E., Clark, P.U., Haley, B.A., Klinkhammer, G.P., Simmons, K., Brook, E.J., and Meissner, K.J., 2007, Geochemical proxies of North American freshwater routing during the Younger Dryas cold event.: Proceedings of the National Academy of Sciences of the United States of America, v. 104, p. 6556–6561, doi: 10.1073/pnas.0611313104.

deMenocal, P., Ortiz, J., Guilderson, T., Adkins, J., Sarnthein, M., Baker, L., and Yarusinsky, M., 2000, Abrupt onset and termination of the African Humid Period:rapid climate responses to gradual insolation forcing: Quaternary Science Reviews, v. 19, p. 347-361.

Donnelly, J.P., Driscoll, N.W., Uchupi, E., Keigwin, L.D., Schwab, W.C., Thieler, E.R., and Swift, S. a., 2005, Catastrophic meltwater discharge down the Hudson Valley: A potential trigger for the Intra-Allerød cold period: Geology, v. 33, p. 89–92, doi: 10.1130/G21043.1.

Garcin, Y., Vincens, A., Williamson, D., Buchet, G., and Guiot, J., 2007, Abrupt resumption of the African Monsoon at the Younger Dryas-Holocene climatic transition: Quaternary Science Reviews, v. 26, p. 690–704, doi: 10.1016/j.quascirev.2006.10.014.

Gasse, F., Arnold, M., Fontes, J.C., Fort, M., Gibert, E., Huc, a., Bingyan, L., Yuanfang, L., Qing, L., Mélières, F., Campo, E. Van, Fubao, W., and Qingsong, Z., 1991, A 13,000-year climate record from western Tibet: Nature, v. 353, p. 742–745, doi: 10.1038/353742a0.

He, F., 2011, Simulating Transiet Climate Evolution of the Last Deglaciation with CCSM3: University of Wisconsin-Madison, 1-185 p.

IPCC, 2013, Climate Change 2013: The Physical Science Basis. Contribution of Working Group I to the Fifth Assessment Report of the Intergovernmental Panel on Climate Change (T. F. Stocker, D. Qin, G.-K. Plattner, M. Tignor, S. K. Allen, J. Boschung, A. Nauels, Y. Xia, V. Bex, & P. M. Midgley, Eds.): Cambridge, United Kingdom and New York, NY, USA, Cambridge University Press, 1535 p.

Joos, F., and Spahni, R., 2008, Rates of change in natural and anthropogenic radiative forcing over the past 20,000 years: Proceedings of the National Academy of Sciences of the United States of America, v. 105, p. 1425–1430, doi: 10.1073/pnas.0707386105.

Liu, Z., Otto-Bliesner, B.L., He, F., Brady, E.C., Tomas, R., Clark, P.U., Carlson, A.E., Lynch-Stieglitz, J., Curry, W., Brook, E.J., Erickson, D., Jacob, R., Kutzbach, J., and Cheng, J., 2009, Transient simulation of last deglaciation with a new mechanism for Bølling-Allerød warming.: Science, v. 325, p. 310–4, doi: 10.1126/science.1171041.

Manabe, S., and Stouffer, R.J., 1994, Multiple-century response of a coupled ocean-atmosphere model to an increase of atmospheric carbon dioxide: Journal of Climate, v. 7, p. 5–23, doi: 10.1175/1520-0442(1994)007<0005:MCROAC>2.0.CO;2.

Manabe, S., and Stouffer, R.J., 1980, Sensitivity of a global climate model to an increase of CO 2 concentration in the atmosphere: Journal of Geophysical Research, v. 85, p. 5529–5554, doi: 10.1029/JC085iC10p05529.

Manabe, S., and Stouffer, R.J., 1995, Simulation of abrupt climate change induced by freshwater input to the North Atlantic Ocean: Nature, v. 378, p. 165–167.

Mikolajewicz, U., Vizcaíno, M., Jungclaus, J., and Schurgers, G., 2007, Effect of ice sheet interactions in anthropogenic climate change simulations: Geophysical Research Letters, v. 34, p. 1–5, doi: 10.1029/2007GL031173.

Murton, J.B., Bateman, M.D., Dallimore, S.R., Teller, J.T., and Yang, Z.-L., 2010, Identification of Younger Dryas outburst flood path from Lake Agassiz to the Arctic Ocean.: Nature, v. 464, p. 740–3, doi: 10.1038/nature08954.

Peltier, W.R., 2007, Rapid climate change and Arctic Ocean freshening: Geology, v. 35, p. 1147, doi: 10.1130/focus122007.1.

Prell, W., Kutzbach, J., 1987, Monsoon variability over the past 150,000 years: Journal of Geophysical Research, v. 92, p. 8411-8425.

Rooth, C., 1982, Hydrology and ocean circulation: Progress in Oceanography, v. 11, p. 131–149, doi: 10.1016/0079-6611(82)90006-4.

Talbot, M.R., Filippi, M.L., Jensen, N.B., and Tiercelin, J.-J., 2007, An abrupt change in the African monsoon at the end of the Younger Dryas: Geochemistry, Geophysics, Geosystems, v. 8, p. 16, doi: 10.1029/2006GC001465.

Voss, R., and Mikolajewicz, U., 2001, The climate of 6000 years BP in near-equilibrium simulations with a coupled AOGCM: Geophysical Research Letters, v. 28, p. 2213–2216, doi: 10.1029/2000GL012498.

Weijer, W., Maltrud, M.E., Hecht, M.W., Dijkstra, H. a., and Kliphuis, M. a., 2012, Response of the Atlantic Ocean circulation to Greenland Ice Sheet melting in a strongly-eddying ocean model: Geophysical Research Letters, v. 39, p. 1–6, doi: 10.1029/2012GL051611.

Winguth, A., and Winguth, C., 2013, Precession-driven monsoon variability at the Permian-Triassic boundary - Implications for anoxia and the mass extinction: Global and Planetary Change, v. 105, p. 160–170, doi: 10.1016/j.gloplacha.2012.06.006.

Yancheva, G., Nowaczyk, N.R., Mingram, J., Dulski, P., Schettler, G., Negendank, J.F.W., Liu, J., Sigman, D.M., Peterson, L.C., and Haug, G.H., 2007, Influence of the intertropical convergence zone on the East Asian monsoon: Nature, v. 445, p. 74–77, doi: 10.1038/nature05431.

Zhisheng, A., Porter, S.C., Weijian, Z., Yanchou, L., Donahue, D.J., Head, M.J., Xihuo, W., Jianzhang, R., and Hongbo, Z., 1993, Episode of Strengthened Summer Monsoon Climate of Younger Dryas Age on the Loess Plateau of Central China: Quaternary Research, v. 39, p. 45–54, doi: 10.1006/qres.1993.1005.

Chapter 3

Effects of Freshwater Discharge on the Younger Dryas Climate in CCSM3

Abstract

The Younger Dryas cooling event was the most recent period of abrupt climate change in the geologic record. The cause of this event is controversial, and many hypotheses have been proposed including a massive freshwater pulse from the Laurentide Ice Sheet, change in storm tracks with the melting of the glaciers, and a bolide impact. In this study, the freshwater forcing hypothesis is reevaluated with different possible drainage routes via the Mackenzie River and St. Lawrence River into the North Atlantic Ocean. The Community Climate System Model version 3 has been applied to test the sensitivity of the Atlantic meridional overturning circulation (AMOC) and stable carbon isotope changes during the Younger Dryas in response to maximum freshwater discharges. The experiments indicate that the AMOC is slightly more sensitivity to the Mackenzie River discharge as opposed to St. Lawrence River discharge. This sensitivity suggests that the AMOC may be influenced by the location of the freshwater forcing and not just the freshwater volume. Additionally, model results suggest that the surface air temperature for the simulation with freshwater forcing decreased by approximately 10-15 °C over Greenland, which is in agreement with the GISP reconstructions for that region. However, a more substantial cooling of the surface air temperature over the Greenland ice sheet and North America occurs in the simulation without freshwater forcing. The cooler and drier climate condition in this simulation, compared to the scenario with freshwater forcing, leads to a stronger AMOC. Additional analysis would be required to determine the causes of the cooling of the surface air temperature over North America and the Greenland ice sheet because of the complexity of the various climate feedbacks. In the scenario with freshwater foricng, a discontinuation of freshwater forcing leads to an increase in AMOC within the first 10 years and recovery continues for the next 170 years. Analysis of the distribution of density indicating increased ocean heat transport by decreased freshwater input in the North Atlantic Ocean. The simulated cooling event of the Younger Dryas freshwater forcing scenario has a lower $\delta^{13}C$ bias to the reconstructed $\delta^{13}C$ values from the sedimentary record compared to scenario without freshwater forcing.

3.1 Introduction

The deep sea circulation acts as a flywheel of the climate and can be compared to a conveyor belt (Broecker, 1991; Drange et al., 2005). Warm and saline water masses from the low latitudes are transported northward (Hastenrath 1982, Broecker et al., 1988; Srokosz et al., 2012; Rahmstorf, 2006) into the northern North Atlantic (Greenland, Iceland, Norwegian or Labrador Sea) where convective overturning occurs by heat loss to the atmosphere, changes in salinity, and wind-induced mixing. When the surface water reach the polar latitudes, the heat from the surface water is given off to the atmosphere as a latent heat flux (Broecker et al., 1988; Srokosz et al., 2012). The loss of heat from the water mass causes a cooling of the sea surface temperatures, and along with the increase in salinity from formation of sea ice, the density of the water mass increases and it sinks to the bottom of the ocean. The colder and denser deep water flows across the Denmark Strait and partially across the Iceland-Faroe Ridge along the western boundary southward.

The strength of the AMOC as well as the wind stress over the surface ocean influences the poleward heat transport into the northern North Atlantic Ocean substantially. For this study, the focus will be on the processes related to the strength of the AMOC. On average, the volume transport of the oceanic circulation is approximately 17.0 ± 4 Sverdrups (Sv) and carries approximately 1.2 ± 0.2 PW of heat over the North Atlantic (Levitus, 1983; Hall and Bryden, 1982; Rintoul and Wunsch, 1991). Overall, the heat transport response to changes in the AMOC from approximately 2004 to 2011 is approximately 0.06 PW/Sv (Srokosz et al., 2012; Srokosz and Bryden, 2015; Johns et al., 2011).

Rerouting of freshwater drainage from the Mississippi River to the St. Lawrence River into the North Atlantic Ocean (Rooth, 1982; Broecker et al. 1989) could have effected the strength of the AMOC by enhanced vertical stability of water masses during the Younger Dryas (Broecker and Denton, 1989; Rooth, 1982). When freshwater is discharged into the northern Atlantic Ocean, deep water formation in the GIN and Labrador sea decreases (Rahmstorf, 2000; Stocker and Marchal, 2000; Stocker and Wright, 1991; Rahmstorf, 1996), poleward heat transport decreases, and the Northern Atlantic cools (Seager and Battisti, 2007; Peltier, 2007; Cheng et al., 2011).

Moderate changes in the oceanic circulation due to a different location and amount of the freshwater input can change the regional climate of the North Atlantic substantially. It has been shown that a maximum surface air temperature cooling of approximately 10°C can occur in the Nordic Seas (Rahmstorf, 1996, 2006).

Another cause of the YD cooling event may be linked to the amount of freshwater input into the Northern Atlantic Ocean. A decreased rate of NADW formation by the freshening could have resulted to in a weakening of the AMOC (Tarasov and Peltier, 2005; Boyle and Keigwin, 1987; McManus et al., 2004; Broecker et al., 1988; Hughen et al., 2000). There is evidence of a strong salinity reduction at the onset of the YD as well as indication of meltwater discharge in the oxygen isotope records from sediment core within Gulf of Mexico (Broecker and Denton, 1989). Sea surface temperature along with $\delta^{18}O$ records show water masses in the poles were less saline and colder at the onset of the YD (Bakke et al., 2009).

Evidences for the change in AMOC as well as the location for possible drainage paths at the onset of the YD are supported by marine sediment cores (see Chapter 1). AMOC reduction at the YD is also inferred from a sediment core off Northern Norway in which sea surface temperatures change between interglacial to glacial values, ~10 °C and ~2 °C respectively, as well as the Bermuda Rise (Ebbesen and Hald, 2004; McManus et al., 2004). Cd/Ca records from benthic foraminifera in a western south Atlantic Ocean sediment core indicate weaker deep and intermediate water circulation during the YD (Came et al., 2003). A reduction in deepwater production in the northern Atlantic Ocean is also supported by analysis of radiocarbon from marine sediment records in the Cariaco Basin and the Caribbean Sea (Hughen et al., 1998; Broecker et al., 1982). Changes in the AMOC at the onset of the YD affected the tropical atmospheric circulation and regional aridity and increased salinity in the Gulf of Mexico as inferred from $\delta^{18}O_{SW}$ values from the Florida Straits (Schmidt and Lynch-Stieglitz, 2011).

One possibility for the input of freshwater is the disappearance of glacial ice sheets during the BA event (Bard et al., 1996). With the abrupt warming of the northern Atlantic climate, the Laurentide Ice Sheet (LIS) could have melted and drained rapidly into the proglacial Lake Agassiz followed by an estimated ~9500 km^3 of water drainage to the northern Atlantic Ocean

(Broecker and Denton, 1989; Rooth, 1982; Teller et al., 2002). Lacustrine sediments in the region indicate that the water level of Lake Agassiz fell at the onset of the YD (Teller, 2013). Although this hypothesis is the most widely accepted, the path of the LIS drainage out of Lake Agassiz is controversial. There are three established LIS drainage routes: the northern route through the Mackenzie River, the eastern route through the St. Lawrence River, and the southern route through the Mississippi River (Huang and Tian, 2008; Murton et al., 2010; Broecker and Denton, 1989).

Geological evidence has suggested that originally Lake Agassiz drained through the Mississippi River, but around the onset of the YD, this drainage was diverted to the St. Lawrence River (Teller, 1990; Broecker et al., 1988; Leverington and Teller, 2003; Teller, 2003; Dyke, 2004). Evidence from ice margin fluctuations of the LIS indicate increased freshwater flow through the St. Lawrence River corresponding to reductions in deep water formation at the time of the YD. Timing from sediment records of Glacial Lake Iroquois also indicate increased meltwater discharge through the region (Clark et al., 2001; Donnelly et al., 2005). Planktonic foraminiferal geochemical proxies from a core extracted at the mouth of the St. Lawrence estuary indicate an increase of freshwater discharge occurred at the start of the YD at a volume capable of reducing the AMOC to the point of causing the cooling that occurred in the YD (Carlson et al., 2007). Additionally, lithic grains from the southwestern Labrador sea show ice movement through the Labrador Sea during the YD (Bond and Lotti, 1995).

However, new geologic evidence suggest that the northern route through the Mackenzie River is the most likely path of freshwater discharge (Peltier, 2007; Murton et al., 2010). Cores from the region of lake Nipigon indicate that the Great Lakes area, and therefore the St. Lawrence River may not have been deglaciated until after the YD (Teller et al., 2005). Evidence from gravel and erosion surfaces in the region suggest the occurrence of a flood into the Arctic Ocean from the Mackenzie River corresponding to the onset of the YD (Murton et al., 2010). Freshwater pulses from the Arctic Ocean could have been transported with the East Greenland Current through the Fram Strait at the onset of the YD as inferred from $\delta^{18}O$ and $\delta^{13}C$ values from a sedimentation record on the Yermak Plateau (Knies et al., 2007). Additionally, discharge from

this location has been supported to be more effective in reducing the AMOC because the Arctic Ocean water column is particular stable because of fresh surface water masses, as opposed to higher saline water masses from North Atlantic current in the area south of Greenland (Peltier, 2007). Because of this differences in vertical stability of the water masses, freshwater discharge does not entrain into the ocean along isopycnal surfaces and is transported southward through the Fram Strait, partially in the form of pack ice which eventually melts in the Greenland Sea (Peltier, 2007).

3.2 Sensitivity of the AMOC to freshwater perturbations

Climate simulations indicate that a freshwater discharge into the northern North Atlantic Ocean lead to reduction of the AMOC and associated decrease of air temperature and poleward heat transport over the entire region (Manabe and Stouffer, 2000; Mikolajewicz, 1996; Manabe and Stouffer, 1999; Schiller et al.,1997; Rahmstorf, 2006). In the CMIP/PMIP experiments, a 0.1 Sv freshwater discharge into the northern Atlantic causes a 30% weakening of the AMOC; however, no collapse of the AMOC is induced (Stouffer et al., 2006). When the freshwater discharge is increased to 1.0 Sv, the AMOC collapses completely in all of the simulations (Stouffer et al., 2006). Similarly, a 0.25 Sv freshwater discharge induces a slight shut down of the deep water formation and increasing the discharge to 0.5 Sv or higher collapses the AMOC completely, thus causing a cooling in the Northern Hemisphere (Knutti et al., 2004). Freshwater hosing simulations, one with an open and another with a closed Bering Strait, result in a nearly collapsed AMOC; however, full recovery is faster in the open Bering Strait simulation (Hu et al., 2004). Otto-Bliesner and Brady (2010) simulated freshwater forcing with 0.1 Sv and 1.0 Sv. This simulation resulted in reduced surface air temperatures over Greenland by 6-8°C, and the magnitude, location, and duration of freshwater input were not found to be substantially influential. The strength and pathway of the Atlantic deep sea circulation by freshwater hosing is also dependent on the model resolution (Otto-Bliesner et al., 2006), particularly if eddies are explicitly resolved (Weijer et al., 2012).

Several studies have been performed testing how the AMOC responds to freshwater discharged through the St. Lawrence River and the Mackenzie River independently. Freshwater discharge into the Arctic Ocean during the YD and transport of these fresh water masses through the Fram Strait could have influenced the strength of the AMOC (Tarasov and Peltier, 2005). It has also been suggested that the response of the AMOC and the surface air temperature in the North Atlantic region to drainage by St. Lawrence River and the Mackenzie River are approximately similar (Peltier, 2007). A reduction by 44% of the AMOC during the YD cooling event may have plausible by a 0.1 Sv discharge directed through the St. Lawrence river (Carlson et al., 2007) as inferred from Trace21 glacial-interglacial transient simulations (He, 2011). Based on these simulations, however, it was concluded that input from the Mackenzie River into the Arctic Ocean reduces the AMOC more substantially as compared to the St. Lawrence River (He, 2011). The AMOC response appears to be sensitive to the position of the ice margin of northern North Atlantic Ocean (Hostetler et al., 2000), but less sensitive to freshwater drainage to regions outside the northern North Atlantic Ocean (i.e. to the Gulf of Mexico; Manabe and Stouffer, 1997). Therefore, it is important to reevaluate these uncertainties with a complex climate model.

3.3 Model Description

3.3.1 Introduction to the Climate System Model version 3 (CCSM3)

The sensitivity experiments described in this study were performed using the Community Climate System Model version 3 (CCSM3, Collins et al., 2006; http://www.cesm.ucar.edu/models/ccsm3.0/), a comprehensive, fully coupled comprehensive climate system model. The model consist of the Community Atmospheric Model (CAM3; Collins et al., 2004), an atmospheric general circulation model, the Parallel Ocean Program version 1.4 (POP1.4; Doney et al., 2006), an ocean general circulation model, a community sea ice model version 5 (CSIM5; Schramm et al., 2004; Briegleb et al., 2004) and community land model version 3 (CLM3; Oleson et al., 2004). The low-resolution 3°x3° grid system was used (T31_gx3v5) for the sensitivity experiments conducted in this study. The ocean and ice models use the same grid (gx3v5) with the North Pole displaced to Greenland while the atmosphere and land utilize a horizontal Gaussian grid that has a 3.75-degree resolution (T31; Collins et al., 2004;

Oleson et al., 2004; Schramm et al., 2004; Briegleb et al., 2004; Doney et al., 2006). The nominal gx3v5 grid has a variable resolution in the latitudinal direction of approximately 0.9 degrees near the equator, 3.6-degree longitudinal resolution, and has 116 latitudes and 100 longitudes of grid cells horizontally (Schramm et al., 2004; Briegleb et al., 2004; Doney et al., 2006). The governing equations for CAM3 and POP1.4 are summarized in Appendix D. CCSM3 exchanges boundary conditions, physical state, and physical and geochemical flux information between four components (land, ocean, atmosphere and sea-ice) linked by a central coupler. Physical constants that are shared by the geophysical models are presented in Appendix B. The detailed descriptions of the four main components of CCSM3 are summarized below.

3.3.2 The Community Atmosphere Model

The Community Atmosphere Model version 3 (CAM3) is the National Center for Atmospheric Research's fifth generation of the global three-dimensional atmospheric general circulation model (AGCM; Collins et al., 2006). New dynamics and physics were included in the major improvements from CAM 2 to CAM 3.0 including the new treatment of precipitation and cloud processes (Boville et al., 2006), new aerosol data sets (He, 2011), the insuring of conservation of energy via new calculation of thermodynamic tendencies (Boville and Bretherton, 2003), a finite-volume dynamical core (Lin and Rood, 1996; Lin, 2004), and new radiative parameterization involving long- and short-wave radiation interactions with water vapor and cloud geometry (Neale et al., 2004).

The CAM3 uses a generalized terrain following vertical coordinates to develop the primitive equations (Neale et al., 2004). A semi-implicit Eulerian spectral dynamical core is coupled with the total parameterization package and consists of clouds and radiation, turbulent mixing, moist precipitation processes, and a surface model (Neale et al., 2004). Precipitation processes include moist penetrative convection, large-scale stable condensation, shallow convection, and dry adiabatic adjustment for the stratosphere. The radiation parameterization utilizes the cloud parameterization. Longwave absorptivity and emissivity have new parameterizations that, using the absorptivity/emissivity method, preserve the radiative transfer equation (Neale et al., 2004). This is used for water vapor, which is considered a prognostic

variable. The surface model provides surface fluxes obtained from the ocean, sea-ice, and land models. Lower flux boundary conditions required for the surface fluxes include vertical diffusion, gravity wave drag, and the planetary boundary layer parameterization. Zhang and McFarlane (1995) developed the deep convection parameterization, which is based on saturated downdrafts and the related convective scale updrafts existing in the lower troposphere whenever the atmosphere is conditionally unstable. Formulas used for the deep convective parameterization can be found in Zhang and McFarlane (1995). A summary of the CAM3.0 formulations can be found in the CAM3.0 User's Guide (Neale et al., 2004) and at http://www.cesm/ucar.edu/models/atm-cam/.

3.3.3 The Community Land Model

The biogeophysical processes of the Community Land Model version 3 (CLM3) are forced by atmospheric surface fluxes that provide sensible heat flux, latent heat flux, upward long-wave radiation, surface albedos, zonal and meridional surface stresses, and water vapor flux to CAM (Oleson et al., 2004). Several hydrological and ecological factors partially regulate the previously mentioned processes. The model can account for processes such as stomatal physiology and leaf phenology as well as the ecological differences between vegetation typed. Multiple land cover types within grid cells are calculated via thermal and hydrological differences in soil types (Oleson et al., 2004).

The land model is forced by the current state of the atmosphere per time step (Appendix C). CLM3.0 calculates momentum, radiative surface energy, and constituent fluxes using hydrologic states of snow and soil from the previous time step. The coupler receives these fields from the atmospheric model. Surface albedos, fluxes (momentum, radiative, sensible, and latent), soil temperature and hydrology, and ecosystem structure and composition details can be found in Oleson et al. (2004; http://www.cgd.ucar.edu/tss/clm/distribution/clm3.0/).

3.3.4 The Parallel Ocean Program

The Parallel Ocean Program version 1.4 (POP1.4) uses a dipole grid with 25 vertical levels and a nominal horizontal resolution of 3° (gx3v5), as well as the three-dimensional primitive equations for ocean dynamics (Smith and Gent, 2004; Vertenstein et al., 2004). With the use of a dipole-mesh grid, the poles are displaced over land, and the vertical dimension has a finer resolution (approximately 8 m thick) at the surface ocean. The deep ocean has a resolution of greater than 300 m. POP1.4 is an improved version of the Los Alamos National Laboratory POP model. Details are documented in Smith and Gent (2004; http://www.cesm/ucar.edu/models/ccsm3.0/pop/).

3.3.5 The Community Sea Ice Model

The Community Sea Ice Model version 5 (CSIM5) utilizes the same vertical and horizontal grid as POP. CSIM uses Bitz and Lipscomb's (1999) energy conservation thermodynamics and includes a subgrid-scale ice thickness distribution (Schramm et al., 2004). The exchange of salt between the ocean and sea-ice as well as ice dynamics and sea-ice albedo are included in the model. CSIM details can be found in Briegleb et al. (2004) and Schramm et al. (2004) as well as the website for the model at http://www.cesm.ucar.edu/models/ccsm3.0/csim/.

3.3.6 Ocean Carbon Cycle

An adaptation of the Ocean-Carbon Cycle Model Intercomparison Project (OCMIP) has been used in conjunction with CCSM3 to simulate the carbon cycle for the Younger Dryas. This model followed the design of a previous carbon cycle model by Doney et al. (2006). Seven prognostic variables including phosphate, dissolved organic phosphorous, dissolved organic and inorganic iron, dissolved inorganic carbon, total alkalinity and dissolved oxygen are simulated by the carbon cycle model. Dissolved inorganic carbon (DIC) is defined as the summation of the amount of bicarbonate, carbonate and aqueous carbon dioxide in the surface ocean, as shown:

$$DIC = \left[HCO_3^-\right] + \left[CO_3^{-2}\right] + \left[CO_{2(aq)}\right] \quad (3\text{-}1)$$

Nutrient uptake from biological processes assumes a constant Redfield ratio and is similar to the Hamburg Model of the Ocean Carbon Cycle (HAMOCC; Maier-Reimer, 1993).

Biological production is regulated by biomass turnover, surface solar irradiance, temperature, and micro- and macronutrients. The Martin power-law curve is used to describe the vertical flux of particulate organic phosphorus in the water column (for details see Winguth and Winguth, 2011). Air-sea gas exchange of CO_2 depends on difference of the partial pressure of CO_2 between the ocean and the atmosphere. The net flux of CO_2will exchange ΔF across the boundary between the ocean and the atmosphere in dependence on the wind speed and temperature (Doney et al., 2009) as:

$$\Delta F = F_{ao} - F_{oa} = K_u\left[(pCO_2)_a - (pCO_2)_o\right](1-f_{ice}) \tag{3-2}$$

$$(pCO_2)_o = \beta_T[CO_2] \tag{3-3}$$

where F_{ao} and F_{oa} are the flux of CO_2 from the atmosphere to the ocean and from the ocean to the atmosphere respectively, K_u is a wind-dependent coefficient for air-sea gas exchange (Wanninkhof, 1992), $(pCO_2)_a$ and $(pCO_2)_o$ are the partial pressure of CO_2 in the atmosphere and ocean respectively, β_T is the solubility of CO_2 based on temperature, and $[CO_2]$ is the concentration of CO_2 dissolved in the uppermost layer of the ocean. $(1-f_{ice})$ represents the reduction of CO_2 flux between the ocean and atmosphere reservoirs by the sea-ice coverage when it is present at the poles.

Primary production in the surface ocean is determined by nutrient availability, temperature, light, and biomass, which can be represented by an equation proposed by Doney et al. (2006):

$$J_{Prod} = \frac{F_T F_N F_I B_{max}\left(1, \frac{z_{ml}}{z_c}\right)}{\tau} \tag{3-4}$$

where

$$F_T = \frac{T+2}{T+10} \tag{3-5}$$

$$F_N = \min\left(\frac{PO_4}{PO_4 - K_{PO4}}, \frac{Fe}{Fe - K_{Fe}}\right) \tag{3-6}$$

$$F_I = \frac{I}{I+K_I} \tag{3-7}$$

$$B = \min\left(PO_4, \frac{Fe}{rFe:B}\right) \tag{3-8}$$

Limiting factors of nutrient uptake are temperature (F_T), the availability of iron and phosphate (F_N), and light (F_I). In equation 3-4, T is temperature, and in equation 6, I and K_I are the short wave radiation and light limiting term respectively. K_I is equal to 20 W/m^2 (Winguth and Winguth, 2013). B represents the biomass proxy where the ratio of uptake between Fe and PO_4 (~5.85 x 10^{-4}) is shown by *rFe:B* (Winguth and Winguth, 2013). The ratio of z_{ml}/z_c must be positive, as productivity can only take place above 75 m, which is the compensation depth (Winguth and Winguth, 2013). Redfield ratios are fixed at 117/16/1 (Doney et al., 2006).

3.3.7. Diagnostic stable isotope model

The stable carbon isotope $\delta^{13}C$ is defined as:

$$\delta^{13}C = \left[\frac{\left(\frac{13C}{12C}\right)_{sample}}{\left(\frac{13C}{12C}\right)_{standard}} - 1 \right] \times 1000 \qquad (3\text{-}9)$$

Where $\left(\frac{13C}{12C}\right)_{standard}$ is the Vienna PDB Marine Carbonate Standard of 0.0112372000 derived from the Pee Dee Belemnite, a Cretaceous fossil, *Belemnitella americana*, from the Pee Dee Formation in South Carolina (NIST-1; Verkouteren and Klinedinst, 2004; Keith et al., 1964; Aitken, 1990). *B. americana* has a higher ratio of $^{13}C/^{12}C$ than most fossils, which allows for most $\delta^{13}C$ values to be negative. Processes that influence the marine carbon isotopes ratio include air-sea gas exchange (Mook et al., 1974), photosynthesis and respiration (Broecker and Peng, 1982). In this study we focus on $\delta^{13}C$ values in intermediated and deep waters follow the approach of Broecker and Maier-Reimer (1992) and Winguth et al. (1999) where $\delta^{13}C$ values are highly correlated to nutrient levels.

Photosynthesis by phytoplankton occurs in surface waters when carbon dioxide levels are able to sustain a high level of production. Respiration occurs when the lack of carbon dioxide forces phytoplankton to respire in order to survive. $\delta^{13}C$ will increase as photosynthesis occurs and will decrease during respiration, as organisms tend to preferentially take up ^{12}C (Lynch-Stieglitz et al., 1995; Broecker, 1995). A fractionation factor of approximately -19‰ occurs during photosynthesis, causing $\delta^{13}C$ to be high in surface waters and low in deep waters (Lynch-Stieglitz

et al., 1995). Biological production responds to changes in temperature; therefore, surface water temperatures could directly affect stable carbon isotopes.

In approximation of Broecker and Maier-Reimer (1992), stable carbon isotopes can be diagnostically computed from the phosphate concentration [PO_4] for the deep sea

$$\delta^{13}C=2.9-1.1[PO_4] \quad (3\text{-}10)$$

where the fraction of stable carbon isotopes by the air sea gas exchange is assumed to be in equilibrium and constant.

3.4 Experimental Design

The present day simulation is a continuation of a previous simulation from Yeager et al. (2006), which was integrated for an additional 1,300 years by Winguth (pers. comm.). The present day simulation in this study uses prescribed global vegetation and is integrated with the marine carbon cycle described in section 3.3.6 for 50 years. No changes were made to the present day experiment.

Two Younger Dryas experiments, one with freshwater hosing as discussed below and a second simulation without freshwater hosing, are conducted with CCSM3, which included the carbon model described in section 3.3.6. Both simulations used 13.1 ka initial conditions from He (2011) and were integrated for 1,600 years.

The scheme for freshwater forcing for the onset of the Younger Dryas was adapted from He (2011). Figure 3-1 and Table 3-1 shows the fresh water fluxes for the different drainage locations from the LIS as well as the geological timing of the river routing scheme. The first instance of maximum freshwater input originates from the St. Lawrence River at approximately 900 years of integration, with a second instance from the Mackenzie River at approximately 1200 years. Freshwater forcing is terminated at approximately 1600 years of integration. Also included are the Hudson River, Arctic, North Sea, and Barents Sea. The magnitudes of freshwater forcing have been implemented into the model and the simulations have been run as a control for an integration period of approximately 1,800 years, spanning the entirety of the Younger Dryas cooling event.

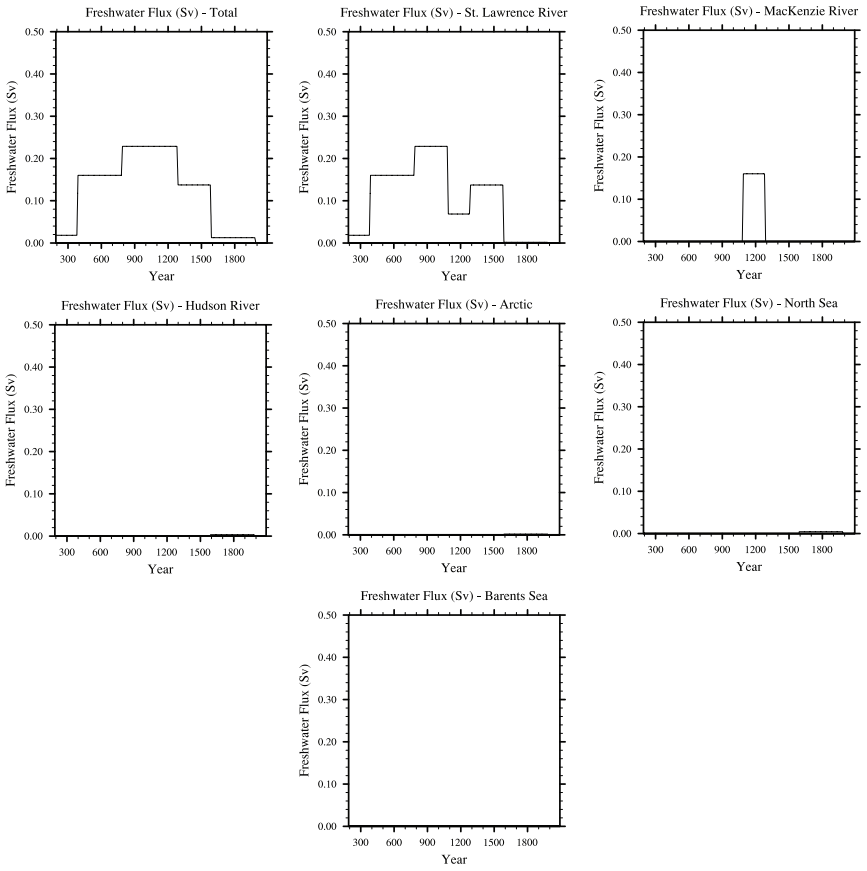

Figure 3-1 Magnitude and Timing of Freshwater Input during the Younger Dryas for the CCSM3 simulations. These figures show the magnitude in Sverdrups, Sv, and the timing of freshwater input for each river system for the duration of the Younger Dryas cooling event. The total amount of freshwater input from all sources is shown in the top left figure, (a). The most substantial input originates from the St. Lawrence (b) and Mackenzie rivers (c), while the Hudson River (d), Arctic (e), North Sea (f), and Barents Sea (g) only provide a small amount of freshwater input toward the end of the event. The maximum amount of forcing occurs around 800 years into the simulation, or approximately 12.3 ka. The onset of the Younger Dryas, or 12.9 ka, occurs approximately 200 years after the simulation begins. The start date of the simulation is 13.1 ka.

Table 3-1 Freshwater Forcing Scheme for the Younger Dryas (CCSM3 Experiments)

Age (ka)	Model Year	Flux (m/kyr)	Flux (Sv)	Flux Location	Flux Lat	Flux Long
13.1-12.9	191-391	1.6	0.0183	St. Lawrence River	50°N~70°N	80°W~20°E
12.9-12.5	391-791	14	0.1602			
12.5-12.2	791-1091	20	0.2288			
12.2-12.0	1091-1291	6	0.0686			
		14	0.1602	Mackenzie River	65°N~75°N	210°W~240°E
12.0-11.7	1291-1591	12	0.1373	St. Lawrence River	50°N~70°N	80°W~20°E
11.7-11.3	1591-1991	0.15	0.0017			
		0.29	0.0033	Hudson Strait	55°N~70°N	280°W~312°E
		0.15	0.0017	Arctic	70°N~76°N	200°W~275°E
		0.38	0.0043	North Sea	45°N~62°N	0°E~12°E
		0.13	0.0015	Barents Sea	65°N~80°N	25°W~55°E

Initial and boundary conditions are shown in Table 3-2. Topography was changed to represent 13 ka for both the ocean and ice sheets (ICE-5G; Table 3-2; Peltier, 2004), while atmospheric aerosol optics, ozone, and absorption and emission were adjusted to reflect that of the YD (Table 3-2; Joos and Spahni, 2008). The solar constant was adjusted to 1,365 W m^{-2} based on calculations for the LGM (Table 3-2; Otto-Bliesner, Brady, et al., 2006). The simulation utilized a Dynamic Global Vegetation Model (DGVM), allowing for vegetation to adapt with changing conditions as the model progressed (Table 3-2). Orbital settings were adjusted for 13,000 years BP using the formula of Berger and Loutre (1991; Table 3-2).

Table 3-2 Initial and Boundary Conditions for the CCSM3 experiments

Initial and Boundary Conditions			
Parameter	Preindustrial	Younger Dryas	Reference
Incoming Solar Radiation	1,365 W m^{-2}	1,364 W m^{-2}	Adapted from Otto-Bliesner et al. (2006)
Orbital Parameters			
Year	1990	13.0 ka	
Precession	0.01690	-0.01824	Berger and Loutre (1991)
Eccentricity	0.017236	0.020175	
Obliquity	23.446°	24.093°	
Greenhouse Gases			
CO_2	284.7 ppmv	237.6 ppmv	Preindustrial values from Brady et al. (2013) YD values from Joos and Spahni (2008)
CH_4	791.6 ppbv	632.0 ppbv	
N_2O	275.7 ppbv	265.0 ppbv	
Other Parameters			
Vegetation	Preindustrial	Preindustrial	Brady et al. (2013)
Ice Sheet	Present Day	Ice5G	Peltier (2004)
Ocean Salinity	34.73 psu	35.71 psu	Present day from Labeyrie et al. (1992) Younger Dryas calculated from Chappell et al. (1996) and Siddall et al. (2003)

3.5 Results

Climate variables such as salinity, sea surface temperature, surface air temperature, and precipitation are influenced by several parameters including greenhouse gas fluctuations, orbital changes, and freshwater forcing.

Warm western boundary currents, like the Gulf Stream, with high latent heat fluxes have a significant influence of the atmospheric circulation (Levitus, 1983; Hall and Bryden, 1982; Rintoul and Wunsch, 1991; Srokosz et al., 2012; Seager and Battisti, 2007; Peltier, 2007; Cheng et al., 2011). The poleward heat transport by the Gulf Stream is in turn influenced by deepwater formation around Greenland. Convective overturning of water masses and the strength of the AMOC is increased with colder temperatures and increased salinity, whereas warmer temperature and decreased salinity causes a reduction of the strength of the AMOC (Rooth, 1982; Broecker and Denton, 1989). Therefore, a freshwater input into the surface ocean would cause salinity to decrease, which would cause surface density, convective overturning, and AMOC to decrease. The reduced AMOC would contribute to a cooling of the sea surface, which

decreases the saturation value of water vapor in the atmosphere, and atmospheric moisture content.

A lower than preindustrial pCO_2 in the atmosphere (ΔpCO_2=47.1 ppmv) and associated greenhouse gases radiative forcing lead to surface cooling and lower precipitation and thus contribute to an increased strength of the AMOC (Manabe and Stouffer, 1994; Voss and Mikolajewicz, 2001).

Changes in orbital parameters affect the climate by changing the distance the Earth is from the sun annually, as well as how much incoming solar radiation reaches both hemispheres on a seasonal basis (Berger, 1988). The more incoming solar radiation that reaches the surface, the warmer the troposphere will be, and the less incoming solar radiation, the cooler the troposphere will be (see Chapter 2).

The following are results from the CCSM3 simulations with and without freshwater forcing. The results for the preindustrial simulation are given in Appendix A.1. In this study, the analysis of the results focuses on the North Atlantic region where the largest changes occur.

3.5.4 Salinity

For the period of 13.1-11.5 ka, the sea surface salinity for the simulation without freshwater forcing is approximately 35.0 psu, an increase of 1-2 psu from the preindustrial simulation (Figure 3-2 A and C). For the simulation with freshwater forcing during the same period, the sea surface salinity is approximately 34 psu, or a decrease of approximately 1 psu from the preindustrial simulation (Figure 3-2 B and D).

For the model year 900, or approximately 12.4 ka, freshwater discharge from the St. Lawrence River is at its maximum (Figure 3-1). The sea surface salinity for the simulation without freshwater forcing is ~1.5 psu more saline in the North Atlantic Ocean than the preindustrial simulation because of the larger continental ice masses, while the simulation with freshwater forcing decreased by ~0.5 psu compared to the preindustiral simulation (Figure 3-3 A and B).

During the period in which the maximum freshwater forcing discharge is through the Mackenzie River, 12.1 ka (after a 1,200 year integration of the model), the simulation without

freshwater forcing indicates that the salinity was approximately the same as the preindustrial simulation (Figure 3-3 C). For the same period, the salinity for the simulation with freshwater forcing is ~1 psu lower than the preindustrial simulation (Figure 3-3 D). At 11.7 ka, the simulation without freshwater forcing remains the same as the preindustrial simulation, while the simulation with freshwater forcing indicates an increase of ~1.5 psu compared to the preindustrial salinity (Figure 3-3 E and F). When the model reaches 11.6 ka (1700 model years), the salinity for the simulation without freshwater forcing is approximately 1.5 psu more saline than the preindustrial simulation, and the simulation with freshwater forcing indicates a 1 psu decrease compared to the preindustrial salinity (Figure 3-3 G and H). The sea surface salinity for the experiement with and without fresh water forcing varies between 35 and 36 psu and are ~0.8-1.0 psu fresher compared to the preindustrial simulation (Figures 3-4) because of the time-varying freshwater forcing (Figure 3-1). The simulation without freshwater forcing is fresher than the preindustrial simulation because both simulations (with and without freshwater forcing) were started from a simulation that already had a freshwater forcing scheme in place. With the first instance of freshwater forcing around 300 years into the simulation with freshwater forcing, the salinity decreases from 35.30 to 34.35 psu by 600 and then steadily increases to approximately 35.22 psu at year 900 (Figure 3-4). Upon maximum discharge from the Mackenzie River, the freshening is amplified from 35.22 to 34.74 psu (Figure 3-4). When freshwater forcing is terminated, the salinity steadily rises from 34.74 to 35.52 psu by the end of the simulation (Figure 3-4). For the simulation without freshwater forcing, the salinity increases from 35.07 to 35.67 psu by year 375 and steadily declines to approximately 35.0 psu by year 900 where it remains constant until the end of the simulation (Figure 3-4).

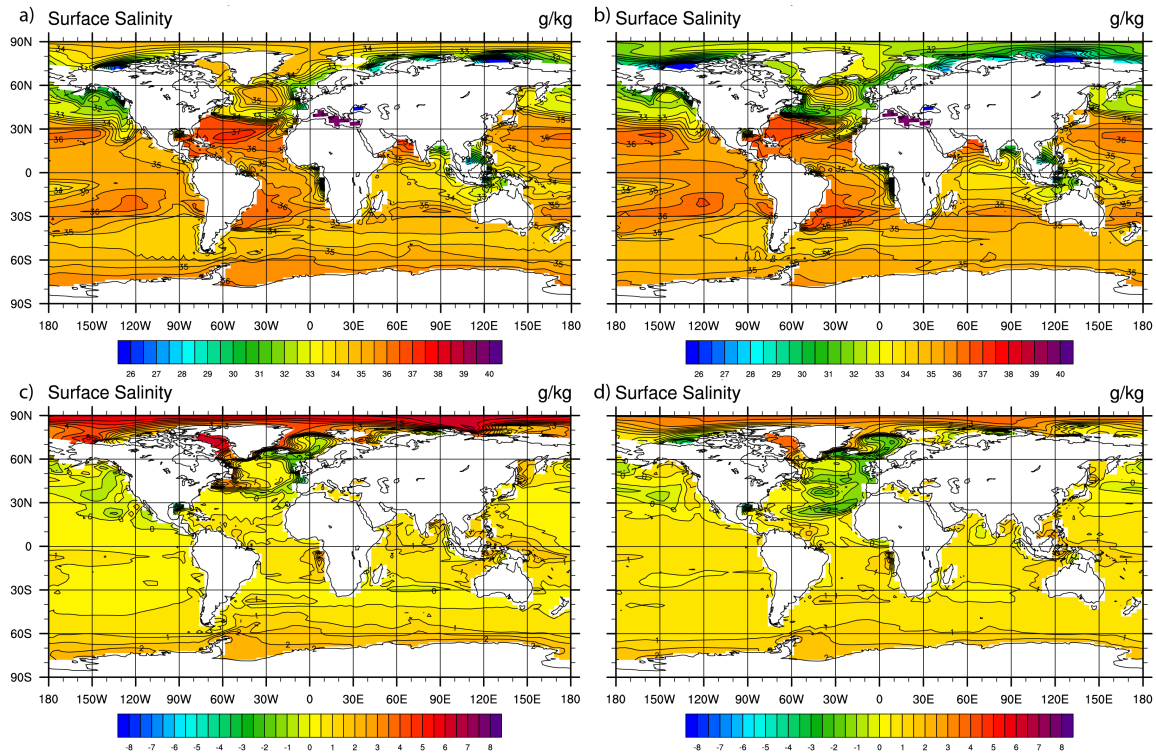

Figure 3-2 Global surface salinity in g kg^{-1} simulated by CCSM3 for 191-1790 simulated years (13.1-11.5 ka). YD simulation A) without and B) with freshwater forcing. Difference between the YD simulation C) without and D) with freshwater forcing and the preindustrial simulation.

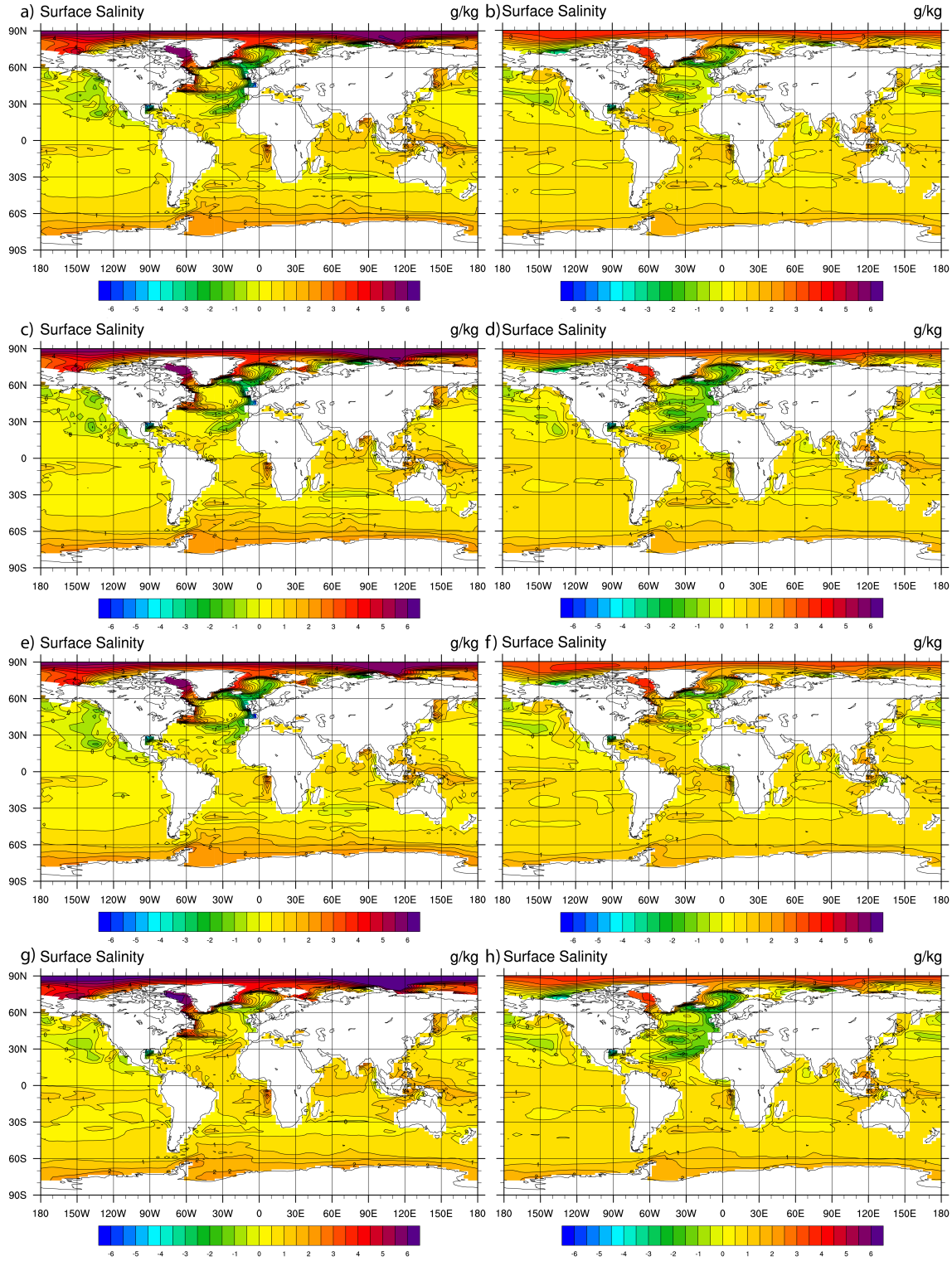

Figure 3-3 Global surface salinity in g kg^{-1} simulated by CCSM3. Right column: difference between the YD simulation without freshwater forcing and the preindutrial simulation for A) 12.4 ka, C) 12.1 ka, E) 11.7 ka, and G) 11.6 ka. Left column: difference between the YD simulation

with freshwater forcing and the preindutrial simulation for B) 12.4 ka. D) 12.1 ka, F) 11.7 ka, and H) 11.6 ka.

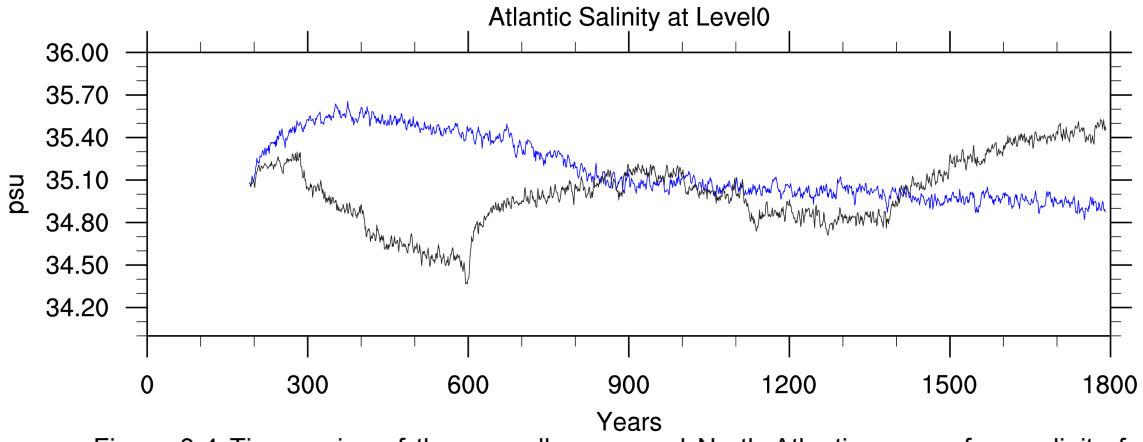

Figure 3-4 Time series of the annually averaged North Atlantic sea surface salinity for 13.1-11.5 ka (191-1790 model years). The black line represents the YD simulation with freshwater forcing, and the blue line represents the simulation without freshwater forcing.

3.5.7 Precipitation

For the period of 13.1-11.5 ka, the annual precipitation rate for both the simulation with and without freshwater forcing is approximately 2.5 mm day^{-1}, which is a decrease of approximately 1.5-2.0 mm day^{-1} compared to the preindustrial simulation (Figure 3-5 A-D).

The precipitation rates for the simulation with freshwater forcing during the time of maximum discharge from the St. Lawrence River (~12.4 ka) averaged at approximately 3 mm day^{-1}, while the simulation without freshwater forcing indicated ~2.5 mm day^{-1} (Figure 3-6 A). Compared to the preindustrial simulation, rainfall decreased by ~ 2 mm day^{-1} for the scenario with freshwater forcing and 2.5 mm day^{-1} for the scenario without freshwater forcing (Figure 3-6 B). During the maximum discharge from the Mackenzie River (12.1 ka), the rate for both the simulation with and without freshwater forcing remained the same (Figure 3-6 C and D). When the freshwater forcing is terminated at 11.7 ka, the simulation without freshwater forcing remains unchanged, and the simulation with freshwater forcing indicates a rate decrease of 1.5 mm day^{-1}

compared to the preindustrial simulation (Figure 3-6 E and F). After 100 years, both the simulation with and without freshwater forcing do not change (Figure 3-6 G, and H).

Rainfall for both simulations decreases overall for the area over Greenland, and the atmosphere over the North Atlantic Ocean becomes drier (Figure 3-5 and 3-6). For the equatorial region in the Atlantic Ocean, the simulation without freshwater forcing indicates an increase in precipitation over the western Atlantic Ocean, and a decrease in precipitation in the eastern Atlantic Ocean (Figure 3-5 and 3-6). For the simulation with freshwater forcing, the equatorial rainfall remains increased for the entirity of the freshwater forcing (13.1-11.7 ka; Figure 3-6 B and D). When the freshwater forcing is terminated at 11.7 ka, the precipitation between 20°N and the equator increases compared to the preindustrial simulation, and continues to increase over the region past 11.6 ka (Figure 3-6 F and H).

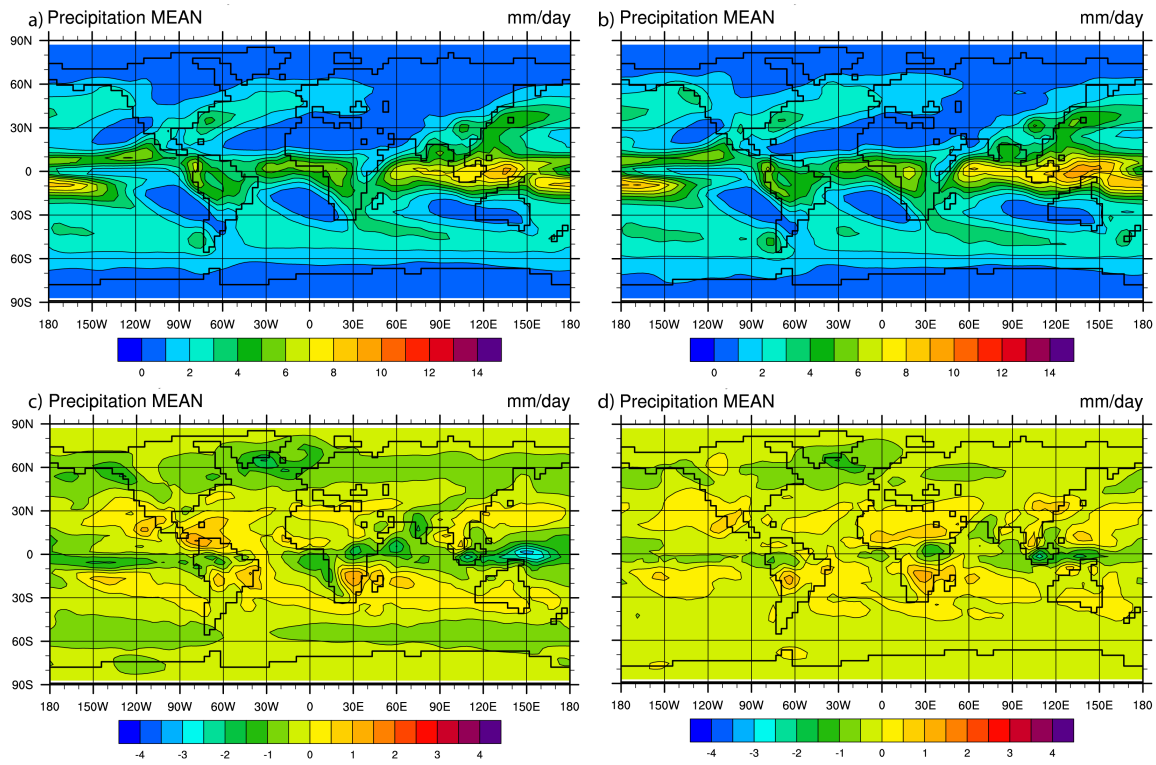

Figure 3-5 Global annual precipitation in mm day^{-1} simulated for the YD by CCSM3 for 191-1790 simulated years (13.1-11.5 ka) A) without freshwater forcing, and B) with freshwater forcing. Difference between the YD simulation C) without and D) with freshwater forcing and the preindustrial simulation.

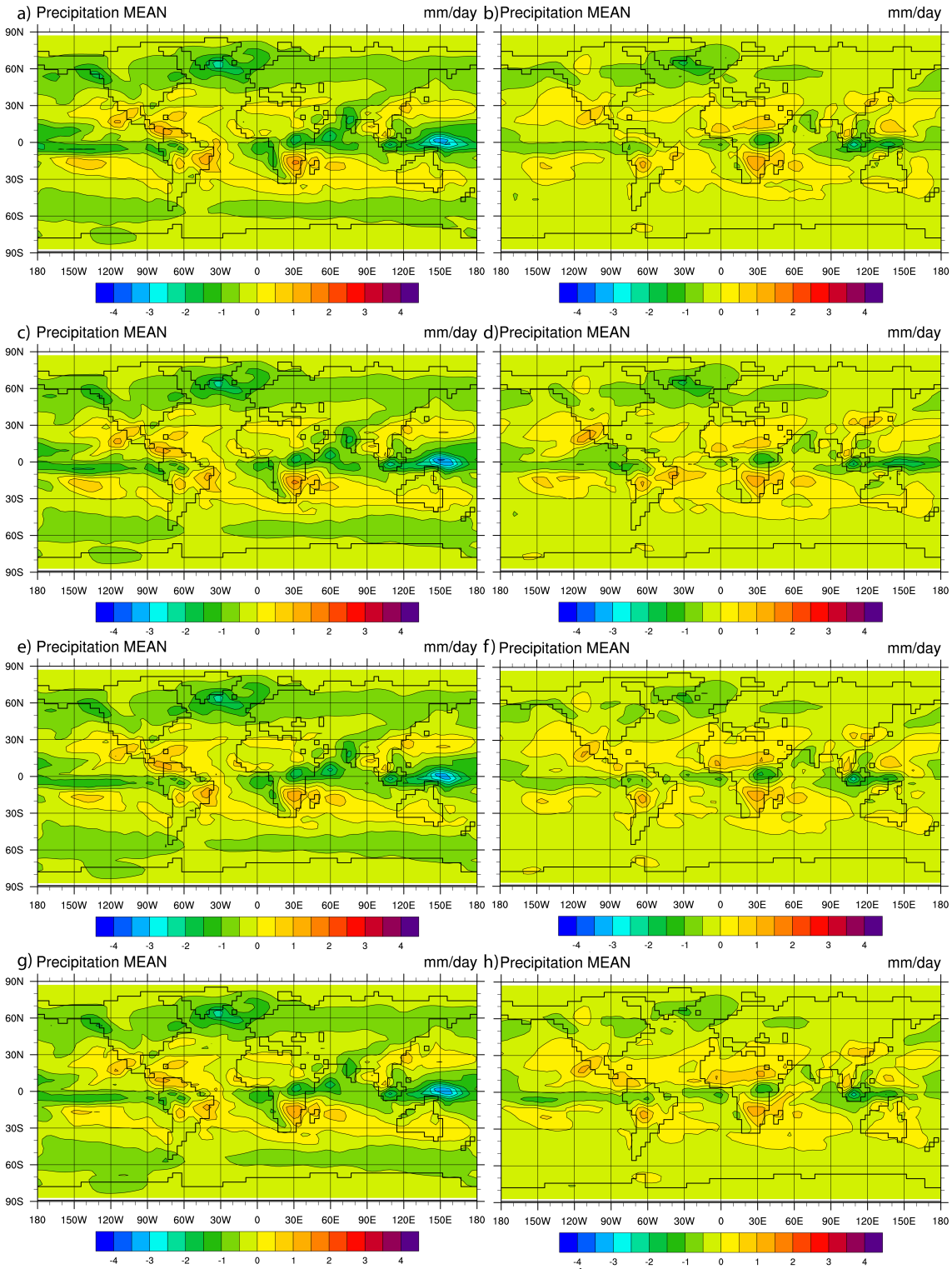

Figure 3-6 Global annual precipitation in mm day^{-1} simulated by CCSM3. Right column: difference between the YD simulation without freshwater forcing and the preindutrial simulation for A) 12.4 ka, C) 12.1 ka, E) 11.7 ka, and G) 11.6 ka. Left column: difference between the YD

simulation with freshwater forcing and the preindutrial simulation for B) 12.4 ka. D) 12.1 ka, F) 11.7 ka, and H) 11.6 ka.

3.5.5 Sea Surface Temperature

For the period of 13.1 to 11.5 ka, simulated sea surface temperature (SST) for the scenario without freshwater forcing cooled by ~2°C while in the simulation with freshwater forcing the SST cooled by ~1°C for the same period (Figure 3-7 A and B). Compared to the preindustrial simulation, the simulation without freshwater forcing is ~7°C cooler, and the simulation with freshwater forcing is ~6°C cooler (Figure 3-7 C and D).

At the maximum discharge of the St. Lawrence River, SST for the simulation with freshwater forcing warms ~2°C in the proximity south of Greenland, which is a decrease of 6.5°C relative to the preindustrial simulation (Figure 3-8 B). The SST for the simulation without freshwater discharge cools by 1°C, or a 10°C cooling compared to the preindustrial simulation (Figure 3-8 A). When the Mackenzie River drainage is at maximum, both SST for both decrease by 1°C (Figure 3-8 C and D). Upon termination of freshwater discharge, the SST warms by 3°C in the simulation with freshwater discharge while the simulation without remains constant (Figure 3-8 E and F). As the simulation progresses, SST for both experiments rises by ~1°C (Figure 3-8 G and H). The timeseries of the SST for the simulation with freshwater forcing continues to adjust to the freshwater forcing, while initially the simulation without freshwater forcing adjusts to cooler state and becomes near steady-state after 900 years of integration (Figure 3-9). Note that the cooler state for the simulation without freshwater forcing is due to enhanced convective overturn, as compared to the simulation with freshwater hosing (Figure 3-9). Additionally, it should be noted that both the simulation with and without freshwater forcing were started from a simulation that already incorporated freshwater forcing.

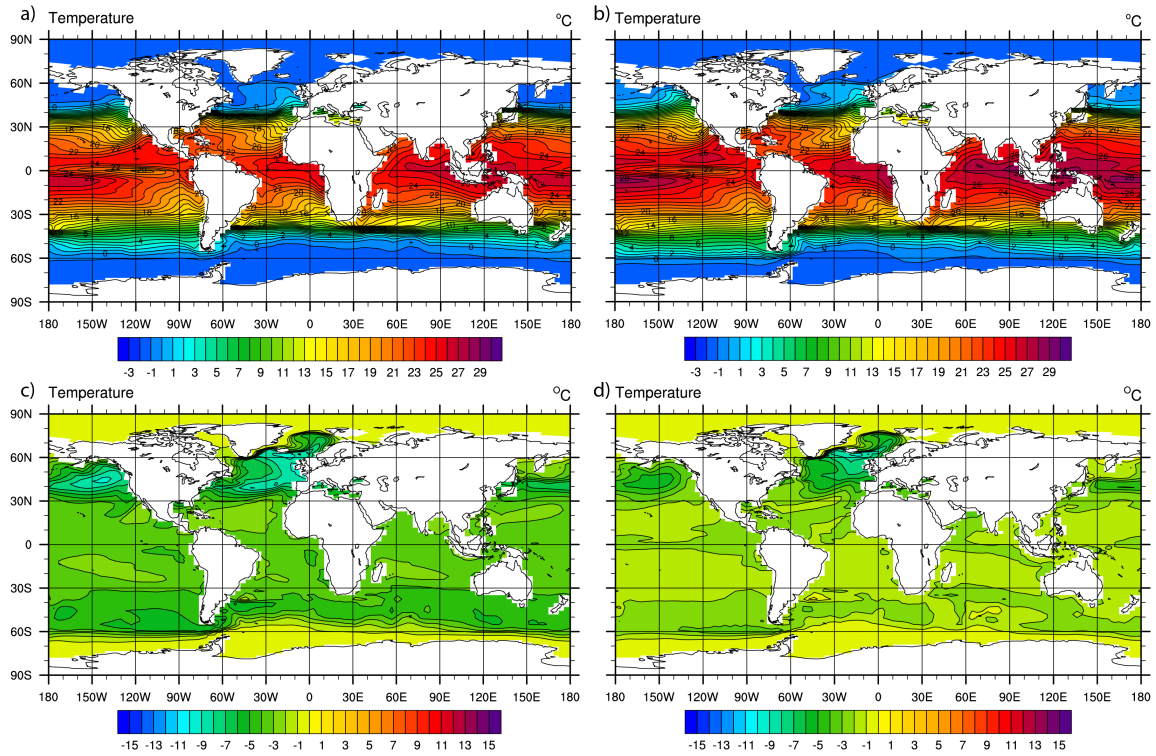

Figure 3-7 Global sea surface temperature in °C simulated by CCSM3 for 191-1790 simulated years (13.1-11.5 ka). YD simulation A) without and B) with freshwater forcing. Difference between the YD simulation C) without and D) with freshwater forcing and the preindustrial simulation.

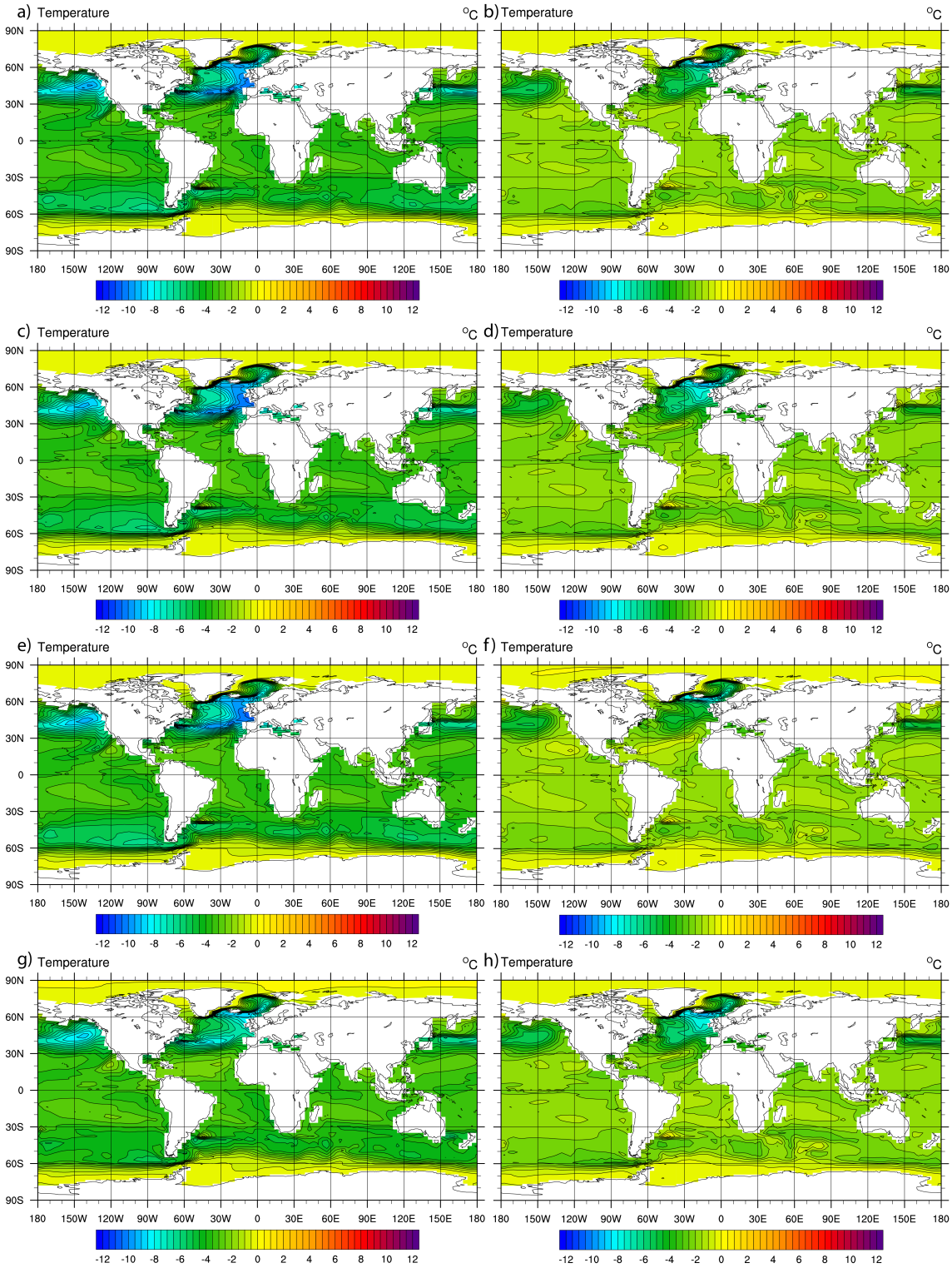

Figure 3-8 Global sea surface temperature in °C simulated by CCSM3. Right column: difference between the YD simulation without freshwater forcing and the preindutrial simulation for A) 12.4 ka, C) 12.1 ka, E) 11.7 ka, and G) 11.6 ka. Left column: difference between the

simulation with freshwater forcing and the preindutrial simulation for B) 12.4 ka. D) 12.1 ka, F) 11.7 ka, and H) 11.6 ka.

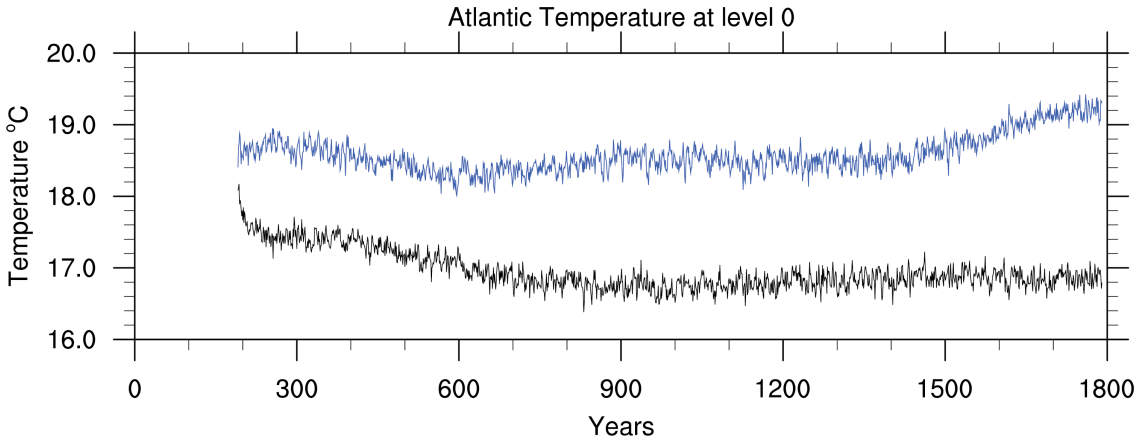

Figure 3-9 Annual sea surface temperature averaged for North Atlantic Ocean and for 13.1-11.5 ka (191-1790 simulated years). The blue line represents the simulation with freshwater forcing, and the black line represents the simulation without freshwater forcing

3.5.6 Surface Air Temperature

For 13.1-11.5 ka, the surface air temperature (SAT) over Greenland for the simulation without freshwater forcing was approximately -40°C, approximately a 20°C cooling compared to the preindustrial simulation (Figure 3-10 A and C). For the simulation with freshwater forcing, the SAT was approximately -36°C, which is a decrease of ~15°C relative to the preindustrial simulation (Figure 3-10 B and D).

The SAT simulated by CCSM3 for the simulation with freshwater forcing over Greenland decreased by approximately 15°C compared to the preindustrial simulation for both the St. Lawrence and Mackenzie River maximum discharges (Figures 3-11 A-D). The simulation without freshwater forcing shows an even larger decrease of ~25°C for both discharge maximums compared to the preindustrial control (Figures 3-11 A-D). The temperature does not change for the remainder of the simulation, maintaining the 15°C and 25°C differences for the simulation with and without freshwater forcing respectively (Figures 3-11 E-H).

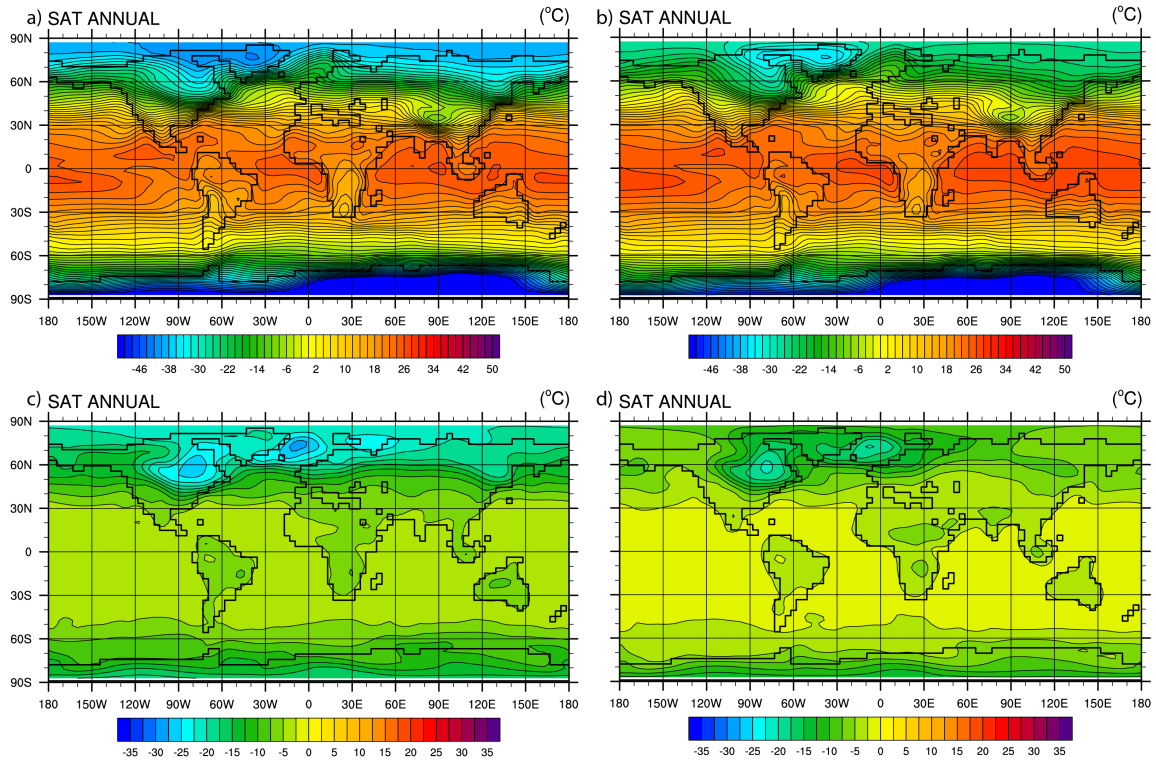

Figure 3-10 Global surface air temperature in °C simulated by CCSM3 for 191-1790 simulated years (13.1-11.5 ka). YD simulation A) without and B) with freshwater forcing. Difference between the YD simulation C) without and D) with freshwater forcing and the preindustrial simulation.

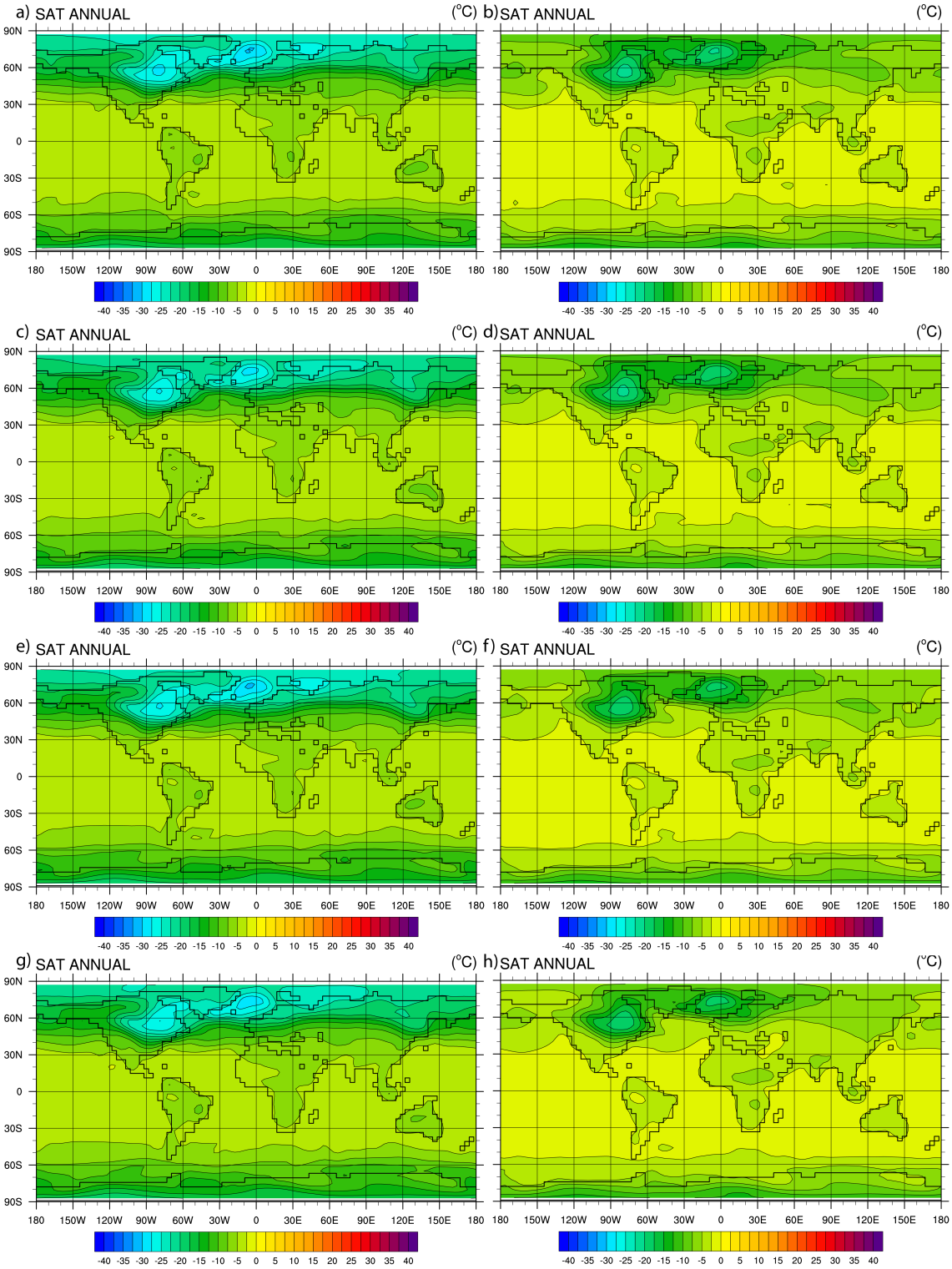

Figure 3-11 Global surface air temperature in °C simulated by CCSM3. Right column: difference between the YD simulation without freshwater forcing and the preindutrial simulation for A) 12.4 ka, C) 12.1 ka, E) 11.7 ka, and G) 11.6 ka. Left column: difference between the YD

simulation with freshwater forcing and the preindutrial simulation for B) 12.4 ka. D) 12.1 ka, F) 11.7 ka, and H) 11.6 ka.

3.5.2 Atlantic Meridional Overturning Circulation

The Atlantic meridional overturning circulation (AMOC) represents the strength of the oceanic circulation as a volume transport in Sv. The AMOC for the simulation without freshwater over the course of 13.1-11.5 ka is ~10 Sv at 30°N and 1000m depth (Figure 3-12 A). For the same time period, the simulation with freshwater forcing indicates an oceanic circulation strength of approximately 5 Sv (Figure 3-12 B). Compared to present day, the AMOC strength has decreased by approximately 6 Sv and 11 Sv for the simulation without freshwater forcing and the simulation with freshwater forcing respectively (Figure 3-12 C and D).

When the freshwater output is at a maximum for the St. Lawrence river, the maximum strength of the AMOC at 1000 m depth and 30°N is ~11 Sv, which is a decrease of ~9 Sv from preindustrial times (Figure 3-13 B). During the same time period for the simulation without freshwater forcing, the AMOC is ~7 Sv, or ~11 Sv weaker than the preindustrial simulation (Figure 3-13 A). Additionally, the furthest vertical extent of deepwater circulation is ~900 m deeper in the simulation without freshwater forcing than the one with freshwater forcing (Figure 3-13 A and B). At the maximum freshwater forcing from the Mackenzie River, the AMOC shows a circulation of ~8 Sv for the simulation with freshwater forcing, while the simulation without freshwater forcing shows a strength of 9 Sv, a decrease of ~10 Sv and 9 Sv respectively compared to the preindustrial simulation (Figure 3-13 C and D). When the freshwater hosing is terminated, the AMOC for the experiment with freshwater forcing increases to 12 Sv, and the simulation without freshwater forcing increases to 10 Sv (Figure 3-13 E and F). Compared to the preindustrial simulation, this is a decrease of 7 and 11 Sv respectively (Figure 3-13 E and F). On continuation of the lack of freshwater, the strength of the AMOC in the experiment with freshwater forcing decreases to 8 Sv, while the simulation without freshwater forcing is approximately 14 Sv (Figure 3-13 G and H). The timeseries for the AMOC for the simulation without freshwater forcing reaches a steady state after approximately 900 model years, and the simulation with freshwater

forcing continues to adjust to the influence of the freshwater forcing through the entirity of the simulation (Figure 3-14).

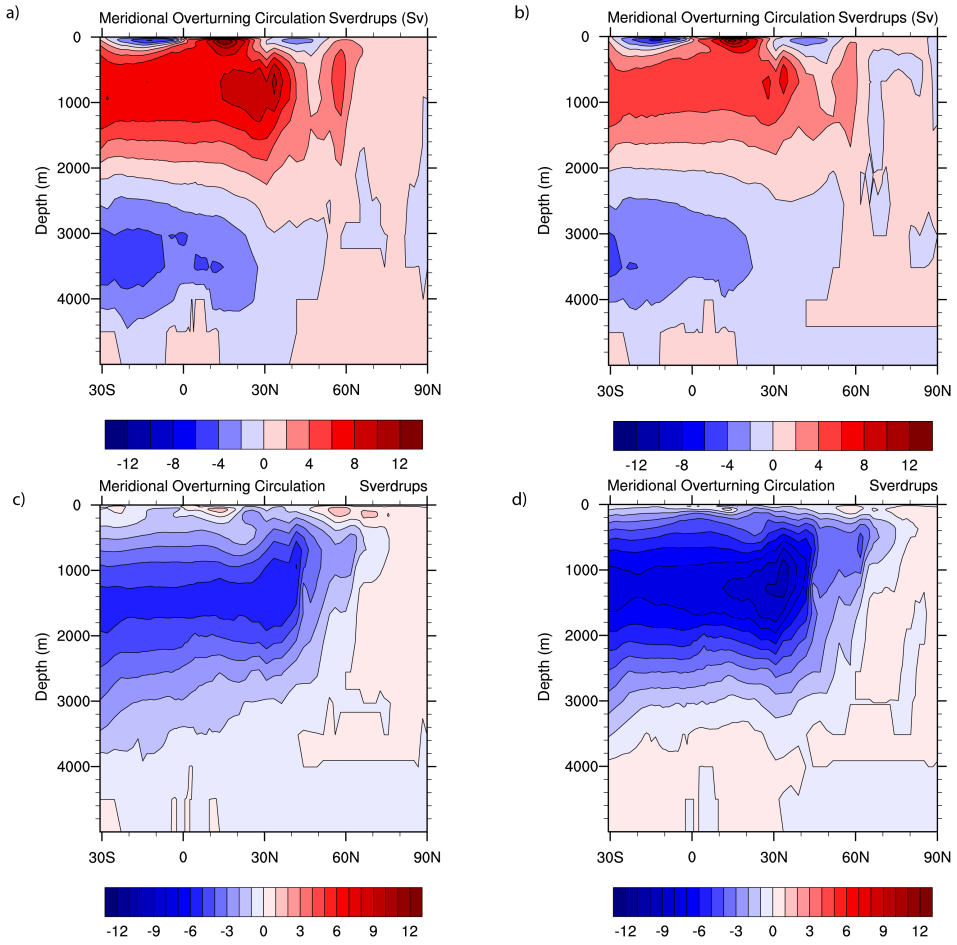

Figure 3-12 Atlantic meridional overturning circulation in Sv simulated by CCSM3 for 191-1790 simulated years (13.1-11.5 ka). YD simulation A) without and with B) freshwater forcing. Difference between the simulation C) without and D) with freshwater forcing and the preindustrial simulation.

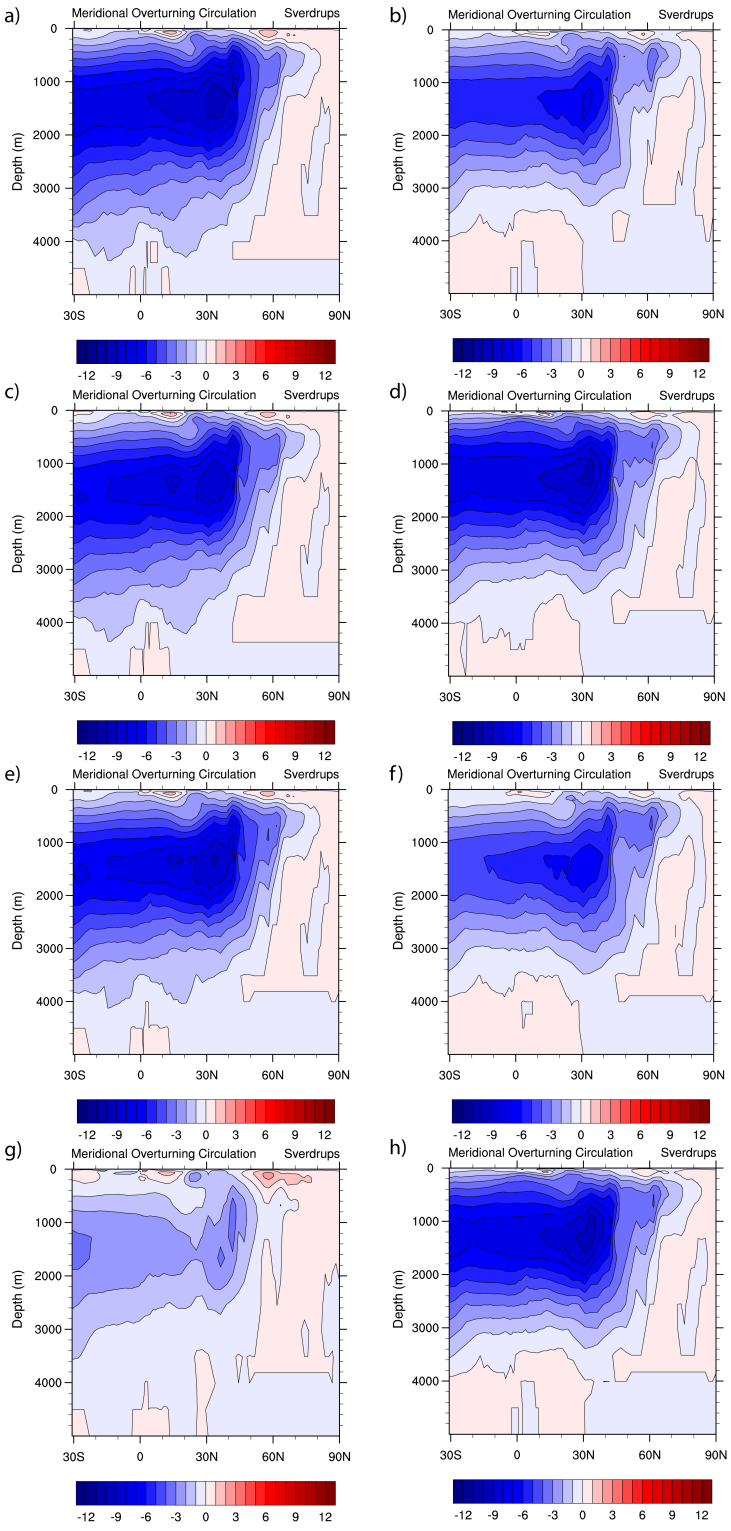

Figure 3-13 Atlantic meridional overturning circulation in Sv simulated by CCSM3. Right column: difference between the YD simulation without freshwater forcing and the preindutrial simulation for A) 12.4 ka, C) 12.1 ka, E) 11.7 ka, and G) 11.6 ka. Left column: difference between

the YD simulation with freshwater forcing and the preindutrial simulation for B) 12.4 ka. D) 12.1 ka, F) 11.7 ka, and H) 11.6 ka.

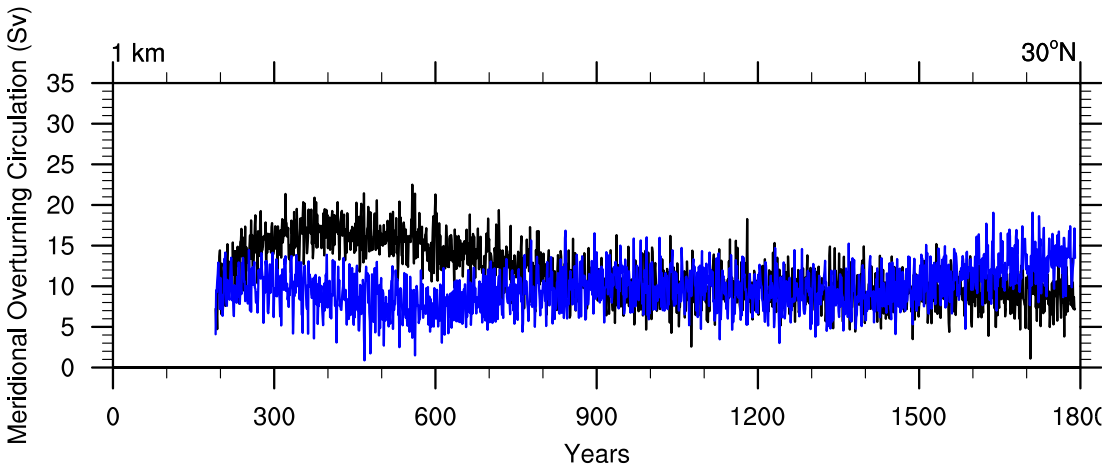

Figure 3-14 Atlantic meridional overturning circulation annually averaged timeseries for 13.1-11.5 ka (191-1790 years). The blue line represents the simulation with freshwater forcing, and the black line represents the simulation without freshwater forcing

3.5.1 Ideal Age of Water Masses

Ideal age of water masses indicates how many years have passed since a parcel of water has contacted the surface ocean (Thiele and Sarmiento, 1990; England, 1995a). The higher the age of a parcel of water, the longer it has been since it has contacted the surface ocean, and can therefore be linked to the strength of the oceanic circulation (Smith et al., 2010).

For the period of 13.1-11.5 ka, the ideal age of water masses for the simulation without freshwater forcing at 2000m depth is approximately 500-600 years, while the simulation with freshwater forcing indicates an ideal age of approxiamtely 900-1000 years (Figure 3-15 A and B). Comapred to the preindustrial simulation, the simulation without freshwater forcing has an increase in ideal age of approximately 200 years (Figure 3-15 C). For the simulation with freshwater forcing, the ideal age has increased by approximately 500-600 years compared to the preindustrial simulation (Figure 3-15 D).

Compared to the preindustrial control simulation, the ideal age of water masses for the period of maximum output from the St. Lawrence River (~900 model years; 12.4 ka) increased by

approximately 700 years in the simulation with freshwater forcing at 2000 m depth (Figure 3-16 B). In the simulation without freshwater forcing at the same depth, the age of the water masses increased by 200 years (Figure 3-16 A). The same magnitude of increase for both simulations is seen for the maximum output of the Mackenzie River (~1200 model years; 12.1 ka) as well (Figure 3-16 C and D). At approximately 1600 years (11.7 ka), the ideal age for the simulation without freshwater forcing is approximately 150 years, while the experiment with freshwater forcing is approximately 400 years at 2000 m depth (Figure 3-16 E and F). At 100 years after the freshwater forcing is terminated, the ideal age of water masses for the simulation with freshwater forcing is 500 years, while the simulation without freshwater forcing is 200 years at 2000 m depth (Figure 3-16 G and H).

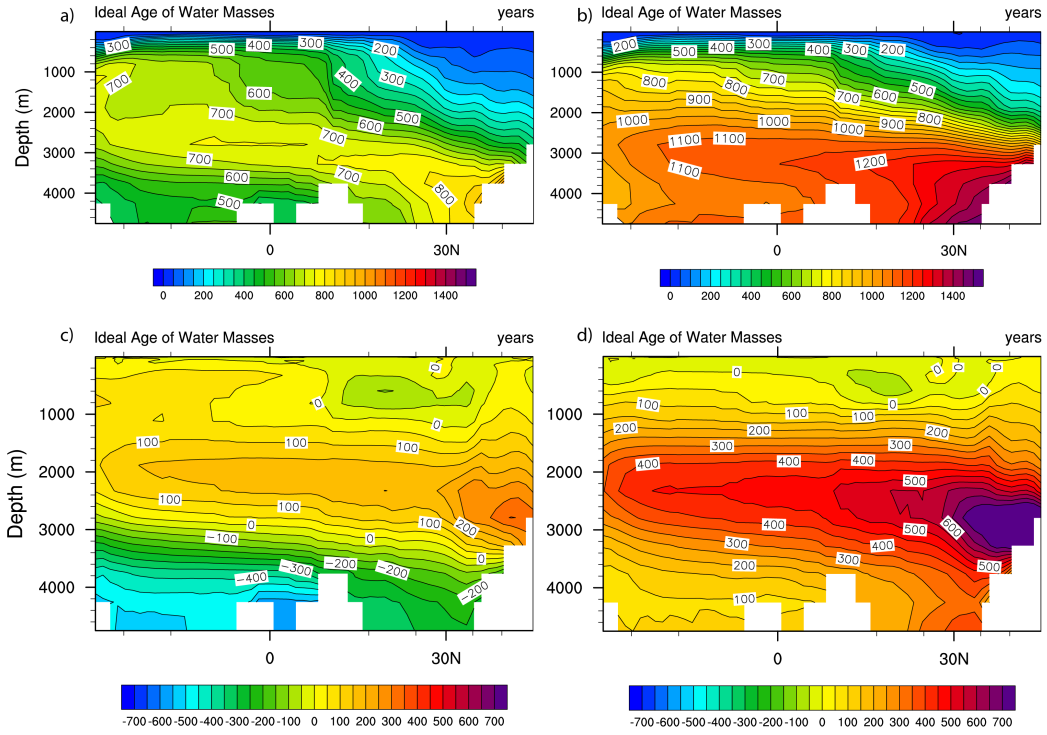

Figure 3-15 Ideal age of water masses in years simulated by CCSM3 for 191-1790 simulated years (13.1-11.5 ka). YD Simulation A) without and B) with freshwater forcing. Difference between the simulation C) without and D) with freshwater forcing and the preindustrial simulation.

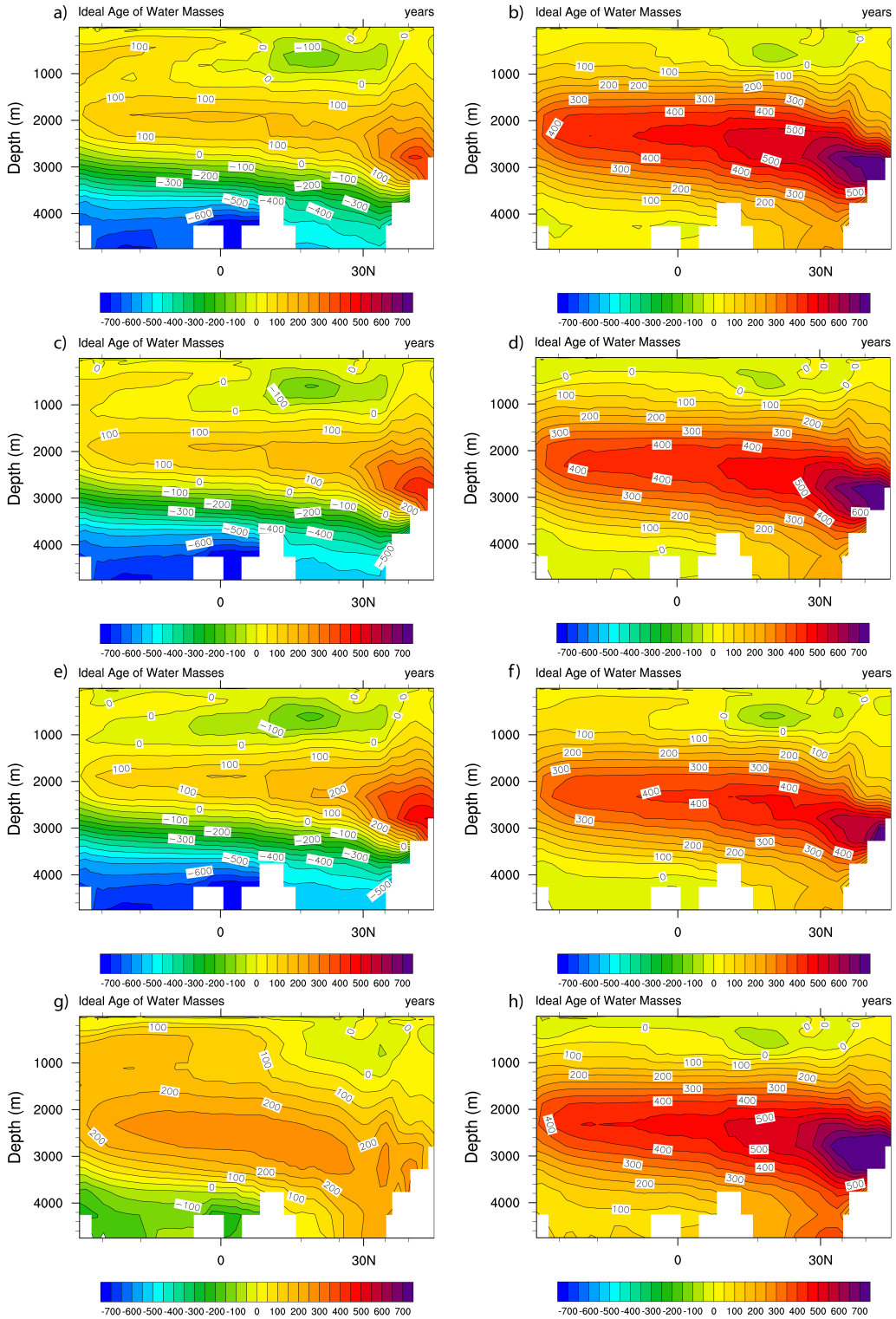

Figure 3-16 Ideal age of water masses in years simulated by CCSM3. Right column: difference between the YD simulation without freshwater forcing and the preindutrial simulation for A) 12.4 ka, C) 12.1 ka, E) 11.7 ka, and G) 11.6 ka. Left column: difference between the YD

simulation with freshwater forcing and the preindutrial simulation for B) 12.4 ka. D) 12.1 ka, F) 11.7 ka, and H) 11.6 ka.

3.5.8 Comparison between simulated and reconstructed $\delta^{13}C$

$\delta^{13}C$ was reconstructed for the Younger Dryas and compared to the 0-4 ka values from Sarnthein et al. (1994). It should be noted that present day values measured in the water column are perturbed by the Suess effect, which occurs when CO_2 from fossil fuels does contain ^{13}C of ~-27‰, and thereby alters the natural atmospheric $^{13}CO_2$ concentrations (Suess, 1955; Keeling et al., 1989). Datasets for $\delta^{13}C$ are obtained for the Younger Dryas time period courtesy of Sarnthein et al. (1994), which will be used to determine accuracy of the model for the data produced.

$\delta^{13}C$ measurements from epibenthic *C. wuellerstorfi* are used to compare simulated $\delta^{13}C$ values for the time period and are shown in Table 3-3 along with references in Table 3-4 (Sarnthein et al., 1994). It is important to note that in order to account for biological processes involved in the carbon cycle, up to 0.04‰ would need to be subtracted from all values (Winguth et al., 1999).

Table 3-3 Observed $\delta^{13}C$ values from *C. wuellerstorfi.*

Core	Latitude	Longitude	Water Depth (m)	YD $\delta^{13}C$	Reference
V28-14	64.78	29.57	1855	0.59	k
BOFS 17K	58	16.5	1150	1.29	m
V28-73	57	20	2063	1.11	t
DSDP 552	56.05	23.23	2311	1	r
NA87-22	55.5	14.7	2161	0.86	b
17049	55.26	26.73	3331	0.81	a
V29-193	55	19	1326	1.31	t
CH73-139c	54.63	16.35	2209	0.89	b
23419	54.96	19.76	1491	1.15	a
17048	54.31	18.18	1859	1.13	b
V23-81	54.25	16.83	2393	0.83	n
23414	53.54	20.29	2196	0.87	a
17054	48.45	27.7	1834	1.08	a

Table 3-3 Continued

Core	Latitude	Longitude	Water Depth (m)	YD $\delta^{13}C$	Reference
17055-1	48.22	27.06	2558	0.86	a
15612	44.69	26.54	3050	0.6	a
SU81-44	44.25	2.7	1173	0.66	b
CHN825020	43.5	29.87	3020	0.94	h
CHN824115	43.37	28.23	2151	1.21	h
SU81-31	42.1	9.78	2280	0.69	b
SU81-18	37.77	10.18	3135	0.5	B
SU92-21	36.57	23.74	4170	0.59	A
11944	35.65	8.06	1765	0.64	A
15666	34.96	7.12	803	1.29	a,w
15670	34.91	7.58	1482	0.98	A
15669-1	34.89	7.82	2022	0.84	A
15672-1/2	34.86	8.12	2455	0.76	a
T86-15P	30.43	37.07	3375	0.73	f
16006	29.27	11.5	796	1.22	a,w
15637	27.01	18.99	3849	0.55	a
12309-2	26.84	15.11	2820	0.55	a
12392	25.17	16.85	2575	0.7	a,s
12310-3/4	23.5	18.72	3080	0.5	a
12379	23.14	17.75	2136	0.4	a
16017	21.25	17.8	812	0.77	a
16030	21.24	18.06	1500	0.8	a
12328	21.15	18.57	2778	0.48	a
ODP 658	20.75	18.587	2263	0.57	a
12329-6	19.37	19.93	3320	0.47	a
13289	18.07	18.01	2490	0.49	a
ALB-226	17.95	21.05	3100	0.37	d
12337	15.95	18.13	3088	0.1	a
12347	15.83	17.86	2576	0.51	a
16402	14.42	20.57	4203	0.04-0.32	a
V22-197	14.17	18.58	3167	0.37	k
V22-196	13.83	18.97	3728	0.67	g
16415	9.57	19.11	3841	0.2	a
16408	9.01	21.5	4336	0.48	a
16459	7.28	26.19	4835	0.24	a

Table 3-3 Continued

Core	Latitude	Longitude	Water Depth (m)	YD $\delta^{13}C$	Reference
13519	5.66	19.85	2862	0.63-0.88	a
ENO66-16	5.46	21.14	3152	0.57	j
16457	5.39	21.72	3291	0.88	a
16458	5.34	22.06	3518	0.77	a
16455	5.27	22.87	4160	0.76	a
ENO66-38	4.92	20.5	2931	0.89	j
16453	4.73	20.95	2675	0.92	a
ENO66-21	4.23	21.63	3995	0.69	j
KW-31	3.52	-5.57	1515	0.19	b,a
ENO66-26	3.09	20.02	4745	0.24	j
13521	3.02	22.03	4504	0.16	a
ENO66-32	2.47	19.73	5003	0.6	j
ENO66-29	2.46	19.76	5104	0.48	j
V25-59	1.37	33.48	3824	0.71	o
V30-40	-0.2	23.15	3706	0.58	q
16773	-0.97	9.44	4662	0.28	a
16867	-2.2	-0.51	3891	0.67	a
BT-4	-4.33	-10.43	1000	0.12	k
MG-237	-5.2	-11.33	1000	-0.15	b
GeoB 1113	-5.75	11.04	2374	0.66	a
V29-135	-19.6	-8.88	2675	0.27	a,c
RC13-229	-25.5	-11.3	4194	0.2	k,x
RC11-83	-41.6	-9.72	4718	0	i

Table 3-4 References for Table 3-3

a	University of Kiel (published and unpublished)
b	Centre des Faibles Radioactivites, Laboratoire mixte CNRS-CEA, Gif-sur Yvette Cedex, France (published and unpublished)
c	Abrantes (unpublished data, 1993)
d	Bornmalm (unpublished data, 1993)
e	Fairbanks (unpublished data, 1992)
f	Ganssen (unpublished data, 1992)
g	Shackleton (unpublished data, 1992)
h	Boyle and Keigwin [1985, 1987]
i	Charles and Fairbanks [1992]
j	Curry and Lohmann [1985]
k	Curry et al. [1988]
l	Duplessy et al. [1984]
m	Labeyrie et al. [1992]
n	Jansen and Veum [1990]
o	Mix and Ruddiman [1985]
p	Mix and Fairbanks [1985]
q	Oppo and Fairbanks [1987]
r	Shackleton and Hall [1984]
s	Shackleton [1977]
t	Oppo and Lehman [1993]
u	Hodell [1993]
w	*C. wuellerstorfi* and *P. ariminensis*
x	*C. kullenbergi*
y	living rose bengal stained *C. wuellerstorfi*, [Ganssen, 1983]
z	*C. pseudoungerianus*

The observed *C. wuellerstorfi* $\delta^{13}C$ values agree generally with zonally averaged $\delta^{13}C$ model output for the 13.1-11.5 time period (Figure 3-17). However, in the bottom water masses, the simulation without freshwater forcing (Figure 3-17 B) suggests a better agreement to the observed data than the simulation with freshwater forcing (Figure 3-17 A). It is important to note that to account for glacial-interglacial changes in the landbiosphere glacial $\delta^{13}C$ values should be approximately 0.04‰ lower than glacial values (Winguth et al., 1999). With this correction, the $\delta^{13}C$ model - data bias is reduced. Additionally, when accounting for this correction, neither simulation represents a best fit to the observed $\delta^{13}C$ data; the best fit to the data is likely between the freshwater and non-freshwater forcing scenarios.

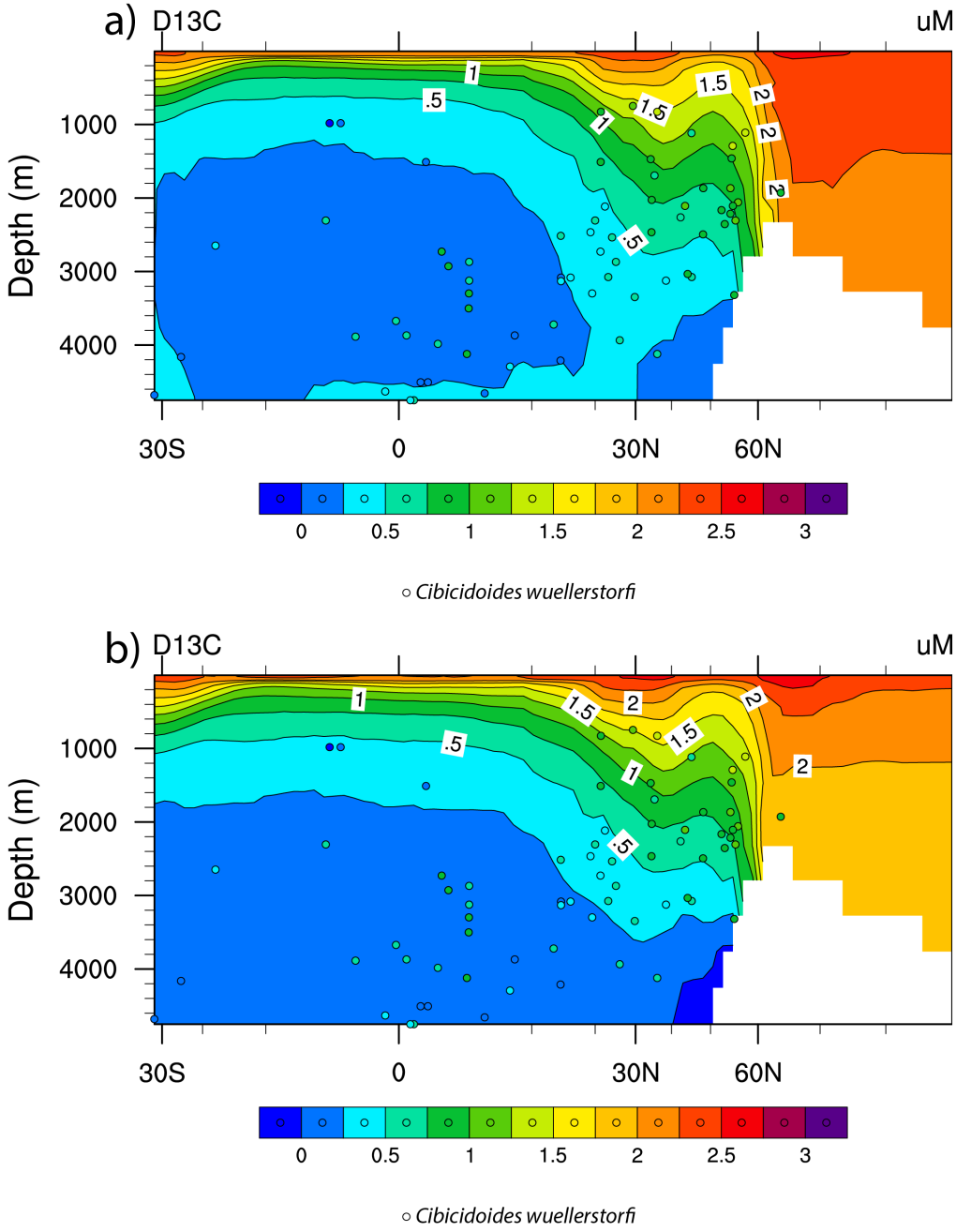

Figure 3-17 Zonally averaged $\delta^{13}C$ in the Atlantic Ocean for the CCSM3 simulations compared with $\delta^{13}C$ reconstructions from epibenthic *C. wuellerstorfi* (Sarnthein et al., 1994). Figures represent years 13.1-11.5 ka (191-1790 simulated years). A) Simulation without freshwater forcing. B) Simulation with freshwater forcing.

3.6 Discussion

The simulation with freshwater forcing indicated an approximately 15 °C decrease in surface air temperature compared to the preindustrial control simulation, in agreement with surface air temperature estimates from the ice core data sampled from the Summit Station, Greenland (Severinghaus et al., 1998). Sea surface temperature data for the freshwater forcing simulation do not exhibit the decreasing trend seen in the proxy reconstructions; instead, the simulation without freshwater forcing indicates a sharp ~1.5-2.0 °C decrease in sea surface temperature at the onset of the Younger Dryas, followed by a steady-state condition. Reconstructions at the onset of the Younger Dryas give sea surface temperature for the area south of Greenland at 18 °C and then temperature decreases to ~8 °C (McManus et al., 2004).

Salinity reconstructions for the Younger Dryas period range from approximately 27.5-30 psu (Schmidt et al., 2004; Clark et al., 2001; DeVernal et al., 1996; Ebbesen and Hald, 2004). Salinity for the freshwater forcing simulation is ~35 psu, which is higher than the reconstructed values. Reduced precipitation at the onset of the Younger Dryas in both the freshwater forcing and non-freshwater forcing simulations agrees with the suggestion of reduced storminess during the Younger Dryas (Alley, 2000).

The AMOC for the simulation with freshwater forcing is approximately 6 Sv, a 10 Sv decrease from the preindustrial, which agrees with reconstructions and previous model simulations in which AMOC strength decreases from 10 Sv to 4 Sv (He, 2011; Liu et al., 2012; McManus et al., 2004; Gherardi et al., 2005).

The analysis of the ideal age of water masses reveals that the circulation in the simulation without freshwater forcing is increasing compared to that of the preindustrial simulation. This could be the result of increasing salinity due to the formation of sea ice in the northern Atlantic Ocean. Increasing salinity would cause the pycnocline to increase, causing the surface water mass to become denser and therefore increase the circulation strength. It is likely that the increase in sea ice formation would be due to the decrease of SAT over Greenland and the North Atlantic Ocean just south of Greenland. The simulation with freshwater forcing shows a decrease in the ideal age of water masses, indicating that the strength of AMOC is decreased

and linked to increased pycnocline by an increase of precipitation over the area, and associated discharge from the continents. It is important to note that SAT in the simulation with freshwater forcing decreased in the North Atlantic Ocean similar to the simulation without freshwater forcing, because the surface salinity is higher by enhanced sea ice formation. Additionally, the temperature change could likely be related to the chances in orbital and greenhouse gas parameters. However, the input of freshwater into the Northern Atlantic Ocean must override the effects of this salinity increase, causing the AMOC to weaken.

The results from the zonally averaged ideal age of water masses are supported by the AMOC, in which the simulation with freshwater forcing by drainage from the LIS shows a more substantial decrease in oceanic circulation than the simulation without freshwater forcing. The lack of freshwater forcing in the later experiment is associated with a more reduced pycnocline (compared to the simulation with hosing) and thus a stronger AMOC. In addition to the decrease in strength, the simulation with freshwater forcing favors a shallow AMOC due to increased entrainment of Antarctic bottom water into the North Atlantic (Danabasoglu et al., 2012; Yeager and Danabasoglu, 2012).

In this study, the transport of the AMOC is reduced to 5 Sv for the YD simulation with freshwater forcing compared to ~16 Sv for the preindustrial simulation (or a 69% change). Comparable to the study of Peltier (2007) with a comparable freshwater hosing of 0.3 Sv into the Atlantic Ocean, the transport of water masses associated with the AMOC in the simulation with fresh input was 65% lower than that of preindustrial simulation. In contrast, the sensitivity of AMOC to freshwater hosing in study of Schiller et al. (1997) is much lower (4-5 Sv changes in transport of the AMOC) relative to a the scenario without hosing (with a transport of 24 Sv). Note that, the freshwater applied in forcing simulation involved in Schiller was more than twice as much (or 0.625 Sv). Difference may be attributed to differences in the diffusive mixing and length of the freshwater perturbation.

A similar simulation, performed by Mikolajewicz (1996) with a model lower of atmospheric complexity involved an input of 0.625 Sv of freshwater into the Labrador sea. With this input, the

AMOC shuts down for several hundred years. However, the AMOC reduces to 5 Sv, a substantial decrease from the preindustrial simulation, which was approximately 16 Sv.

As discussed in section 3.2, a 0.1 Sv freshwater discharge into the northern Atlantic causes a 30% weakening of the AMOC (Stouffer et al., 2006). For this study, the AMOC is reduced by approximately 31.3%, though the maximum freshwater forcing was 0.23 Sv. Therefore, even with a doubling of the freshwater input, the AMOC strength reduced by about the same magnitude.

The findings of this study are also agreeable with freshwater forcing experiment conducted by Rind et al.'s (2001) with a hosing 0.12 Sv of freshwater from the St. Lawrence River. Their analysis suggests that the AMOC decreases by 13 Sv from 20 Sv to 7 Sv (or 65%). In contrast to this study, Rind et al.'s (2001)proposed that NADW production is linear to the freshwater magnitude and duration. However, this study reveals that the magnitude of freshwater forcing does the strength of the AMOC responds non-linear to the freshwater forcing. Therefore, it is important to determine how the location of freshwater forcing affects oceanic circulation.

It should be noted that the strength of the AMOC for the simulation without freshwater forcing is ~11 Sv, and the surface air temperature decrease exceeds the decrease in surface air temperature of the simulation with freshwater forcing by ~10 °C. With the decrease in rainfall over the Northern North Atlantic region, and the subsequent increase in sea surface salinity along with decreasing sea surface temperatures, the AMOC is stronger than the simulation with freshwater forcing, but still decreased by ~6 Sv compared to the preindustrial simulation. Given the increased strength of the AMOC compared to the simulation with freshwater forcing, an increased surface air temperature over Greenland should be expected. However, the surface air temperature is substantially cooler for the simulation without freshwater forcing compared to the simulation with freshwater forcing. The cause for this cooling requires more analysis and further explanation.

When comparing the effects of location of freshwater discharge on the AMOC strength, this simulation shows sensitivity on the same order as noted in previous simulations (He, 2011). During the maximum drainage from the Mackenzie River, the AMOC is reduced by 9 Sv as

opposed to 7 Sv during the maximum drainage is from the St. Lawrence River. Additionally, the salinity of the surface waters of the Northern Atlantic reflect this sensitivity, as there is no reduction in salinity upon the discharge from the St. Lawrence River, but approximately a 0.5 psu reduction when the Mackenzie River output is at its maximum. Therefore, the model shows that there is an increased sensitivity of the AMOC to freshwater location, particularly freshwater discharge coming from the Arctic Ocean.

It is also important to note that upon termination of the freshwater discharge, the AMOC begins to recover within 10 years of shutting off the freshwater forcing, and the temperature increases by 3 °C within that time period. When the simulation is allowed to progress beyond the termination point, the AMOC in the simulation with freshwater forcing begins to weaken again, while temperature begins to increase. This could be due to the melting of sea ice that formed when temperatures were decreased, inputting more freshwater into the surface oceans, causing the AMOC to slow once more.

The difference in the AMOC reduction by freshwater hosing reflects also differences in the response in surface temperature between these simulations. For example, while in this study the North Atlantic sea surface cool by 8.5 °C and the surface air temperature (SAT) cool by 22 °C the changes in Schiller et al. 1997 are less sensitive (with 6 °C cooling of the SST and 15 °C cooling of the SAT). These differences may be attributed to a lower response of the AMOC to the freshwater forcing.

$\delta^{13}C$ observed values generally agree with the zonally averaged $\delta^{13}C$ from model output, however a negative $\delta^{13}C$ shift due changes in the glacial-interglacial land surface and in the ratio of C3 to C4 plants must be considered and adjusted accordingly (see Winguth et al., 1999). When these values are corrected, the zonal averages for the simulation with freshwater forcing have reduced bias to the observed values compared to the simulation without freshwater forcing. The model-data analysis suggest that the simulation without freshwater forcing provide the best fit to the observations and is thus the most plausible scenario for the YD cooling event.

An important note involves the uncertainties of CCSM3 and the model resolution. Bryan et al. (2006) and Saenko et al. (2004), in a series of sensitivity experiments between different

model resolutions, conjecture that the T31x3 resolution has a reduced sensitivity of the thermohaline circulation with increasing ice coverage and decreasing meltwater input. In the same studies, higher resolution simulations do not show this lack of sensitivity. The simulations performed in this study were at T31x3 resolution, and therefore the reduced sensitivity of the thermohaline should be taken into consideration. The T31x3 version of CCSM3 has a bias of >2 W m^{-2} bias in the top of atmosphere energy balance that results from midlatitude grid density that is lower compared to density of grids at higher levels, enhancement of extratropical shortwave cloud forcing, and reduction of deep tropic shortwave cloud forcing (Yeager et al., 2006). Additionally, the T31x3 version of CCSM3 produces biased cold sea surface temperatures that help to regulate the amount of rain produced in the Pacific ocean (Yeager et al., 2006). Sea ice also tends to be too thick and extensive in the Northern hemisphere because of lack of ocean heat transport from the North Atlantic, or lack of sea ice melting (Yeager et al., 2006).

3.7 Conclusion

This study aimed to investigate the validity of the freshwater forcing hypothesis and sensitivity of the North Atlantic climate to location of freshwater discharge with the Community Climate System Model version 3 (CCSM3) for the onset of the Younger Dryas cooling event. Results suggest that the same magnitude of freshwater forcing does not consistently reduce the AMOC. For example, two simulations that input 0.625 Sv of freshwater into the Atlantic Ocean produce different reductions of the AMOC. A simulation with 0.1 Sv freshwater forcing induces a 30% reduction of the AMOC, while in this study, doubling the freshwater forcing reduces the AMOC by 31.25%. Performing a series of simulations with differing magnitudes of freshwater forcing in the same location with the same boundary conditions at a higher resolution would be necessary to determine the consistency of the effect of freshwater magnitude on the AMOC. Additionally, it is found that the AMOC has a higher sensitivity to Mackenzie River discharge as opposed to St. Lawrence discharge, indicating that the AMOC is sensitive to the location of the freshwater forcing. The Mackenzie River discharge weakens the AMOC by approximately 9 Sv, while the St. Lawrence River discharge weakens the AMOC by 7 Sv. A previous simulation in which the Mackenzie River discharge weakens the AMOC by approximately 50%, while discharge from the

St. Lawrence River only reduces oceanic circulation by approximately 44% supports this finding (He, 2011). Higher resolution simulations testing the freshwater location and magnitude would be required to test this issue further. Along with the reduction of the AMOC, surface air temperature for the simulation with freshwater forcing suggests a decrease of approximately 15 °C over Greenland, which is in agreement with the GISP reconstructions for the area. The AMOC shows a recovery within the first 10 years of freshwater termination, and the recovery continues for the next 170 years, temperature and salinity indicating increased ocean heat transport and decreased freshwater input respectively. The simulation without freshwater forcing is in better agreement with the observed $\delta^{13}C$ values although there is substantial model-data bias, partially because changes of the land surface are not considered and the temperature effect on the isotopic ratio is too simplified. Overall, the simulation with freshwater forcing accurately represents what would be expected for the YD cooling event. However, with the more substantial cooling of the surface air temperature over Greenland as well as reduction in the AMOC in the simulation without freshwater forcing, the findings of this study indicate that freshwater forcing is not necessary to cause a reduction of the AMOC and a cooling of the climate. Additional research and analysis is required to determine the causes of the cooling of the surface air temperature in the simulation without freshwater forcing.

References

Alley, R.B., 2000, The Younger Dryas cold interval as viewed from central Greenland: Quaternary Science Reviews, v. 19, p. 213–226, doi: 10.1016/S0277-3791(99)00062-1.

Bakke, J., Lie, Ø., Heegaard, E., Dokken, T., Haug, G.H., Birks, H.H., Dulski, P., and Nilsen, T., 2009, Rapid oceanic and atmospheric changes during the Younger Dryas cold period: Nature, v. 2, p. 202–205, doi: 10.1038/ngeo439.

Bard, E., Hamelin, B., Arnold, M., Montaggioni, L., Cabioch, G., Faure, G., and Rougerie, F., 1996, Deglacial sea-level record from Tahiti corals and the timing of global meltwater discharge: Nature, v. 382, p. 241–244, doi: 10.1038/382241a0.

Berger, A., 1988, Milankovitch Theory and climate: Reviews of Geophysics, v. 26, p. 624, doi: 10.1029/RG026i004p00624.

Berger, A., and Loutre, M.F., 1991, Insolation values for the climate of the last 10 million years: Quaternary Science Reviews, v. 10, p. 297–317, doi: 10.1016/0277-3791(91)90033-Q.

Bitz, C.M., and Lipscomb, W.H., 1999, An energy-conserving thermodynamic model of sea ice: Journal of Geophysical Research, v. 104, p. 15669, doi: 10.1029/1999JC900100.

Bond, G.C., and Lotti, R., 1995, Iceberg discharges into the north atlantic on millennial time scales during the last glaciation.: Science (New York, N.Y.), v. 267, p. 1005–10, doi: 10.1126/science.267.5200.1005.

Boville, B. a., and Bretherton, C.S., 2003, Heating and kinetic energy dissipation in the NCAR Community Atmosphere Model: Journal of Climate, v. 16, p. 3877–3887, doi: 10.1175/1520-0442(2003)016<3877:HAKEDI>2.0.CO;2.

Boville, B.A., Rasch, P.J., Hack, J.J., and McCaa, J.R., 2006, Representation of clouds and precipitation processes in the Community Atmosphere Model version 3 (CAM3): Journal Of Climate, v. 19, p. 2184–2198, doi: 10.1175/JCLI3749.1.

Boyle, E.A., and Keigwin, L., 1987, North Atlantic thermohaline circulation during the past 20,000 years linked to high-latitude surface temperature: Nature, v. 330, p. 35–40, doi: 10.1038/330035a0.

Briegleb, B., Bitz, C.M., Hunke, E.C., Lipscomb, W.H., Holland, M.M., Schramm, J., and Moritz, D., 2004, Scientific Description of the Sea Ice Component in the Community Climate System Model, Version Three: NCAR Technical Note, v. NCAR/TN-46, p. 70, doi: 10.5065/D6HH6H1P.

Broecker, W., 1991, The Great Ocean Conveyor: Oceanography, v. 4, p. 79–89, doi: 10.5670/oceanog.1991.07.

Broecker, W.S., Andree, M., Wolfli, W., Oeschger, H., Bonani, G., Kennett, J., and Peteet, D.M., 1988, The Chronology of the Last Deglaciation: Impications to the Cause of the Younger Dryas Event: Paleoceanography, v. 3, p. 1–19, doi: 10.1029/PA003i001p00001.

Broecker, W.S., and Denton, G.H., 1989, The role of ocean-atmosphere reorganizations in glacial cycles: Geochimica et Cosmochimica Acta, v. 53, p. 2465–2501, doi: 10.1016/0016-7037(89)90123-3.

Broecker, W.S., Peng, T.-H., and Beng, Z., 1982, Tracers in the sea (Lamont-Doherty Geological Observatory, Ed.): Lamont-Doherty Geological Observatory, Columbia University, Eldigio Press, 690 p.

Bryan, F.O., Danabasoglu, G., Nakashiki, N., Yoshida, Y., Kim, D.-H., Tsutsui, J., and Doney, S.C., 2006, Response of the North Atlantic Thermohaline Circulation and Ventilation to Increasing Carbon Dioxide in CCSM3: Journal of Climate, v. 19, p. 2382–2397, doi: 10.1175/JCLI3757.1.

Came, R.E., Oppo, D.W., and Curry, W.B., 2003, Atlantic Ocean circulation during the Younger Dryas: Insights from a new Cd/Ca record from the western subtropical South Atlantic: Paleoceanography, v. 18, p. n/a–n/a, doi: 10.1029/2003PA000888.

Carlson, A.E., Clark, P.U., Haley, B.A., Klinkhammer, G.P., Simmons, K., Brook, E.J., and Meissner, K.J., 2007, Geochemical proxies of North American freshwater routing during the Younger Dryas cold event.: Proceedings of the National Academy of Sciences of the United States of America, v. 104, p. 6556–6561, doi: 10.1073/pnas.0611313104.

Cheng, J., Liu, Z., He, F., Otto-Bliesner, B.L., and Colose, C., 2011, Impact of North Atlantic – GIN Sea exchange on deglaciation evolution of the Atlantic Meridional Overturning Circulation: Climate of the Past, v. 7, p. 935–940, doi: 10.5194/cp-7-935-2011.

Clark, P.U., Marshall, S.J., Clarke, G.K., Hostetler, S.W., Licciardi, J.M., and Teller, J.T., 2001, Freshwater forcing of abrupt climate change during the last glaciation.: Science, v. 293, p. 283–287, doi: 10.1126/science.1062517.

Collins, W.D., Bitz, C.M., Blackmon, M.L., Bonan, G.B., Bretherton, C.S., Carton, J.A., Chang, P., Doney, S.C., Hack, J.J., Henderson, T.B., Kiehl, J.T., Large, W.G., McKenna, D.S., Santer, B.D., et al., 2006, The community climate system model version 3 (CCSM3): Journal of Climate, v. 19, p. 2122–2143, doi: 10.1175/JCLI3761.1.

Danabasoglu, G., Yeager, S.G., Kwon, Y.-O., Tribbia, J.J., Phillips, A.S., and Hurrell, J.W., 2012, Variability of the Atlantic Meridional Overturning Circulation in CCSM4: Journal of Climate, v. 25, p. 5153–5172, doi: 10.1175/JCLI-D-11-00463.1.

DeVernal, A., Hillaire-Marcel, C., and Bilodeau, G., 1996, Reduced meltwater outflow from the Laurentide ice margin during the Younger Dryas: Nature, v. 381, p. 774–777, doi: 10.1038/381774a0.

Doney, S.C., Lima, I., Feely, R. a., Glover, D.M., Lindsay, K., Mahowald, N., Moore, J.K., and Wanninkhof, R., 2009, Mechanisms governing interannual variability in upper-ocean inorganic carbon system and air-sea CO2 fluxes: Physical climate and atmospheric dust: Deep-Sea Research Part II: Topical Studies in Oceanography, v. 56, p. 640–655, doi: 10.1016/j.dsr2.2008.12.006.

Doney, S.C., Lindsay, K., Fung, I., and John, J., 2006, Natural variability in a stable, 1000-yr global coupled climate-carbon cycle simulation: Journal of climate, v. 19, p. 3033–3054, doi: 10.1175/JCLI3783.1.

Donnelly, J.P., Driscoll, N.W., Uchupi, E., Keigwin, L.D., Schwab, W.C., Thieler, E.R., and Swift, S. a., 2005, Catastrophic meltwater discharge down the Hudson Valley: A potential trigger for the Intra-Allerød cold period: Geology, v. 33, p. 89–92, doi: 10.1130/G21043.1.

Drange, H., Dokken, T., Furevik, T., Gerdes, R., and Berger, W., 2005, The Nordic Seas: An Integrated Perspective: Oceanography, Climatology, Biogeochemistry, and Modeling: Washington, DC, American Geophysical Union, 1-366 p.

Duplessy, J.C., Bard, E., Labeyrie, L., Duprat, J., and Moyes, J., 1993, Oxygen-Isotope Records and Salinity Changes in the Northeastern Atlantic-Ocean during the Last 18,000 Years: Paleoceanography, v. 8, p. 341–350.

Dyke, A.S., 2004, An outline of North American deglaciation with emphasis on central and northern Canada: Developments in Quaternary Science, v. 2, p. 373–424, doi: 10.1016/S1571-0866(04)80209-4.

Ebbesen, H., and Hald, M., 2004, Unstable Younger Dryas climate in the northeast North Atlantic: Geology, v. 32, p. 673 –676, doi: 10.1130/G20653.1.

England, M.H., 1995, The Age of Water and Ventilation Timescales in a Global Ocean Model: Journal of Physical Oceanography, v. 25, p. 2756–2777, doi: 10.1175/1520-0485(1995)025.

Gherardi, J.M., Labeyrie, L., McManus, J.F., Francois, R., Skinner, L.C., and Cortijo, E., 2005, Evidence from the Northeastern Atlantic basin for variability in the rate of the meridional overturning circulation through the last deglaciation: Earth and Planetary Science Letters, v. 240, p. 710–723, doi: 10.1016/j.epsl.2005.09.061.

Hall, M.M., and Bryden, H.L., 1982, Direct estimates and mechanisms of ocean heat transport: Deep Sea Research Part A. Oceanographic Research Papers, v. 29, p. 339–359, doi: 10.1016/0198-0149(82)90099-1.

He, F., 2011, Simulating Transiet Climate Evolution of the Last Deglaciation with CCSM3: University of Wisconsin-Madison, 1-185 p.

Hu, A., Meehl, G.A., Washington, W.M., and Dai, A., 2004, Response of the Atlantic Thermohaline Circulation to Increased Atmospheric CO_2 in a Coupled Model: Journal of Climate, v. 17, p. 4267–4279, doi: 10.1175/JCLI3208.1.

Huang, E., and Tian, J., 2008, Melt-Water-Pulse (MWP) events and abrupt climate change of the last deglaciation: Chinese Science Bulletin, v. 53, p. 2867–2878, doi: 10.1007/s11434-008-0206-8.

Hughen, K. a, Overpeck, J.T., Lehman, S.J., Kashgarian, M., Southon, J., Peterson, L.C., Alley, R., and Sigman, D.M., 1998, Deglacial changes in ocean circulation from an extended radiocarbon calibration: Nature, v. 391, p. 65–68, doi: 10.1038/34150.

Hughen, K.A., Southon, J.R., Lehman, S.J., and Overpeck, J.T., 2000, Synchronous radiocarbon and climate shifts during the last deglaciation.: Science (New York, N.Y.), v. 290, p. 1951–1955, doi: 10.1126/science.290.5498.1951.

Johns, W.E., Baringer, M.O., Beal, L.M., Cunningham, S. a., Kanzow, T., Bryden, H.L., Hirschi, J.J.M., Marotzke, J., Meinen, C.S., Shaw, B., and Curry, R., 2011, Continuous, array-based estimates of atlantic ocean heat transport at 26.5°N: Journal of Climate, v. 24, p. 2429–2449, doi: 10.1175/2010JCLI3997.1.

Joos, F., and Spahni, R., 2008, Rates of change in natural and anthropogenic radiative forcing over the past 20,000 years: Proceedings of the National Academy of Sciences of the United States of America, v. 105, p. 1425–1430, doi: 10.1073/pnas.0707386105.

Keeling, C.D., Bacastow, R.B., Carter, A.F., Piper, S.C., Whorf, T.P., Heimann, M., Mook, W.G., and Roeloffzen, H., 1989, A three-dimensional model of atmospheric CO2 transport based on observed winds: 1. Analysis of observational data, *in* Aspects of Climate Variability in the Pacific and the Western Americas, p. 165–236.

Knies, J., Matthiessen, J., Mackensen, A., Stein, R., Vogt, C., Frederichs, T., and Nam, S.-I., 2007, Effects of Arctic freshwater forcing on thermohaline circulation during the Pleistocene: Geology, v. 35, p. 1075, doi: 10.1130/G23966A.1.

Knutti, R., Flückiger, J., Stocker, T.F., and Timmermann, A., 2004, Strong hemispheric coupling of glacial climate through freshwater discharge and ocean circulation.: Nature, v. 430, p. 851–856, doi: 10.1038/nature02786.

Leverington, D.W., and Teller, J.T., 2003, Paleotopographic reconstructions of the eastern outlets of glacial Lake Agassiz: Canadian Journal of Earth Sciences, v. 40, p. 1259–1278, doi: 10.1139/e03-043.

Levitus, S., 1983, Climatological Atlas of the World Ocean: Eos, Transactions American Geophysical Union, v. 64, p. 962, doi: 10.1029/EO064i049p00962-02.

Lin, S.-J., 2004, A "Vertically Lagrangian" Finite-Volume Dynamical Core for Global Models: Monthly Weather Review, v. 132, p. 2293–2307, doi: 10.1175/1520-0493(2004)132<2293:AVLFDC>2.0.CO;2.

Lin, S.-J., and Rood, R.B., 1996, Multidimensional Flux-Form Semi-Lagrangian Transport Schemes: Monthly Weather Review, v. 124, p. 2046–2070, doi: 10.1175/1520-0493(1996)124<2046:MFFSLT>2.0.CO;2.

Liu, Z., Carlson, A.E., He, F., Brady, E.C., Otto-Bliesner, B.L., Briegleb, B.P., Wehrenberg, M., Clark, P.U., Wu, S., Cheng, J., Zhang, J., Noone, D., and Zhu, J., 2012, Younger Dryas cooling and the Greenland climate response to CO_2.: Proceedings of the National Academy of Sciences of the United States of America, v. 109, p. 11101–4, doi: 10.1073/pnas.1202183109.

Maier-Reimer, E., 1993, Geochemical cycles in an ocean general circulation model. Preindustrial tracer distributions: Global Biogeochemical Cycles, v. 7, p. 645–677, doi: 10.1029/93GB01355.

Manabe, S., and Stouffer, R.J., 1997, Coupled ocean-atmosphere model response to freshwater input: Comparison to Younger Dryas event: Paleoceanography, v. 12, p. 321–336, doi: 10.1029/96PA03932.

Manabe, S., and Stouffer, R.J., 1994, Multiple-century response of a coupled ocean-atmosphere model to an increase of atmospheric carbon dioxide: Journal of Climate, v. 7, p. 5–23, doi: 10.1175/1520-0442(1994)007<0005:MCROAC>2.0.CO;2.

Manabe, S., and Stouffer, R.J., 2000, Study of abrupt climate change by a coupled ocean-atmosphere model: Quaternary Science Reviews, v. 19, p. 285–299, doi: 10.1016/S0277-3791(99)00066-9.

Manabe, S., and Stouffer, R.J., 1999, The role of thermohaline circulation in climate: Tellus B, v. 51, p. 91–109, doi: 10.1034/j.1600-0889.1999.00008.x.

McManus, J.F., Francois, R., Gherardi, J.-M., Keigwin, L.D., and Brown-Leger, S., 2004, Collapse and rapid resumption of Atlantic meridional circulation linked to deglacial climate changes.: Nature, v. 428, p. 834–7, doi: 10.1038/nature02494.

Mikolajewicz, U., 1996, A meltwater induced collapse of the `conveyor belt' thermohaline circulation and its influence on the distribution of $\delta^{14}C$ and $\delta^{18}O$ in the oceans: Technical Report, Max Plank Institute for Meteorology, v. 189, p. 25.

Murton, J.B., Bateman, M.D., Dallimore, S.R., Teller, J.T., and Yang, Z.-L., 2010, Identification of Younger Dryas outburst flood path from Lake Agassiz to the Arctic Ocean.: Nature, v. 464, p. 740–3, doi: 10.1038/nature08954.

Neale, R.B., Gettelman, A., Park, S., Chen, C.-C., Lauritzen, P.H., Williamson, D.L., Conley, A., Kinnison, D., Marsh, D., Smith, A.K., Vitt, F., Garcia, R., Lamarque, J.-F., Mills, M., et al., 2004, Description of the NCAR Community Atmosphere Model (CAM3): NCAR Technical Note, v. NCAR/TN-46, p. 214.

Oleson, K.W., Dai, Y., Bonan, G.B., Bosilovich, M., Dickinson, R.E., Dirmeyer, P., Hoffman, F., Houser, P., Levis, S., Niu, G.-Y., Thornton, P., Vertenstein, M., Yang, Z.-L., and Zeng, X., 2004, Technical Description of the Community Land Model (CLM): NCAR Technical Note, v. NCAR/TN-46, p. 186, doi: 10.5065/D6N877R0.

Otto-Bliesner, B.L., Brady, E.C., Clauzet, G., Tomas, R., Levis, S., and Kothavala, Z., 2006, Last Glacial Maximum and Holocene Climate in CCSM3: Journal of Climate, v. 19, p. 2526–2544, doi: 10.1175/JCLI3748.1.

Otto-Bliesner, B.L., Tomas, R., Brady, E.C., Caspar, A., Kothavala, Z., and Clauzet, G., 2006, Climate Sensitivity of Moderate- and Low-Resolution Versions of CCSM3 to Preindustrial Forcings: Journal of Climate, v. 3, p. 2567–2583, doi: 10.1175/JCLI3754.1.

Peltier, W.R., 2004, GLOBAL GLACIAL ISOSTASY AND THE SURFACE OF THE ICE-AGE EARTH: The ICE-5G (VM2) Model and GRACE: Annual Review of Earth and Planetary Sciences, v. 32, p. 111–149, doi: 10.1146/annurev.earth.32.082503.144359.

Peltier, W.R., 2007, Rapid climate change and Arctic Ocean freshening: Geology, v. 35, p. 1147, doi: 10.1130/focus122007.1.

Rahmstorf, S., 1996, Bifurcations of the Atlantic Thermohaline circulation in response to changes in the hydrological cycle: Nature, v. 378, p. 145–149, doi: 10.1038/378145a0.

Rahmstorf, S., 2000, The Thermohaline Ocean Circulation: A System with Dangerous Thresholds? Climatic Change, v. 46, p. 247–256, doi: 10.1023/A:1005648404783.

Rahmstorf, S., 2006, Thermohaline Ocean Circulation, *in* Encyclopedia of Quaternary Sciences, p. 1–10.

Rind, D., DeMenocal, P., Russell, G., Sheth, S., Collins, D., Schmidt, G., and Teller, J., 2001, Effects of glacial meltwater in the GISS coupled atmosphereocean model: 1. North Atlantic Deep Water response: Journal of Geophysical Research: Atmospheres, v. 106, p. 27335–27353, doi: 10.1029/2000JD000070.

Rintoul, S.R., and Wunsch, C., 1991, Mass, heat, oxygen and nutrient fluxes and budgets in the North Atlantic Ocean: Deep Sea Research Part A. Oceanographic Research Papers, v. 38, Supple, p. S355–S377, doi: http://dx.doi.org/10.1016/S0198-0149(12)80017-3.

Rooth, C., 1982, Hydrology and ocean circulation: Progress in Oceanography, v. 11, p. 131–149, doi: 10.1016/0079-6611(82)90006-4.

Saenko, O.A., Eby, M., and Weaver, A.J., 2004, The effect of sea-ice extent in the North Atlantic on the stability of the thermohaline circulation in global warming experiments: Climate Dynamics, v. 22, p. 689–699, doi: 10.1007/s00382-004-0414-0.

Sarnthein, M., Winn, K., Jung, S.J.A., Duplessy, J.-C., Labeyrie, L., Erlenkeuser, H., and Ganssen, G., 1994, Changes in East Atlantic Deepwater Circulation over the last 30,000 years: Eight time slice reconstructions: Paleoceanography, v. 9, p. 209–267, doi: 10.1029/93PA03301.

Schiller, A., Mikolajewicz, U., and Voss, R., 1997, The stability of the North Atlantic thermohaline circulation in a coupled ocean-atmosphere general circulation model: Climate Dynamics, v. 13, p. 325–347, doi: 10.1007/s003820050169.

Schmidt, M.W., and Lynch-Stieglitz, J., 2011, Florida Straits deglacial temperature and salinity change: Implications for tropical hydrologic cycle variability during the Younger Dryas: Paleoceanography, v. 26, p. 1–16, doi: 10.1029/2011PA002157.

Schmidt, M.W., Spero, H.J., and Lea, D.W., 2004, Links between salinity variation in the Caribbean and North Atlantic thermohaline circulation.: Nature, v. 428, p. 160–3, doi: 10.1038/nature02346.

Schramm, J., Bitz, C.M., Briegleb, B., Holland, M.M., Hunke, E.C., Lipscomb, B., and Moritz, D., 2004, Community Sea Ice Model (CSIM) User's Guide version 5.0: National Center for Atmospheric Research, Boulder, CO, p. 32.

Seager, R., and Battisti, D.S., 2007, Challenges to our understanding of the general circulation: abrupt climate change, *in* Global Circulation of the Atmosphere, p. 332–372.

Severinghaus, J.P., Sowers, T., Brook, E.J., Alley, R.B., and Bender, M.L., 1998, Timing of abrupt climate change at the end of the Younger Dryas interval from thermally fractionated gases in polar ice: Nature, v. 391, p. 141–146.

Smith, R., and Gent, P., 2004, Reference manual for the parallel ocean program (POP): Los Alamos Unclassified Report LA-UR-02-2484, p. 76.

Smith, R., Jones, P., Briegleb, B., Bryan, F., Danabasoglu, G., Dennis, J., Dukowicz, J., Eden, C., Fox-Kemper, B., Gent, P., Hecht, M., Jayne, S., Jochum, M., Large, W., et al., 2010, The Parallel Ocean Program (POP) reference manual: Ocean component of the Community Climate System Model (CCSM): Rep. LAUR-01853, v. 141, p. 1–141.

Srokosz, M., Baringer, M., Bryden, H., Cunningham, S., Delworth, T., Lozier, S., Marotzke, J., and Sutton, R., 2012, Past, Present, and Future Changes in the Atlantic Meridional Overturning Circulation: Bulletin of the American Metoeorlogical Society, v. 93, p. 1663–1676, doi: 10.1175/BaMs-d-11-00151.1.

Srokosz, M. a., and Bryden, H.L., 2015, Observing the Atlantic Meridional Overturning Circulation yields a decade of inevitable surprises: Science, v. 348, p. 1255575–1255575, doi: 10.1126/science.1255575.

Stocker, T.F., and Marchal, O., 2000, Abrupt climate change in the computer: is it real? Proceedings of the National Academy of Sciences of the United States of America, v. 97, p. 1362–5.

Stocker, T.F., and Wright, D.G., 1991, Rapid transitions of the ocean's deep circulation induced by changes in surface water fluxes: Nature, v. 351, p. 729–732, doi: 10.1038/351729a0.

Stouffer, R.J., Yin, J., Gregory, J.M., Dixon, K.W., Spelman, M.J., Hurlin, W., Weaver, A.J., Eby, M., Flato, G.M., Hasumi, H., Hu, A., Jungclaus, J.H., Kamenkovich, I. V., Levermann, A., et al., 2006, Investigating the Causes of the Response of the Thermohaline Circulation to Past and Future Climate Changes: Journal of Climate, v. 19, p. 1365–1387, doi: 10.1175/JCLI3689.1.

Suess, H.E., 1955, Radiocarbon Concentration in Modern Wood: Avian diseases, v. 122, p. 415–417, doi: 10.1126/science.122.3166.415-a.

Tarasov, L., and Peltier, W.R., 2005, Arctic freshwater forcing of the Younger Dryas cold reversal.: Nature, v. 435, p. 662–5, doi: 10.1038/nature03617.

Teller, J.T., 2003, Controls, history, outbursts, and impact of large late-Quaternary proglacial lakes in North America, *in* Developments in Quaternary Science, Developments in Quaternary Sciences, Elsevier, p. 45–61.

Teller, J.T., 2013, Lake Agassiz during the Younger Dryas: Quaternary Research (United States), v. 80, p. 361–369, doi: 10.1016/j.yqres.2013.06.011.

Teller, J.T., 1990, Meltwater and precipitation runoff to the North Atlantic, Arctic, and Gulf of Mexico from the Laurentide Ice Sheet and adjacent regions during the Younger Dryas: Paleoceanography, v. 5, p. 897–905, doi: 10.1029/PA005i006p00897.

Teller, J.T., Boyd, M., Yang, Z.-L., Kor, P.S.G., and Fard, A.M., 2005, Alternative routing of Lake Agassiz overflow during the Younger Dryas: new dates, paleotopography, and a re-evaluation: Quaternary Science Reviews, v. 24, p. 1890–1905, doi: 10.1016/j.quascirev.2005.01.008.

Teller, J.T., Leverington, D.W., and Mann, J.D., 2002, Freshwater outbursts to the oceans from glacial Lake Agassiz and their role in climate change during the last deglaciation: Quaternary Science Reviews, v. 21, p. 879–887, doi: 10.1016/S0277-3791(01)00145-7.

Thiele, G., and Sarmiento, J.L., 1990, Tracer Dating and Ocean Ventilation: Journal of Geophysical Research, v. 95, p. 9377–9391, doi: 10.1029/JC095iC06p09377.

Vertenstein, M., Craig, T., Henderson, T.B., Murphy, S., Carr Jr, G.R., and Norton, N., 2004, CCSM3.0 User's Guide: National Center for Atmospheric Research, Boulder, CO, p. 69.

Voss, R., and Mikolajewicz, U., 2001, The climate of 6000 years BP in near-equilibrium simulations with a coupled AOGCM: Geophysical Research Letters, v. 28, p. 2213–2216, doi: 10.1029/2000GL012498.

Weijer, W., Maltrud, M.E., Hecht, M.W., Dijkstra, H. a., and Kliphuis, M. a., 2012, Response of the Atlantic Ocean circulation to Greenland Ice Sheet melting in a strongly-eddying ocean model: Geophysical Research Letters, v. 39, p. 1–6, doi: 10.1029/2012GL051611.

Winguth, A.M.E., Archer, D., Duplessy, J.-C., Maier-Reimer, E., and Mikolajewicz, U., 1999, Sensitivity of paleonutrient tracer distribution and deep-sea circulation to glacial boundary conditions: Paleoceanography, v. 14, p. 304–323, doi: 10.1029/1999PA900002.

Winguth, A., and Winguth, C., 2013, Precession-driven monsoon variability at the Permian-Triassic boundary - Implications for anoxia and the mass extinction: Global and Planetary Change, v. 105, p. 160–170, doi: 10.1016/j.gloplacha.2012.06.006.

Winguth, a. M.E., and Winguth, C., 2011, Simulating Permian-Triassic oceanic anoxia distribution: Implications for species extinction and recovery: Geology, v. 40, p. 127–130, doi: 10.1130/G32453.1.

Yeager, S., and Danabasoglu, G., 2012, Sensitivity of atlantic meridional overturning circulation variability to parameterized Nordic Sea overflows in CCSM4: Journal of Climate, v. 25, p. 2077–2103, doi: 10.1175/JCLI-D-11-00149.1.

Yeager, S.G., Shields, C.A., Large, W.G., and Hack, J.J., 2006, The low-resolution CCSM3: Journal of Climate, v. 19, p. 2545–2566, doi: 10.1175/JCLI3744.1.

Zhang, G.J., and McFarlane, N. a., 1995, Sensitivity of climate simulations to the parameterization of cumulus convection in the Canadian climate centre general circulation model: Atmosphere-Ocean, v. 33, p. 407–446, doi: 10.1080/07055900.1995.9649539.

Chapter 4

Sensitivity of the Climate to Younger Dryas Orbital parameters and Greenhouse Gas concentrations – a model study with CESM1.0.5

Abstract

Younger Dryas to Holocene differences in the Atlantic meridional ocean circulation can be explained by changes in the discharge of freshwater into the surface ocean, in atmospheric greenhouse gas concentrations, in Earth's orbital parameters, and in other factors. This study utilizes the Community Earth System Model (CESM1.0.5) to evaluate how changes in orbital and greenhouse gas concentration, primarily CO_2, affect the Younger Dryas to Holocene change and seasonal climate variability. The Younger Dryas to present-day changes by the Earth's orbital parameters have a larger influence on the decline in the AMOC than changes induced by relative small changes in the CO_2 radiative forcing (orbitally-driven changes in AMOC are 1.4 times larger than pCO_2-driven changes). The reduction of atmospheric pCO_2 and the changes in orbital cycles leads both to increased precipitation over the northern North Atlantic and to reduced transport of water masses associated with the AMOC. The strength of the AMOC may be more affected by the heat and freshwater fluxes due to the seasonal radiative forcing changes by orbital parameters. The combined effects of orbital and CO_2 forcing alone are not substantial enough to trigger a Younger Dryas climate state as inferred from the observations, indicating that additional mechanisms are required. The addition of an ice sheet and freshwater forcing may be crucial to forcing the system into the climatic scheme desired. African Monsoons are more greatly affected by changes in the orbital parameters compared to changes in the atmospheric pCO_2 values. However, as seen with the AMOC results, the change in orbital and greenhouse gas forcings alone were not enough to induce a YD climate state for the monsoonal seasons. Additional mechanisms are required to produce the feedbacks necessary for a dry YD monsoon season compared to the "African Humid Period" it interrupted.

4.1 Introduction

4.1.1 Orbital Parameters

The Younger Dryas climate change is affected by a combination of the three orbital parameters (precession, obliquity, and eccentricity). Eccentricity, or the degree of ellipticity of Earth's orbit around the sun, involves a 100,000-year cycle, though can also be seen weakly in larger cycles of approximately 410,000 years (Berger, 1988). Obliquity, or the tilt of the Earth's axis toward the sun, involves a 41,000-year cycle. Precession of the equinoxes, composed of the Earth's wobble and the precession of the ellipse, involves a 23,000-19,000 year cycle. The precession of the equinoxes is defined as the changing position of the equinoxes on the elliptic pathway of the Earth around the sun, thus altering the distance to sun the amount of radiation at the equinoxes (Crowley and North, 1991).

The monsoon circulation is influenced by precession of the equinox, which is modulated by the eccentricity (Imbrie and Imbrie, 1979). An increase in summer solar radiation in the subtropics by precessional maxima increases the warming over land, creating a more intense low-pressure area over the land and a high-pressure area over the ocean (Kutzbach, 1981, Zhisheng et al., 1993). The enhanced low-pressure over land leads to an increase of advected warm moist marine air towards the land where the convection and associated latent heat release by condensation of water vapor as well as intense monsoonal precipitation occurs. During the winter, incoming solar radiation during precessional maxima is weaker causing larger cooling and intensification of the high-pressure system over land whereas the low-pressure system over the warmer ocean decreases. During the Younger Dryas, the precession of the equinox and eccentricity were more extreme than during preindustrial times (Table 3-1) and thus monsoonal circulation was stronger (Figure 4-1; Kutzbach, 1998).

Obliquity changes also affect seasonality by the amount of solar radiation received particularly in high latitudes. For example, when the Earth's obliquity is larger, the seasonality in polar regions become more extreme, as more solar radiation is exposed to the Northern Hemisphere during the summer, and less during the winter.

In addition, the solar constant during the Younger Dryas was 1 W m^{-2} lower than its preindustrial value of 1,365 W m^{-2} because solar radiation increases over time (Table 3-1; Otto-Bliesner et al., 2006b).

In summary, summer insolation during the Younger Dryas was significantly higher than that of present day with an increase of approximately 28 W m^{-2} (Figure 4-1; Kutzbach et al., 1998). Similarly, the winter insolation was decreased by approximately 18 W m^{-2} at 13 ka compared to present day (Figure 4-1). This indicates that the seasonal climate variations during the Younger Dryas were likely more extreme than during the late Holocene. Thus, seasonal climate feedbacks were also more amplified during the Younger Dryas.

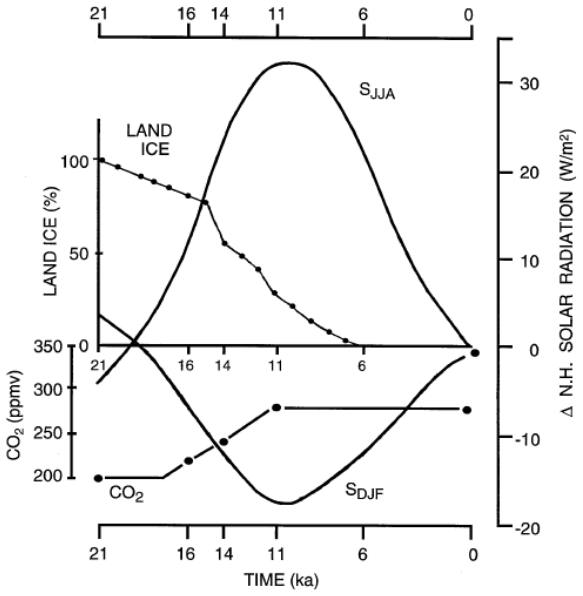

Figure 4-1 Climate forcing during the deglaciation including changes in insolation in the northern hemisphere, extent of land ice, and atmospheric pCO_2 (from Kutzbach et al., 1998). It should be noted that the seasonal radiative forcing changes due to orbital changes exceeds the annual changes due to greenhouse gas changes in the North Atlantic region.

4.1.1.1 Obital-induced Changes in the Monsoon Circulation

The West African monsoonal system involves the northward and southward seasonal migration of the Intertropical convergence zone (ITCZ), which is the zone where the northeast and southeast trade winds converge (Griffiths, 1972; Chiang et al., 2002). During January, when the high pressure system is over Northwestern Africa and a low-pressure system exists over the equatorial region, the ITCZ is to the north of the equator (Griffiths, 1972). In the spring, the low-pressure systems continue to migrate northward over the northern desert, and with it the ITCZ, which moves to the region just south of the desert, known as the Sahel (Nicholson, 2013; Folland et al., 1986; Gasse, 2000; Kröpelin et al., 2008; Griffiths, 1972). In the summer, the ITCZ reaches its northernmost location, which is at approximately 20°N latitude (Griffiths, 1972).

The West African monsoon is represented in terrestrial and lacustrine sediment cores. Analysis of Lake Masoko sediment records in Tanzania represent pollen assemblages that suggest a decline in the southern African monsoon intensity during the Younger Dryas (Garcin et al., 2007) because of a northward migration of the ITCZ over the African Continent (Garcin et al., 2007). This arid period is also inferred from lacustrine sediment cores from the southern African subtropics, south of 10°S, where drought conditions prevailed (Gasse, 2000; Talbot et al., 2007). The presence of the increased precipitation in the northern tropics is supported by lacustrine cores from Lakes Malawi, Tanganyika and Bosumtwi in Tropical Africa (Talbot et al., 2007) and in pollen grain records from the mouth of the Niger River during the Younger Dryas period (Lézine et al., 2005), and is known as the “African Humid Period”. Northern hemispheric African summer monsoon appeared to strengthened during this period, likely a result of increased solar radiation from orbital changes (Kutzbach, 1981; Kutzbach and Guetter, 1986). The sediments from Lakes Masoko, Malawi, and Tanganyika are all located in South Africa, while the Lake Bosumtwi and Niger River sediments are located in Northern Africa. This indicates that the northern African monsoon is strengthened with more precipitation, and the southern African monsoon is weakened, with dry conditions prevailing.

Otto-Bliesner et al., (2014) performed sensitivity experiments that isolated the effects of orbital and greenhouse gas forcings for the Last Glacial Maximum and suggested precipitation

increases in the southern Sahel for the simulation with greenhouse gas changing only. In the simulation with only orbital changes, precipitation increased in the Sahel and the monsoonal rains expanded further northward (Otto-Bliesner et al., 2014).

4.1.1.2 Orbital-driven Changes in the Atlantic Meridional Overturing Circulation

The AMOC has been simulated in regards to orbital changes using a variety of climate models. One simulation using the intermediately complex LOVECLIM model indicates that AMOC oscillations are reliant on the obliquity (Friedrich et al., 2009). For example, with a decrease of obliquity from 22.8° to 22.4°, the AMOC begins to transition between a strong state and an intermediate state (~26 Sv and ~17 Sv respectively). Analysis of climate simulations with 6 ka orbital values suggest a cooling in high northern and southern latitudes, a southward-migration of the ITCZ, and an increase in the AMOC strength by 2 Sv at 30°N (Fischer and Jungclaus, 2010).

4.1.2 Global Carbon Cycle Changes at the Younger Dryas

Concentration of greenhouse gases in the atmosphere during the Younger Dryas period were substantial lower than for 1850 (Table 4-1; Joos and Spahni, 2008a). For example, a decrease of 47.13 ppmv in atmospheric pCO_2 (due to change in the atmospheric pCO_2 from the YD to 1850; Table 3-1) would result in a decline of radiative forcing of 1.04 W m^{-2} and cooling of 0.76 °C if we assume an equilibrium climate sensitivity of CEM1.05 of 3.2 ± 0.1 °C (Bitz et al., 2011; Danabasoglu and Gent, 2009) for a doubling of atmospheric pCO_2 (IPCC, 2007; Manabe and Bryan Jr, 1985; Hansen et al., 1988; Winguth et al., 2015).

4.1.2.1 Atmospheric pCO_2-driven Changes in the Atlantic Meridional Overturning Circulation

Change in the thermohaline circulation, specifically the shutdown of the AMOC, is the proposed mechanism for the onset of the Younger Dryas cooling event (Broecker and Denton, 1989; Rooth, 1982; Murton et al., 2010; Manabe and Stouffer, 1995; Donnelly et al., 2005; Broecker, 2003; Carlson et al., 2007; Tarasov and Peltier, 2005; Huang and Tian, 2008; Manabe and Stouffer, 1997; Hostetler et al., 2000; Teller et al., 2005; Broecker, 2006; Licciardi et al., 1999). Antarctic ice cores indicate climate changes are directly related to increasing greenhouse

gases at the end of the last three deglaciations, and it has been shown that large CO_2 emissions lead to the collapse of the AMOC (Fischer et al., 1999; Broecker, 1997). Analysis of climate simulations suggest that the AMOC may be nearly shutdown if atmospheric CO_2 concentrations are about half of present-day, which is equivalent to the LGM pCO_2 concentrations (Stouffer and Manabe, 2003; Shin et al., 2003). In contrast, increasing atmospheric CO_2 can also causes a weakening or collapse of the AMOC (Wood et al., 1999; Hu et al., 2004; Rahmstorf, 2000; Gregory et al., 2005; Stouffer et al., 1989; Manabe and Stouffer, 1999; Klockmann et al., 2015; Manabe and Stouffer, 1994; Voss and Mikolajewicz, 2001). An increase in the amount of greenhouse gases in the troposphere increases the amount of thermal radiation that is back radiated to the Earth's surface, which causes the temperature of the troposphere to increase. Increasing temperature raises the water vapor concentration at saturation level in the atmosphere, which may result in an increase in precipitation during convection or updraft of moist air masses. Such an increase in precipitation causes a freshening of the surface oceans, an increase in vertical stratification, and a reduction of the AMOC (Broecker and Denton, 1989; Rooth, 1982). Thus, lower greenhouse gas concentration in the atmosphere may lead to more arid climatic conditions.

4.2 Model Description

The sensitivity simulations for this study were performed using the National Center for Atmospheric Research's Community Earth System Model version 1.0.5 (NCAR CESM1.0), a predecessor to CCSM3. CESM is a comprehensive coupled climate system model that has the ability to simulate future, present, and past climates (Gent et al., 2011). The four components of CESM1 are the Community Atmospheric Model version 4 (CAM4; Neale et al., 2010), the Community Land Model version 4 (CLM4; Oleson et al., 2010), the Parallel Ocean Program version 2 (POP2; Smith et al., 2010), and the Los Alamos Sea Ice Model (CICE; Hunke et al., 2013). Fluxes of these four components are exchanged with a central coupler (CPL7). The central coupler allows for the exchange of information between the model components and an inclusive view of the climatic conditions for the time-period that is being investigated.

The horizontal resolution in this study consists of a finite volume grid for the atmosphere with a resolution of 0.9°x1.25° and a nominal 1°x1° grid for the ocean (gx1v6). The ocean and ice models have a displaced North Pole to Greenland and utilize the same grid. The atmospheric grid in CAM4 is vertically resolved with 26 layers and the oceanic grid in POP2, and consists of 60 vertical layers.

Orbital parameters, such as obliquity and precession are calculated by empirical series expansions that are solutions for Earth's orbit (Neale et al., 2010):

$$\epsilon=\epsilon^{*}+\sum_{j=1}^{47} A_j \cos(f_j t+\delta_j) \quad (4\text{-}11)$$

$$\psi=\tilde{\psi}t+\zeta+\sum_{j=1}^{78} F_j \sin\left(f_j^{'} t+\delta_j^{'}\right) \quad (4\text{-}12)$$

For equation 1, $\boldsymbol{\epsilon}$ is obliquity and $\boldsymbol{\epsilon}^{*} = 23.320556°$. A_j, f_j, and δ_j are determined by numerical fitting, and t is time in years (Neale et al., 2010). For equation 2, $\boldsymbol{\psi}$ denotes the general precession, $\tilde{\psi}$ = 50.439273", and $\zeta = 3.392506°$. F_j, $\boldsymbol{f_j'}$, and δ_j' are estimated from the numerical solution of Earth's orbit.

4.2.1 The Community Atmosphere Model

The atmospheric component, the Community Atmospheric Model version 4 (CAM4), is the seventh generation of the global atmospheric general circulation model within CESM1 with a uniform horizontal resolution of 1.25° x 0.9° and 26 vertical levels (Neale et al., 2010).

The CAM4 utilizes the same governing equations as CAM3 (Neale et al., 2004). The Eulerian spectral dynamical core has been coupled with a hybrid vertical coordinate following the approach of Simmons and Strüfing (1981). The parameterization suite for CAM4 includes a moist turbulence scheme, shallow convection scheme, deep convection, cloud micro- and macrophysics, aerosols, condensed phase optics, radiative transfer, and surface fluxes (Neale et al., 2010). The moist turbulence scheme is based on the diagnostic turbulent kinetic energy (TKE) formulation of Bretherton and Park (2009). It serves to simulate stratus radiation-turbulence interactions and vertically transport moisture, tracers, horizontal momentum and heat by symmetric turbulences. The shallow convection scheme uses the plume dilution equation of Park and Bretherton (2009) to simulate the spatial distribution of shallow convective activity. The same

deep convection scheme from Zhang and McFarlane (1995) used in CAM3 was changed to include the convective momentum transports of Richter and Rasch (2008) and Raymond and Blyth's (1986, 1992) dilute plume calculation. The parameterization for cloud microphysics is based on that of Morrison and Gettelman (2008). The parameterization involves a two-moment scheme that predicts mixing ratios and number concentrations of cloud droplets and ice. The physical processes that make up the cloud macrophysics suite include cloud fractionation, cloud overlaps, and condensation processes, thus allowing for the simulation of cloud microphysics, radiative transfer, moist turbulent processes, cloud droplet nucleation and activation, and the wet scavenging of aerosols. Aerosols are represented by two modal schemes, the 3-mode modal aerosol scheme (MAM-3; Neale et al., 2010) and the 7-mode modal aerosol scheme (MAM-7). Aerosol modes include accumulation, fine and coarse dust and sea salt, Aitken, and primary carbon (Neale et al., 2010). Parameters included in condensed phase optics are aerosols, hydrometeors, ice crystals and liquid cloud droplets. These parameters are specified for the longwave and shortwave radiation code bands. The Rapid Radiative Transfer Method of GSMs (RRTMG) is used for the longwave and shortwave radiative transfer calculations (Iacono, 2008; Mlawer et al., 1997). The surface fluxes between the atmosphere and the other components (ocean, ice, and land) use a bulk exchange formula that includes heat, moisture and momentum.. Additional details on CAM can be found in Neale et al. (2010) and at http://www.cesm.ucar.edu/models/cesm1.2/cam/.

4.2 2 The Community Land Model

NCAR's Community Land Model version 4 (CLM4) is a descendant of the Land Surface Model and is the land component of CESM1. CLM4 is an improved version of CLM3.5. Major improvements include land surface process representation and understanding, model capabilities, and atmospheric and surface forcing datasets (Oleson et al., 2010). Additional improvements include soil evaporation, snow cover fraction and aging, black carbon and dust deposition, vertical distribution of snow solar energy, soil column and ground water interactions, the burial of vegetation by snow, and aerodynamic parameters for canopies. Biogeophysical

processes for CLM4 include momentum, sensible and latent heat fluxes, heat transfer, canopy hydrology, longwave radiation absorption and emission, solar radiation absorption, transmittance and reflection, vegetation structure, phenology and composition, snow, soil and canopy hydrology, stomatal physiology and photosynthesis, temperature and fluxes of lakes, deposition and fluxes of dust, and a dynamic global vegetation model. CLM4 uses the same horizontal resolution as CAM4. Additional information for CLM4 can be found in Oleson et al. (2010) and at http://www.cesm.ucar.edu/models/cesm1.2/clm/.

4.2.3 The Parallel Ocean Program version 2

The ocean component of CESM1 is a general ocean circulation model, the Parallel Ocean Program version 2 (POP2) from the Los Alamos National Laboratory (LANL) that solves the ocean dynamic three-dimensional primitive equations (Smith et al., 2010). The primitive equations use the Boussinesq and hydrostatic approximations for a thin, stratified fluid (Smith et al., 2010). Improvements in POP2 from POP include surface-pressure formulation of barotropic mode, latitudinal scaling of horizontal diffusion, pressure-averaging, free-surface boundary condition, and redesigning it for parallel computers (Smith et al., 2010). POP2 has a displaced pole grid located over Greenland and a 1.11° horizontal resolution with 60 vertical levels with uniform 10 m spacing for <200 m (Gent et al., 2011). The lower 40 levels are of a lower resolution due to the lack of heat transfer between them. Further details of POP2 can be found in Smith et al. (2010) and Gent et al. (2011) as well as at http://www.cesm.ucar.edu/models/cesm1.2/pop2/.

4.2.4 The Los Alamos Sea Ice Model

The Los Alamos Sea Ice Model (CICE) has an identical horizontal resolution as POP2. The components within CICE include an ice dynamic model, a transport model and a thermodynamic model as well as a ridging parameterization (Hunke et al., 2013). The thermodynamic model calculates the growth rates of ice and snow from vertical turbulent, conductive and radiative fluxes. The ice dynamics model uses the strength of the ice to calculate the velocity field of the ice pack (Hunke et al., 2013). The transport model involves advection of

ice volumes, areal concentration and other variables. More information on CICE can be found in Hunke et al. (2013) and at http://www.cesm.ucar.edu/models/cesm1.0/cice/.

4.2.5 Biogeochemical Elemental Cycling Model

The marine biogeochemical elemental cycling (BEC) model includes multiple phytoplankton functional groups, semi-labile organic matter, sinking particulates, dissolved nutrients (nitrate, ammonium, phosphate, iron, silicate, oxygen, inorganic carbon, and alkalinity), and water column denitrification (Moore et al., 2013). This model simulates ocean biogeochemistry, lower trophic level marine ecosystem dynamics, and the cycling of key elements in the ocean (C, N, P, Fe, Si, and O; Moore et al., 2004). Processes that govern the distribution of variables such as dissolved O_2, nutrients and carbon include biological productivity in the euphotic zone, organic matter export out of the surface-ocean, organic matter remineralization, and the air-sea gas exchange.

4.2.5 Boundary and Initial Conditions

Boundary and initial conditions for the preindustrial 1850 control simulation and for the Younger Dryas are summarized in Table 4-1. Orbital parameters are calculated within CESM1 after Neale et al. (2010) as a function of the calendar year referenced to January 1, 1950 (considered present day); therefore, any date before January 1, 1950 is referenced as before present (BP). The orbital year chosen for the preindustrial simulation was 1990 (Brady et al., 2013). For the Younger Dryas simulations, the orbital year has been set to the equivalent of 13,000 yrs BP. Greenhouse gas concentrations for the preindustrial simulation are 284.7 ppmv, 791.6 ppb, and 275.68 ppb for CO_2, CH_4, and N_2O respectively (Table 4-1; Brady et al., 2013). For the Younger Dryas the greenhouse gas concentrations are simulated at 237.57 ppmv, 632.0 ppbv, and 265.0 ppbv for CO_2, CH_4, and N_2O respectively (Table 3-1 and Table 4-1; Joos and Spahni, 2008).

Incoming solar radiation for preindustrial simulations was set to 1.366×10^6 W m^{-2} and adjusted for the Younger Dryas to 1.365×10^6 W m^{-2} based on calculations for the Last Glacial Maximum (Brady et al., 2013; Otto-Bliesner, Tomas, et al., 2006). Modern ice sheets were used

for the preindustrial simulations. In the Younger Dryas simulations, the ice sheets were adjusted using the 1-degree Ice-5G mask for 13.0ka, which changed the vegetation over most of Canada to ice (Peltier, 2004). Due to a ~65 m fall in sea level at the Younger Dryas (Huang and Tian, 2008), ocean salinity was adjusted from the preindustrial level of 34.73 psu to 35.272 psu (Labeyrie et al., 1992).

Table 4-1 Initial and Boundary Conditions for CESM1.0 Sensitivity Experiments

Initial and Boundary Conditions			
Parameter	Preindustrial	Younger Dryas	Reference
Incoming Solar Radiation	1,365 W m^{-2}	1,364W m^{-2}	Adapted from Otto-Bliesner et al. (2006)
Orbital Parameters			
Year	1990	13.0 ka	
Precession	0.01690	-0.01824	Berger and Loutre (1991)
Eccentricity	0.017236	0.020175	
Obliquity	23.446°	24.093°	
Greenhouse Gases			
CO_2	284.7 ppmv	237.6 ppmv	Preindustrial values from Brady et al. (2013) YD values from Joos and Spahni (2008)
CH_4	791.6 ppbv	632.0 ppbv	
N_2O	275.7 ppbv	265.0 ppbv	
Other Parameters			
Vegetation	Preindustrial	Preindustrial	Brady et al. (2013)
Ice Sheet	Present Day	Ice5G	Peltier (2004)
Ocean Salinity	34.73 psu	35.71 psu	Present day from Labeyrie et al. (1992) Younger Dryas calculated from Chappell et al. (1996) and Siddall et al. (2003)

4.3 Experimental Design

This study aims to reproduce the sensitivity of the climate to Younger Dryas boundary conditions using a moderate-resolution climate model (CESM 1.0.5) integrated over approximately 500 years and initialized from preindustrial initial conditions (Table 5-1). Sensitivity studies involving the change of orbital parameters and of greenhouse gas concentrations will provide more detailed insights on how climate system responds during the Younger Dryas cooling event.

The control experiment with preindustrial conditions (PI) for the year 1850 was initialized from a 1000-year simulation from NCAR, and used the same boundary conditions of Brady et al. (2013; Table 4-2). CESM 1.0.5 was integrated for an additional 100 years after the input of the

initial and boundary conditions. Initial conditions include a solar constant of 1,365 W m^{-2} (Otto-Bliesner et al., 2006), orbital settings are set to year 1990, preindustrial atmospheric greenhouse gas concentration, present-day ice sheet extent, and preindustrial land surface coverage.

In the first sensitivity experiment (hereafter named YDORB) orbital values of 13,000 BP were used, and all other boundary and initial conditions were set to preindustrial values (see Chapter 2; Table 4-1; Table 4-2). This simulation addresses objective 3, how the mean climate and seasonal climate variability in the North Atlantic region (including West Africa) respond to Younger Dryas to preindustrial changes in orbital forcing.

In a second experiment (hereafter named YDCO2) the atmospheric CO_2 concentration was adjusted to Younger Dryas levels and all other boundary and initial conditions were set to preindustrial values (see Chapter 2; Table 5-2). The YDCO2 scenario addresses, how the Younger Dryas climate and the AMOC respond to changes in CO_2 radiative forcing (objective 2).

Table 4-2 Experiment Design and Boundary Conditions for Sensitivity Experiments

Experiment Design and Boundary Conditions						
Simulation	*GHGs*	*Ice Sheet*	*Orbital Year*	*Vegetation cover*	*Aerosol forcing*	*Length of Simulation*
PI	CO_2 = 284.7 ppmv CH_4 = 791.6 ppbv N_2O = 275.68 ppbv	Modern Greenland and Antarctica	1990	Preindustrial	Preindustrial	100 yr
YD	CO_2 = 237.57 ppmv CH_4 = 632.0 ppbv N_2O = 265.00 ppbv	Ice5G	13 ka	PI	PI	500 yr
$YDCO_2$	CO_2 = 237.57 ppmv CH_4 = 791.6 ppbv N_2O = 275.68 ppbv	PI	PI	PI	PI	500 yr
YDORB	CO_2 = 284.7 ppmv CH_4 = 791.6 ppbv N_2O = 275.68 ppbv	PI	13 ka	PI	PI	500 yr

4.4 Results

This chapter is organized as followed. First, differences in the radiative forcing due to orbital and greenhouse gas changes are discussed. Second, the reponse of the mean climate in the North Atlantic region and AMOC to these forcing changes is evaluated. Finally, the seasonal variability of precipitation and surface level wind and pressure are analyzed in regards to the African monsoon circulation. For comparision, key results from the preindustrial simulation are discussed in Appendix A.2.

4.4.1 Difference in radiative forcing changes between orbital and greenhouse gas forcing

Of important note is the difference between the radiative forcing changes brought on by changes in orbital and greenhouse gas forcing. The YD to 1850 change in atmospheric pCO_2 of ~47.13 ppmv (Section 4.1.2) results in a decrease of radiative forcing of ~1.0 W m^{-2} and a subsequent decrease in temperature of ~0.8 °C. Compared to the radiative changes due to orbital forcing changes, the decrease of radiative forcing due to CO_2 is relatively small. The change in summer insolation is >30 W m^{-2} higher than the preindustrial control simulation, and the winter insolation change is ~-30 W m^{-2} lower than the preindstrial simulation (Figure 4-2). Therefore, seasonality for the YDORB simulation is more extreme compared to the YDCO2 simulation.

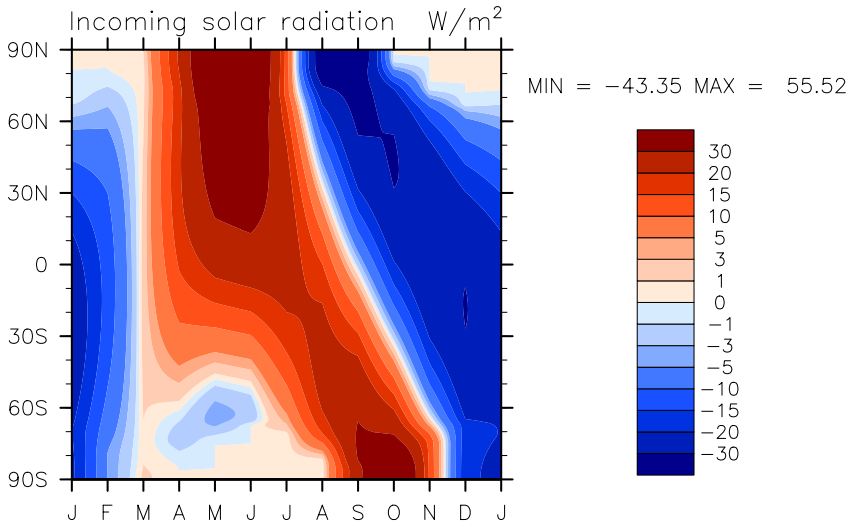

Figure 4-2. Radiative forcing due differences between the YDORB experiment and the preindustrial simulation in W m^{-2} as simulated by CESM1.

4.4.2 Effects of orbital forcing on the Younger Dryas climate

4.4.2.1 Changes in annual variability due to orbital forcing changes – the AMOC

The sea surface temperature (SST) was annually averaged for all experiments and were taken from the Norwegian Sea. The SST for the simulation was approximately 8-10 °C in the northern North Atlantic Ocean, approximately 1.5 °C cooler than the preindustrial simulation (Figure 4-3) whereas the surface air temperature over Summit Station, Greenland (-28°C) was 1.2 °C warmer than the preindustrial simulation (Figure 4-4). The warming over Greenland and the Arctic Ocean is associated to the annual increase in radiation (Figure 4-2), whereas the cooling of the sea surface is linked to changes in the AMOC (see Chapter 3). Annual precipitation rate over the northern North Atlantic Ocean was approximately 4 mm day^{-1}, and increased by 0.3 mm day^{-1} compared to the preindustrial simulation (Figure 4-5), leading to a decline of 0.2 psu in sea surface salinity for the YDORB simulation relative to the preindustrial simulation (Figure 4-6). Sea level pressure is unsubstantially lower over the northern North Atlantic for the YDORB simulation compared to the preindustrial (Figure 4-7).The AMOC strength was approximately 25 Sv, and AMOC strength for the YDORB simulation was approximately 3.5 Sv weaker (Figure 4-8) than the preindustrial simulation due to increased freshwater fluxes by precipitation

(Figure 4-5). These results are supported by the ideal age of water masses. At the depth which North Atlantic Deep Water production occurs, the ideal age of water masses ranged from 250-300 years, which was 30-40 years younger than the preindustrial simulation (Figure 4-9).

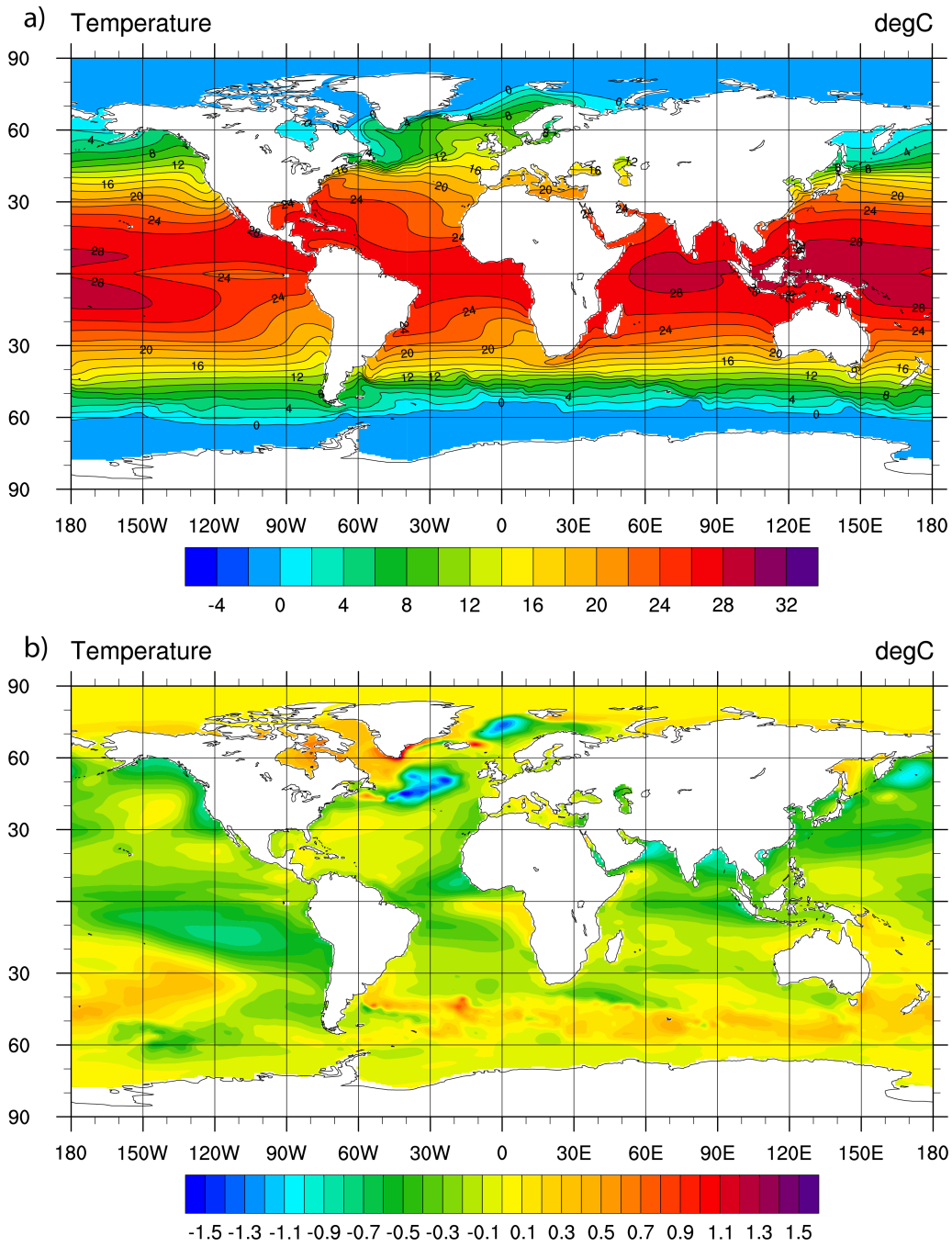

Figure 4-3 Sea surface temperature (°C) simulated by CESM1 for the A) YDORB experiment and B) the difference between the YDORB and preindustrial experiment.

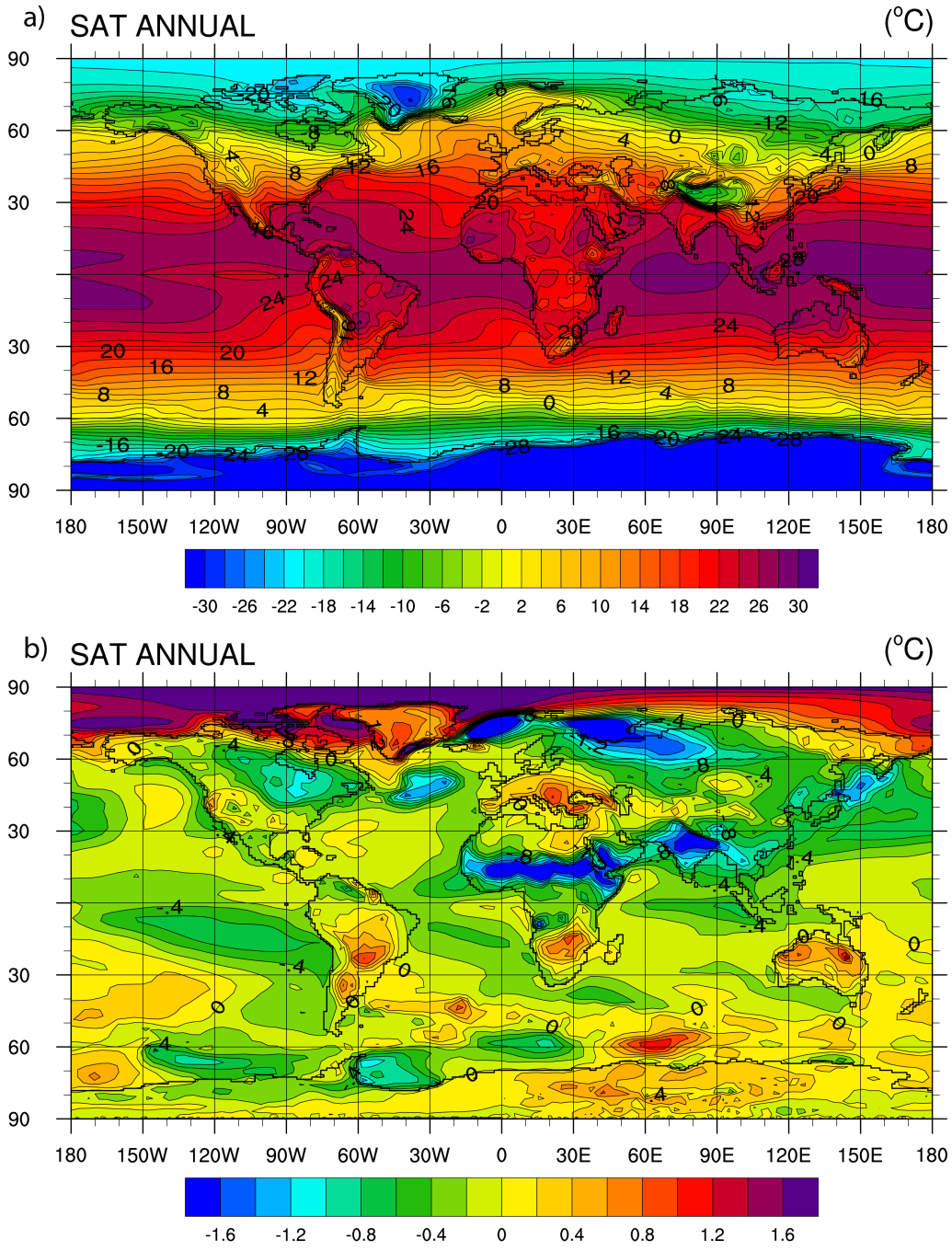

Figure 4-4 Simulated surface air temperature (°C) simulated by CESM1 for the A) YDORB experiment and B) the difference between the YDORB and preindustrial experiment.

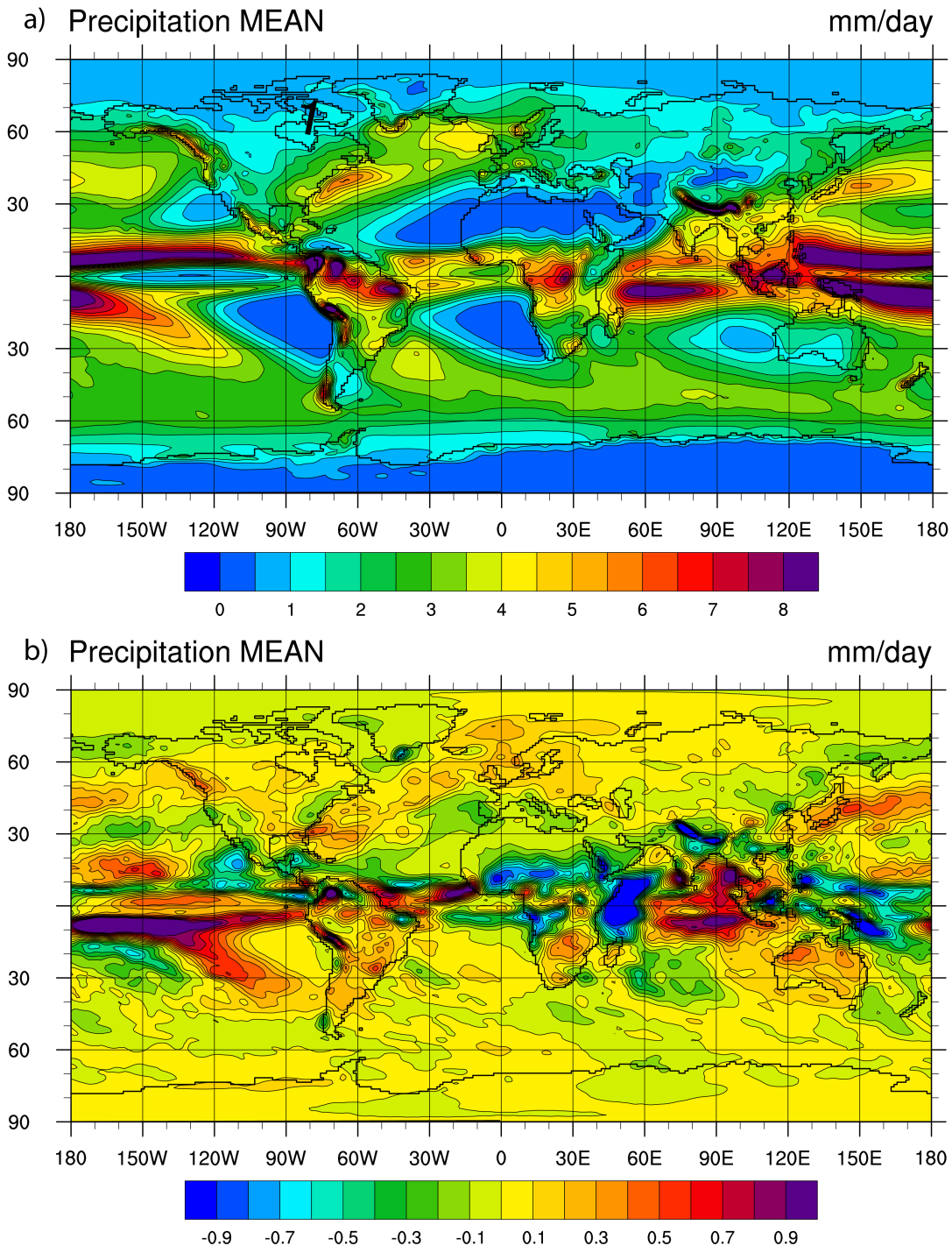

Figure 4-5 Simulated annual precipitation rates for the YDORB experiment in mm day^{-1} from CESM1. A) The YDORB Simulation. B) The difference between the YDORB and preindustrial simulation.

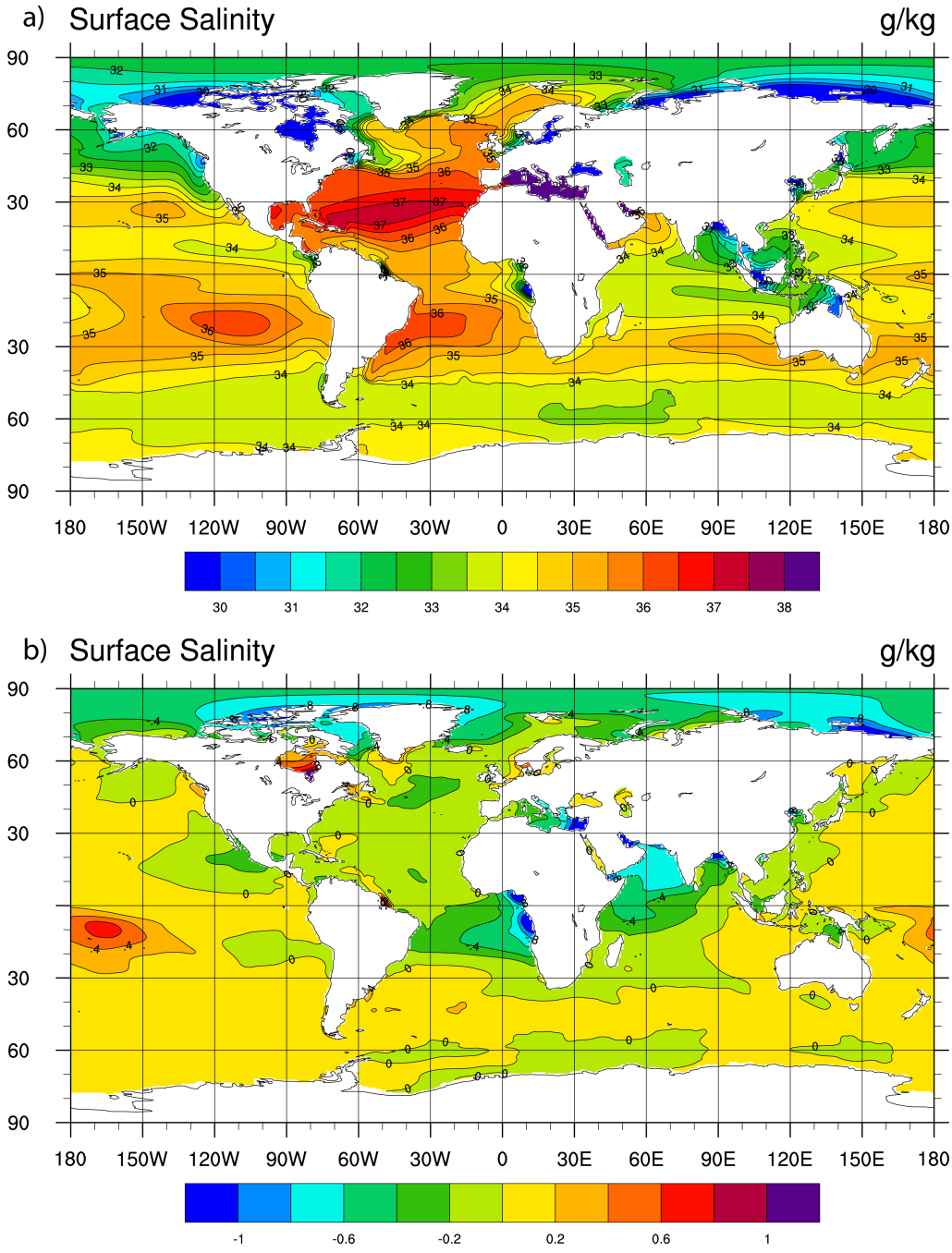

Figure 4-6 Sea surface salinity (psu) simulated by CESM1 for the A) YDORB experiment and B) the difference between the YDORB and preindustrial experiment.

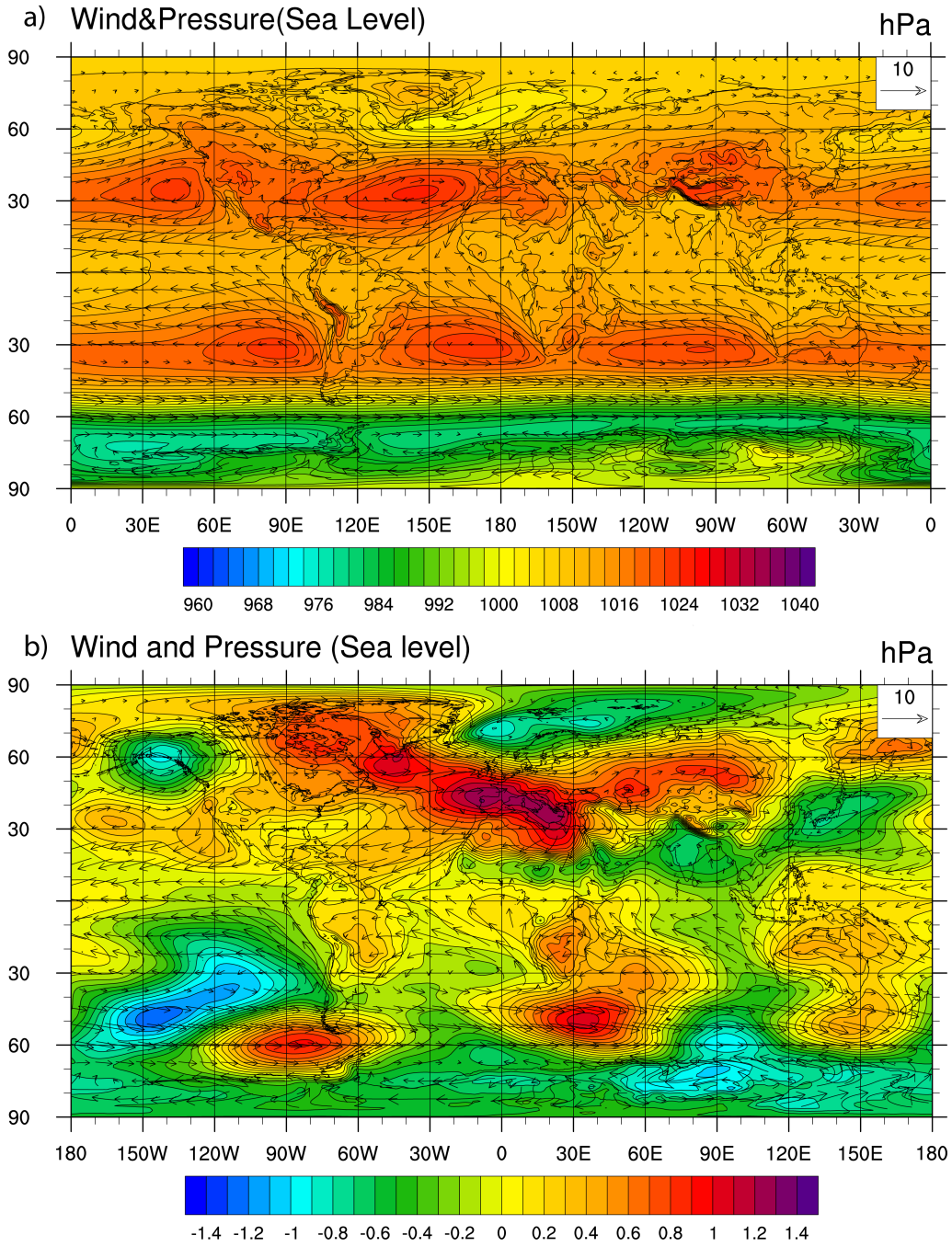

Figure 4-7 Sea level pressure (hPa) and surface level winds (m s^{-1}) simulated by CESM1 for the A) YDORB experiment and B) the difference between the YDORB and preindustrial experiment.

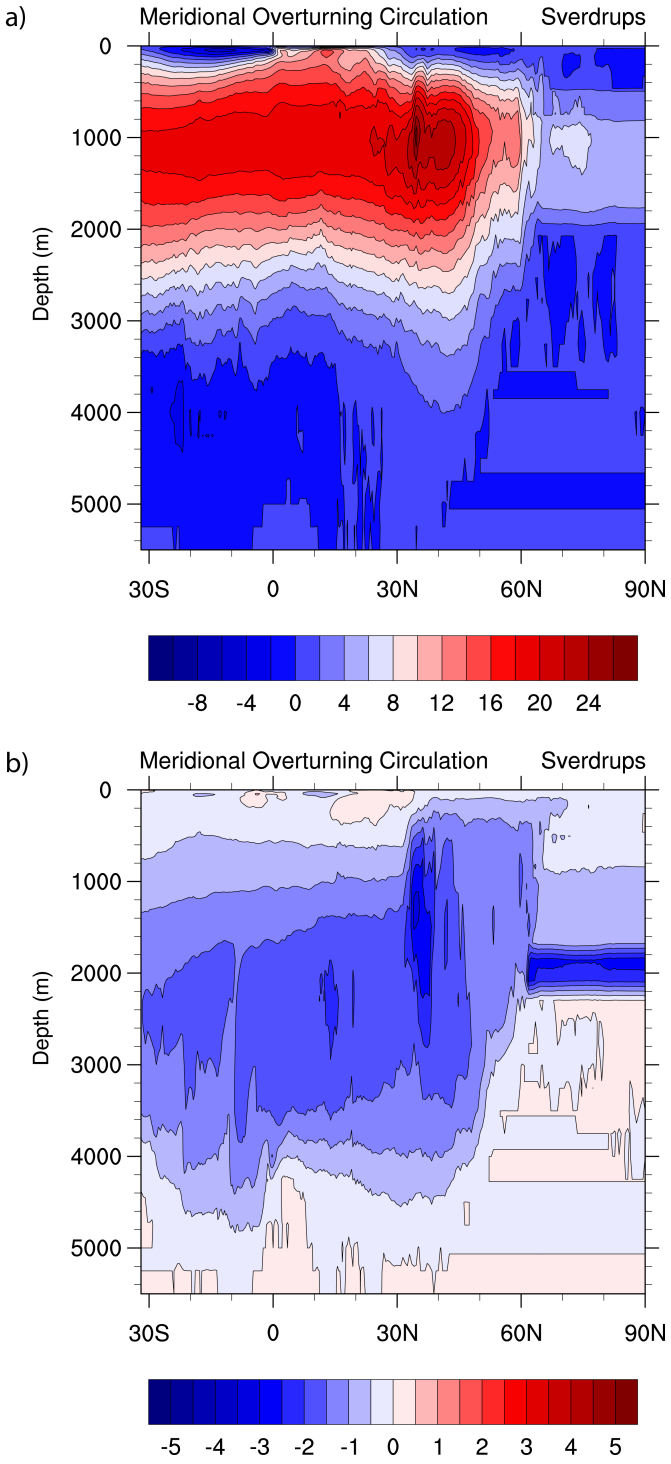

Figure 4-8 Atlantic meridional overturning circulation (Sv) simulated by CESM1 for the A) YDORB experiment and B) the difference between the YDORB and preindustrial experiment.

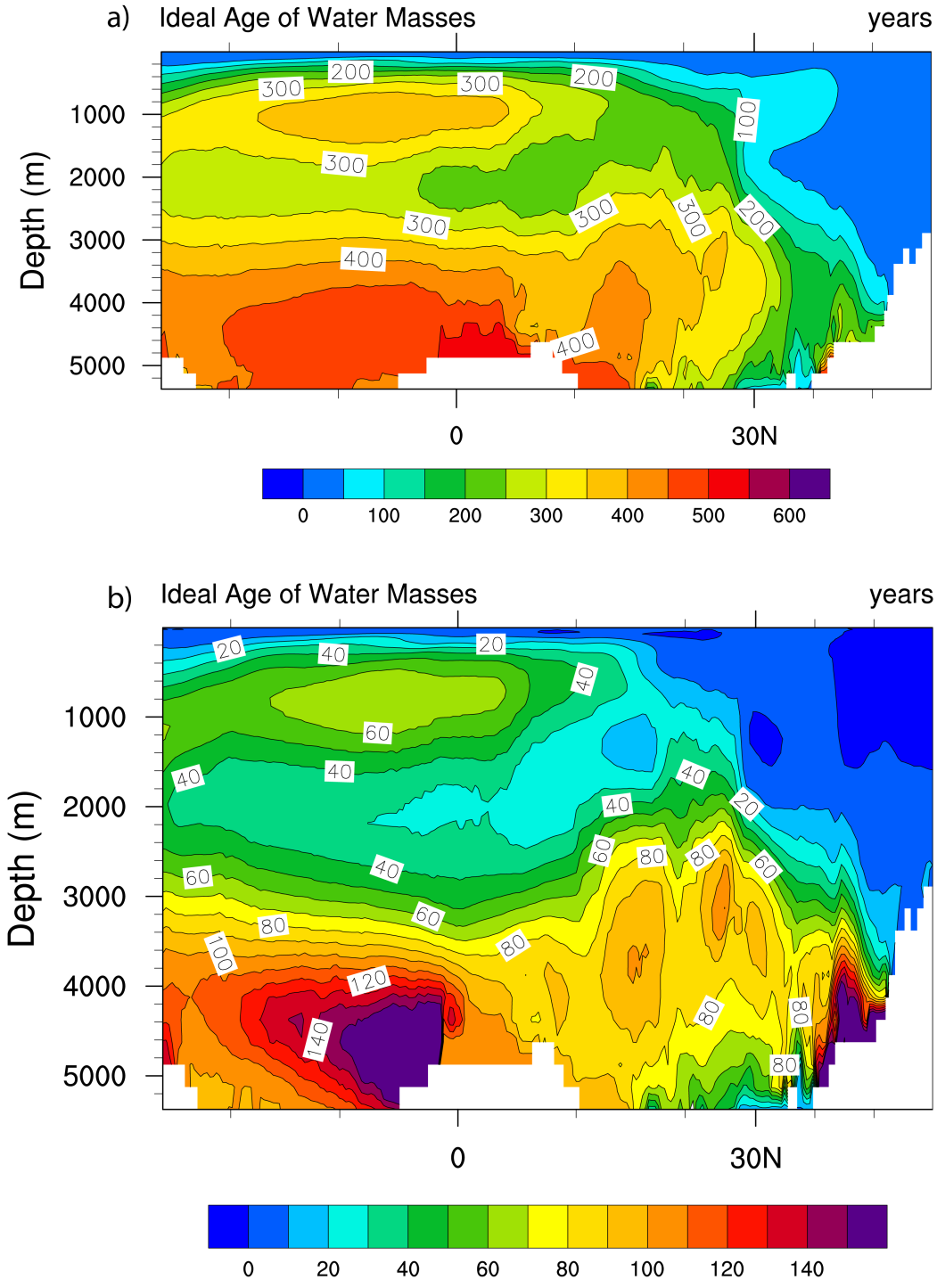

Figure 4-9 Ideal age of water masses (yrs) simulated by CESM1 for the A) YDORB experiment and B) the difference between the YDORB and preindustrial experiment.

4.4.2.2 Changes in seasonal variability due to orbital forcing changes – monsoon circulation

The break up of the climatic zones of Africa will follow that of Griffiths (1972) with one minor change (Figure 4-10). Region IV will be broken into two regions, the one south of region V being the South Tropics, and the region to the north of region V being the North Tropics (Figure 4-10).

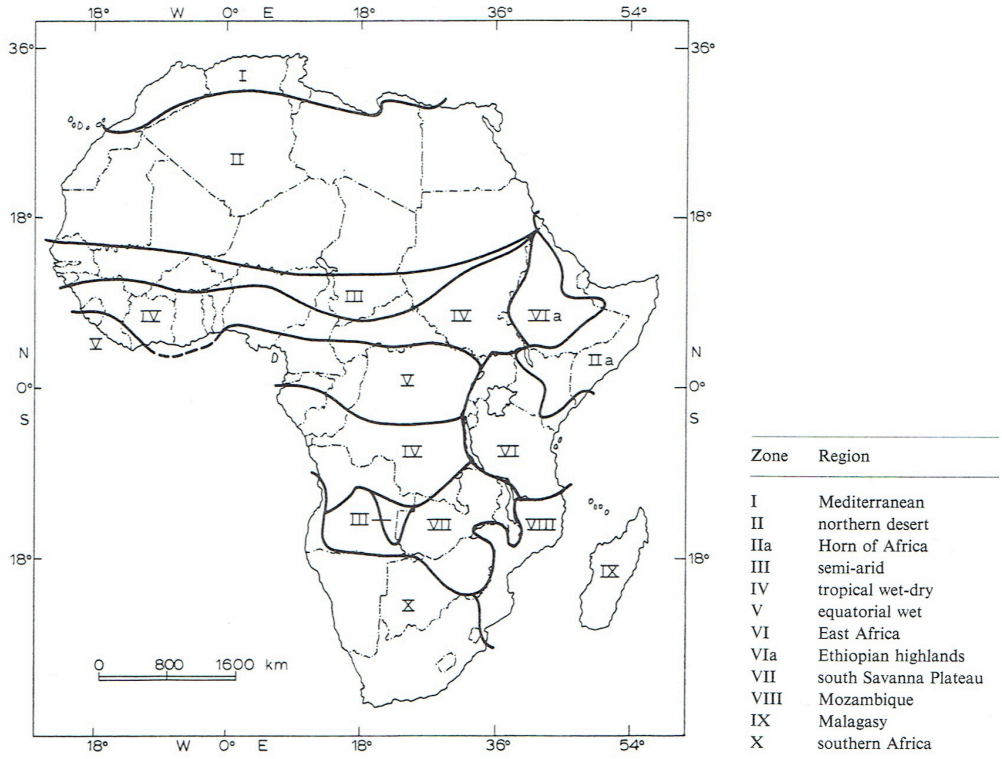

Figure 4-10 Climatic regions of Africa. The focus of this study will be the equatorial regions III, IV, and V. Region IV, for the purpose of this study, has been subdivided into the “northern tropical region” and the “southern tropical region” for the regions north and south of region V respectively. (Figure from Griffiths, 1972)

Winter precipitation in the YDORB scenario over the semi-arid region (Zone III) and northern part of the tropical region (Zone IV) of Africa were both ~1 mm day^{-1} or a decrease of 5 mm day^{-1} and 15 mm day^{-1} compared to the preindustrial simulation, respectively (Figure 4-11 A and C). For the equatorial wet region (Zone V), the winter precipitation was approximately 5 mm day^{-1}, which increased 5 mm day^{-1} compared to the preindustrial simulation (Figure 4-11 A and C). In the southern tropical region, the winter

precipitation rate was approximately 10 mm day^{-1} higher than the preindustrial simulation (Figure 4-11 A and C).

Summer precipitation values in the YDORB scenario for the semi-arid region were approximately 5 mm day^{-1}, which is ~1-2 mm day^{-1} higher than the preindustrial simulation (Figure 4-11 B and D). The northern tropical precipitation in the summer was approximately 15 mm day^{-1}, an increase of 2 mm day^{-1}, and the southern tropical summer precipitation was approximately 1 mm day^{-1} (Figure 4-11 B and D). The equatorial wet region had a summer precipitation rate of approximately 5 mm day^{-1} (Figure 4-11 B and D).

The low-pressure system and the ITCZ, the convergence of the northeast and southeast trade winds, migrates meridionally with the seasons over the central African continent (Griffiths, 1972; Chiang et al., 2002). This low-pressure system is at its northernmost location in the summer, and at its southernmost point in the winter following the seasonal variation in insolation (Waliser and Gautier, 1993; Nicholson, 2013). In the winter, the low-pressure system simulated by the YDORB scenario decreases to 1010 hPa and is located approximately over the southern region of tropical Africa (Figure 4-12 A). This low-pressure system is approximately 2 hPa lower than the pressure system in the preindustrial simulation (Figure 4-12 C). A large high-pressure system is located over the Mediterranean and northern desert regions (Zones I and II), with a surface level pressure of approximately 1030 hPa, which is 16 hPa higher than the system in the preindustrial simulation (Figures 4-12 A and C). The convergence of the equatorial trade winds occurs at approximately 4°S latitude (Figure 4-12 A). In the summer, the low-pressure system migrates northward with the position of the sun, and is situated over the northern desert (Figure 4-12 B). The lowest region of pressure is approximately 1005 hPa, and is ~4 hPa lower than the pressure in the preindustrial simulation (Figure 4-12 B and D). The high-pressure system is located over the wet and southern tropics with a pressure of approximately 1012 hPa (Figure 4-12 B and D). The convergence of the trade winds in the summer is located at ~10°N latitude (Figure 4-12 B).

Surface air temperature over the Mediterranean region during winter is ~5 °C, which is 20 °C cooler than the preindustrial simulation for the same region (Figure 4-13 A and C). During winter, the northern desert in the YDORB scenario is approximately 18°C cooler than the preindustrial simulation, and the semi-arid region is ~7 °C cooler (Figure 4-13 A and C). Surface air temperature continues to

increase the further south over the continent, though all values are ~2-3 °C cooler than the preindustrial values (Figure 4-13 A and C). In the summer, the maximum surface air temperature (~38 °C) occurs over the northern desert, which is 5 °C warmer compare to the preindustrial simulation (Figure 4-13 B and D). The Mediterranean region is ~4 °C warmer than the preindustrial simulation at 29 °C, and the semi-arid region is ~3 °C cooler than the preindustrial at 26 °C (Figure 4-13 B and D). The temperature differences at 10° latitude follow the seasonal pattern of rainfall (Figure 4-13 B and D).

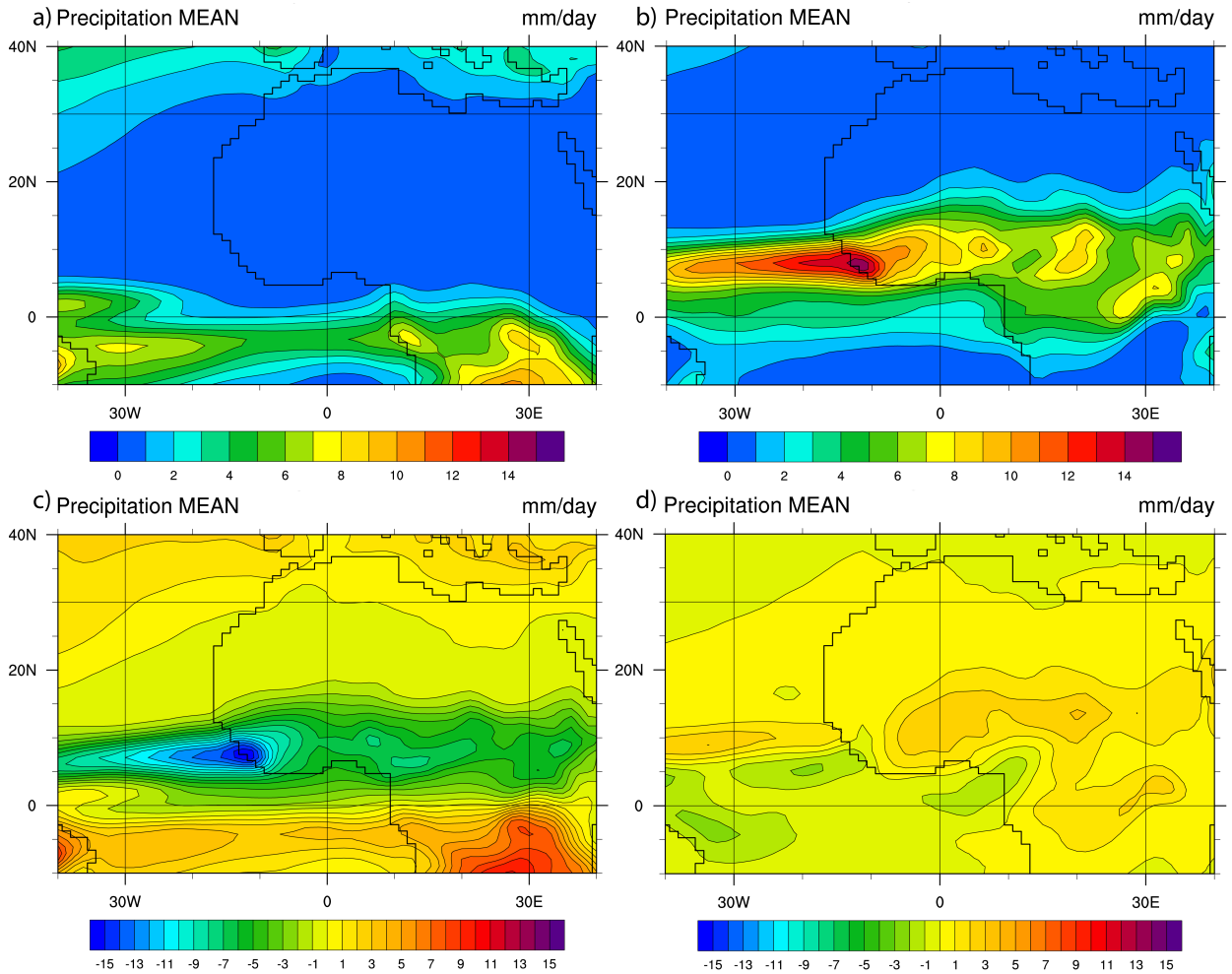

Figure 4-11 Seasonally averaged precipitation in mm day^{-1} simulated by CESM1.0.5 for the region of Africa. A) YDORB values for DJF. B) YDORB values for JJA. C) The difference between the YDORB simulation and Preindustrial control for DJF. D) The difference between the YDORB simulation and Preindustrial control for JJA.

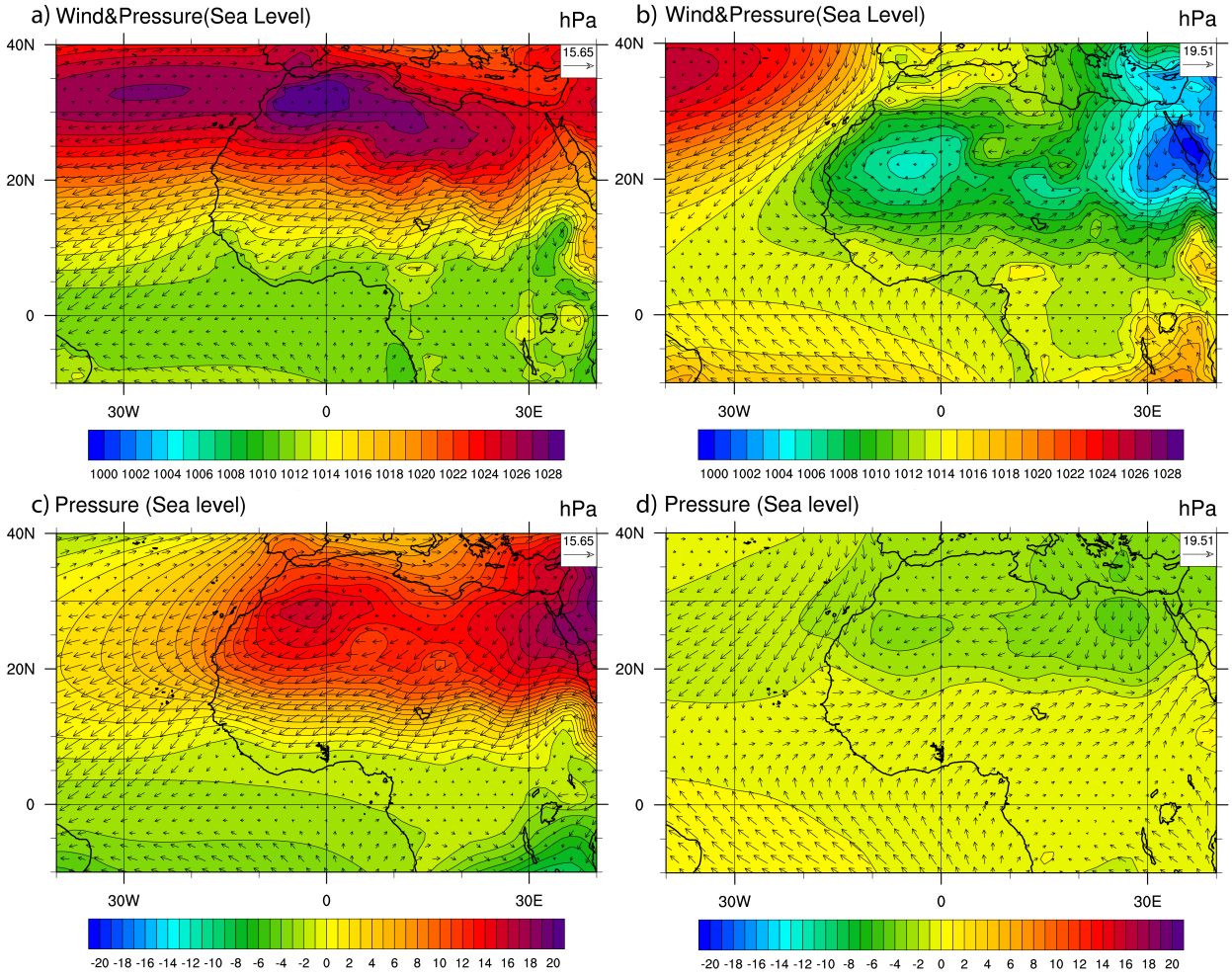

Figure 4-12 Seasonally averaged surface pressure for the region of Africa for the YDORB simulation. A) Winter (DJF). B) Summer (JJA). C) The difference between the YDORB and Preindustrial simulation for winter. D) The difference between the YDORB and Preindustrial simulation for summer.

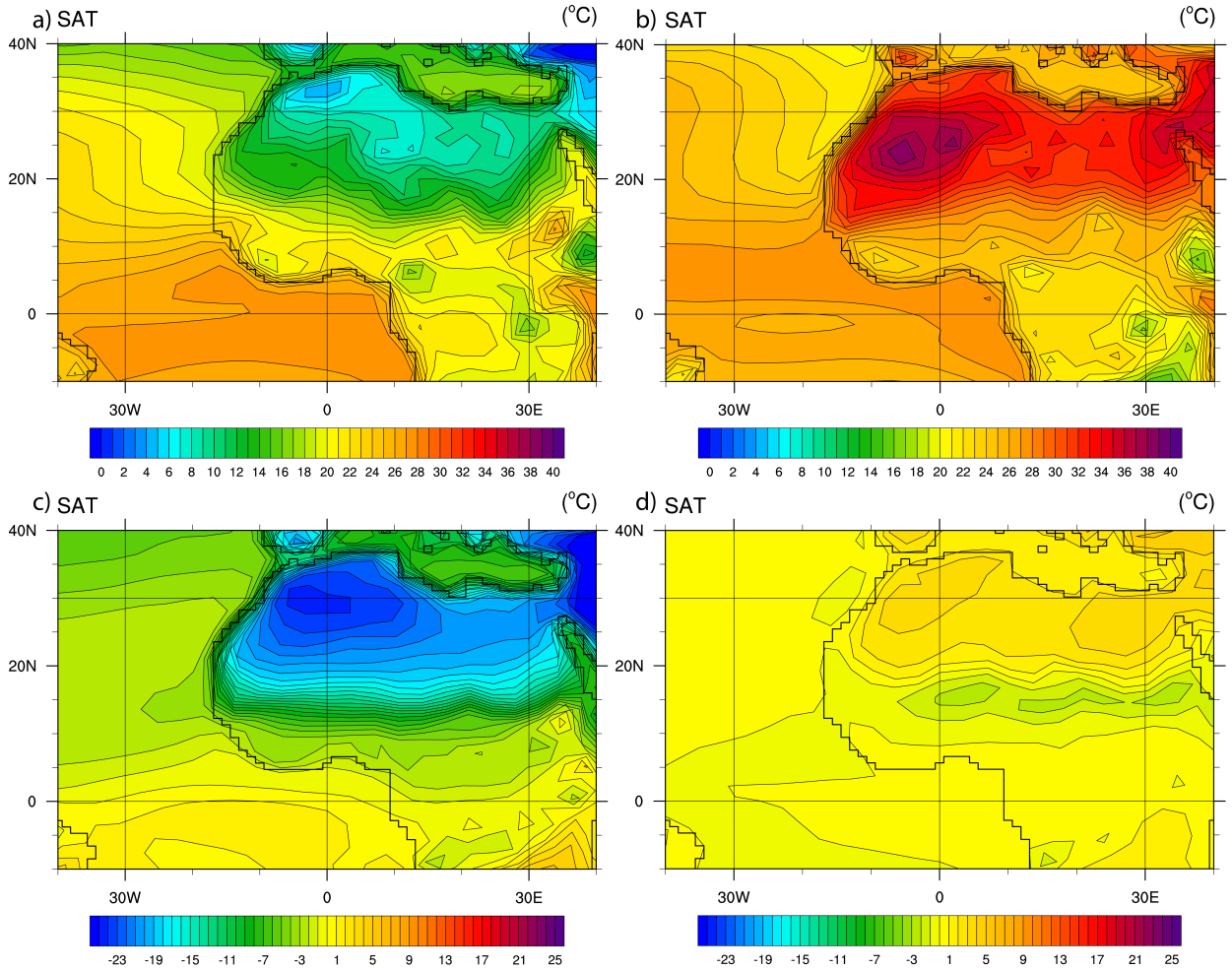

Figure 4-13 Seasonally averaged surface air temperature for the region of Africa for the YDORB simulation. A) Winter (DJF). B) Summer (JJA). C) The difference between the YDORB and Preindustrial simulation for winter. D) The difference between the YDORB and Preindustrial simulation for summer.

4.4.3 Effects of greenhouse gas forcing on the Younger Dryas climate

4.4.3.1 Changes in annual variability due to greenhouse gas forcing changes – the AMOC

In the simulation with YD greenhouse gas forcing, YDCO2 scenario, annually averaged sea surface temperature in the northern North Atlantic Ocean was approximately 13 °C, which is a -1.2 °C departure from the preindustrial control simulation (Figure 4-14). For the YDCO2 simulation, annually averaged surface air temperature over the location of GISP2, Summit Station in Greenland, was approximately -30 °C, which was a 2°C increase relative to the preindustrial simulation (Figure 4-15).

Precipitation over the northern North Atlantic increased of 0.2 mm day^{-1} compared to the preindustrial simulation (Figure 4-16). This increase in freshwater fluxes lead the YDCO2 scenario to an ~0.2 psu fresher salinity (Figure 4-18). The surface pressure over the Greenland Sea was ~1000 hPa, which was ~0.5 hPa lower than the pressure for the same region in the preindustrial simulation (Figure 4-17). The cooling and freshening in the YDCO2 scenarion lead to a decrease in AMOC of 2.5 Sv compared to the preindustrial simulation (Figure 4-19). This slowing of the oceanic circulation is supported by the ideal age of water masses of approximately 200-600 years in the YDCO2 scenario, which is an increase of approximately 10 years compared to the preindustrial simulation (Figure 4-20).

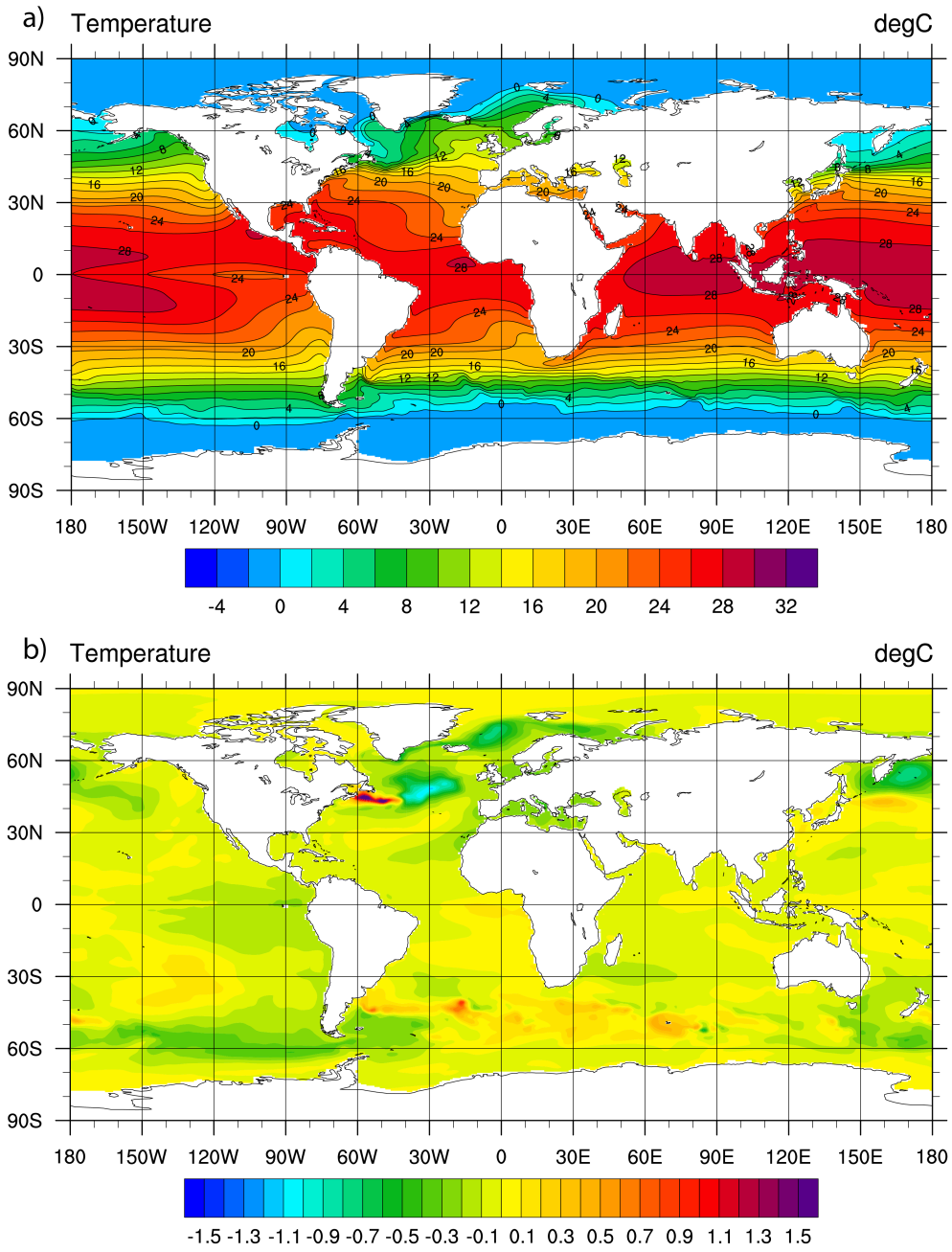

Figure 4-14 Sea surface temperature (°C) simulated by CESM1 for the A) YDCO2 experiment and B) the difference between the YDCO2 and preindustrial experiment.

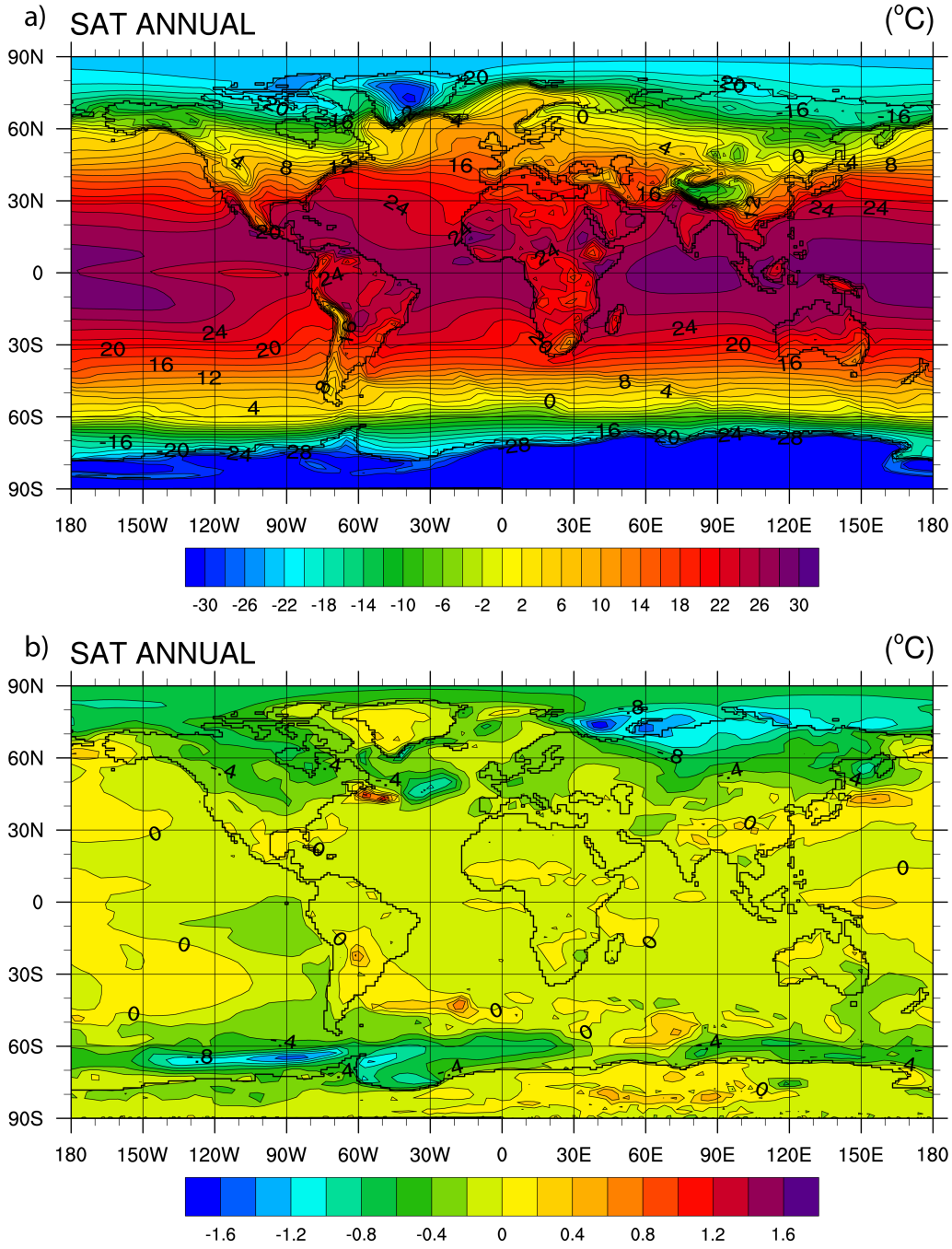

Figure 4-15 Surface air temperature (°C) simulated by CESM1 for the A) YDCO2 experiment and B) the difference between the YDCO2 and preindustrial experiment.

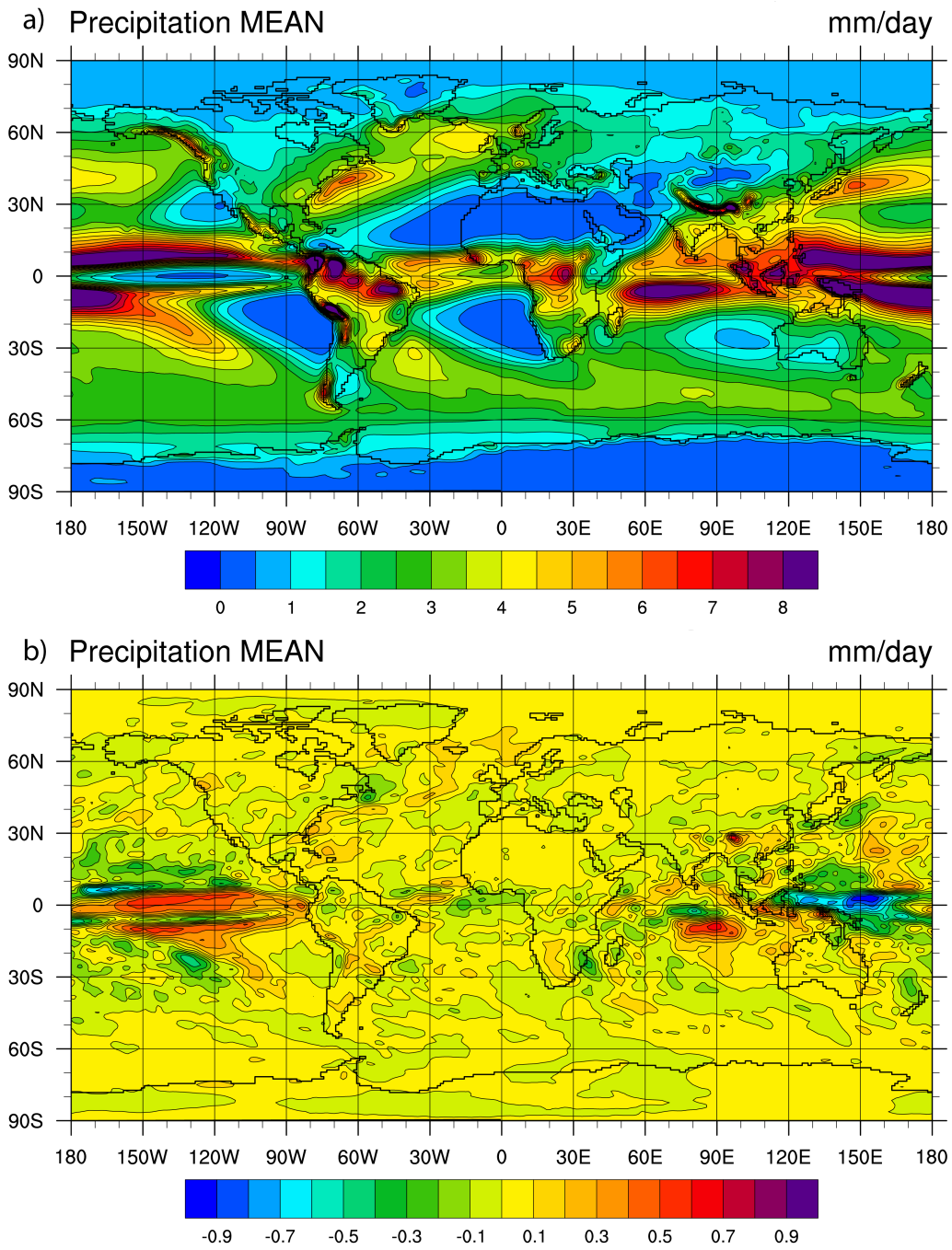

Figure 4-16 Annual precipitation (mm day^{-1}) for simulated by CESM1 for the A) YDCO2 experiment and B) the difference between the YDCO2 and preindustrial experiment.

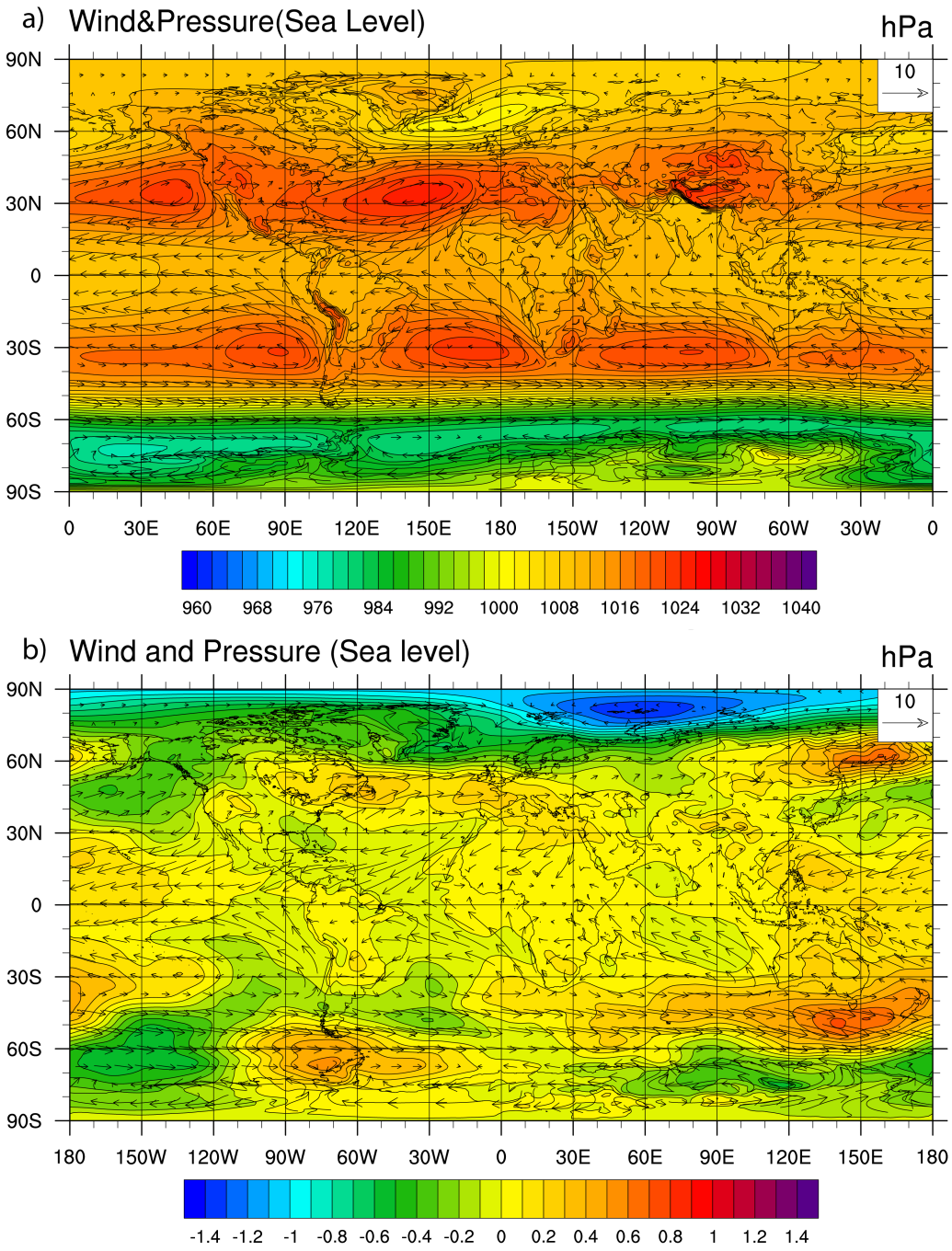

Figure 4-17 Sea level pressure (hPa) and surface level winds (m s^{-1}) simulated by CESM1 for the A) YDCO2 experiment and B) the difference between the YDCO2 and preindustrial simulation.

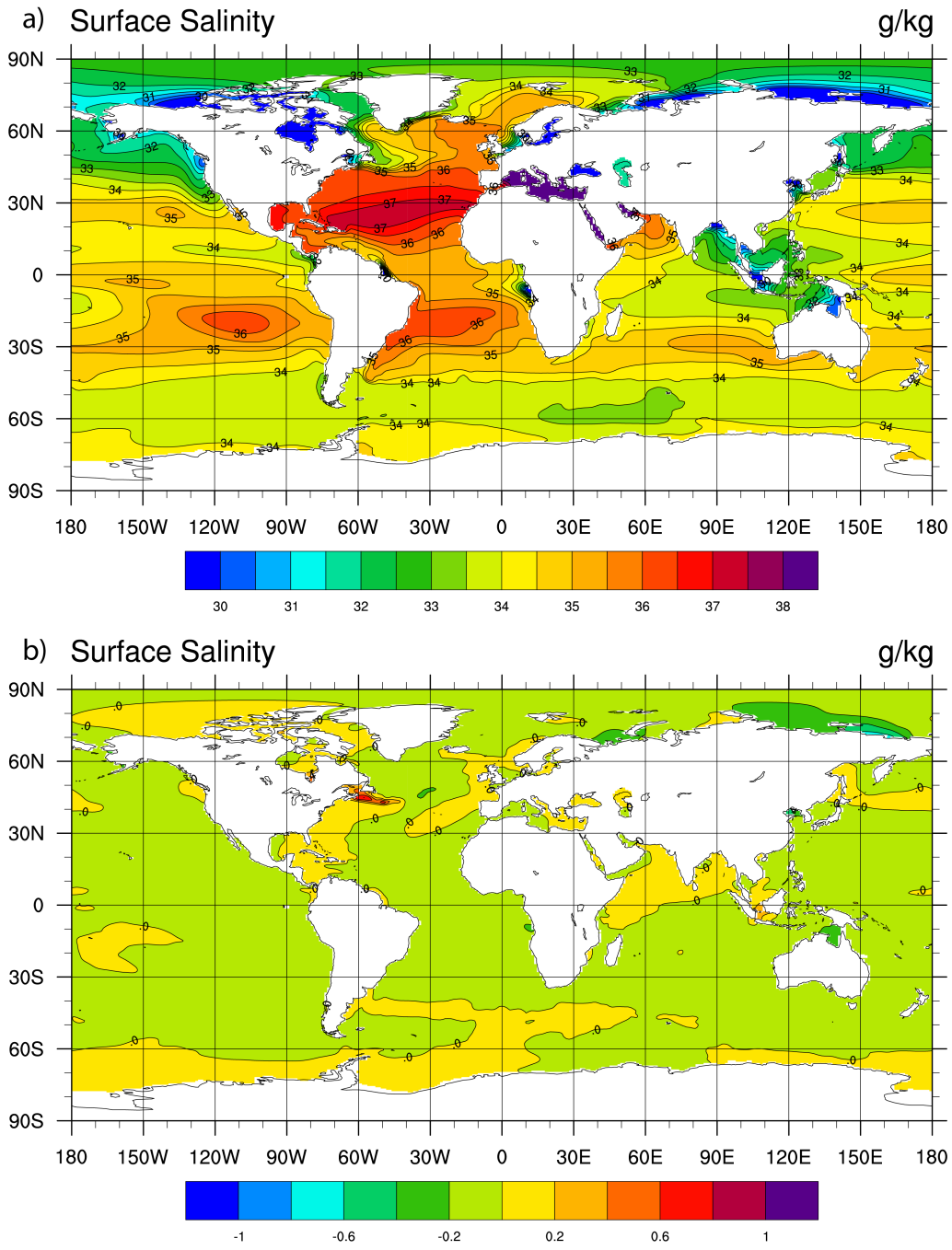

Figure 4-18 Sea surface salinity (psu) simulated by CESM1 for the A) YDCO2 experiment and B) the difference between the YDCO2 and preindustrial experiment.

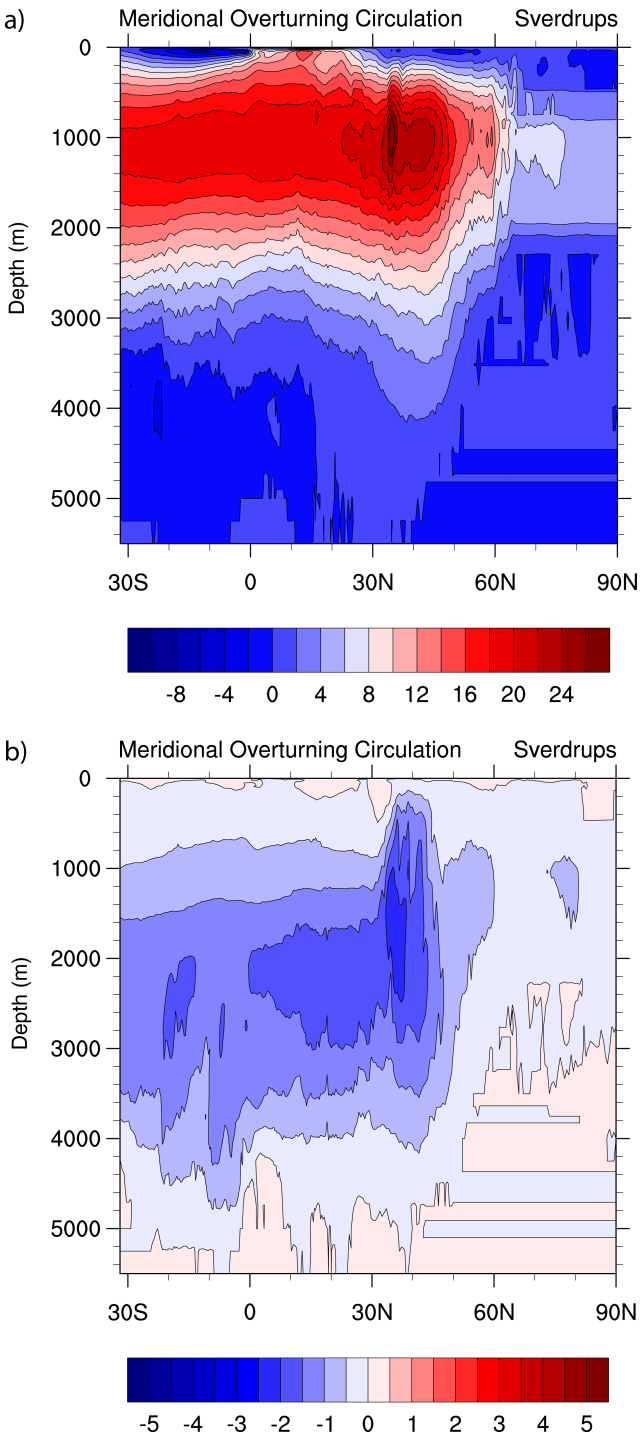

Figure 4-19 Atlantic meridional overturning circulation (Sv) simulated by CESM1 for the A) YDCO2 experiment and B) the difference between the YDCO2 and preindustrial experiment.

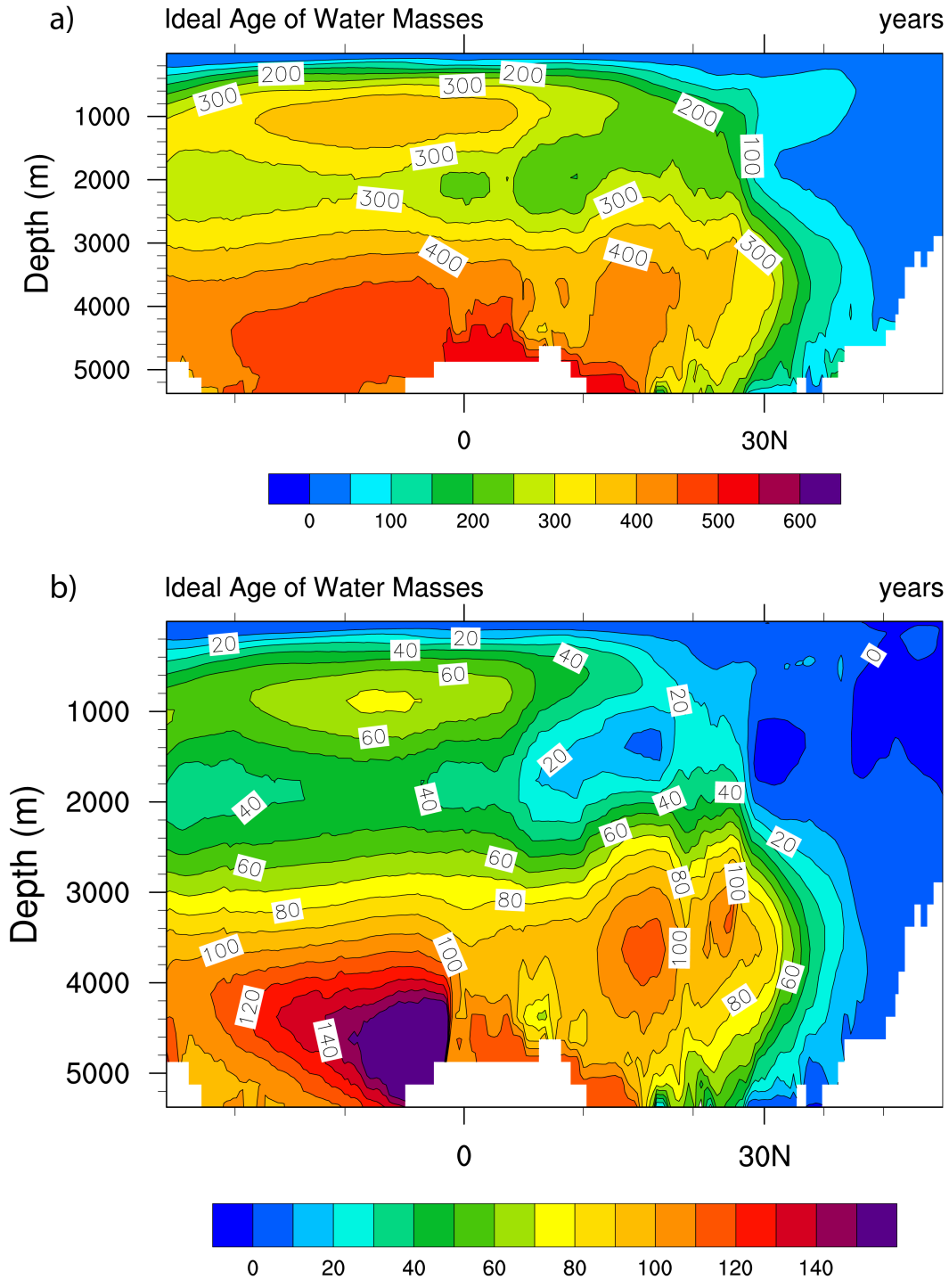

Figure 4-20 Idealized age of water masses (yrs) simulated by CESM1 for the A) YDCO2 experiment and B) the difference between the YDCO2 and preindustrial experiment.

4.4.3.2 Changes in seasonal variability due to greenhouse gas forcing changes – monsoon circulation

Simulated winter precipitation in the YDCO2 scenario over the semi-arid and northern tropical regions is ~0-1 mm day^{-1}, which is approximately 2-3 mm day^{-1} lower than the preindsutrial simulation (Figure 4-21 B and D). Winter precipitation increases southward over the African continent, with the northern tropical region averaging 5 mm day^{-1}, and the southern tropical averging 7-8 mm day^{-1} (Figure 4-21 B and D). This is an increase of 3 mm day^{-1} and 5 mm day^{-1} respectively (Figure 4-21 B and D). Precipitation migrates northward in the summer months with the low pressure systems and the ITCZ. Maximum rainfall for Africa occurrs over the northern tropical region (Figure 4-21 A). Maximum rainfall for this region is ~13 mm day^{-1} near the coast, which is 12 mm day^{-1} less than in the preindustrial simulation (Figure 4-21 A and C). The precipitation over the equatorial wet, and southern tropical regions average ~3 mm day^{-1}, whereas rainfall over the semi-arid region is ~1-2 mm day^{-1} (Figure 4-21 A and C). The rainfall over the equatorial wet region is 3 mm day^{-1} higher than in the preindustrial simulation, and 8 mm day^{-1} higher over the sourthern tropical region (Figure 4-21 A and C).

During the winter, the high-pressure system in the YDCO2 scenario is located over the Mediterranean, northern desert, and semi-arid regions, with the highest pressure of 1024 hPa located over the latter two (Figure 4-22 A). This high in the YDCO2 scenario is ~8 hPa higher than the preindustrial simulation (Figure 4-22 C). The low is located over the equatorial wet and the southern tropics regions with minimum pressure of 1010 hPa, which is ~2 hPa lower than the preindustrial simulation (Figure 4-22 A and C). The convergence of the northern and southern equatorial trade winds during the winter is situated at approximately 1°N latitude (Figure 4-22 A). In the summer, the high pressure system is located over the Mediterranean at 1020 hPa, which is 6 hPa higher than the preindustrial simulation (Figure 4-22 B and D). The lowest part of the low pressure system is over the northern desert, and is 1008 hPa, 4 hpa higher than the preindustrial pressure system (Figure 4-22 B and D). The ITCZ during the summer is positioned at ~7°N (Figure 4-22 B).

During the winter, the surface air temperature of 20-23 °C simulated by the YDCO2 scenario is comparable uniform between the northern desert to the southern tropical region, which is approximately 2-4 °C cooler than the preindustrial simulation (Figure 4-23 A and C). The northern desert, however, is 7

°C cooler than the preindustrial simulation. The Mediterranean region in the YDCO2 scenario is ~16 °C cooler (~10 °C) compared to the preindustrial simulation (Figure 4-23 A and C). The northern desert, the region with the maximum summer temperatures of 34 °C, is 10 °C cooler than the preindustrial simulation (Figure 4-23 B and D). All other regions have a temperature of ~24 °C, which is ~4 °C cooler than the preindustrial values for the Mediterranean and semi-arid regions (Figure 4-23 B and D). At 10 °N, the temperature is ~2 °C cooler, and in the equatorial wet and at 10 °S, the temperature is 1 °C warmer than the preindustrial values (Figure 4-23 D).

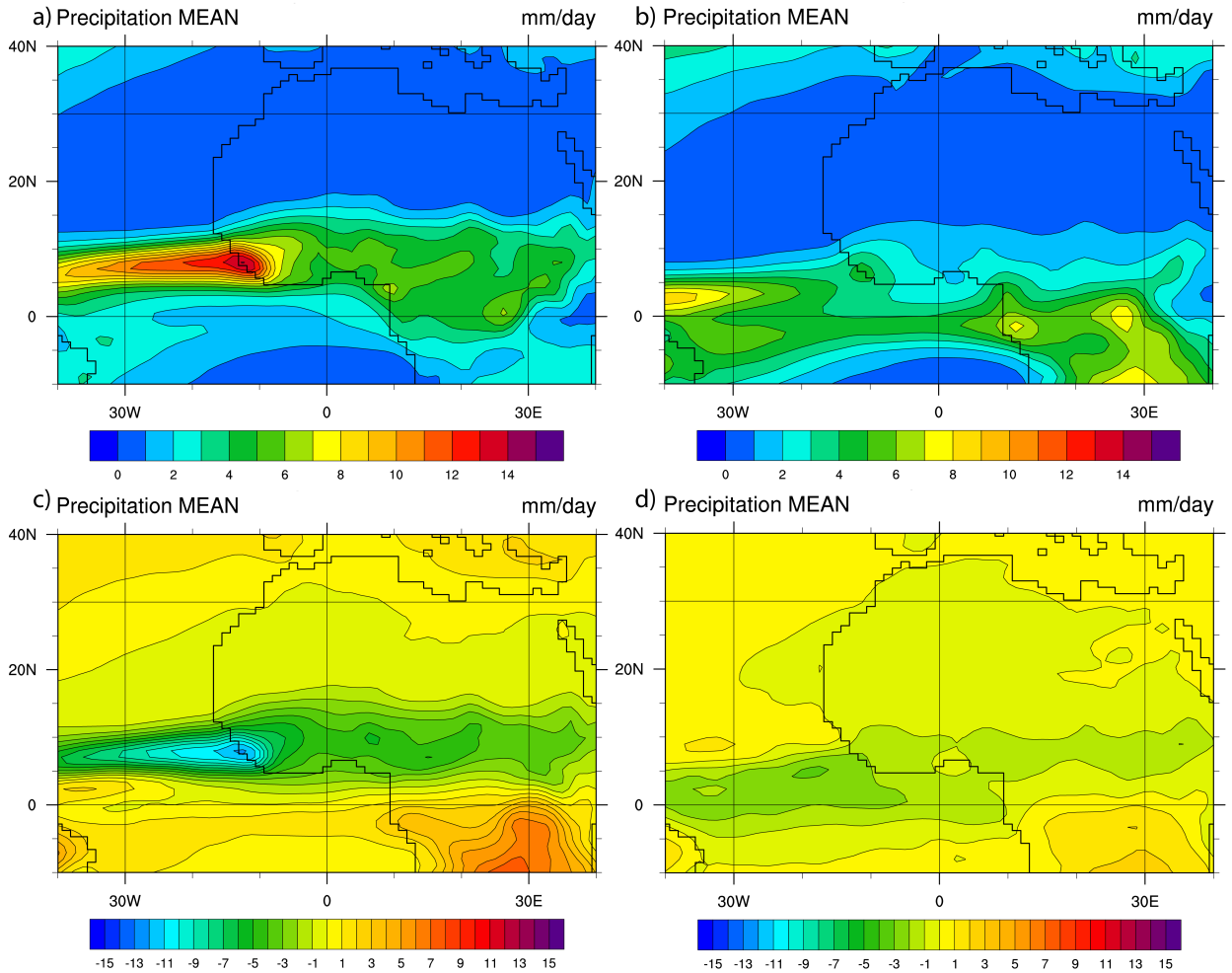

Figure 4-21 Seasonally averaged precipitation for Africa. A) YDCO2 scenario for summer (JJA). B) YDCO2 scenario for winter (DJF). C) The difference between the YDCO2 and preindustrial control simulation for summer. D) The difference between the YDCO2 and Preindustrial control simulation for winter.

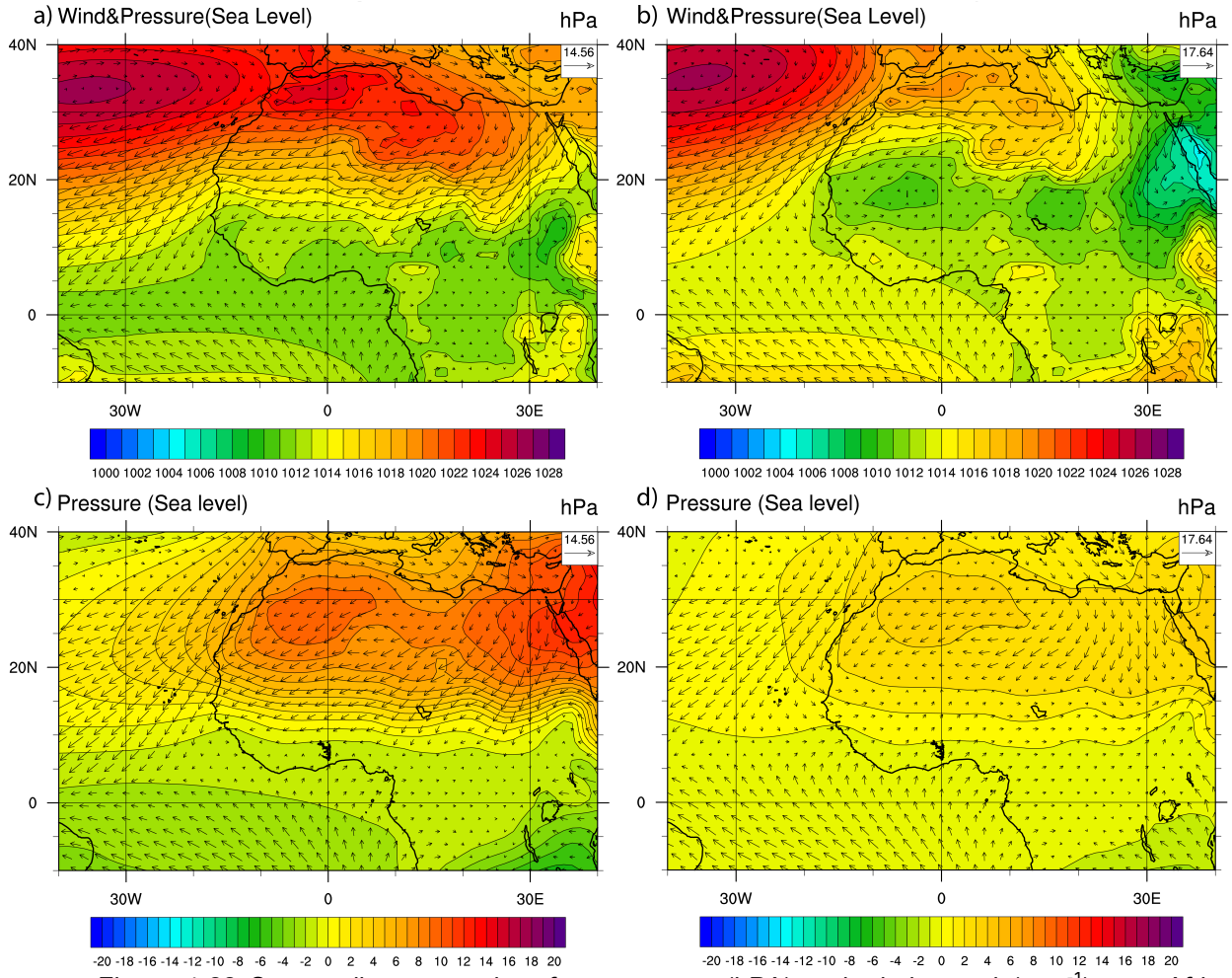

Figure 4-22 Seasonally averaged surface pressure (hPA) and wind speed (m s^{-1}) over Africa simulated by CESM1.0.5 for A) YDCO2 scenario for winter (DJF), B) YDCO2 scenario for summer (JJA), C) the difference between the YDCO2 and preindustrial control simulation for winter, and D) the difference between the YDCO2 and preindustrial control simulation for summer.

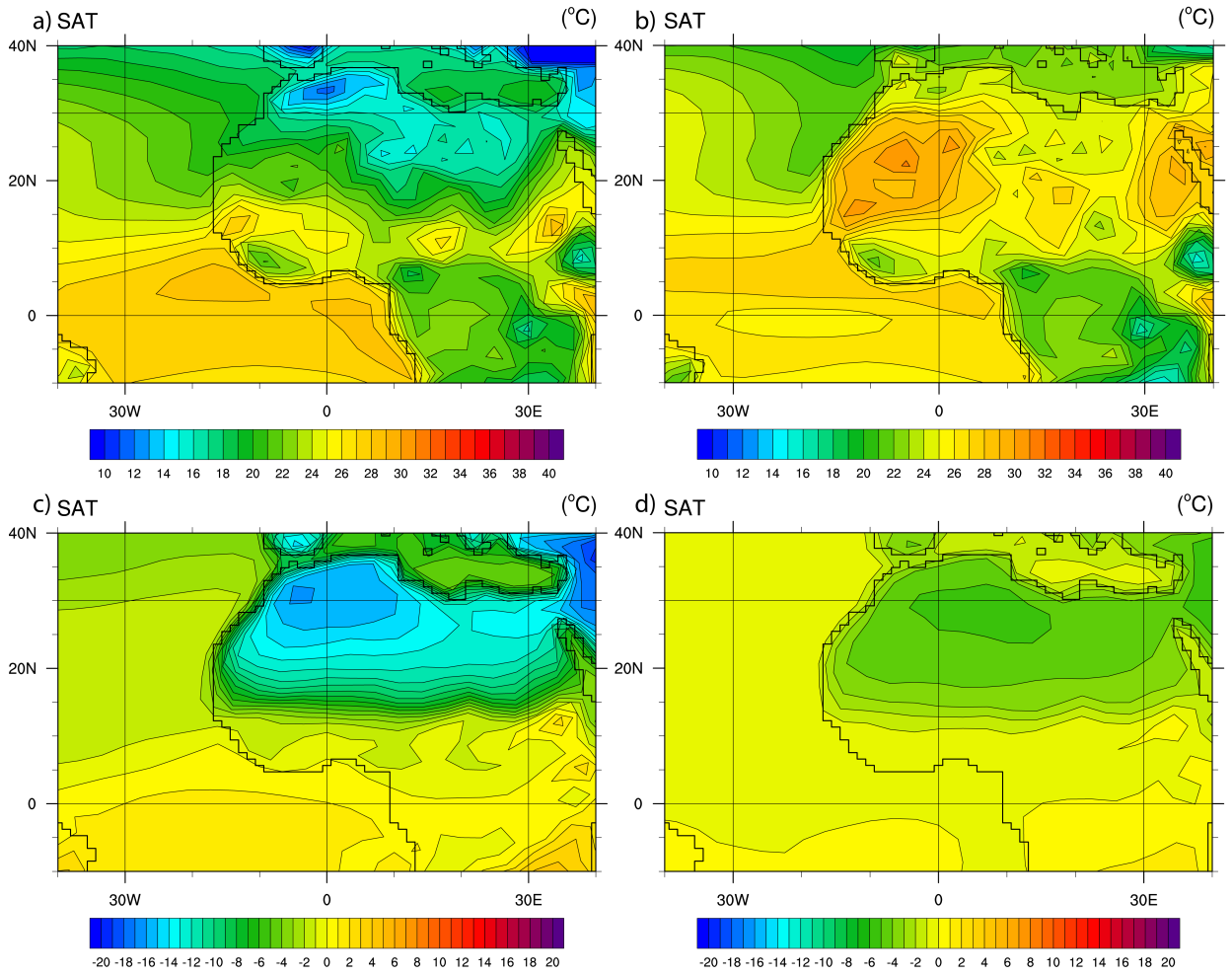

Figure 4-23 Seasonally averaged surface air temperature (°C) over Africa simulated by CESM1.0.5 for A) YDCO2 scenario for winter (DJF), B) YDCO2 scenario for summer (JJA), C) the difference between the YDCO2 and preindustrial control simulation for winter, and D) the difference between the YDCO2 and preindustrial control simulation for summer

4.5 Discussion

4.5.1 Atlantic Meridional Overturning Circulation

In this section, several parameters and their feedbacks are evaluated to determine the effects of orbital and CO_2 parameters on the AMOC. The primary mechanisms that need to be considered are climate change due to freshwater fluxes (e.g. precipitation minus evaporation, river runoff, and melting

and freezing of sea ice), and climate change due to heat fluxes (related to incoming shortwave radiation, outgoing longwave radiation, latent heat fluxes and sensible heat fluxes) that effect both the surface air temperature and sea surface temperature. Freshwater flux into the ocean increases with precipitation if evaporation and the other flux components remains the same. As the surface water masses begin to freshen by enhanced rainfall, the vertical density gradient in the ocean becomes larger, and the water masses of the ocean begin to stratify (Rooth, 1982; Broecker and Denton, 1989) thus reducing the AMOC (Chapter 1). Increasing the surface air temperature and the sea surface temperature also affects the AMOC as a warming of the surface ocean causes the density to decrease and the water masses stratify. With an increase in radiative forcing, the amount of incoming solar radiation that reaches the surface is higher, and therefore the temperature is increased (Berger, 1988). As noted before, changes in radiative forcing due to orbital forcing changes is much higher than the changes due to greenhouse gas forcing (Section 4.4.1). This means that the climatic changes and changes in the AMOC for the simulation with orbital changes should be greater than the simulation with greenhouse gas forcing.

Sea surface temperature of ~10°C - 11 °C for the YDORB simulation around Greenland, and is cooled ~2°C more compared to the YDCO2 simulation. Oxygen isotope proxy reconstructions from the GISP2 ice core reveal that the sea surface temperature is approximately 18 °C at the onset of the YD and then ~8 °C at the termination (McManus et al., 2004). Thus, it appears that the YDCO2 and YDORB simulation both underestimate the cooling at the termination. Other climate simulations in which only orbital parameters were altered predicted an even lower cooling in the sea surface temperature (~1 °C) (Fischer and Jungclaus, 2010). This study is also agreeable with Rind et al., (1986) that during the YD the effects orbital parameters on the North Atlantic sea surface temperature is small. The surface air temperature increased in both simulations compared to the preindustrial values by approximately 1 °C, which in no way agrees with the proposed 15 °C cooling associated with the onset of the YD as inferred by Severinghaus et al. (1998). These differences are likely attributed to the counteracting affect of greenhouse gas forcing and orbital forcing on the sea surface temperature (see section 4.4.1). Surface air temperature, when compared to a Holocene orbital forcing sensitivity experiment, is to be expected warmer (Fischer and Jungclaus, 2010). The sensitivity of Greenland surface temperature to orbital

changes, as suggested by this study, is agreeable with an Eemian climate simulation (~125 ka; Lohmann and J. Lorenz, 2007) and with a CESM1 climate scenario for Last Glacial Maximum (~21 ka; Brady et al., 2013). For the Younger Dryas, the seasonal changes in temperature due to orbital forcing appear to be more substantial than the changes in temperature due to relatively small changes in greenhouse gas concentration and associated forcing.

Precipitation increases by 8.16% for YDORB and by 6.25% for YDCO2 simulations in the North Atlantic Ocean near Greenland compared to the preindustrial reference simulation. The proxy reconstructions indicate that the storminess of the YD was decreased for this region, and with both simulations increasing, they do not match the proxy reconstructions (Alley, 2000). The stronger increase in the YDORB is likely due to the warmer of the YD surface air temperature in the Labrador Sea, which is seen in both simulations, but is more pronounced in the YDORB simulation than the YDCO2 simulation. Though the results do not agree with the proxy reconstructions for the YD, they do agree with Holocene orbital sensitivity experiments in which the precipitation increase over the Norwegian seas (Fischer and Jungclaus, 2010). The warmer the SST in this region could stimulate extratropical storm systems and more precipitation (Eisenman et al., 2009). Compared to the preindustrial simulation, sea surface salinity is slightly decreased in both the YDCO2 and YDORB simulations with sea surface salinity at approximately 36 psu and 35.5 psu. The proxy reconstructions indicate that the sea surface salinity was much lower during the YD than the modeled results with a range of 27.5-30 psu (Schmidt et al., 2004; Clark et al., 2001; DeVernal et al., 1996; Ebbesen and Hald, 2004). It should be noted that at ~30 m depth, the salinity decreases by 0.02 psu for the YDORB simulation, whereas changes relative to the preindustrial experiment in the YDCO2 are not substantial.

The transport of water masses associated to the AMOC in YDORB is decreased compared to the preindustrial experiment, which is supported by changes in the idealized age tracer. The AMOC in YDORB scenario decreased by approximately -3.5 Sv, while the AMOC in the YDCO2 scenario decreased by -2.5 Sv. However, the strength of the AMOC during the YD inferred from paleoproxies (McManus et al., 2004; Gherardi et al., 2005) was substantially weaker at 7-10 Sv than the transport of ~24 Sv simulated by both the YDORB and YDCO2 experiments. For the Holocene, orbital forcing caused

a decrease of the AMOC by approximately 1.5 Sv, which is not as a strong response as the AMOC weakening in this study (Fischer and Jungclaus, 2010). In a greenhouse gas sensitivity experiment for the Last Glacial Maximum, the AMOC strength for the Northern North Atlantic was approximately 23.5 Sv, which is in very close agreement with the results presented here (Brady et al., 2013). Gildor and Tziperman (2000) predicted also small changes (2.5 Sv) in the AMOC due to changes in orbital forcing. Increased precipitation over the Northern North Atlantic Ocean likely caused a stratification of the surface ocean because of the increased input of freshwater into the region, as well as warming of the sea surface and associated poleward retreat of sea ice margin. Thus YD to preindustrial changes in the AMOC may be more affected by the seasonal radiative forcing changes by orbital parameters and associated changes in freshwater fluxes than by the relative low changes in CO_2 radiative forcing (Figure 4-1). However, the sensitivity of climate change by both orbital and CO_2 forcing alone are too small to be consistent with the observed climate state during the YD indicating that additional mechanisms are required. The addition of an ice sheet and freshwater forcing may be of importance to force the system rapidly into the Younger Dryas cooling event.

4.5.2 West African Monsoon

The intensity of the West African monsoon is affected by, among other radiative forcings, both changes in orbital parameters and changes in atmospheric pCO_2. These changes in the radiative forcing affect regional temperature, precipitation, and wind and pressure patterns. Largest annual surface air temperature is simulated in the YDORB and YDCO2 scenario over the semi-arid and northern tropical regions. In the YDCO2 experiment, there is northward extension of surface warming into the northern desert region. In contrast to the YDORB experiment, the YDCO2 experiment simulates a ~4 °C warming for the equatorial wet and southern tropics region.

The YDORB simulation indicates a more extreme seasonality because of more extreme seasonal insolation in which the summer season is hotter and winter season is colder. The same trend is seen for the YDCO2 simulation, though the amplitude of increased seasonality is less weak compared to the YDORB simulation. For example, the areas of maximum and minimum temperature for the YDORB

simulation are located in the Mediterranean and northern African desert regions for both the winter and the summer. In these regions, the maximum temperature in the summer is ~39 °C, whereas the minimum temperature in the winter is ~4 °C. Compared to the preindustrial simulation, this is an increase of temperature of ~5 °C for the summer and a decrease of ~23 °C for the winter. Temperature extremes for the YDCO2 simulation are located in the same regions discussed above, however the changes are substantially lower. For example, the temperature for the summer is actually decreased over the entire Mediterranean and northern African desert regions for the summer by ~8 °C, and in the winter, the temperature is decreased further by ~16 °C.

Changes in gradients in the air surface temperature over the African continent effects surface pressure systems, with warmer air masses leading to lower surface pressure and cooler air masses leading to higher surface pressures. For example, in the YDORB simulation the decrease in surface air temperature over the Mediterranean and northern desert regions of Africa in the winter months leads to a high-pressure system over the region with maximum pressures in excess of 1028 hPa. The higher temperatures in the equatorial wet and southern tropics regions lead to a formation of a 1008 hPa low. In the summer, the higher temperatures over the Mediterranean and northern desert regions produces a weak 1005 hPa low, while cooling occurs more southward and thus intensifies the high-pressure system. The same pattern is simulated by YDCO2 experiment, but not as extreme as in the YDORB simulation. The high-pressure system that is over the Mediterranean and Northern desert in the winter has a maximum pressure of 1022 hPa, and the low-pressure system is approximately 1010 hPa. In the summer, the low-pressure system over the northern desert region has a minimum pressure of 1010 hPa, and the high-pressure system further south has a maximum of ~1019 hPa.

The shift in surface air temperature gradients and pressure systems affects the convergence of the trade winds at the ITCZ and associated of pattern of precipitation. In the YDORB simulation there are stronger latitudinal gradients of the precipitation near the ITCZ compared to the YDCO2 experiment. The convergence of the north and south equatorial trades in the summer for the YDORB simulation occurs at approximately 10 °N, and in the winter it occurs at 4 °S. For the YDCO2 simulation, the summer position of the trade convergence is at 7 °N and the winter position is at 1 °N.

This migration of the ITCZ can be verified by the location of the bands of precipitation over the African continent. For the summer, the location of the precipitation for the YDORB experiment is the semi-arid, the northern tropics, and the equatorial wet regions, and the precipitation spans 20 °N to ~5 °S. The maximum amount of precipitation is on the coast of the northern tropics region at ~7 °N. In the winter, the precipitation band migrates southward to ~5 °S and extends from the equatorial wet region to the southern tropics region where the maximum precipitation is located. For the YDCO2 experiment, the band of precipitation is located at approximately 6-7 °N for the summer, and at approximately 1 °S for the winter. The maximum precipitation for both seasons is in the same regions as the YDORB simulation, though the maximum amount of precipitation, like the temperature and pressure, is not as extreme. For example, maximum precipitation in the summer for the YDORB simulation is ~15 mm day^{-1}, and maximum precipitation for the winter is ~10 mm day^{-1}. The maximum precipitation for the summer and winter for the YDCO2 experiment are 13 mm day^{-1} and 8 mm day^{-1}. Thus, the YD to preindustrial changes in the West African monsoon are likely more affected by orbital changes than by the change in YD to present change in CO_2 radiative forcing.

There is general consensus that orbital and greenhouse gas forcing enhances the variability of monsoonal circulation. This study is agreeable with previous sensitivity studies that increased northern summer insolation increases the strength of the West African monsoon (Kutzbach et al., 2007; Trauth et al., 2009; Prell and Kutzbach, 1987; Timm et al., 2010; Talbot et al., 2007; Kitoh et al., 1997; Voss and Mikolajewicz, 2001; Otto-Bliesner, Tomas, et al., 2006; Kutzbach and Guetter, 1986; Kutzbach, 1981; He, 2011). This study is also agreeable with Otto-Bliesner et al., (2014) suggesting that a decline in greenhouse gas forcing lead to increasing precipitation in the southern Sahel, the semi-arid and northern tropical regions of Africa. In addition, this study's results concur with Otto-Bliesner et al. (2014) that orbital changes only produced an increase in precipitation in the Sahel along with a northward expansion of the rains toward the northern desert region, whereas orbital-induced increases in summer insolation may lead to decline in precipitation (Renssen et al., 2006). The African monsoon could have also weakened by the cooling in the Northern hemisphere (Alley and Clark, 1999).

An important note to make is the fact that the orbital and CO_2 forcing changes do not induce a YD like state for the monsoonal seasons. Proxy evidence indicates that the YD was a dry period in the midst of the "African Humid Period" (Tierney et al., 2008; Gasse, 2000; Lézine et al., 2005; Garcin et al., 2007; Overpeck et al., 1996; Weldeab et al., 2011), and the results from this study indicate a strengthening of the monsoons and increase of precipitation. Therefore, other forcing mechanisms must be considered in order to explain a dry period for the monsoons as seen during the Younger Dryas cooling event.

4.6 Conclusion

By using a comprehensive high-resolution climate model, this study aimed to determine how changes between the Younger Dryas and the Holocene (pre-industrial) orbital and greenhouse gas parameters affect the AMOC and North Atlantic climate. Model results indicate YD to preindustrial changes in the AMOC may be more affected by the seasonal radiative forcing changes by orbital parameters and associated changes in freshwater fluxes than by the relative low changes in CO_2 radiative forcing (Figure 4-1). Higher climate variability in the YDORB simulation exists compared to the YDCO2 scenario and the preindustrial simulation. However, the climatic changes by orbital and CO_2 forcing alone are not sufficient enough to explain the YD cooling event, indicating that additional forcings are required. These findings are supported by the simulated changes in the AMOC which did not decrease in either scenario to 7-10 Sv, as suggest by the proxy record. In addition, the YDORB and YDCO2 simulation did not reproduce the substantial surface air temperature of ~15 °C, as inferred from the GISP record. The consideration of an YD ice sheet and freshwater forcing may thus be of importance to explain the observed changes. The West African monsoonal system is more greatly affected by changes in orbital parameters than by YD to Holocene changes in CO_2 radiative forcing. Seasonal variability in surface air temperature and associated changes in the wind and pressure pattern along with the position of the ITCZ for the YDORB simulation were greater than the changes for the YDCO2 scenario. However, these changes in orbital and greenhouse gas forcings alone were not large enough to explain the YD monsoonal circulation, as inferred from the proxy record. Additional mechanisms are required to produce the feedbacks necessary for a dry YD monsoon season compared to the African

Humid Period it interrupted. Overall, all results imply orbital YD to Holocene changes appear to affect the seasonal climate to a greater magnitude than CO_2 changes, possibly because seasonal radiative forcing of orbital changes were substantial greater than those by the relative small increase in atmospheric pCO_2.

References

Alley, R.B., 2000, The Younger Dryas cold interval as viewed from central Greenland: Quaternary Science Reviews, v. 19, p. 213–226, doi: 10.1016/S0277-3791(99)00062-1.

Alley, R.B., and Clark, P.U., 1999, THE DEGLACIATION OF THE NORTHERN HEMISPHERE: A Global Perspective: Annual Review of Earth and Planetary Sciences, v. 27, p. 149–182, doi: 10.1146/annurev.earth.27.1.149.

Berger, A., 1988, Milankovitch Theory and climate: Reviews of Geophysics, v. 26, p. 624, doi: 10.1029/RG026i004p00624.

Bitz, C.M., Shell, K.M., Gent, P.R., Bailey, D., Danabasoglu, G., Armour, K.C., Holland, M.M., and Kiehl, J.T., 2011, Climate Sensitivity of the Community Climate System Model Version 4: Journal of Climate, p. 111209062051003, doi: 10.1175/JCLI-D-11-00290.1.

Brady, E.C., Otto-bliesner, B.L., Kay, J.E., and Rosenbloom, N., 2013, Sensitivity to glacial forcing in the CCSM4: Journal of Climate, v. 26, p. 1901–1925, doi: 10.1175/JCLI-D-11-00416.1.

Bretherton, C.S., and Park, S., 2009, A New Moist Turbulence Parameterization in the Community Atmosphere Model: Journal of Climate, v. 22, p. 3422–3448, doi: 10.1175/2008JCLI2556.1.

Broecker, W.S., 2003, Does the trigger for abrupt climate change reside in the ocean or in the atmosphere? Science (New York, N.Y.), v. 300, p. 1519–22, doi: 10.1126/science.1083797.

Broecker, W.S., 1997, Thermohaline Circulation, the Achilles Heel of Our Climate System: Will Man-Made CO2 Upset the Current Balance? Science, v. 278, p. 1582–1588, doi: 10.1126/science.278.5343.1582.

Broecker, W.S., 2006, Was the Younger Dryas triggered by a flood? Science, v. 312, p. 1146–1148, doi: 10.1126/science.1123253.

Broecker, W.S., and Denton, G.H., 1989, The role of ocean-atmosphere reorganizations in glacial cycles: Geochimica et Cosmochimica Acta, v. 53, p. 2465–2501, doi: 10.1016/0016-7037(89)90123-3.

Carlson, A.E., Clark, P.U., Haley, B.A., Klinkhammer, G.P., Simmons, K., Brook, E.J., and Meissner, K.J., 2007, Geochemical proxies of North American freshwater routing during the Younger Dryas cold

event.: Proceedings of the National Academy of Sciences of the United States of America, v. 104, p. 6556–6561, doi: 10.1073/pnas.0611313104.

Chiang, J.C.H., Kushnir, Y., and Giannini, A., 2002, Deconstructing Atlantic Intertropical Convergence Zone variability: Influence of the local cross-equatorial sea surface temperature gradient and remote forcing from the eastern equatorial Pacific: Journal of Geophysical Research, v. 107, p. 4004, doi: 10.1029/2000JD000307.

Clark, P.U., Marshall, S.J., Clarke, G.K., Hostetler, S.W., Licciardi, J.M., and Teller, J.T., 2001, Freshwater forcing of abrupt climate change during the last glaciation.: Science, v. 293, p. 283–287, doi: 10.1126/science.1062517.

Crowley, T.J., and North, G.R., 1991, Paleoclimatology: New York, New York, Oxford University Press, 339 p.

Danabasoglu, G., and Gent, P.R., 2009, Equilibrium climate sensitivity: Is it accurate to use a slab ocean model? Journal of Climate, v. 22, p. 2494–2499, doi: 10.1175/2008JCLI2596.1.

DeVernal, A., Hillaire-Marcel, C., and Bilodeau, G., 1996, Reduced meltwater outflow from the Laurentide ice margin during the Younger Dryas: Nature, v. 381, p. 774–777, doi: 10.1038/381774a0.

Donnelly, J.P., Driscoll, N.W., Uchupi, E., Keigwin, L.D., Schwab, W.C., Thieler, E.R., and Swift, S. a., 2005, Catastrophic meltwater discharge down the Hudson Valley: A potential trigger for the Intra-Allerød cold period: Geology, v. 33, p. 89–92, doi: 10.1130/G21043.1.

Ebbesen, H., and Hald, M., 2004, Unstable Younger Dryas climate in the northeast North Atlantic: Geology, v. 32, p. 673 –676, doi: 10.1130/G20653.1.

Eisenman, I., Bitz, C.M., and Tziperman, E., 2009, Rain driven by receding ice sheets as a cause of past climate change: Paleoceanography, v. 24, p. 12, doi: 10.1029/2009PA001778.

Fischer, N., and Jungclaus, J.H., 2010, Effects of orbital forcing on atmosphere and ocean heat transports in Holocene and Eemian climate simulations with a comprehensive Earth system model: Climate of the Past, v. 6, p. 155–168, doi: 10.5194/cp-6-155-2010.

Fischer, H., Wahlen, M., Smith, J., Mastroianni, D., and Deck, B., 1999, Ice Core Records of Atmospheric CO2 Around the Last Three Glacial Terminations: Science, v. 283, p. 1712–1714, doi: 10.1126/science.283.5408.1712.

Folland, C.K., Palmer, T.N., and Parker, D.E., 1986, Sahel rainfall and worldwide sea temperatures, 1901–85: Nature, v. 320, p. 602–607, doi: 10.1038/320602a0.

Friedrich, T., Timmermann, A., Timm, O., Mouchet, A., and Roche, D.M., 2009, Orbital modulation of millennial-scale climate variability in an earth system model of intermediate complexity: Climate of the Past Discussions, v. 5, p. 2019–2051, doi: 10.5194/cpd-5-2019-2009.

Garcin, Y., Vincens, A., Williamson, D., Buchet, G., and Guiot, J., 2007, Abrupt resumption of the African Monsoon at the Younger Dryas-Holocene climatic transition: Quaternary Science Reviews, v. 26, p. 690–704, doi: 10.1016/j.quascirev.2006.10.014.

Gasse, F., 2000, Hydrological changes in the African tropics since the Last Glacial Maximum: Quaternary Science Reviews, v. 19, p. 189–211, doi: 10.1016/S0277-3791(99)00061-X.

Gent, P.R., Danabasoglu, G., Donner, L.J., Holland, M.M., Hunke, E.C., Jayne, S.R., Lawrence, D.M., Neale, R.B., Rasch, P.J., Vertenstein, M., Worley, P.H., Yang, Z.L., and Zhang, M., 2011, The community climate system model version 4: Journal of Climate, v. 24, p. 4973–4991, doi: 10.1175/2011JCLI4083.1.

Gherardi, J.M., Labeyrie, L., McManus, J.F., Francois, R., Skinner, L.C., and Cortijo, E., 2005, Evidence from the Northeastern Atlantic basin for variability in the rate of the meridional overturning circulation through the last deglaciation: Earth and Planetary Science Letters, v. 240, p. 710–723, doi: 10.1016/j.epsl.2005.09.061.

Gildor, H., and Tziperman, E., 2000, Sea ice as the glacial cycles' climate switch: Role of seasonal and orbital forcing: Paleoceanography, v. 15, p. 605–615, doi: 10.1029/1999PA000461.

Gregory, J.M., Dixon, K.W., Stouffer, R.J., Weaver, A.J., Driesschaert, E., Eby, M., Fichefet, T., Hasumi, H., Hu, A., Jungclaus, J.H., Kamenkovich, I., Levermann, A., Montoya, M., Murakami, S., et al., 2005, A model intercomparison of changes in the Atlantic thermohaline circulation in response to

increasing atmospheric CO 2 concentration: Geophysical Research Letters, v. 32, p. L12703, doi: 10.1029/2005GL023209.

Griffiths, J.F., 1972, Climates of Africa, Volume 10: Elsevier Pub. Co., 604 p.

Hansen, J., Fung, I., Lacis, A., Rind, D., Lebedeff, S., Ruedy, R., Russell, G., and Stone, P., 1988, Global Climate Changes as Forecast by Goddard Institute for Space Studies Three-Dimensional Model: Journal of Geophysical Research, v. 93, p. 9341–9364, doi: 10.1029/JD093iD08p09341.

He, F., 2011, Simulating Transiet Climate Evolution of the Last Deglaciation with CCSM3: University of Wisconsin-Madison, 1-185 p.

Hostetler, S.W., Bartlein, P.J., Clark, P.U., Small, E.E., and Solomon, A.M., 2000, Simulated influences of Lake Agassiz on the climate of central North America 11 , 000 years ago: Nature, v. 405, p. 334–337, doi: 10.1038/35012581.

Hu, A., Meehl, G.A., Washington, W.M., and Dai, A., 2004, Response of the Atlantic Thermohaline Circulation to Increased Atmospheric CO 2 in a Coupled Model: Journal of Climate, v. 17, p. 4267–4279, doi: 10.1175/JCLI3208.1.

Huang, E., and Tian, J., 2008, Melt-Water-Pulse (MWP) events and abrupt climate change of the last deglaciation: Chinese Science Bulletin, v. 53, p. 2867–2878, doi: 10.1007/s11434-008-0206-8.

Hunke, E.C., Hebert, D.A., and Lecomte, O., 2013, Level-ice melt ponds in the Los Alamos sea ice model, CICE: Ocean Modelling, v. 71, p. 26–42, doi: 10.1016/j.ocemod.2012.11.008.

Iacono, M.J., 2008, Radiative Forcing by Long-Lived Greenhouse Gases: Calculations with the AER Radiative Transfer Models: Journal of Geophysical Research: Atmospheres, v. 113, p. 8.

Imbrie, J., and Imbrie, K.P., 1979, Ice Ages: Solving the Mystery: Harvard University Press, 224 p.

IPCC, 2007, Climate Change 2007: The Physical Science Basis. Contribution of Working Group I to the Fourth Assessment Report of the Intergovernmental Panel on Climate Change [Solomon, S., D. Qin, M. Mann9ing, Z. Chen, M. Marquis, K.B. Averyt, M. Tignor and H.L. Miller (eds.)]. Cambridge University Press, Cambridge, United Kingdom and New York, NY, USA.

Joos, F., and Spahni, R., 2008, Rates of change in natural and anthropogenic radiative forcing over the past 20,000 years: Proceedings of the National Academy of Sciences of the United States of America, v. 105, p. 1425–1430, doi: 10.1073/pnas.0707386105.

Kitoh, A., Yukimoto, S., Noda, A., and Motoi, T., 1997, Simulated Changes in the Asian Summer Monsoon at Times of Increased Atmospheric CO2: Journal of the Meteorological Society of Japan, v. 75, p. 1019–1031.

Klockmann, M., Mikolajewicz, U., and Marotzke, J., 2015, The response of the glacial AMOC to changing greenhouse gas forcing: Geophysical Research Abstracts, v. 17, p. 1.

Kröpelin, S., Verschuren, D., Lézine, A.-M., Eggermont, H., Cocquyt, C., Francus, P., Cazet, J.-P., Fagot, M., Rumes, B., Russell, J.M., Darius, F., Conley, D.J., Schuster, M., von Suchodoletz, H., et al., 2008, Climate-driven ecosystem succession in the Sahara: the past 6000 years.: Science (New York, N.Y.), v. 320, p. 765–8, doi: 10.1126/science.1154913.

Kutzbach, J.E., 1981, Monsoon Climate of the Early Holocene: Climate Experiment with the Earth's Orbital Parameters for 9000 Years Ago: Science, v. 214, p. 59–61, doi: 10.1126/science.214.4516.59.

Kutzbach, J., Gallimore, R., Harrison, S., Behling, P., Selin, R., and Laarif, F., 1998, Climate and Biome simulations for the past 21,000 years: Quaternary Science Reviews, v. 17, p. 473–506, doi: 10.1016/S0277-3791(98)00009-2.

Kutzbach, J.E., and Guetter, P.J., 1986, The Influence of Changing Orbital Parameters and Surface Boundery Conditions on Climate Simulations for the Past 18000 Years: Journal of the Atmospheric Sciences, v. 43, p. 1726–1759.

Kutzbach, J.E., Liu, X., Liu, Z., and Chen, G., 2007, Simulation of the evolutionary response of global summer monsoons to orbital forcing over the past 280,000 years: Climate Dynamics, v. 30, p. 567–579, doi: 10.1007/s00382-007-0308-z.

Lézine, A.-M., Duplessy, J., and Cazet, J., 2005, West African monsoon variability during the last deglaciation and the Holocene: Evidence from fresh water algae, pollen and isotope data from

core KW31, Gulf of Guinea: Palaeogeography, Palaeoclimatology, Palaeoecology, v. 219, p. 225–237, doi: 10.1016/j.palaeo.2004.12.027.

Licciardi, J.M., Teller, J.T., and Clark, P.U., 1999, Freshwater routing by the Laurentide Ice Sheet During the Last Deglaciation: Geophysical Monograph Series, v. 112, p. 177–201.

Liu, Z., Carlson, A.E., He, F., Brady, E.C., Otto-Bliesner, B.L., Briegleb, B.P., Wehrenberg, M., Clark, P.U., Wu, S., Cheng, J., Zhang, J., Noone, D., and Zhu, J., 2012, Younger Dryas cooling and the Greenland climate response to CO2.: Proceedings of the National Academy of Sciences of the United States of America, v. 109, p. 11101–4, doi: 10.1073/pnas.1202183109.

Lohmann, G., and J. Lorenz, S., 2007, Orbital forcing on atmospheric dynamics during the last interglacial and glacial inception: Elsevier, 527-545 p.

Manabe, S., and Bryan Jr, K., 1985, C02-Induced Change in a Coupled Ocean-Atmosphere Model and Its Paleoclimatic Implications: Journal of Geophysical Research, v. 90, p. 11689–11707, doi: 198510.1029/JC090iC06p11689.

Manabe, S., and Stouffer, R.J., 1997, Coupled ocean-atmosphere model response to freshwater input: Comparison to Younger Dryas event: Paleoceanography, v. 12, p. 321–336, doi: 10.1029/96PA03932.

Manabe, S., and Stouffer, R.J., 1994, Multiple-century response of a coupled ocean-atmosphere model to an increase of atmospheric carbon dioxide: Journal of Climate, v. 7, p. 5–23, doi: 10.1175/1520-0442(1994)007<0005:MCROAC>2.0.CO;2.

Manabe, S., and Stouffer, R.J., 1995, Simulation of abrupt climate change induced by freshwater input to the North Atlantic Ocean: Nature, v. 378, p. 165–167.

Manabe, S., and Stouffer, R.J., 1999, The role of thermohaline circulation in climate: Tellus B, v. 51, p. 91–109, doi: 10.1034/j.1600-0889.1999.00008.x.

McManus, J.F., Francois, R., Gherardi, J.-M., Keigwin, L.D., and Brown-Leger, S., 2004, Collapse and rapid resumption of Atlantic meridional circulation linked to deglacial climate changes.: Nature, v. 428, p. 834–7, doi: 10.1038/nature02494.

Mlawer, E.J., Taubman, S.J., Brown, P.D., Iacono, M.J., and Clough, S.A., 1997, Radiative transfer for inhomogeneous atmospheres: RRTM, a validated correlated-k model for the longwave: Journal of Geophysical Research, v. 102, p. 16663, doi: 10.1029/97JD00237.

Moore, J.K., Doney, S.C., and Lindsay, K., 2004, Upper ocean ecosystem dynamics and iron cycling in a global three-dimensional model: Global Biogeochemical Cycles, v. 18, p. 1–21, doi: 10.1029/2004GB002220.

Moore, J.K., Lindsay, K., Doney, S.C., Long, M.C., and Misumi, K., 2013, Marine Ecosystem Dynamics and Biogeochemical Cycling in the Community Earth System Model [CESM1(BGC)]: Comparison of the 1990s with the 2090s under the RCP4.5 and RCP8.5 Scenarios: Journal of Climate, v. 26, p. 9291–9312, doi: 10.1175/JCLI-D-12-00566.1.

Morrison, H., and Gettelman, A., 2008, A New Two-Moment Bulk Stratiform Cloud Microphysics Scheme in the Community Atmosphere Model, Version 3 (CAM3). Part I: Description and Numerical Tests: Journal of Climate, v. 21, p. 3642–3659, doi: 10.1175/2008JCLI2105.1.

Murton, J.B., Bateman, M.D., Dallimore, S.R., Teller, J.T., and Yang, Z.-L., 2010, Identification of Younger Dryas outburst flood path from Lake Agassiz to the Arctic Ocean.: Nature, v. 464, p. 740–3, doi: 10.1038/nature08954.

Neale, R.B., Gettelman, A., Park, S., Chen, C.-C., Lauritzen, P.H., Williamson, D.L., Conley, A., Kinnison, D., Marsh, D., Smith, A.K., Vitt, F., Garcia, R., Lamarque, J.-F., Mills, M., et al., 2004, Description of the NCAR Community Atmosphere Model (CAM3): NCAR Technical Note, v. NCAR/TN-46, p. 214.

Neale, R.B., Richter, J.H., Conley, A.J., Park, S., Lauritzen, P.H., Gettelman, A., Williamson, D.L., Rasch, P.J., Vavrus, S., Taylor, M.A., Collins, W.D., Zhang, M., and Lin, S.-J., 2010, Description of the NCAR Community Atmosphere Model (CAM 4.0): NCAR Technical Note, v. NCAR/TN-48, p. 212.

Nicholson, S.E., 2013, The West African Sahel: A Review of Recent Studies on the Rainfall Regime and Its Interannual Variability: ISRN Meteorology, v. 2013, p. 1–32, doi: 10.1155/2013/453521.

Oleson, K.W., Lawrence, D.M., Gordon, B., Flanner, M.G., Kluzek, E., Peter, L.J., Levis, S., Swenson, S.C., and Thornton, P.E., 2010, Technical Description of version 4.0 of the Community Land Model (CLM): NCAR/TN-478+STR NCAR Technical Note, p. 266.

Otto-Bliesner, B.L., Brady, E.C., Clauzet, G., Tomas, R., Levis, S., and Kothavala, Z., 2006, Last glacial maximum and Holocene climate in CCSM3: Journal of Climate, v. 19, p. 2526–2544, doi: 10.1175/JCLI3748.1.

Otto-Bliesner, B.L., Russell, J.M., Clark, P.U., Liu, Z., Overpeck, J.T., Konecky, B., DeMenocal, P., Nicholson, S.E., He, F., and Lu, Z., 2014, Coherent changes of southeastern equatorial and northern African rainfall during the last deglaciation.: Science, v. 346, p. 1223–7, doi: 10.1126/science.1259531.

Otto-Bliesner, B.L., Tomas, R., Brady, E.C., Caspar, A., Kothavala, Z., and Clauzet, G., 2006, Climate Sensitivity of Moderate- and Low-Resolution Versions of CCSM3 to Preindustrial Forcings: Journal of Climate, v. 3, p. 2567–2583, doi: 10.1175/JCLI3754.1.

Overpeck, J., Anderson, D., Trumbore, S., and Prell, W., 1996, The southwest Indian Monsoon over the last 18000 years: Climate Dynamics, v. 12, p. 213–225, doi: 10.1007/BF00211619.

Park, S., and Bretherton, C.S., 2009, The University of Washington Shallow Convection and Moist Turbulence Schemes and Their Impact on Climate Simulations with the Community Atmosphere Model: Journal of Climate, v. 22, p. 3449–3469, doi: 10.1175/2008JCLI2557.1.

Peltier, W.R., 2004, GLOBAL GLACIAL ISOSTASY AND THE SURFACE OF THE ICE-AGE EARTH: The ICE-5G (VM2) Model and GRACE: Annual Review of Earth and Planetary Sciences, v. 32, p. 111–149, doi: 10.1146/annurev.earth.32.082503.144359.

Prell, W.L., and Kutzbach, J.E., 1987, Monsoon variability over the past 150,000 years: Journal of Geophysical Research, v. 92, p. 8411–8425, doi: 10.1029/JD092iD07p08411.

Rahmstorf, S., 2000, The Thermohaline Ocean Circulation: A System with Dangerous Thresholds? Climatic Change, v. 46, p. 247–256, doi: 10.1023/A:1005648404783.

Raymond, D.J., and Blyth, A.M., 1986, A Stochastic Mixing Model for Nonprecipitating Cumulus Clouds: Journal of the Atmospheric Sciences, v. 43, p. 2708–2718, doi: 10.1175/1520-0469(1986)043<2708:ASMMFN>2.0.CO;2.

Raymond, D.J., and Blyth, A.M., 1992, Extension of the Stochastic Mixing Model to Cumulonimbus Clouds: Journal of the Atmospheric Sciences, v. 49, p. 1968–1983, doi: 10.1175/1520-0469(1992)049<1968:EOTSMM>2.0.CO;2.

Renssen, H., Brovkin, V., Fichefet, T., and Goosse, H., 2006, Simulation of the Holocene climate evolution in Northern Africa: The termination of the African Humid Period: Quaternary International, v. 150, p. 95–102, doi: 10.1016/j.quaint.2005.01.001.

Richter, J.H., and Rasch, P.J., 2008, Effects of Convective Momentum Transport on the Atmospheric Circulation in the Community Atmosphere Model, Version 3: Journal of Climate, v. 21, p. 1487–1499, doi: 10.1175/2007JCLI1789.1.

Rind, D., Peteet, D., Broecker, W.S., McInyre, A., and Ruddiman, W., 1986, The impact of cold North Atlantic sea surface temperatures on climate: implications for the Younger Dryas cooling (11-10 k): Climate Dynamics, v. 1, p. 3–33, doi: 10.1007/BF01277044.

Rooth, C., 1982, Hydrology and ocean circulation: Progress in Oceanography, v. 11, p. 131–149, doi: 10.1016/0079-6611(82)90006-4.

Schmidt, M.W., Spero, H.J., and Lea, D.W., 2004, Links between salinity variation in the Caribbean and North Atlantic thermohaline circulation.: Nature, v. 428, p. 160–3, doi: 10.1038/nature02346.

Severinghaus, J.P., Sowers, T., Brook, E.J., Alley, R.B., and Bender, M.L., 1998, Timing of abrupt climate change at the end of the Younger Dryas interval from thermally fractionated gases in polar ice: Nature, v. 391, p. 141–146.

Shin, S.-I., Liu, Z., Otto-Bliesner, B.L., Kutzbach, J., and Vavrus, S., 2003, Southern Ocean sea-ice control of the glacial North Atlantic thermohaline circulation: Geophysical Research Letters, v. 30, p. 68–71, doi: 10.1029/2002GL015513.

Simmons, A.J., and Strufing, R., 1981, An energy and angular momentum conserving finite-difference scheme, hybrid coordinates and medium-range weather prediction: Technical Report ECMWF Report No. 28, European Centre for Medium-Range Weather Forecasts, Reading, U.K., p. 68.

Smith, R., Jones, P., Briegleb, B., Bryan, F., Danabasoglu, G., Dennis, J., Dukowicz, J., Eden, C., Fox-Kemper, B., Gent, P., Hecht, M., Jayne, S., Jochum, M., Large, W., et al., 2010, The Parallel Ocean Program (POP) reference manual: Ocean component of the Community Climate System Model (CCSM): Rep. LAUR-01853, v. 141, p. 1–141.

Stouffer, R.J., and Manabe, S., 2003, Equilibrium response of thermohaline circulation to large changes in atmospheric CO2 concentration: Climate Dynamics, v. 20, p. 759–773, doi: 10.1007/s00382-002-0302-4.

Stouffer, R.J., Manabe, S., and Bryan, K., 1989, Interhemispheric asymmetry in climate response to a gradual increase of atmospheric CO2: Nature, v. 342, p. 660–662, doi: 10.1038/342660a0.

Talbot, M.R., Filippi, M.L., Jensen, N.B., and Tiercelin, J.-J., 2007, An abrupt change in the African monsoon at the end of the Younger Dryas: Geochemistry, Geophysics, Geosystems, v. 8, p. 16, doi: 10.1029/2006GC001465.

Tarasov, L., and Peltier, W.R., 2005, Arctic freshwater forcing of the Younger Dryas cold reversal.: Nature, v. 435, p. 662–5, doi: 10.1038/nature03617.

Teller, J.T., Boyd, M., Yang, Z.-L., Kor, P.S.G., and Fard, A.M., 2005, Alternative routing of Lake Agassiz overflow during the Younger Dryas: new dates, paleotopography, and a re-evaluation: Quaternary Science Reviews, v. 24, p. 1890–1905, doi: 10.1016/j.quascirev.2005.01.008.

Tierney, J.E., Russell, J.M., Huang, Y., Damste, J.S.S., Hopmans, E.C., and Cohen, a. S., 2008, Northern Hemisphere Controls on Tropical Southeast African Climate During the Past 60,000 Years: Science, v. 322, p. 252–255, doi: 10.1126/science.1160485.

Timm, O., Köhler, P., Timmermann, A., and Menviel, L., 2010, Mechanisms for the Onset of the African Humid Period and Sahara Greening 14.5–11 ka BP: Journal of Climate, v. 23, p. 2612-2633.

Trauth, M.H., Larrasoaña, J.C., and Mudelsee, M., 2009, Trends, rhythms and events in Plio-Pleistocene African climate: Quaternary Science Reviews, v. 28, p. 399–411, doi: 10.1016/j.quascirev.2008.11.003.

Voss, R., and Mikolajewicz, U., 2001, The climate of 6000 years BP in near-equilibrium simulations with a coupled AOGCM: Geophysical Research Letters, v. 28, p. 2213–2216, doi: 10.1029/2000GL012498.

Waliser, D.E., and Gautier, C., 1993, A satellite-derived climatology of the ITCZ: Journal of Climate, v. 6, p. 2162–2174, doi: 10.1175/1520-0442(1993)006<2162:ASDCOT>2.0.CO;2.

Weldeab, S., Frank, M., Stichel, T., Haley, B., and Sangen, M., 2011, Spatio-temporal evolution of the West African monsoon during the last deglaciation: Geophysical Research Letters, v. 38, p. 5, doi: 10.1029/2011GL047805.

Winguth, A.M.E., Shields, C.A., and Winguth, C., 2015, Transition into a Hothouse World at the Permian-Triassic boundary-A model study: Palaeogeography, Palaeoclimatology, Palaeoecology, v. 440, p. 316–327, doi: 10.1016/j.palaeo.2015.09.008.

Wood, R.A., Keen, A.B., Mitchell, J.F.B., and Gregory, J.M., 1999, Changing spatial structure of the thermohaline circulation in response to atmospheric CO2 forcing in a climate model: v. 399, p. 572–575, doi: 10.1038/21170.

Zhang, G.J., and McFarlane, N. a., 1995, Sensitivity of climate simulations to the parameterization of cumulus convection in the Canadian climate centre general circulation model: Atmosphere-Ocean, v. 33, p. 407–446, doi: 10.1080/07055900.1995.9649539.

Zhisheng, A., Porter, S.C., Weijian, Z., Yanchou, L., Donahue, D.J., Head, M.J., Xihuo, W., Jianzhang, R., and Hongbo, Z., 1993, Episode of Strengthened Summer Monsoon Climate of Younger Dryas Age on the Loess Plateau of Central China: Quaternary Research, v. 39, p. 45–54, doi: 10.1006/qres.1993.1005.

Chapter 5

The Role of Freshwater Forcing on the Younger Dryas Climate in CESM1.2

Abstract

A common hypothesis for the cause of the onset of the Younger Dryas cooling event is a massive input of freshwater into the North Atlantic Ocean by the rapid retreat of the Laurentide Ice Sheet during the last deglaciation. Such a freshwater pulse likely caused reduction of surface density, increase in vertical stratification, and decrease in the Atlantic meridional overturning circulation. In this study, the reponse of the Younger Dryas climate to a freshwater pulse into the North Atlantic Ocean is simulated by the Community Earth System Model version 1 (CESM1). With a freshwater pulse, the AMOC during the Younger Dryas is substantially reduced compared to preindustrial conditions. This freshwater forcing together with the larger cover of icesheets in during the Younger Dryas result in cooler than present surface air temperature in agreement with the temperature reconstruction from the Greenland ice cores. The changes in the AMOC by Younger Dryas freshwater forcing and ice sheets exceeds those with YD greenhouse gas and orbital forcing. The simulated Younger Dryas African monsoon was colder and drier compared to the preindustrial scenario. Thus, the input of freshwater and the consideration of the ice sheet for the Younger Dryas may be of importance to explain the weakening the West African monsoon that is also inferred from proxy reconstructions. A simulated southward shift in the ITCZ due to the Northern hemispheric cooling is in agreement with previous studies.

5.1 Introduction

5.1.1 The Freshwater Forcing Hypothesis

Freshwater input into the Northern Atlantic Ocean causes vertical stratification of the oceanic water masses as the density of the surface water decreases with decreasing salinity (Rahmstorf, 2000; Stocker and Marchal, 2000; Stocker and Wright, 1991; Rahmstorf, 1995). An associated decrease in the density-driven circulation causes a decrease in the poleward heat transport and cooling of the North Atlantic region (Seager and Battisti, 2007; Peltier, 2007; Srokosz et al., 2012; Cheng et al., 2011). The freshwater forcing hypothesis is supported by a number of numerical simulations (e.g. Tarasov and

Peltier, 2005; Murton et al., 2010; Huang and Tian, 2008), discussed later in this chapter, as well as proxy records at the onset of the YD (Boyle and Keigwin, 1987; McManus et al., 2004; Broecker et al., 1988; Hughen et al., 2000b; Broecker and Denton, 1989). In addition, the change in location of meltwater discharge at the onset of the Younger Dryas from the Mississippi River is inferred from oxygen isotope records from sediment cores obtained from the Gulf of Mexico (Bakke et al., 2009). Several studies suggest that the Lake Agassiz glacial meltwater was diverted from the Mississippi River to the St. Lawrence River during the Younger Dryas (Teller, 1990; Broecker et al., 1988; Leverington and Teller, 2003; Teller, 2003; Dyke, 2004). This hypothesis is supported by oxygen isotope evidence from the Florida Straits that indicate an increase in sea surface salinity in the Gulf of Mexico from a decrease in freshwater input (Schmidt and Lynch-Stieglitz, 2011). Additionally, a record from the glacial Lake Iroquois and the LIS ice margin indicate increased freshwater flow through the region (Clark et al., 2001; Donnelly et al., 2005). However, more recently the northern route through the Mackenzie River as the suggested flood path has been proposed based on gravel beds, erosional surfaces, and optically stimulated luminescence dating (Murton et al., 2010) as well as climate modeling (Tarasov and Peltier, 2005; Peltier, 2007). Deglacial timing of the Great Lakes region from the lake Nipigon core do not suggest the St. Lawrence was completely deglaciated at the onset of the YD (Teller et al., 2005). Additionally, sediment analysis suggests an outburst flood through the Mackenzie River occurred around the onset of the YD (Murton et al., 2010). This evidence is supported by additional cores from the Yermak Plateau, in which freshwater from the Arctic Ocean moved through the Fram Strait during this time (Knies et al., 2007). Flooding through the Mackenzie River is also suggested to be more effective in altering AMOC strength due to the stability of the Arctic Ocean water column, which allows for the cold water to move across the surface ocean instead of sinking and affecting deep water masses (Peltier, 2007).

Change in the AMOC during the onset of the Younger Dryas can be inferred from isotopic ratios, e.g. $^{13}C/^{12}C$, $^{18}O/^{16}O$, and $^{231}Pa/^{230}Th$, and cadmium calcium from marine sediment cores (see Chapter 1). For example, stable carbon isotope reconstructions from the Cariaco Basin and the Caribbean Sea imply a reduction in deepwater production in the Northern Atlantic Ocean (Hughen et al., 1998; Broecker et al., 1982). Northern Norway sediment cores sea surface temperature reconstructions indicate the onset of

the YD where temperatures fluctuate from interglacial to glacial values, from 10°C to 4°C at the onset of the YD (Ebbesen and Hald, 2004). Tropical Atlantic atmospheric circulation reduction linked to AMOC reduction is also suggested by stable oxygen isotope proxies from the Florida Straits (Schmidt and Lynch-Stieglitz, 2011). A sediment core from the Bermuda Rise conveys the abrupt decline in the AMOC at the onset of the YD where $^{231}Pa/^{230}Th$ increases from 0.06 to 0.08 (McManus et al., 2004).

Glacial ice sheet disappearance owing to warming from the Bølling-Allerød event is a commonly discussed hypothesis for the input of freshwater into the North Atlantic Ocean (Bard et al., 1996). It is suggested that the Laurentide Ice Sheet (LIS) underwent melting as the northern hemisphere warmed during the BA event, and an estimated 9500 km^3 of glacial melt was discharged from the proglacial Lake Agassiz as a result (Broecker and Denton, 1989; Rooth, 1982; Teller et al., 2002) into the northern North Atlantic Ocean. It remains uncertain which path the meltwater used to reach the northern North Atlantic Ocean; the northern route through the Mackenzie River, the eastern route through the St. Lawrence River, and/or the southern route through the Mississippi River (Huang and Tian, 2008; Murton et al., 2010; Broecker and Denton, 1989).

In this chapter, the AMOC response to freshwater hosing under Younger Dryas boundary conditions will be investigated. The sensitivity of the AMOC with present-day boundary conditions has been already discussed in chapter 4. Reduced strength in the AMOC by 90% could have reduce the surface air temperature in the Nordic Seas by approximately 10°C (Rahmstorf, 2006, 1996; Rind et al., 2001).

5.1.2 The African monsoon circulation

A review of the West African monsoon circulation can be found in Chapter 4. The basic features of the West African Monsoon are the low level southwesterly flow from the Atlantic Ocean and the Inter-Tropical Convergence Zone (ITCZ) north of the equator. The ITCZ is characterized by a narrow band of increased precipitation that is positioned approximately 7 °N during winter and is controlled latitiudinally by the convergence of the Atlantic trade winds (Chiang et al., 2002). Over the course of the year, the ITCZ migrates from its southernmost extent in winter over the northern tropical region and to its

northernmost extent of 20 °N over the northern desert region in summer (Waliser and Gautier, 1993; Hastenrath, 2002). In simulations performed with coupled atmospheric general circulation models, it is shown that the addition of the land ice sheet during the Last Glacial Maximum (LGM) imparts a southward movement of the ITCZ away from the cooler hemisphere (Chiang et al., 2003; Chiang and Bitz, 2005). This is suggested to be a result of stronger trade winds in the Northern Atlantic Ocean compared to present day (Chiang et al., 2003). The suggested feedback mechanism for this southward shift of the ITCZ involves the drying of air and abrupt cooling of the northern part of the hemisphere (Chiang and Bitz, 2005). This causes the progression of cold sea surface temperatures toward the lower latitudes and the ITCZ, causing a southward shift of the ITCZ (Chiang and Bitz, 2005). The input of freshwater forcing in addition to the ice sheet would amplify the feedback mechanism by inducing a further cooling and forcing the ITCZ further south.

In chapter 4 the effects of orbital and greenhouse gas forcing on the African monsoon circulation were investigated, but substantial bias occurred between these simulations and rainfall and temperature proxy data that suggest a cool and dry climate over Africa during the Younger Dryas (Tierney et al., 2008; Gasse, 2000; Lézine et al., 2005; Garcin et al., 2007; Overpeck et al., 1996; Weldeab et al., 2011). Thus the sensitivity of the West African Monsoon to freshwater forcing as well as the 13 ka ice sheet were explored in this chapter in order to reduce to model-data bias.

5.2 Previous Simulations

In simulation experiments, model complexity and resolution affect how the AMOC responds to the amount of freshwater input into the ocean and where the freshwater is discharged. 80-year freshwater hosing simulations with CCSM 2 and 3 show that the AMOC nearly collapses (Hu et al., 2004). In other numerical experiment, the AMOC does not collapse and only weakens after a 500-year freshwater discharge (Manabe and Stouffer, 2000; Mikolajewicz, 1996; Manabe and Stouffer, 1999). The critical value of a potential collapse of the AMOC appears to be if freshwater hosing exceeds 0.5 Sv (Stouffer et al., 2006; Knutti et al., 2004). However, the AMOC strength may not change if a certain threshold value for the freshwater forcing is reached (Otto-Bliesner and Brady, 2010). The response of the AMOC in

model simulations is based on the complexity of the model as well as the resolution, with higher complexity models and higher resolution showing a heightened sensitivity of the AMOC to freshwater perturbations (Weijer et al., 2012; Otto-Bliesner et al., 2006).

Studies regarding the AMOC response to the location of freshwater input have been performed in a variety of numerical experiments. For the greatest affect on the AMOC strength, freshwater needs to be discharged within the North Atlantic latitudes, i.e. the eastern or northern routes (Manabe and Stouffer, 1997). A transient simulation performed with a freshwater discharge scheme adapted from Carlson et al. (2007) provided evidence that the St. Lawrence River discharge location weakened the AMOC strength by 44%, while the Mackenzie River discharge location weakened the AMOC by 50%, indicating that the AMOC is more sensitive to discharge from the Mackenzie River (He, 2011). This conclusion was also reached in chapter 3 of this study. While the strength of the AMOC seems to be more affected by discharge from the Mackenzie River, studies in climate models show that reduction of surface air temperature is similar for both freshwater discharge locations (Peltier, 2007).

5.3 Model Description

The National Center for Atmospheric Research's Community Earth System Model version 1.0.5 (NCAR CESM1.0) was used for the simulations in this study. Detailed information regarding CESM1.0 can be found in chapter 4. The four components of CESM1 are the Parallel Ocean Program version 2 (POP2; Smith et al., 2010), the Community Atmospheric Model version 5 (CAM5), the Los Alamos Sea Ice Model (CICE; Hunke et al., 2013), and the Community Land Model version 4 (CLM4; Oleson et al., 2010) along with a central coupler (CPL7). Carbon nitrogen dynamics for the land is included as described by Lindsay et al. (2014). The coupler exchanges information between the model components and allows for an inclusive view of the climatic conditions for the time-period that is being investigated.

Major updates for the Community Earth System Model version 1.2.1 (CESM1.2) compared to CESM1.0 are detailed at NCAR's CESM Models website (http://www.cesm.ucar.edu/models/cesm1.2/tags/cesm1_2/whatsnew_science.html). Modification related to this study includes the implementation of the Community Land Model version 4.5 (CLM4.5; Oleson et

al., 2013). Modifications include a revised canopy scheme, improved hydrologic processes, a new snow cover fraction parameterization, a more realistic lake model, new soil biogeochemistry, improved litter and soil nitrogen and carbon pool structures, a new fire model, and an update of the biogenic volatile organic compounds model (Oleson et al., 2013; Bonan et al., 2011; Sun et al., 2012; Swenson et al., 2012; Swenson and Lawrence, 2012; Subin et al., 2012; Koven et al., 2013; Li et al., 2012, 2013; Guenther et al., 2012). New additions to the model include extending the crop model to include irrigation, organ pools and interactive fertilization, a methane model that simulates production, oxidation and emissions, inclusion of the Variable Infiltration Capacity (VIC) model, and a multilayer canopy option (Oleson et al., 2013; Sacks et al., 2009; Drewniak et al., 2013; Riley et al., 2011; Li et al., 2011; Bonan et al., 2012).

5.4 Forcing Boundary Conditions and Experimental Design

Two simulations were created in collaboration with Arne Winguth and analyzed for this study, a present day control simulation and a Younger Dryas simulation. The boundary conditions for both simulations are summarized in Table 5-1.

The present day control simulation uses present day topography (Figure 5-1). Orbital parameters were set to 1990, which is present day in the model, and the solar constant is 1.366×10^6 W m^{-2}. Greenhouse gas concentrations for CO_2, CH_4, and N_2O are 284.7 ppmv, 791.6 ppbv, and 275.68 ppbv respectively (Brady et al., 2013). Salinity was set to present-day conditions (34.73 psu), and the carbon cycle used in the model is the BDRD, meaning that the biogeochemical processes and radiative CO_2 forcing (B and R respectively) uses prescribed atmospheric concentrations within the model (D).

The boundary conditions for the Younger Dryas simulation are listed in Table 5-1. The solar constant was decreased by ~0.001×10^6 W m^{-2}. The Younger Dryas orbital forcing (Obliquity = 24.093°, eccentricity = 0.020175, and the precession of the equinox = -0.01824), is adjusted according to Berger and Loutre (1991). Greenhouse gas concentrations (Table 3-1) were set to 237.57 ppmv, 632.0 ppbv, and 265.00 ppbv for CO_2, CH_4, and N_2O respectively (Joos and Spahni, 2008). Salinity was adjusted to 35.27 to reflect the 65 m sea level fall during 13ka (Clark et al., 2009). The Ice-5G ice sheet for 13ka was added to the topography (Figure 5-1; Peltier, 2004). Freshwater forcing was added to the simulation and

discharged into the Northern Atlantic between Greenland and Europe (47.34-60.45°N and 321.63-343.50°E; Figure 5-2). The freshwater discharge involved a steady ramping of freshwater forcing by 0.003 Sv per year every 10 years for the first 100 years of the simulation to reach a maximum of 0.3 Sv, after which it was held constant until the end of the 500 yr simulation (Figure 5-3).

Table 5-1. Initial and Boundary Conditions for the Younger Dryas and Preindustrial CESM1.2 Experiments

Initial and Boundary Conditions			
Parameter	Preindustrial	Younger Dryas	Reference
Incoming Solar Radiation	1,365 W m^{-2}	1,364 W m^{-2}	Adapted from Otto-Bliesner et al. (2006)
Orbital Parameters			
Year	1990	13.0 ka	
Precession	0.01690	-0.01824	Berger and Loutre (1991)
Eccentricity	0.017236	0.020175	
Obliquity	23.446°	24.093°	
Greenhouse Gases			
CO_2	284.7 ppmv	237.6 ppmv	Preindustrial values from Brady et al. (2013) YD values from Joos and Spahni (2008)
CH_4	791.6 ppbv	632.0 ppbv	
N_2O	275.7 ppbv	265.0 ppbv	
Other Parameters			
Vegetation	Preindustrial	Preindustrial	Brady et al. (2013)
Ice Sheet	Present Day	Ice5G	Peltier (2004)
Ocean Salinity	34.73 psu	35.71 psu	Present day from Labeyrie et al. (1992) Younger Dryas calculated from Chappell et al. (1996) and Siddall et al. (2003)

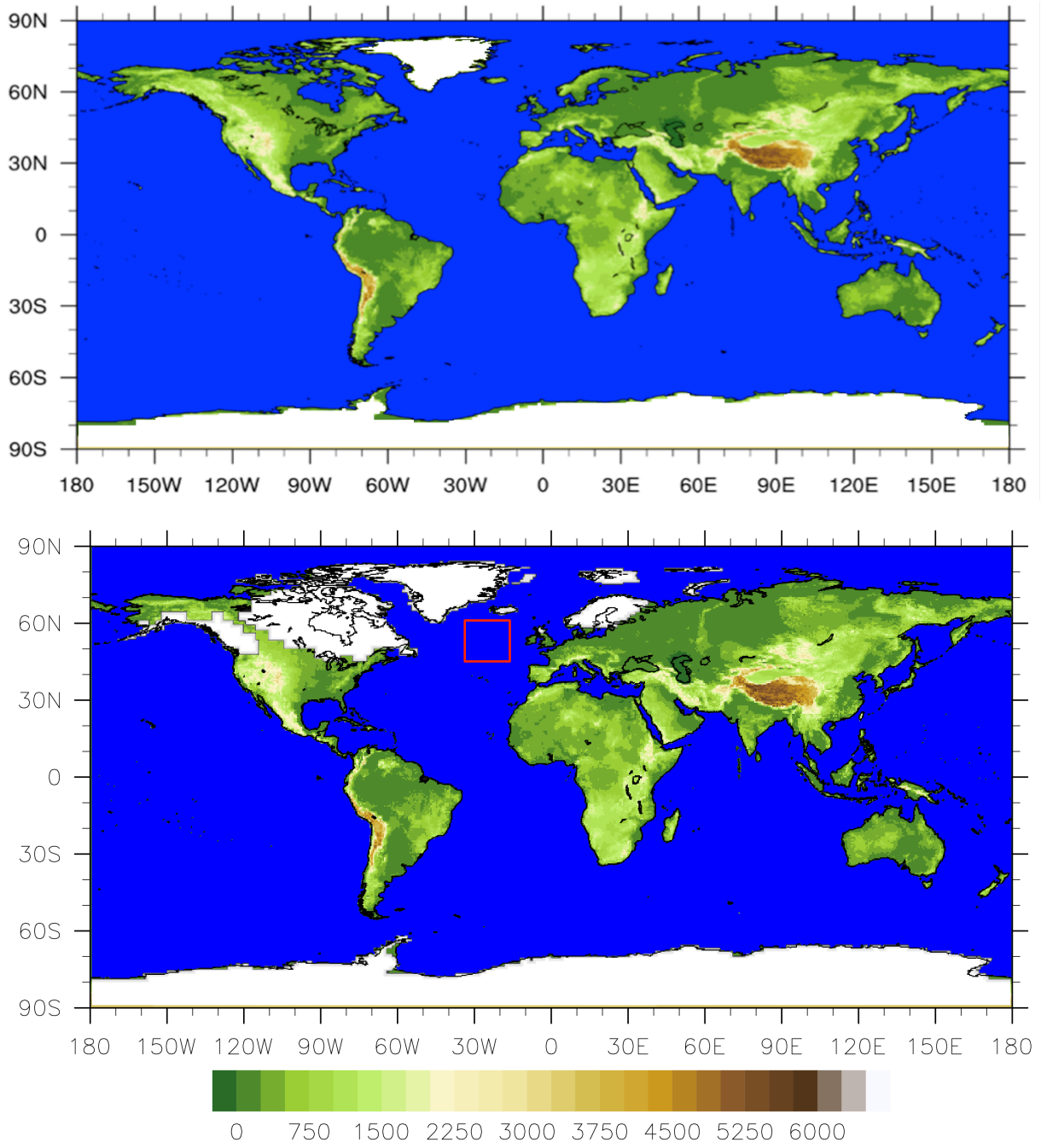

Figure 5-1 Topography for the present day simulation (top figure) and the Younger Dryas simulation (bottom figure). The ice sheet is shown as covering the Hudson Bay in the Younger Dryas simulation. The location of freshwater forcing is shown as the red box (merdional extent from 47.34°N to 60.45°N and zonal extent 321.63°E to 343.50°E) in the bottom figure.

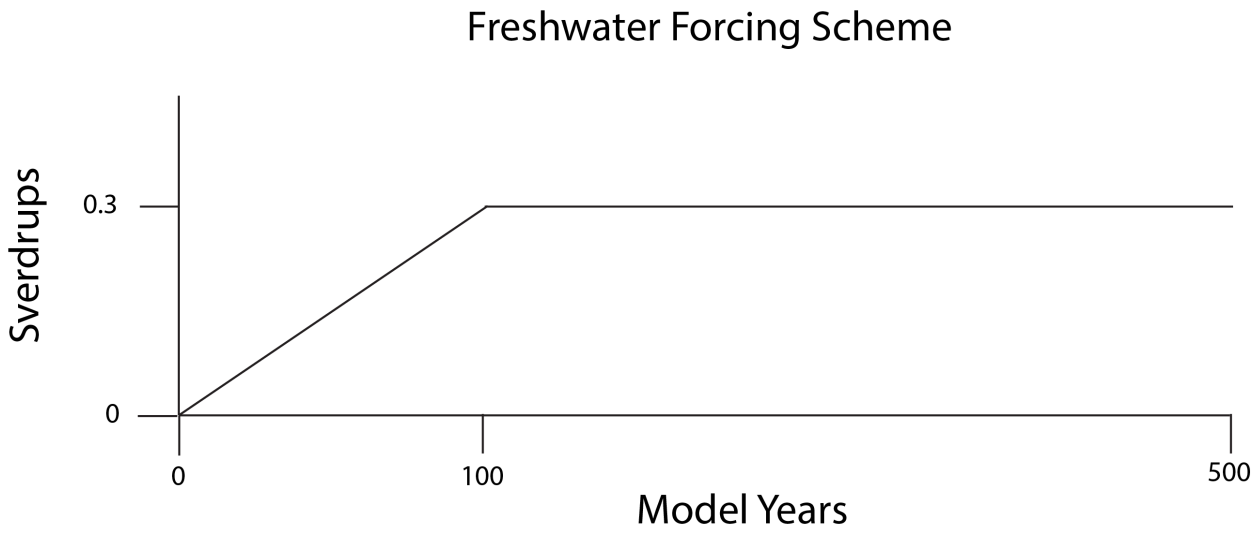

Figure 5-2 The freshwater forcing scheme used for the CESM1 Younger Dryas simulation.

It should be noted that the main difference to the existing preindustrial simulation is the use of CAM5 instead of CAM4 (see Chapter 4). Major improvements between CAM4 and CAM5 include physical processes that make CAM5 the first version of CAM to simulate the indirect radiative effects of cloud-aerosol interactions (Neale et al., 2010). Additional improvements include a new moist turbulent scheme, a new shallow convection scheme, stratiform microphysical processes, a new cloud macrophysics scheme, 3-mode modal aerosol scheme (MAM3; Neale et al., 2010), specifications and calculations for condensed phase optics, and the radiation scheme was updated to the Rapid Radiative Transfer Method for GSMs (RRTMG; Iacono, 2008).

5.5 Results

5.5.1. Atlantic meridional overturning circulation

In the following section, the atmospheric surface properties (air temperature, precipitation, wind and pressure field) in reponse to the Younger Dryas boundary conditions (Section 5.4) are discussed. For comparison, results for the preindustrial simulation are presented in Appendix A.3.

As described by Manabe and Stouffer (1994) and Voss and Mikolajewicz (2001) reduced greenhouse radiative forcing leads to surface cooling and a decline in the water vapor saturation value.

Thus, a glacial troposphere with lower atmospheric pCO_2 appears to be dryer. In colder climate, tropospheric air masses are generally more dense and the mean surface pressure is higher. Higher amounts of precipitation enhance the freshwater flux into the ocean if precipitation exceeds evaporation. An increased freshwater flux to the sea surface salinity (6 psu lower in the Younger Dryas scenario than the preindustrial scenario; Figure 5-3 A and B) can lead to an increase in vertical stability and thus reduced AMOC. Contrarily, if sea surface salinity increases and surface water masses become more dense vertically stability is reduced and the AMOC strength increases (Rooth, 1982; Broecker and Denton, 1989). Thus, changes in heat and freshwater fluxes by orbital and greenhouse gas forcing (Berger, 1988; Broecker and Denton, 1989) can affect the strength of the AMOC (see also Chapter 4).

Poleward heat transport by the Gulf Stream and North Atlantic Current (Seager and Battisti, 2007; Peltier, 2007; Srokosz et al., 2012; Cheng et al., 2011) contribute to the balance of the net radiative differences between the equatorial and polar region. These warm poleward current, are associated with a high sensible and latent heat that contribute to warming of the atmosphere above the surface (Levitus, 1983; Hall and Bryden, 1982; Rintoul and Wunsch, 1991; Srokosz et al., 2012). The reduction of the AMOC and cooling by increased freshwater during the Younger Dryas lead to decrease in the poleward heat transport (Schiller et al., 1997). Sea surface temperature in near Greenland is -12°C cooler in YD simulation compared to the preindustrial experiment (Figure 5-4 A & B). This cooling of the sea surface also leads to reduced latent heat flux and decrease in precipitation. Additionally, when the climate cools, the lower 2 m of air cools faster than the sea surface, and colder (denser) air leads to an increase in the surface pressure.

The furthest extent of the ice margin for the preindustrial simulation for the Northern Atlantic is ~87°N, and the Hudson Bay is covered in annual average ~50-60% by sea ice (Figure 5-5 A). For the Younger Dryas simulation, the ice margin is positioned at ~50°N to 55°N or 30° to 35° more southward than the preindustrial simulation and the Hudson Bay has been covered by the Laurentide ice sheet (Figure 5-5 B). In the preindustrial simulation, all areas where sea ice is present are coverd with <99% sea ice, while in the Younger Dryas, the the area near the North Pole is completely covered by ice (Figure 5-5 A and B).

The average AMOC strength during the Younger Dryas (7-10 Sv) was substantially weaker (~16-19 Sv) than the preindustrial circulation (for the control simulation at 1000 m depth was approximately 26 Sv, Figure 5-6; See Appendix A.3). The reduction of the AMOC strength and increased stratification during Younger Dryas is also revealed by the increase in the the ideal age of water masses by ~200 years at the core of the North Atlantic Deep Water in 2000 m depth (Figure 5-7). Ideal age of water masses is defined as the amount of time that has passed since a parcel of water has last made contact with the surface of the ocean (Chapter 3; Thiele and Sarmiento, 1990; England, 1995).

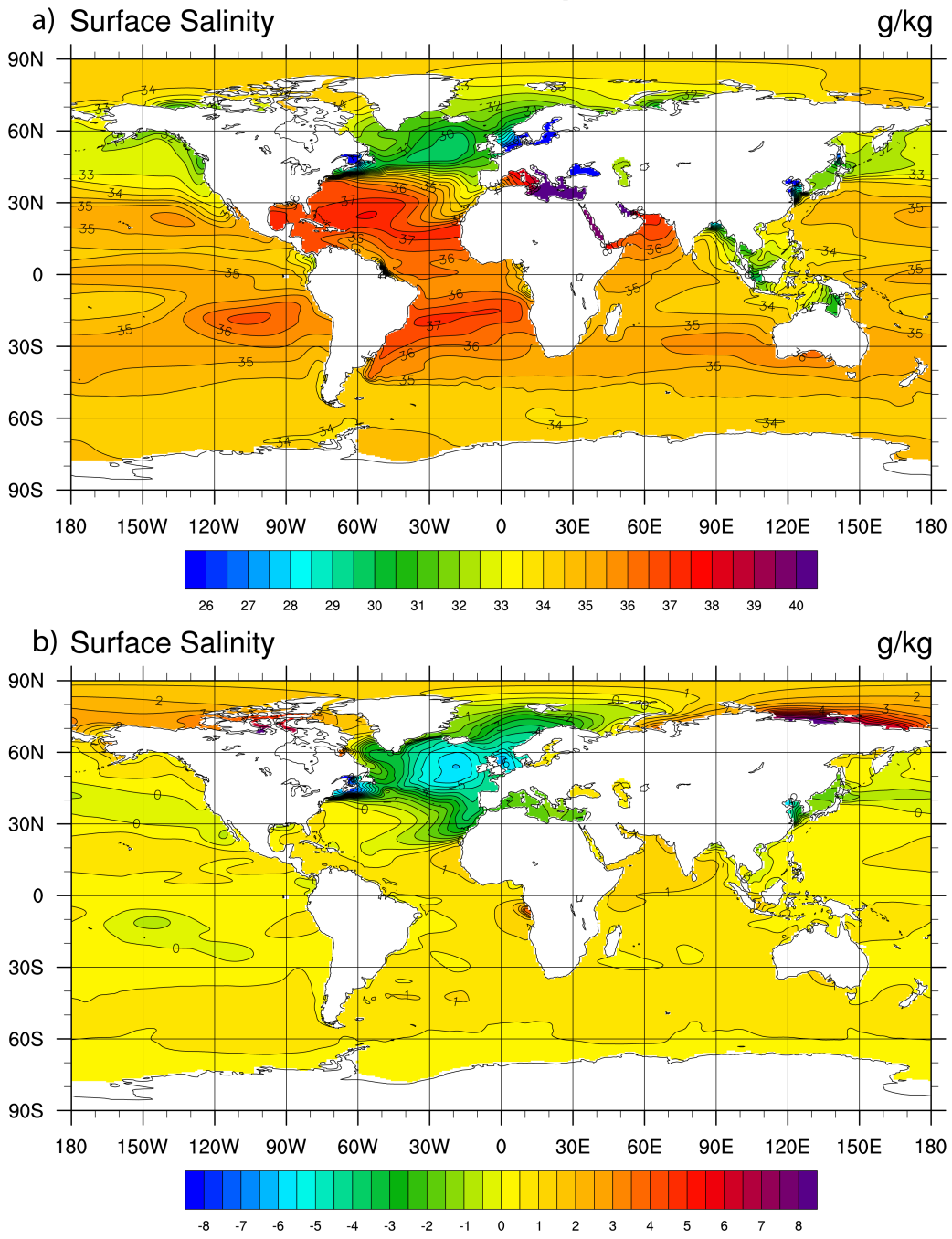

Figure 5-3 Sea surface salinity simulated by CESM1.2. A) The Younger Dryas climate and B) difference between the Younger Dryas and the preindustrial climate.

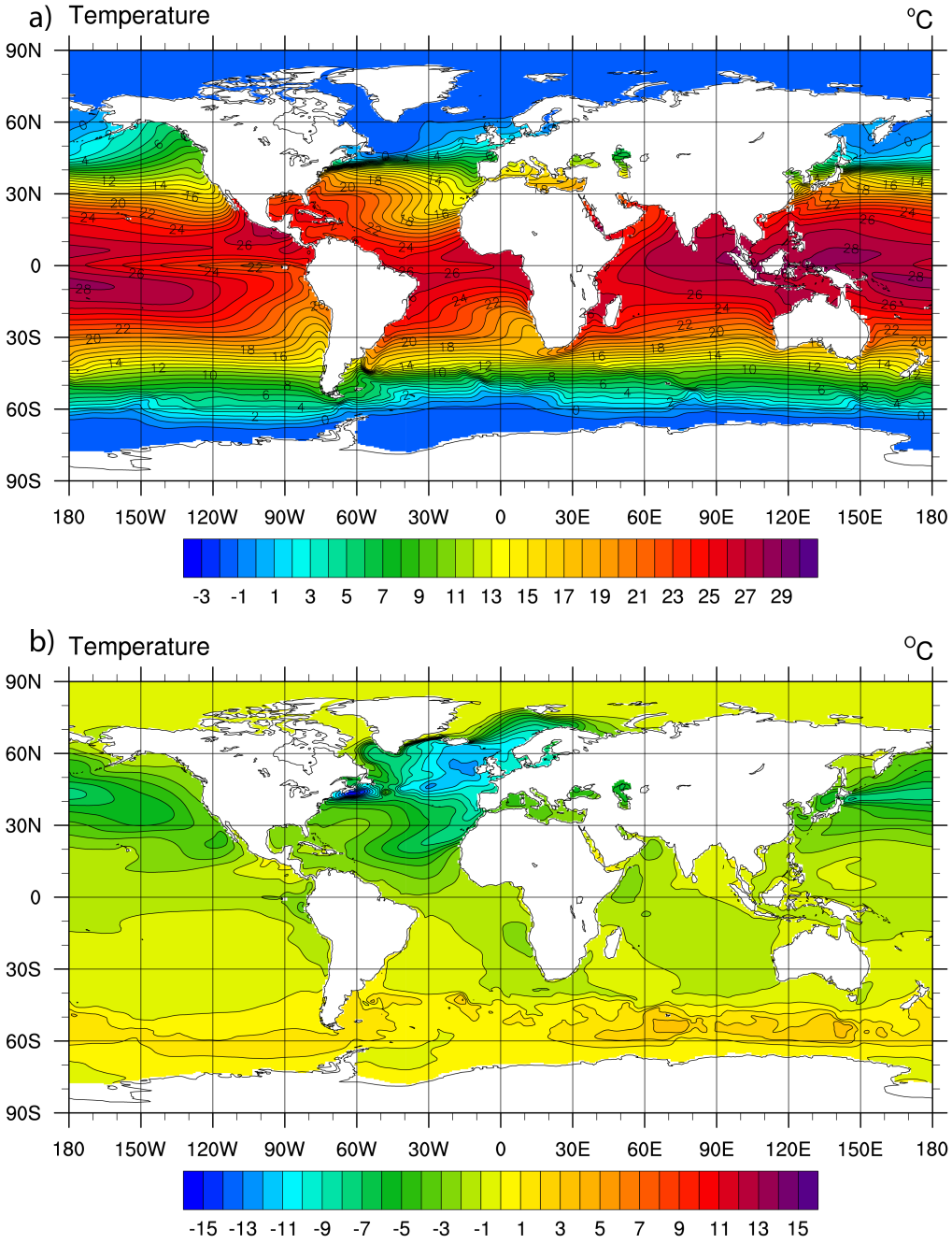

Figure 5-4 Sea surface temperatures simulated by CESM1.2 for A) the Younger Dryas climate and B) the difference between the Younger Dryas and the preindustrial simulations.

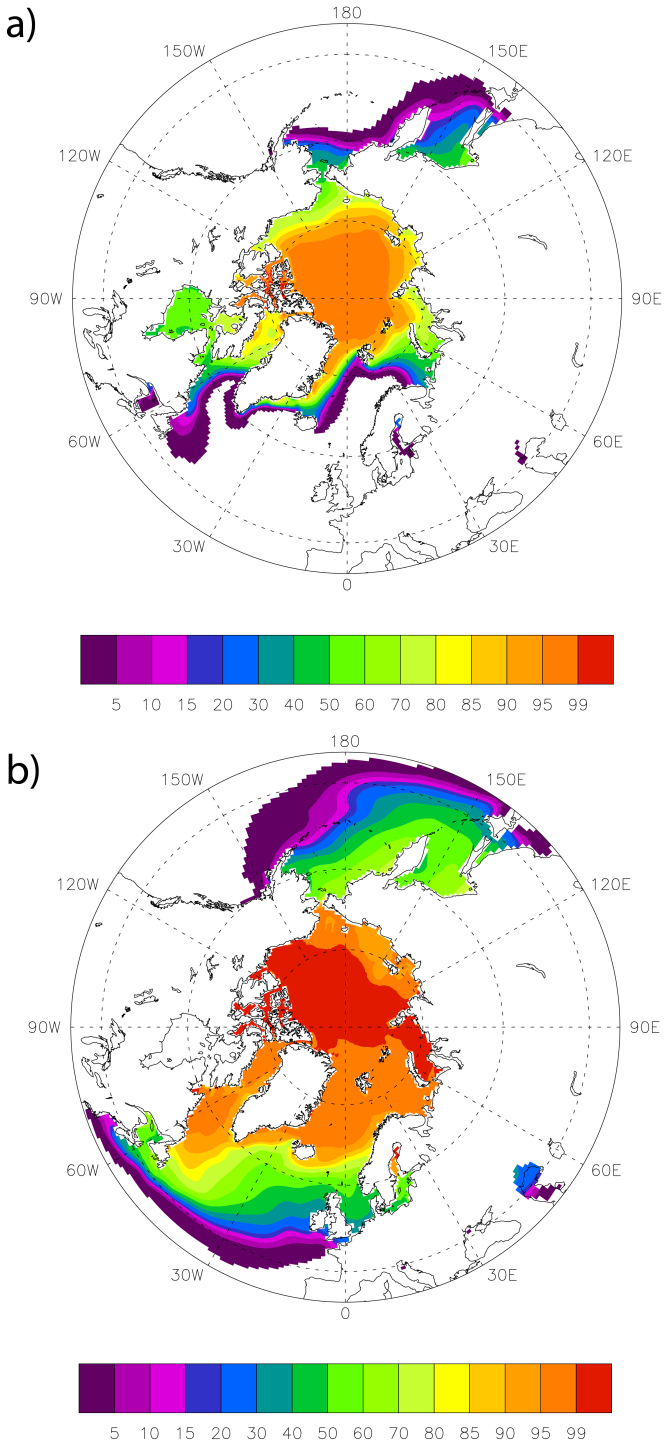

Figure 5-5 Sea ice area in % as simulated CESM1.2 for A) the preindustrial. B) Younger Dryas scenario.

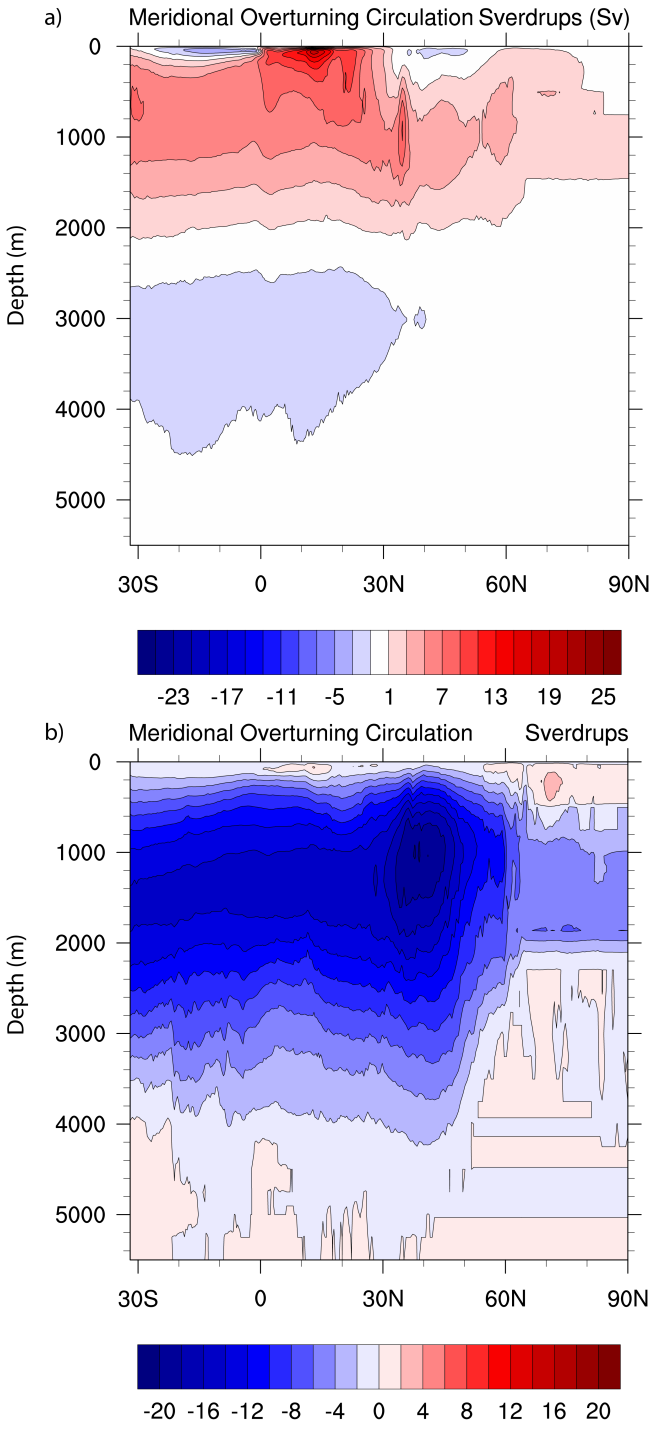

Figure 5-5 Zonally averaged Atlantic meridional overturning circulation from the CESM1 simulation A) for present day climate and B) for Younger Dryas climate. C) Difference between the Younger Dryas and the present day simulations.

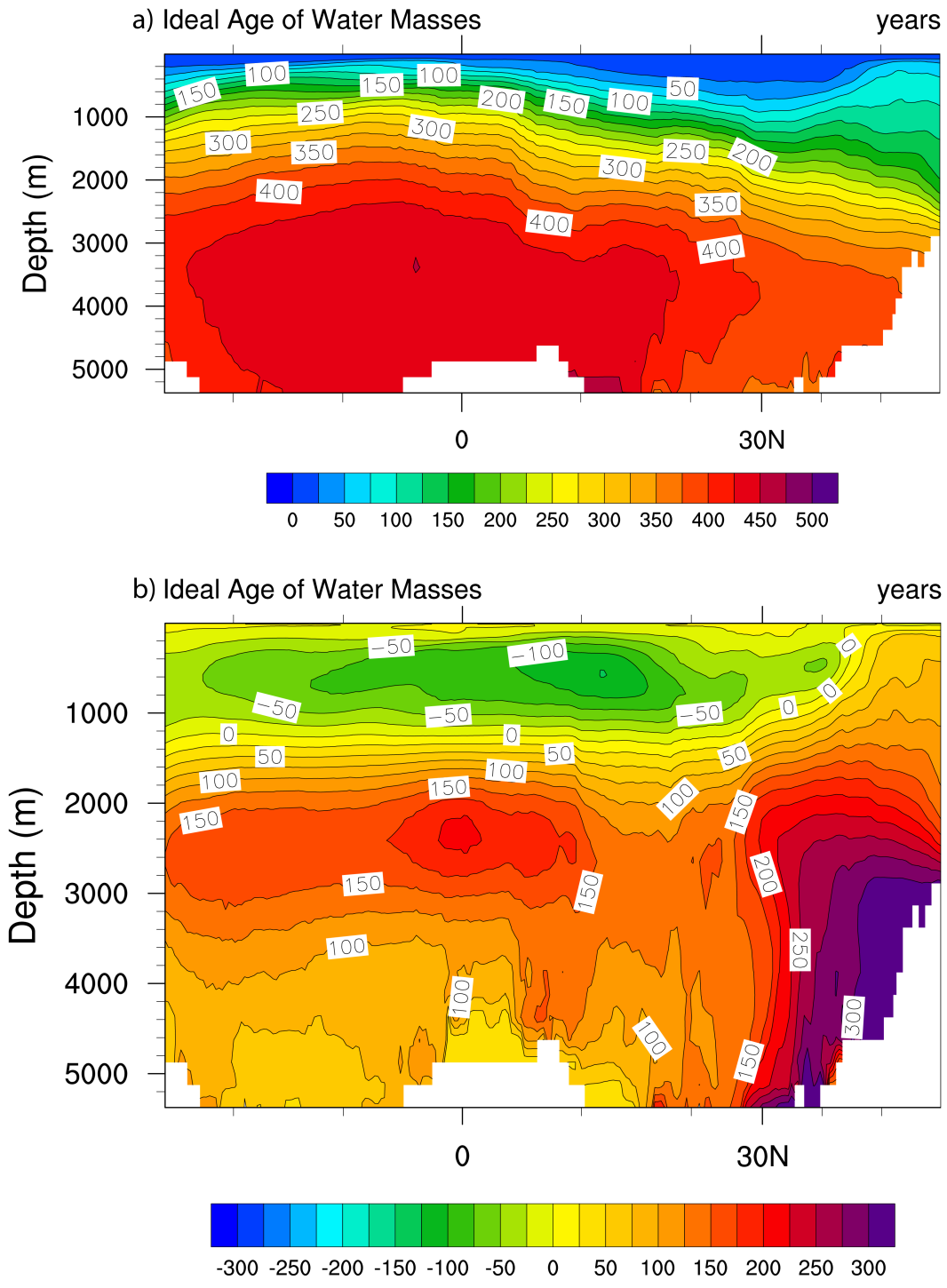

Figure 5-6 Zonally averaged ideal age of water masses simulated by CESM1.2. A) The Younger Dryas climate and B) difference between the Younger Dryas and the preindustrial climate.

Increase in precipitation increases freshwater forcing to the ocean and declines the AMOC strength, whereas decrease in rainfall decreases the freshwater flux to the ocean and increases the AMOC strength. Annual averaged precipitation in the North Atlantic Ocean for the Younger Dryas is 2.5 mm day^{-1}, a 2 mm day^{-1} decrease in the Younger Dryas simulation compared to the preindustrial simulation (Figure 5-8).

Surface air temperature also decreases in the Younger Dryas simulation compared to present day by ~-16°C, resulting in temperature of -48°C for the Younger Dryas simulation (Figure 5-9).

Surface winds and sea level pressure were averaged annually for the last twenty years of both simulations. Sea level pressure over the North Atlantic Ocean in the proximity of South Greenland during the Younger Dryas was approximately 1018 hPa, or 16 hPa higher than in the preindustrial run (Figure 5-10). Younger Dryas wind speeds over the North Atlantic were 5.2 m s^{-1} (Figure 5-10), or about 2.0 m s^{-1} higher than during the preindustrial scenario. Over Greenland, the average surface level pressure is lower compared to the adjacent ocean (1016 hPa) due to higher elevation of the ice sheet during the Younger Dryas (Figure 5-10). Younger Dryas wind speeds for the same area are approximately 1.8 m s^{-1} faster compared to the preindustrial simulation (Figure 5-10).

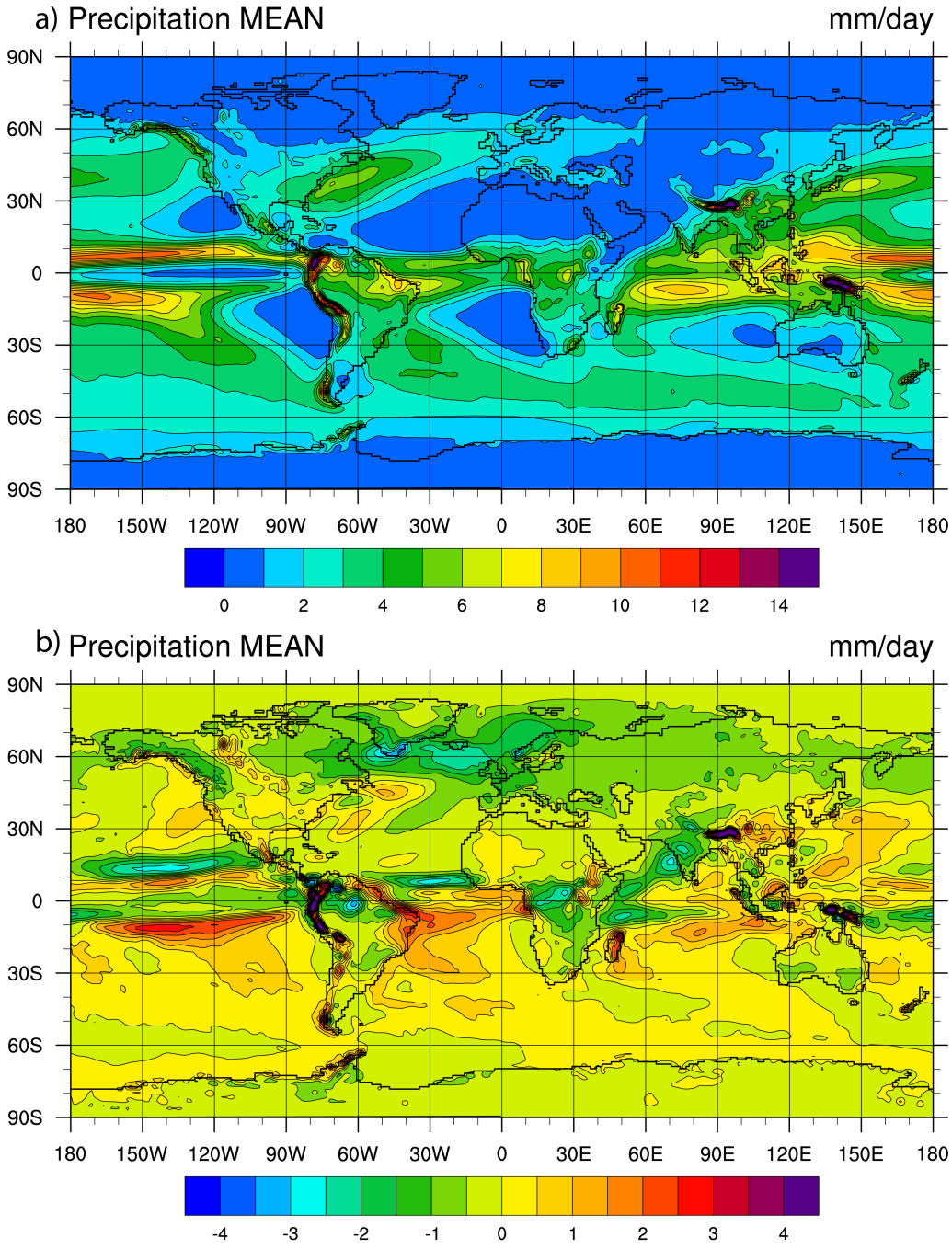

Figure 5-7 Annually averaged precipitation in mm day^{-1} simulated by CESM1.2. A) The Younger Dryas climate and B) difference between the Younger Dryas and the preindustrial climate.

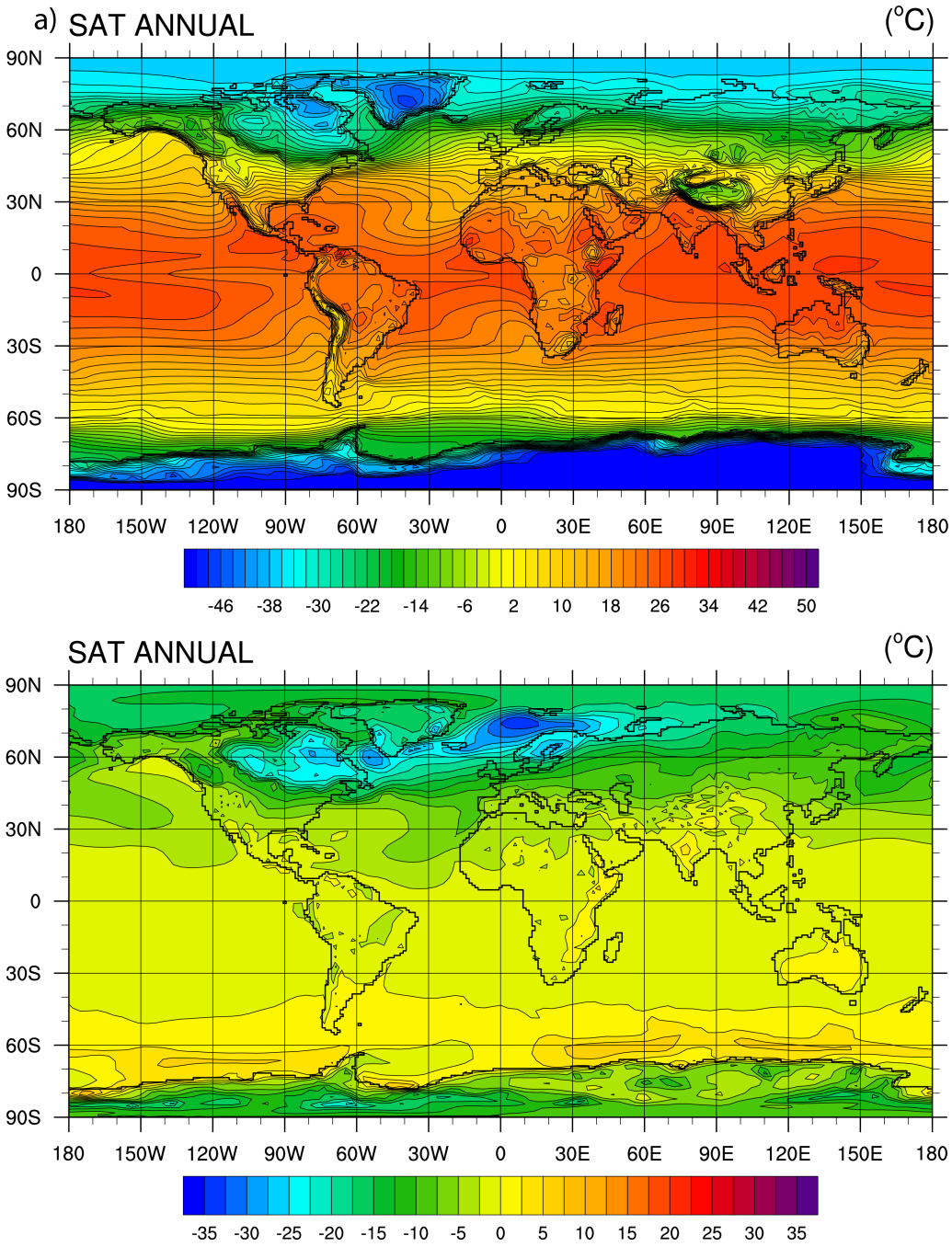

Figure 5-8 Surface air temperatures in °C simulated by CESM1.2. A) The Younger Dryas climate and B) the difference between the Younger Dryas and the preindustrial climate.

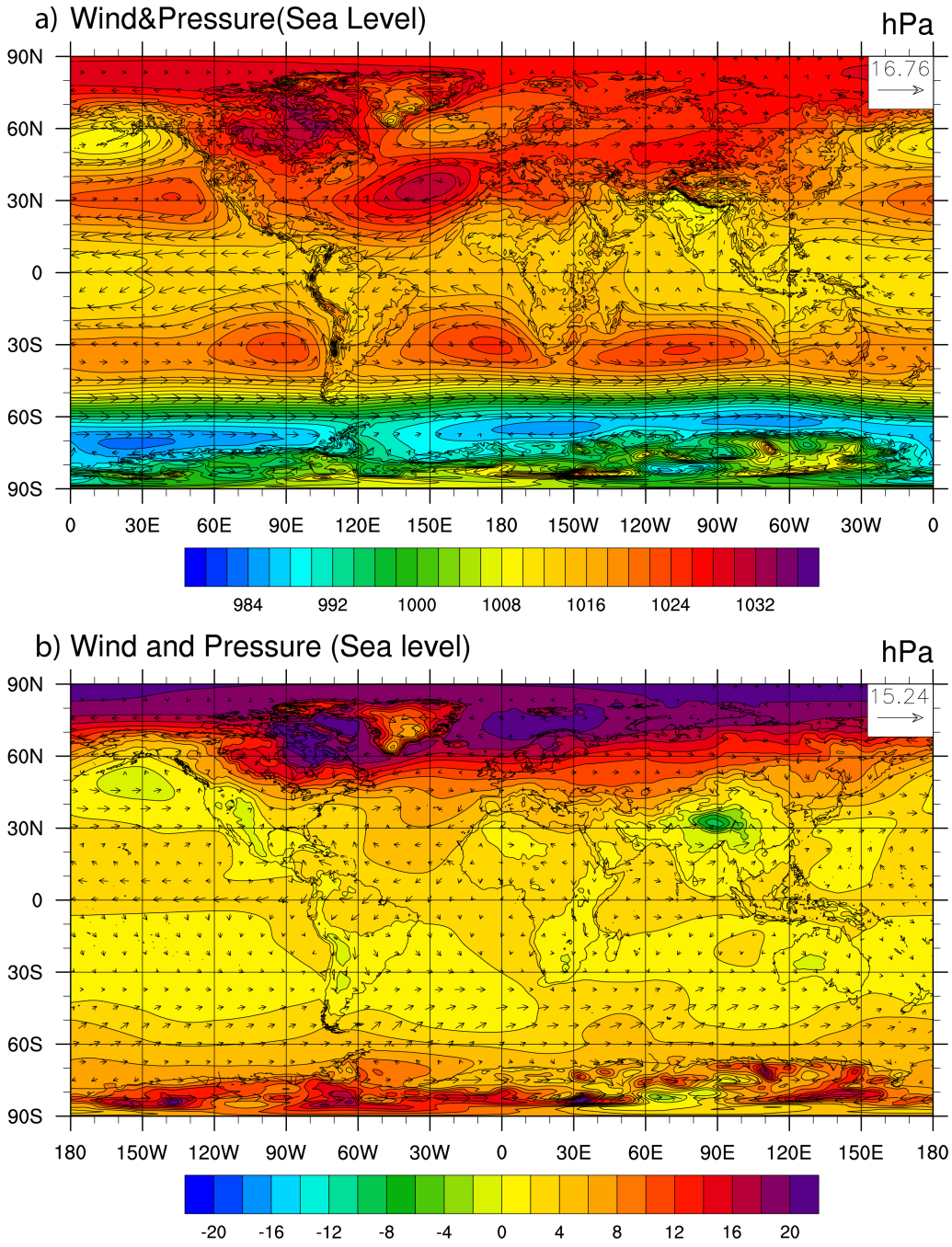

Figure 5-9 Sea level pressure in hPa and surface winds in m s^{-1} simulated by CESM1.2. A) The Younger Dryas climate and B) difference between the Younger Dryas and the preindustrial climate.

5.5.2 African monsoonal circulation

Classification of the African climatic zones in this study (see Chapter 4.4.2.2) follows those of Griffiths (1972; Figure 4-2). Annual precipitation over the semi-arid region was approximately 2 mm day^{-1}, which is approxiamately 0-1 mm day^{-1} less than the preindustrial simulation (Figure 5-11 A and B). For the northern tropical region, precipitation is ~7 mm day^{-1}, or 2 mm day^{-1} lower than the preindustrial simulation (Figure 5-11 A and B). The precipitation rates in the equatorial wet and southern tropics regions are 5 mm day^{-1} and 3 mm day^{-1} respectively, a difference of -4 mm day^{-1} and -2 mm day^{-1} respecitvely compared to the preindustrial simulation (Figure 5-11 A and B). Winter precipitation for the Younger Dryas simulation over the semi-arid and northern tropics regions is ~1 mm day^{-1}, which is 1-2 mm day^{-1} lower than the preindustrial simulation (Figure 5-12 A and B). Over the equatorial wet region, the average winter precipitation is 2 mm day^{-1}, which is 6 mm day^{-1} lower than the preindustrial simulation (Figure 5-12 A and B). The southern tropical region has the maximum rainfall of all the regions, which is ~5 mm day^{-1}, a 3 mm day^{-1} decrease compared to the preindustrial simulation (Figure 5-12 A and B). Summer precipitation for the semi-arid region is ~4 mm day^{-1}, which is an increase of 2 mm day^{-1} compared to the preindustrial experiement (Figure 5-12 C and D). The region with the maximum rainfall is the northern tropical region with a maximum precipitation rate of 12 mm day^{-1}, which is the same rate as the preindustrial rate (Figure 5-12 C and D). The precipitation rate for the equatorial wet and southern tropical regions is 5 mm day^{-1} and 2 mm day^{-1} respectively, a 1 mm day^{-1} compared to the preindustrial simulation (Figure 5-12 C and D). Thus, precipitation for the Younger Dryas decreases from North to South over the West African continent.

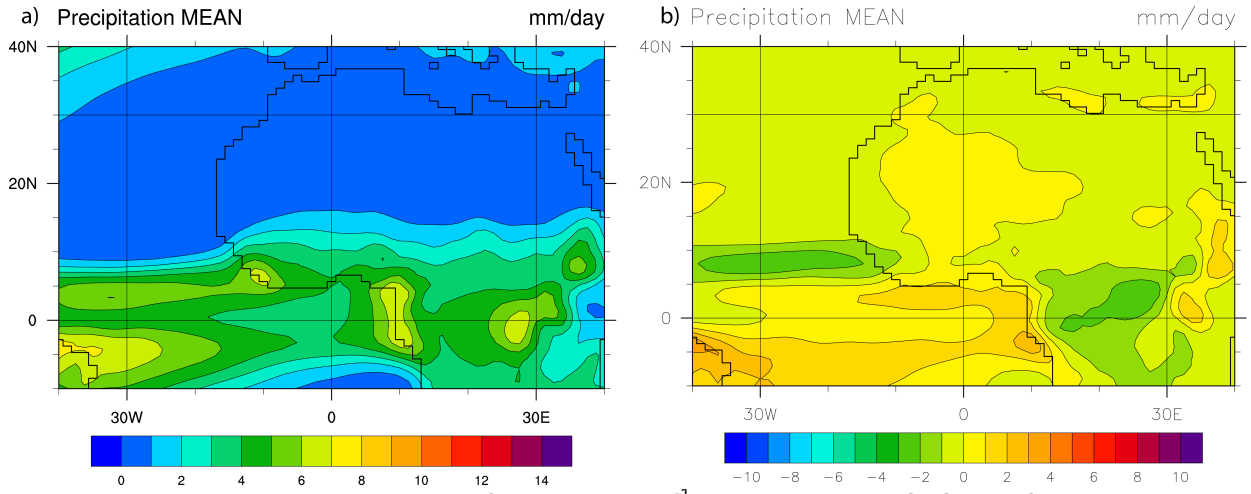

Figure 5-10 Precipitation over Africa in mm day^{-1} as simulated by CESM1.2 for A) the Younger Dryas scenario (annual average), B) the difference between Younger Dryas and preindustrial scenario (annual average).

.

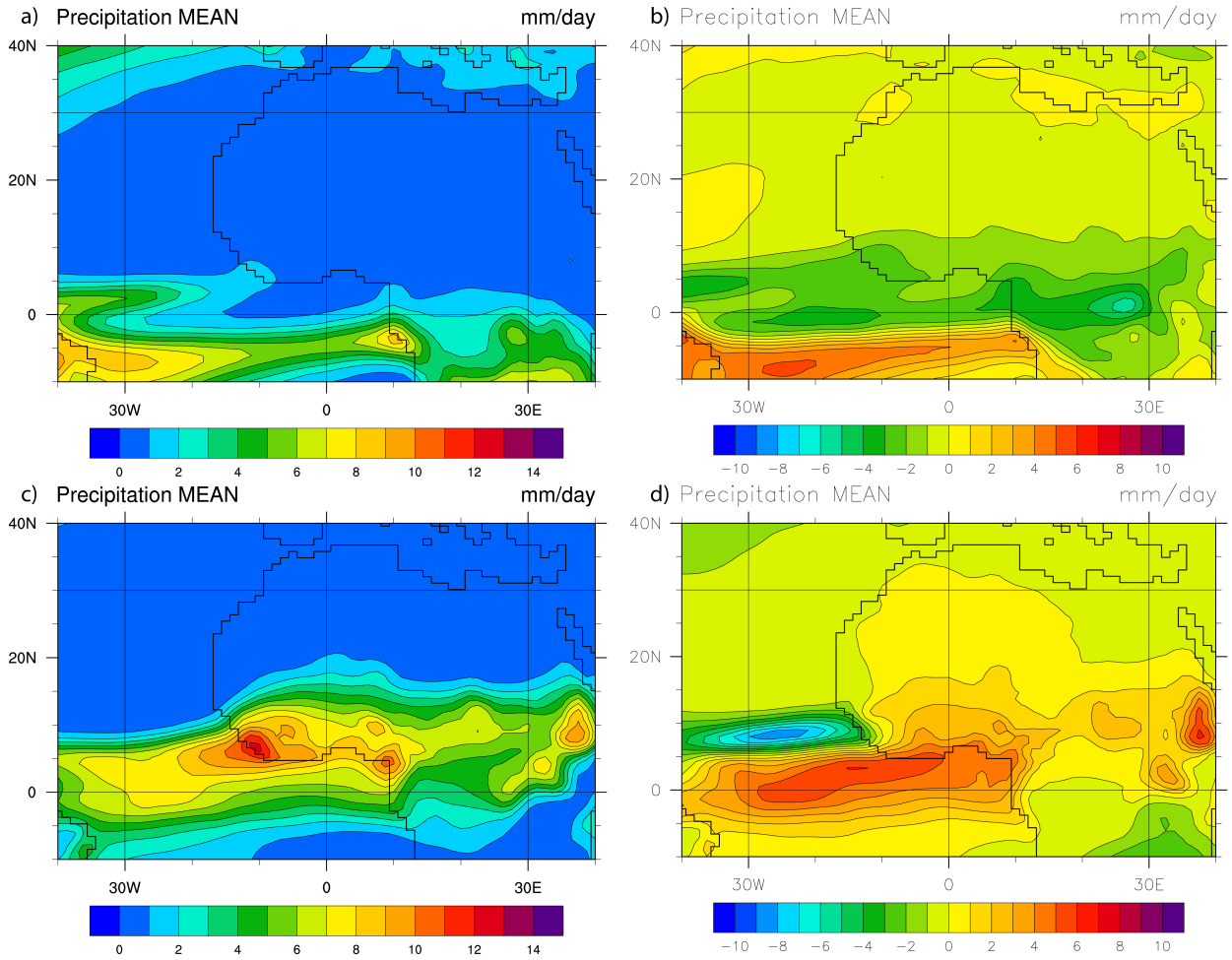

Figure 5-11 Precipitation over Africa in mm day^{-1} as simulated by CESM1.2 A) the Younger Dryas scenario (DJF), B) difference between Younger Dryas and preindustrial scenario (DJF), C) the Younger Dryas scenario (JJA), and D) difference between Younger Dryas and preindustrial scenario (JJA).

Annual sea level pressure for the Mediterranean region of the African continent is approximately 4 hPa higher than the preindustrial simulation at 1024 hPa (Figure 5-13 A and B). The sea surface pressure decreases from North Africa to Central Africa with maximal surface pressure of 1018 hPa over the northern desert, and minimal surface pressure of 1012 hPa over the semi-arid and northern tropical region (Figure 5-13 A). The pressure difference for each of these regions compared to the preindustrial simulation is +4 hPa (Figure 5-13 B). The Northeast and Southwest trade winds converge at approximatley at 2 °S latitude (Figure 5-13 A).

In the winter, a high pressure system is located over the Mediterranean and northern desert regions, with maximum pressure in the Mediterranean at 1030 hPa, a 7 hPa increase from the preindustrial simulation (Figure 5-14 A and B). The northern desert region has a maximal surface pressure of 1024 hPa, which is 6 hPa higher than the preindustrial simulation (Figure 5-14 A and B). Winter convergence in the Younger Dryas simulation with of the trade winds is approximately located at 7 °S (Figure 5-14 A).

Maximum summer sea level pressure for the Younger Dryas simulation is located over the Mediterranean region, which is approximately 1020 hPa, and a 1 hPa decrease compared to the preindustrial value (Figure 5-14 C and D). In this scenario, the minimum surface pressure of 1008 hPa is located over the northern desert (Figure 5-14 C), a 4 hPa decrease compared to preindustrial scenario (Figure 5-14 D). The surface pressure decreases from the semi-arid region (1015 hPa) to the southern tropical region (1013 hPa), but it is generally 2 hPa higher than the preindustrial simulation (Figure 5-14 C and D). The trades wind converges over western tropical Africa at 5 °N (Figure 5-14 C).

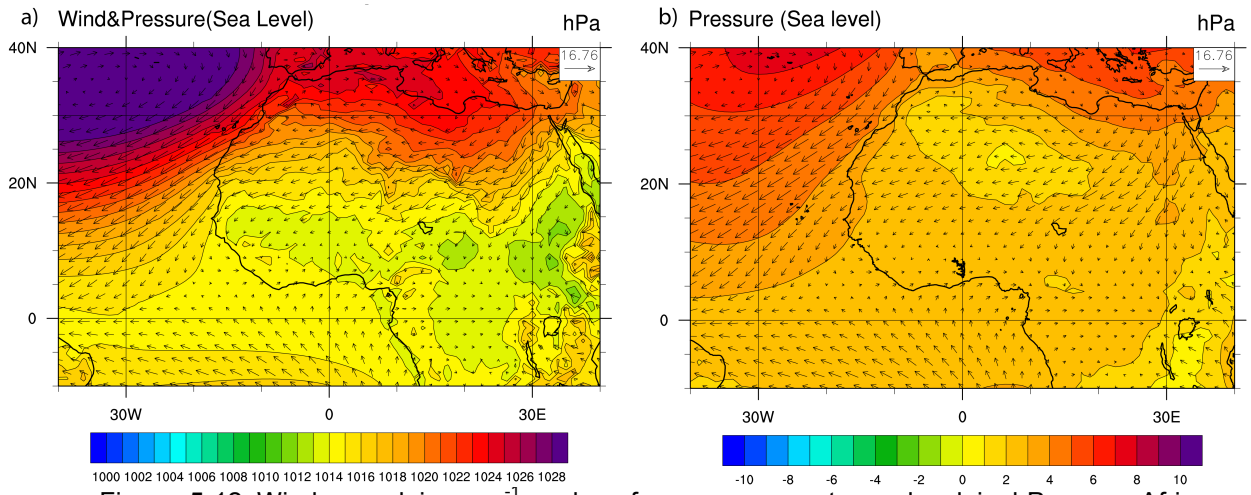

Figure 5-12 Wind speed in m s^{-1} and surface pressure at sea level in hPa over Africa as simulated by CESM1.2. for A) the Younger Dryas scenario (annual average), B) the difference between Younger Dryas and preindustrial scenario (annual average).

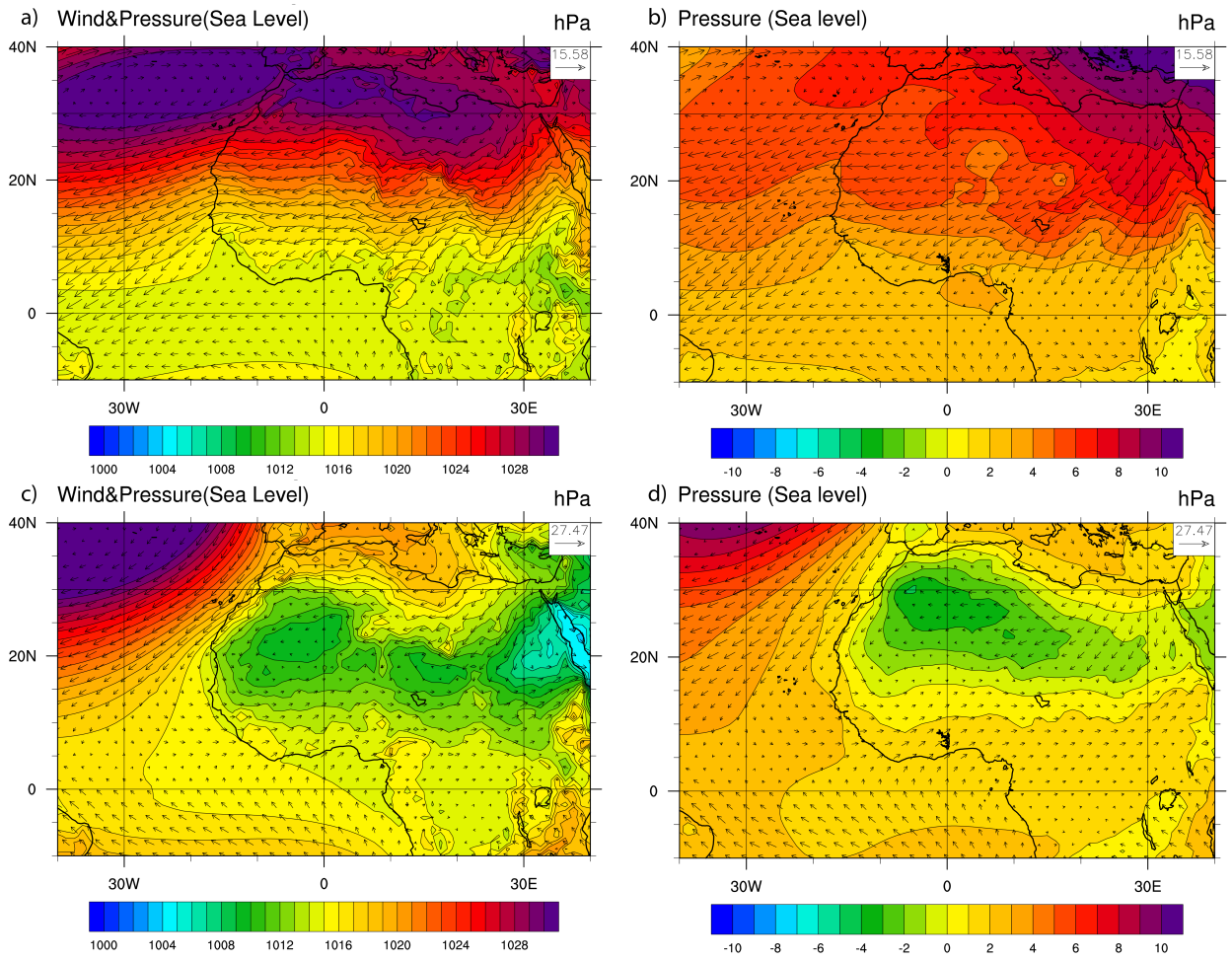

Figure 5-13 Wind speed in m s^{-1} and surface pressure at sea level over Africa in hPa as simulated by CESM1.2. for A) the Younger Dryas scenario in the winter (DJF), B) difference between Younger Dryas and preindustrial scenario in the winter, C) the Younger Dryas scenario in the summer (JJA), and D) difference between Younger Dryas and preindustrial scenario in the summer.

Annual surface air temperature for the Younger Dryas simulation is highest in the northern desert region at 26 °C, though this is a 4 °C decrease from the preindustrial simulation (Figure 5-15 A and B). The Mediterranean region is 7 °C cooler than the preindustrial simulation at 14 °C (Figure 5-15 A and B). Surface air temperature remains between 22 °C and 24 °C for the semi-arid to the southern tropical regions, which is approximatley 2 °C cooler than the prendustrial simulation (Figure 5-15 A and B). Winter surface air temperature is highest around the semi-arid through southern tropical regions, which is

approximately 20 °C (Figure 5-16 A). Note that the difference between the Younger Dryas and preindustrial simulation for these regions is substantial; the semi-arid region is 6 °C cooler, the northern tropic region is 4 °C cooler, and the equatorial wet and southern tropics region are both 3 °C cooler (Figure 5-16 B) for the Younger Dryas scenario compared to preindustrial scenario. Maximum summer temperature occurs over the northern desert region (~36 °C) and is 6 °C warmer than the preindustrial simulation (Figure 5-16 C and D). The Mediterranean region is ~28 °C, a 4 °C increase from the preindustrial temperature (Figure 5-16 C and D). Temperature decreases from the semi-arid region to the southern tropics (Figure 5-16 C). The semi-arid region is 1 °C cooler than the preindustrial at 25 °C, and the northern tropics and equatorial wet regions are both 22 °C and 2° cooler (Figure 5-16 C and D). The southern tropics are 4 °C cooler than the preindustrial simulation at 20 °C (Figure 5-16 C and D).

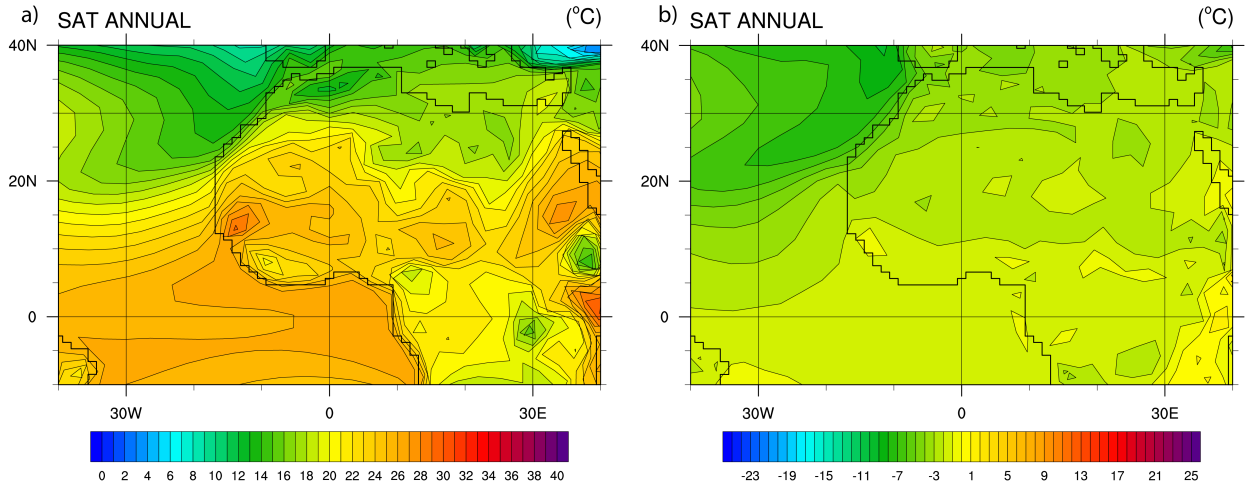

Figure 5-14 Surface air temperature over Africa in °C as simulated by CESM1.2 for A) the Younger Dryas scenario (annual average), B) the difference between Younger Dryas and preindustrial scenario (annual average).

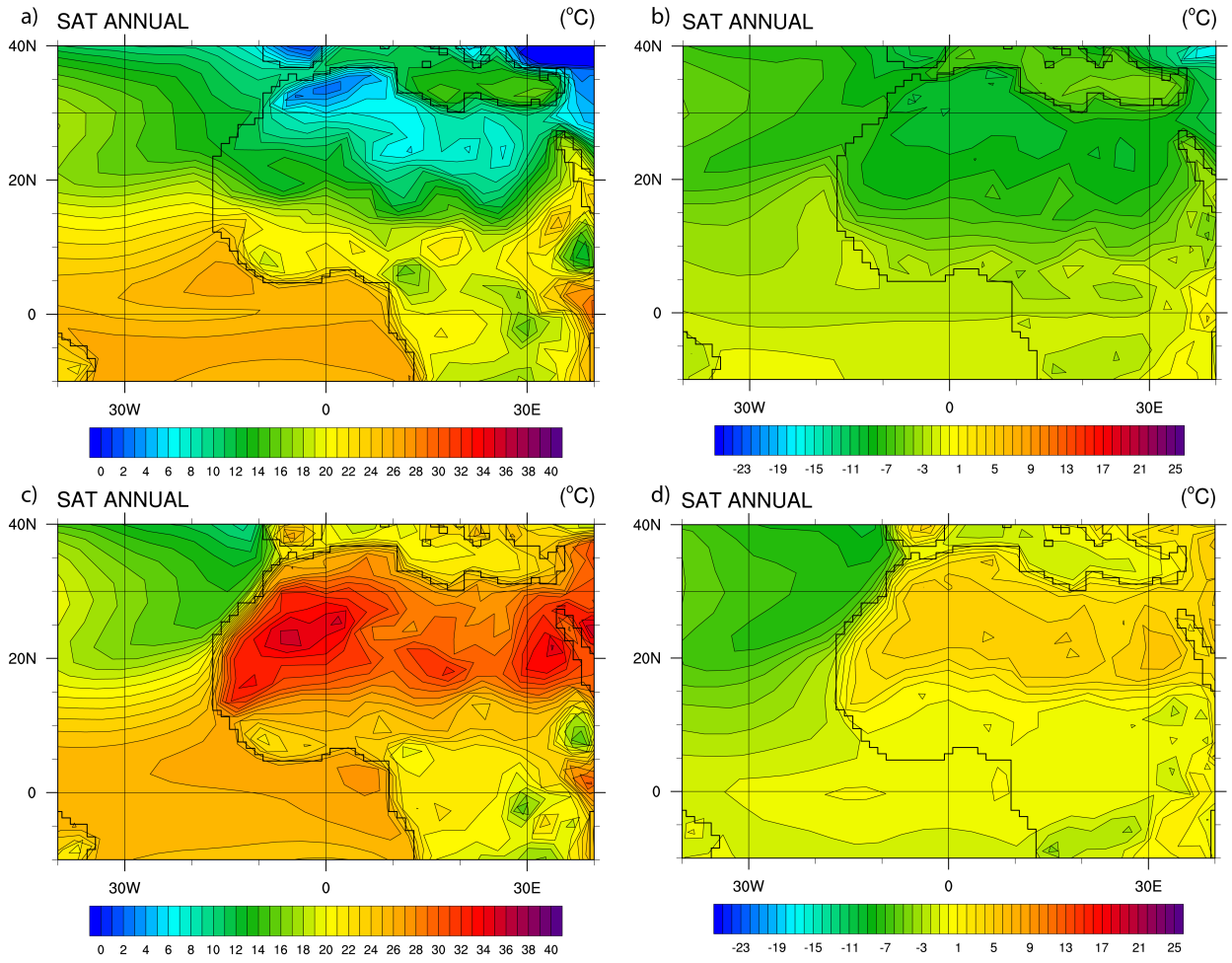

Figure 5-15 Surface air temperature over Africa in °C as simulated by CESM1.2 for A) the Younger Dryas scenario (DJF), B) difference between Younger Dryas and preindustrial scenario (DJF), C) the Younger Dryas scenario (JJA), and D) difference between Younger Dryas and preindustrial scenario (JJA).

5.6 Discussion

This study utilized a moderate resolution comprehensive climate model in the first Younger Dryas simulation that utilized all Younger Dryas boundary conditions, freshwater forcing, and ice sheets. Surface air temperature for central Greenland in the model decreased by ~15°C for the Younger Dryas simulation compared to the preindustrial control simulation. This is in agreement with reconstructions for the Younger Dryas (Severinghaus et al., 1998). The sea surface temperature bias of 9 °C bewteen

observations and the Younger Dryas experiment for the Northern North Atlantic (McManus et al., 2004) may be related to the intial conditions and forcing boundary conditions. For example, intial contions are taken from preindustial values, and the computational expense of the model in its current resolution limits a long integration into a steady state. This model data-bias is partially attributed to the magnitude of freshwater forcing since it is constant after the 100-year spinup thus leading to a substantial cooling in the North Atlantic Ocean. Another approximation is that radiative forcing (prescribed orbital parameters and greenhouse gas concentration) for the Younger Dryas simulation were set to 13.0 ka conditions and did not vary through the simulation transiently.

Salinity for the Younger Dryas simulation is approximately 29.5 psu just south of Greenland, which is in agreement with Younger Dryas salinity reconstructions of 30-27.5 psu (Schmidt et al., 2004; Clark et al., 2001; DeVernal et al., 1996; Ebbesen and Hald, 2004). The reduced precipitation in the North Atlantic region at the onset of the Younger Dryas coincides with the reduced convergence in the wind fields, the increase in surface pressure, and decline in storminess as suggested by ice core reconstructions from Greenland (Alley, 2000).

The simulated strength of the AMOC for the Younger Dryas of 7-10 Sv is agreeable with Pa/Th reconstructions (McManus et al., 2004; Gherardi et al., 2005) and with other model simulations (He, 2011; Liu et al., 2012). The increase in the ideal age of water masses and increase in vertical stratification of the water masses is consistent with the reduced AMOC.

In a simulation in which freshwater forcing on the magnitude of 0.3 Sv was released into the Arctic, the AMOC strength decreased from ~23.5 Sv to ~9 Sv (Peltier, 2007), in agreement with findings from this study. A substantial freshwater hosing as inferred from Schiller et al.(1997) and this study leads to significant cooling in the North Atlantic region. Such a freshwater forcing can lead to shut down of the AMOC, if freshwater is drained into the Labrador Sea (Mikolajewicz, 1996). Given that the freshwater forcing in this study is only half as strong, the reduction of the AMOC is comparable. A freshwater hosing from the St. Lawrence River of ~0.12 Sv could already lead to a reduction of the AMOC (Rind et al., 2001). Depending on the sensitivty of the climate model, an 0.2 Sv freshwater pulse may be suffient to

shut down the AMOC. However, climate simulations with CESM1.2 (this study) suggest that a higher freshwater hosing input of >0.3 Sv may be required to achieve a shutdown of the AMOC.

This study suggests that freshwater forcing appears to be important to explain the cooling over the Greenland dome as well as the decline in the AMOC strength as inferred from the paleoproxies. The input of freshwater forcing into the Northern North Atlantic Ocean leads to following feedback process: An increase in the freshwater flux into the Northern Atlantic caused a decrease in salinity in the surface waters. This decrease in salinity and associated enhanced sea ice cover, albeit cooler surface temperature due to the sea ice albedo effect, caused an enhanced vertical stratification of the water masses as indicated by the ideal age of water masses and a decreased the oceanic poleward heat transport at the surface. The increase in sea ice cover and decrease in in the sea surfarce temperature, together with substantial land ice cover during the Younger Dryas, yield to signifcant surface air temperature changes over Greenland relative to preindustrial conditions. The atmospheric moisture content for the region decreases with the decrease in temperature in the troposphere, thus leading to more aridity. Additionally, high pressure systems formed over the area as the air temperature became colder, and thus enhances the aridity.

Overall, the African monsoon for the Younger Dryas appears to be cooler and drier, as proposed by the paleoproxy reconstructions and other model simulations (Tierney et al., 2008; Gasse, 2000; Lézine et al., 2005; Garcin et al., 2007; Overpeck et al., 1996; Weldeab et al., 2011). For example, the annual averaged surface air temperature is 2-7 °C cooler than the preindustrial simulation. The seasonal YD temperatures are thus also cooler compared to the preindustrial state. Average winter temperature in the YD simulation is 3 °C to 10 °C cooler than the preindustrial experiment. The patterns of mean summer temperature in the YD simulation are more variable (with maxima 4-6 °C warmer and minima 1-4 °C cooler) than the preindustrial simulation. The denser, cooler air over the African continent leads to an overall increase in the surface pressure and increase in aridity. For the annual averages, the monsoonal precipitation range from 0-4 mm day^{-1} lower than the preindustrial simulation. The same trend is seen for the winter averages of rainfall in the range of 1-6 mm day^{-1} lower during the Younger Dryas scenario compared to the preindustrial scenario. The summer semi-arid region during the Younger Dryas

increases in precipitation of ~2 mm day^{-1} compared to the preindustrial simulation, whereas other regions the changes where even smaller.

The consideration of the YD ice sheet and the freshwater forcing has a substantially larger impact on the YD to preindustrial climate changes compared to the simulation with only orbital and greenhouse gas forcing (Chapter 4). For example both scenarios, the orbital and greenhouse gas forcing scenarios, increased with the warming of the surface air masses over Greenland, whereas increased albedo due to rise in the adjacent extent of sea ice to lower in latitude by freshwater forcing and the larger than present ice sheet during the YD led to a cooling and compensated the warming effect by greenhouse gas and orbital forcing.

The colder the northern latitudes, the weaker the monsoonal circulation is over Africa (Marzin et al., 2013). Freshwater input and enhanced cooling by the 13 ka ice sheet weakened the strength of the monsoon circulation during the YD as inferred from paleoproxy record. However, separate simulations that isolate the effects of freshwater forcing and ice sheet extent and height on the monsoon circulation need to be carried out.

The position of the ITCZ shifted from approximately 10°S during the YD to 7°N during the late Holocene. Such a southward shift of the ITCZ during glacial climate is consistent to rainfall changes as inferred observations and modeling (Waliser and Gautier, 1993; Hastenrath, 2002; Chiang et al., 2003; Chiang and Bitz, 2005). Higher sea ice and land cover and a 2°C decrease cooler surface temperatures during the Younger Dryas in the North Atlantic Ocean lead to more intense Azores high pressure system compared to the preindustrial simulation. Intensification of the Azores high-pressure system increases the strength of the NE trade winds and a southward shift of the ITCZ. This study support previous findings that a sea surface temperature decrease of >1°C compared to present day is required in order to shift the ITCZ southward (Chiang and Bitz, 2005).

5.7 Conclusion

Model results for this study indicate that the freshwater forcing by melting of continental ice masses into the Northern Atlantic Ocean causes a decrease in AMOC strength and a decrease in surface

air temperature in agreement with surface air temperature reconstructions for the Younger Dryas. The decrease in surface air temperature for the Younger Dryas simulation compared to the preindustrial simulation was ~15 °C, and the AMOC strength at the end of the freshwater forcing was approximately 7 Sv. The addition of the Younger Dryas freshwater forcing and 13 ka ice sheet were large enough to balance or even compensate the effects of the greenhouse gas and orbital forcing discussed in chapter 4. This study also agrees with proxy reconstructions that inferrred that the Younger Dryas African monsoon was colder and drier. A simulated southward shift in the ITCZ due to the Northern hemispheric cooling is in agreement with previous studies. This weakening of the West African monsoon can be attributed to freshwater input and the consideration of the 13ka ice sheet. However, to understand the Younger Dryas to present changes in the monsoon circulation more effectively simulations that isolate the effects of freshwater forcing and Younger Dryas ice sheet need to be carried out.

References

Alley, R.B., 2000, The Younger Dryas cold interval as viewed from central Greenland: Quaternary Science Reviews, v. 19, p. 213–226, doi: 10.1016/S0277-3791(99)00062-1.

Berger, A., 1988, Milankovitch Theory and climate: Reviews of Geophysics, v. 26, p. 624, doi: 10.1029/RG026i004p00624.

Berger, A., and Loutre, M.F., 1991, Insolation values for the climate of the last 10 million years: Quaternary Science Reviews, v. 10, p. 297–317, doi: 10.1016/0277-3791(91)90033-Q.

Boyle, E.A., and Keigwin, L., 1987, North Atlantic thermohaline circulation during the past 20,000 years linked to high-latitude surface temperature: Nature, v. 330, p. 35–40, doi: 10.1038/330035a0.

Broecker, W.S., Andree, M., Wolfli, W., Oeschger, H., Bonani, G., Kennett, J., and Peteet, D.M., 1988, The Chronology of the Last Deglaciation: Impications to the Cause of the Younger Dryas Event: Paleoceanography, v. 3, p. 1–19, doi: 10.1029/PA003i001p00001.

Broecker, W.S., and Denton, G.H., 1989, The role of ocean-atmosphere reorganizations in glacial cycles: Geochimica et Cosmochimica Acta, v. 53, p. 2465–2501, doi: 10.1016/0016-7037(89)90123-3.

Chiang, J.C.H., Biasutti, M., and Battisti, D.S., 2003, Sensitivity of the Atlantic Intertropical Convergence Zone to Last Glacial Maximum boundary conditions: Paleoceanography, v. 18, p. 18, doi: 10.1029/2003PA000916.

Chiang, J.C.H., and Bitz, C.M., 2005, Influence of high latitude ice cover on the marine Intertropical Convergence Zone: Climate Dynamics, v. 25, p. 477–496, doi: 10.1007/s00382-005-0040-5.

Chiang, J.C.H., Kushnir, Y., and Giannini, A., 2002, Deconstructing Atlantic Intertropical Convergence Zone variability: Influence of the local cross-equatorial sea surface temperature gradient and remote forcing from the eastern equatorial Pacific: Journal of Geophysical Research, v. 107, p. 4004, doi: 10.1029/2000JD000307.

Clark, P.U., Marshall, S.J., Clarke, G.K., Hostetler, S.W., Licciardi, J.M., and Teller, J.T., 2001, Freshwater forcing of abrupt climate change during the last glaciation.: Science, v. 293, p. 283–287, doi: 10.1126/science.1062517.

DeVernal, A., Hillaire-Marcel, C., and Bilodeau, G., 1996, Reduced meltwater outflow from the Laurentide ice margin during the Younger Dryas: Nature, v. 381, p. 774–777, doi: 10.1038/381774a0.

Ebbesen, H., and Hald, M., 2004, Unstable Younger Dryas climate in the northeast North Atlantic: Geology, v. 32, p. 673 –676, doi: 10.1130/G20653.1.

England, M.H., 1995, The Age of Water and Ventilation Timescales in a Global Ocean Model: Journal of Physical Oceanography, v. 25, p. 2756–2777, doi: 10.1175/1520-0485(1995)025.

Garcin, Y., Vincens, A., Williamson, D., Buchet, G., and Guiot, J., 2007, Abrupt resumption of the African Monsoon at the Younger Dryas-Holocene climatic transition: Quaternary Science Reviews, v. 26, p. 690–704, doi: 10.1016/j.quascirev.2006.10.014.

Gasse, F., 2000, Hydrological changes in the African tropics since the Last Glacial Maximum: Quaternary Science Reviews, v. 19, p. 189–211, doi: 10.1016/S0277-3791(99)00061-X.

Gherardi, J.M., Labeyrie, L., McManus, J.F., Francois, R., Skinner, L.C., and Cortijo, E., 2005, Evidence from the Northeastern Atlantic basin for variability in the rate of the meridional overturning circulation through the last deglaciation: Earth and Planetary Science Letters, v. 240, p. 710–723, doi: 10.1016/j.epsl.2005.09.061.

Griffiths, J.F., 1972, Climates of Africa, Volume 10: Elsevier Pub. Co., 604 p.

Hastenrath, S., 2002, Dipoles, temperature gradients, and tropical climate anomalies: Bulletin of the American Meteorological Society, v. 83, p. 735–738, doi: 10.1175/1520-0477(2002)083<0735:WLACNM>2.3.CO;2.

He, F., 2011, Simulating Transiet Climate Evolution of the Last Deglaciation with CCSM3: University of Wisconsin-Madison, 1-185 p.

Huang, E., and Tian, J., 2008, Melt-Water-Pulse (MWP) events and abrupt climate change of the last deglaciation: Chinese Science Bulletin, v. 53, p. 2867–2878, doi: 10.1007/s11434-008-0206-8.

Hughen, K.A., Southon, J.R., Lehman, S.J., and Overpeck, J.T., 2000, Synchronous radiocarbon and climate shifts during the last deglaciation.: Science, v. 290, p. 1951–1955.

Iacono, M.J., 2008, Radiative Forcing by Long-Lived Greenhouse Gases: Calculations with the AER Radiative Transfer Models: Journal of Geophysical Research: Atmospheres, v. 113, p. 8.

Lézine, A.-M., Duplessy, J., and Cazet, J., 2005, West African monsoon variability during the last deglaciation and the Holocene: Evidence from fresh water algae, pollen and isotope data from core KW31, Gulf of Guinea: Palaeogeography, Palaeoclimatology, Palaeoecology, v. 219, p. 225–237, doi: 10.1016/j.palaeo.2004.12.027.

Liu, Z., Carlson, A.E., He, F., Brady, E.C., Otto-Bliesner, B.L., Briegleb, B.P., Wehrenberg, M., Clark, P.U., Wu, S., Cheng, J., Zhang, J., Noone, D., and Zhu, J., 2012, Younger Dryas cooling and the Greenland climate response to CO2.: Proceedings of the National Academy of Sciences of the United States of America, v. 109, p. 11101–4, doi: 10.1073/pnas.1202183109.

Manabe, S., and Stouffer, R.J., 1994, Multiple-century response of a coupled ocean-atmosphere model to an increase of atmospheric carbon dioxide: Journal of Climate, v. 7, p. 5–23, doi: 10.1175/1520-0442(1994)007<0005:MCROAC>2.0.CO;2.

Marzin, C., Braconnot, P., and Kageyama, M., 2013, Relative impacts of insolation changes, meltwater fluxes and ice sheets on African and Asian monsoons during the Holocene: Climate Dynamics, v. 41, p. 2267–2286, doi: 10.1007/s00382-013-1948-9.

McManus, J.F., Francois, R., Gherardi, J.-M., Keigwin, L.D., and Brown-Leger, S., 2004, Collapse and rapid resumption of Atlantic meridional circulation linked to deglacial climate changes.: Nature, v. 428, p. 834–7, doi: 10.1038/nature02494.

Mikolajewicz, U., 1996, A meltwater induced collapse of the `conveyor belt' thermohaline circulation and its influence on the distribution of $\delta^{14}C$ and $\delta^{18}O$ in the oceans: Technical Report, Max Plank Institute for Meteorology, p. 25.

Murton, J.B., Bateman, M.D., Dallimore, S.R., Teller, J.T., and Yang, Z.-L., 2010, Identification of Younger Dryas outburst flood path from Lake Agassiz to the Arctic Ocean.: Nature, v. 464, p. 740–3, doi: 10.1038/nature08954.

Neale, R.B., Richter, J.H., Conley, A.J., Park, S., Lauritzen, P.H., Gettelman, A., Williamson, D.L., Rasch, P.J., Vavrus, S., Taylor, M.A., Collins, W.D., Zhang, M., and Lin, S.-J., 2010, Description of the NCAR Community Atmosphere Model (CAM 4.0): NCAR Technical Note, v. NCAR/TN-48, p. 212.

Overpeck, J., Anderson, D., Trumbore, S., and Prell, W., 1996, The southwest Indian Monsoon over the last 18000 years: Climate Dynamics, v. 12, p. 213–225, doi: 10.1007/BF00211619.

Peltier, W.R., 2007, Rapid climate change and Arctic Ocean freshening: Geology, v. 35, p. 1147, doi: 10.1130/focus122007.1.

Rahmstorf, S., 1996, Bifurcations of the Atlantic Thermohaline circulation in response to changes in the hydrological cycle: Nature, v. 378, p. 145–149, doi: 10.1038/378145a0.

Rahmstorf, S., 2006, Thermohaline Ocean Circulation, *in* Encyclopedia of Quaternary Sciences, p. 1–10.

Rind, D., DeMenocal, P., Russell, G., Sheth, S., Collins, D., Schmidt, G., and Teller, J., 2001, Effects of glacial meltwater in the GISS coupled atmosphereocean model: 1. North Atlantic Deep Water response: Journal of Geophysical Research: Atmospheres, v. 106, p. 27335–27353, doi: 10.1029/2000JD000070.

Rooth, C., 1982, Hydrology and ocean circulation: Progress in Oceanography, v. 11, p. 131–149, doi: 10.1016/0079-6611(82)90006-4.

Schiller, A., Mikolajewicz, U., and Voss, R., 1997, The stability of the North Atlantic thermohaline circulation in a coupled ocean-atmosphere general circulation model: Climate Dynamics, v. 13, p. 325–347, doi: 10.1007/s003820050169.

Schmidt, M.W., Spero, H.J., and Lea, D.W., 2004, Links between salinity variation in the Caribbean and North Atlantic thermohaline circulation.: Nature, v. 428, p. 160–3, doi: 10.1038/nature02346.

Severinghaus, J.P., Sowers, T., Brook, E.J., Alley, R.B., and Bender, M.L., 1998, Timing of abrupt climate change at the end of the Younger Dryas interval from thermally fractionated gases in polar ice: Nature, v. 391, p. 141–146.

Tarasov, L., and Peltier, W.R., 2005, Arctic freshwater forcing of the Younger Dryas cold reversal.: Nature, v. 435, p. 662–5, doi: 10.1038/nature03617.

Thiele, G., and Sarmiento, J.L., 1990, Tracer Dating and Ocean Ventilation: Journal of Geophysical Research, v. 95, p. 9377–9391, doi: 10.1029/JC095iC06p09377.

Tierney, J.E., Russell, J.M., Huang, Y., Damste, J.S.S., Hopmans, E.C., and Cohen, a. S., 2008, Northern Hemisphere Controls on Tropical Southeast African Climate During the Past 60,000 Years: Science, v. 322, p. 252–255, doi: 10.1126/science.1160485.

Voss, R., and Mikolajewicz, U., 2001, The climate of 6000 years BP in near-equilibrium simulations with a coupled AOGCM: Geophysical Research Letters, v. 28, p. 2213–2216, doi: 10.1029/2000GL012498.

Waliser, D.E., and Gautier, C., 1993, A satellite-derived climatology of the ITCZ: Journal of Climate, v. 6, p. 2162–2174, doi: 10.1175/1520-0442(1993)006<2162:ASDCOT>2.0.CO;2.

Weldeab, S., Frank, M., Stichel, T., Haley, B., and Sangen, M., 2011, Spatio-temporal evolution of the West African monsoon during the last deglaciation: Geophysical Research Letters, v. 38, p. n/a–n/a, doi: 10.1029/2011GL047805.

Chapter 6

Future Outlook

The simulations conducted in this study will give valuable insight into the Younger Dryas climate and the mechanisms involved in producing abrupt climate change. Specifically, this study analyzed how orbital, greenhouse gas, and freshwater forcing changes affect the Younger Dryas climate. However, the effects of freshwater alone have not been determined without the influence of an ice sheet. Therefore, in order to isolate how each parameter, freshwater forcing and the ice sheet, affect the climate, additional simulations need to be performed. The following topics would be of interest to explore further to improve the understanding of the causes of the onset of the Younger Dryas cooling event and climate variations during the Younger Dryas.

6.1 Ice Sheet Dynamics

As discussed in section 1.2.2, changes in the ice margin of the Laurentide Ice Sheet is proposed to cause a positive feedback loop that would increase net precipitation at the onset of the Younger Dryas cooling event by affecting atmospheric circulation, sea ice development, and therefore the AMOC (Eisenman et al., 2009). The plausibility of this mechanism has already been confirmed using the NCAR CCSM3, but has not been applied to YD boundary conditions (i.e. orbital parameters, greenhouse gases, and salinity changes).

One can propose a high-resolution transient simulation from the Last Glacial Maximum through the Younger Dryas, if computer resources become available with changing the ice sheets and other forcing boundary conditions. Another experiment of interest would be a YD simulation without freshwater hosing to evaluate the sensitivity of the climate to the continental ice sheet. Once the simulation has been fully integrated, the goal would be to evaluate how changes in the ice margin of the Laurentide Ice Sheet can alter storm tracks and associated location of the jet stream, precipitation patterns, sea surface temperature, sea ice cover and the AMOC. Changes in the AMOC could be compared with the paleoclimatic record, e.g. to the stable carbon isotope reconstructions inferred from epibenthic foraminiferal shells in sedimentary records (Sarnthein et al., 1994).

6.2 El Niño/Southern Oscillation during the YD

The El Niño/Southern Oscillation (ENSO) climate variability is one of the pronounced climate perturbation in the equatorial Pacific (McPhaden, 1999). The Southern Oscillation involves the fluctuation of tropical atmospheric pressure between a low pressure area (e.g. Djakarta) and a high pressure system (e.g. Easter Island) (Berlage, 1966). This fluctuation of pressure affects the circulation over North America during the winter, as well as monsoon rainfall, and can be measured by the Southern Oscillation Index (SOI; Power and Kociuba, 2010; Rasmusson and Wallace, 1983). The SOI measures the difference in pressure over the Pacific ocean from Darwin to Tahiti, and predicts and tracks changes in ENSO (Power and Kociuba, 2010). El Niño is a disturbance of ocean sea surface temperature and ocean currents in the central and eastern Pacific ocean, cool and nutrient-rich water masses upwell along the equatorial divergence (Zebiak and Cane, 1987; AchutaRao and Sperber, 2002; Latif and Keenlyside, 2009). The eastward propagation of warm surface water into the cool water is coupled with a weakening of the Southern Oscillation and NE and SE trade winds every two to seven years, and leads to increased precipitation over the Pacific coastal region of the North American continent (Bacastow et al., 1980; Zebiak and Cane, 1987; AchutaRao and Sperber, 2002; Latif and Keenlyside, 2009) and decrease rainfall over Indonesia and Northern Australia.

Terrestrial and deep sea sedimentary records representing hydrological respectively indicate the variability and strength of ENSO events (Turney et al., 2004; Beaufort et al., 2001). The sedimentary record from Lynch's Crater in Queensland, Australia indicates dry periods on a millennial scale (Turney et al., 2004). In Australia, southern hemisphere summer (September–May) precipitation declines, indicating frequent El Niño events (Turney et al., 2004). The deep sea cores from the Pacific and Indian oceans suggest equatorial productivity variations, correlated precessional cycles and indicative of the variability of glacial-interglacial shifts and changes in the east-west thermocline (Beaufort et al., 2001). A study of the Holocene using the Zebiak-Cane coupled ocean model indicates that an increase in orbital parameters results in a cooling induced by solar radiation, suppression of warm event development, and fewer cold events associated with ENSO behavior change (Clement et al., 2001). Additionally, when forcing the

model with a precession of the equinoxes closer to zero, changes in the solar insolation alters the ENSO character significantly (Clement et al., 2001).

The equatorial net gas air-sea flux of CO_2 exchange is related to Ekman-induced upwelling and thus correlated to ENSO, but in turn changes in the greenhouse gas radiative forcing may also affect ENSO (Fedorov and Philander, 2000; Fedorov et al., 2010; Rayner et al., 1999; Keeling et al., 1989; Winguth et al., 1994), potentially linked to a decrease in the Walker Circulation with an increase in greenhouse gas radiative forcing, or not affect substantially (Tett, 1995; Latif and Keenlyside, 2009; IPCC, 2013). The question remains of how ENSO would be altered with lower than present CO_2 radiative forcing during the Younger Dryas.

To determine how ENSO responds to the YD climate perturbations, such as orbital parameter and greenhouse gas changes along with freshwater forcing and ice sheet adjustments, several parameters and their interactions need to be analyzed. The primary variable that needs to be looked into is the sea surface temperature in the equatorial region of the Pacific Ocean, particularly the SST anomalies for the Nino3 and Nino3.4 regions (Latif and Barnett, 1994; Timmerman et al., 1999; England, 1995b; McPhaden, 1999; Lee and McPhaden, 2010; Latif and Barnett, 1996; Huber and Caballero, 2003; Xue et al., 1997; Roeckner et al., 1996; Torrence and Webster, 1999; Joseph and Nigam, 2006; Wang et al., 2005; Liu et al., 2000; Otto-Bliesner et al., 2003; Zebiak and Cane, 1987; Otto-Bliesner, Brady, et al., 2006a; Capotondi, 2013; Latif and Keenlyside, 2009; Otto-Bliesner, Tomas, et al., 2006; Tziperman et al., 1997). Nino3 is a region from 150°W-90°W, and 5°N-5°S while Nino3.4 is from 170°W-120°W and 5°N-5°S (Timmerman et al., 1999; Lee and McPhaden, 2010; Capotondi, 2013). In addition to sea surface temperature, the severity of the thermocline and the strength of the zonal wind stress would also be of interest, as the change in wind stress could cause a shallowing or deepening of the thermocline due to mixing (McPhaden, 1999; Latif and Barnett, 1996; Xue et al., 1997; Roeckner et al., 1996; Joseph and Nigam, 2006; Hurrell et al., 2006; Liu et al., 2000; Zebiak and Cane, 1987; Capotondi, 2013; England, 1995b). Changes in the strength of the wind stress over the Northern Pacific Ocean would affect the position of high and low pressure systems, which would in turn affect the surface air temperature and the precipitation of the region (Latif and Barnett, 1996; Huber and Caballero, 2003; Roeckner et al., 1996;

Joseph and Nigam, 2006; Hurrell et al., 2006; Capotondi, 2013). A detailed analysis of the interannual climate variability and associated feedbacks would improve the understanding of ENSO during rapid climate change.

.

6.3 Extraterrestrial Impact Hypothesis

Varying dust parameters and determining the size of the meteorite could test the controversial hypothesis of a bolide impact at the start of the Younger Dryas (Firestone et al., 2007; Firestone, 2009). When meteorites impact the earth, enhanced large-scale fires can cause a temporary cooling of the climate as the incoming solar radiation decreases due to increased dust in the atmosphere (Van Der Hammen and Van Geel, 2008; Covey et al., 1994; Toon et al., 1982). This cooling typically only a few years to a decade, and then there is a subsequent warming of the climate due to the increase of carbon emissions from burned material, which leads to an increase in greenhouse gas radiative forcing and surface warming.

To determine the plausibility of an extraterrestrial impact, the size of the meteorite would need to be determined through a series of climate sensitivity experiments as to how much dust a meteorite of a particular size would produce, and then model the climate based on that input of dust. Also of interest would be investigating the amount of freshwater that could be generated by such an impact, inputting that amount of freshwater into the Northern Atlantic, and determining how the climate responds to such an input. Once the size of the meteorite is determined, the likelihood of such an impact can be investigated. Though these simulations would be interesting and beneficial to the scientific community, allocations currently available for simulation use on the super computer Yellowstone may be not large enough to allow for the simulations at this time.

References

AchutaRao, K., and Sperber, K., 2002, Simulation of the El Niño Southern Oscillation: Results from the Coupled Model Intercomparison Project: Climate Dynamics, v. 19, p. 191–209, doi: 10.1007/s00382-001-0221-9.

Bacastow, R.B., Adams, J.A., Keeling, C.D., Moss, D.J., Whorf, T.P., and Wong, C.S., 1980, Atmospheric Carbon Dioxide, the Southern Oscillation, and the Weak 1975 El Nino: Science, v. 210, p. 66–68, doi: 10.1126/science.210.4465.66.

Beaufort, L., de Garidel-Thoron, T., Mix, A.C., and Pisias, N.G., 2001, ENSO-like forcing on oceanic primary production during the Late Pleistocene.: Science (New York, N.Y.), v. 293, p. 2440–4, doi: 10.1126/science.293.5539.2440.

Berlage, H.P., 1966, The southern oscillation and world weather: Koninklijk Nederlands Meteorologisch Instituut, v. 88, p. 152.

Capotondi, A., 2013, ENSO diversity in the NCAR CCSM4 climate model: Journal of Geophysical Research: Oceans, v. 118, p. 4755–4770, doi: 10.1002/jgrc.20335.

Clement, A.C., Cane, M.A., and Seager, R., 2001, An Orbitally Driven Tropical Source for Abrupt Climate Change: Journal of Climate, v. 14, p. 2369–2375, doi: 10.1175/1520-0442(2001)014<2369:AODTSF>2.0.CO;2.

Clement, A.C., Seager, R., and Cane, M.A., 2000, Suppression of El Niño during the Mid-Holocene by changes in the Earth's orbit: Paleoceanography, v. 15, p. 731–737, doi: 10.1029/1999PA000466.

Covey, C., Thompson, S.L., Weissman, P.R., and MacCracken, M.C., 1994, Global climatic effects of atmospheric dust from an asteroid or comet impact on Earth: Global and Planetary Change, v. 9, p. 263–273, doi: 10.1016/0921-8181(94)90020-5.

Eisenman, I., Bitz, C.M., and Tziperman, E., 2009, Rain driven by receding ice sheets as a cause of past climate change: Paleoceanography, v. 24, p. 12, doi: 10.1029/2009PA001778.

England, M.H., 1995, The Age of Water and Ventilation Timescales in a Global Ocean Model: Journal of Physical Oceanography, v. 25, p. 2756–2777, doi: 10.1175/1520-0485(1995)025<2756:TAOWAV>2.0.CO;2.

Fedorov, A. V, Brierley, C.M., and Emanuel, K., 2010, Tropical cyclones and permanent El Niño in the early Pliocene epoch.: Nature, v. 463, p. 1066–1070, doi: 10.1038/nature08831.

Fedorov, A. V., and Philander, S.G., 2000, Is El Nino Changing? Science, v. 288, p. 1997–2002, doi: 10.1126/science.288.5473.1997.

Firestone, R.B., 2009, The Case for the Younger Dryas\nExtraterrestrial Impact Event:\nMammoth, Megafauna, and Clovis Extinction, 12,900 Years Ago: Journal of Cosmology, v. 2, p. 256–285.

Firestone, R.B., West, A., Kennett, J.P., Becker, L., Bunch, T.E., Revay, Z.S., Schultz, P.H., Belgya, T., Kennett, D.J., Erlandson, J.M., Dickenson, O.J., Goodyear, A.C., Harris, R.S., Howard, G.A., et al., 2007, Evidence for an extraterrestrial impact 12,900 years ago that contributed to the megafaunal extinctions and the Younger Dryas cooling.: Proceedings of the National Academy of Sciences of the United States of America, v. 104, p. 16016–21, doi: 10.1073/pnas.0706977104.

Van Der Hammen, T., and Van Geel, B., 2008, Charcoal in soils of the Allerød-Younger Dryas transition were the result of natural fires and not necessarily the effect of an extra-terrestrial impact: Netherlands Journal of Geosciences, v. 87, p. 359–361.

Huber, M., and Caballero, R., 2003, Eocene El Niño: evidence for robust tropical dynamics in the “hothouse”.: Science (New York, N.Y.), v. 299, p. 877–881, doi: 10.1126/science.1078766.

Hurrell, J.W., Hack, J.J., Phillips, A.S., Caron, J., and Yin, J., 2006, The dynamical simulation of the Community Atmosphere Model version 3 (CAM3): Journal of Climate, v. 19, p. 2162–2183, doi: 10.1175/JCLI3762.1.

Joseph, R., and Nigam, S., 2006, ENSO Evolution and Teleconnections in IPCC’s Twentieth-Century Climate Simulations: Realistic Representation? Journal of Climate, v. 19, p. 4360–4377, doi: 10.1175/JCLI3846.1.

Keeling, C.D., Bacastow, R.B., Carter, A.F., Piper, S.C., Whorf, T.P., Heimann, M., Mook, W.G., and Roeloffzen, H., 1989, A three-dimensional model of atmospheric CO2 transport based on observed winds: 1. Analysis of observational data, *in* Aspects of Climate Variability in the Pacific and the Western Americas, p. 165–236.

Latif, M., and Barnett, T.P., 1994, Causes of Decadal Climate Variability over the North Pacific and North America: Science, v. 266, p. 634–637, doi: 10.1126/science.266.5185.634.

Latif, M., and Barnett, T.P., 1996, Decadal climate variability over the North Pacific and North America: Dynamics and predictability: Journal of Climate, v. 9, p. 2407–2423, doi: 10.1175/1520-0442(1996)009<2407:DCVOTN>2.0.CO;2.

Latif, M., and Keenlyside, N.S., 2009, El Nino/Southern Oscillation response to global warming: Proceedings of the National Academy of Sciences of the United States of America, v. 106, p. 20578–83, doi: 10.1073/pnas.0710860105.

Lee, T., and McPhaden, M.J., 2010, Increasing intensity of El Ni??o in the central-equatorial Pacific: Geophysical Research Letters, v. 37, doi: 10.1029/2010GL044007.

Liu, Z., Kutzbach, J., and Wu, L., 2000, Modeling climate shift of El Nino variability in the Holocene: Geophysical Research Letters, v. 27, p. 2265–2268, doi: 10.1029/2000GL011452.

McPhaden, M.J., 1999, Genesis and evolution of the 1997-98 El Nino: Science, v. 283, p. 950–954, doi: 10.1126/science.283.5404.950.

Oldenborgh, G.J. Van, Philip, S.Y., and Collins, M., 2005, El Niño in a changing climate: a multi-model study: Ocean Science, v. 1, p. 81–95.

Otto-Bliesner, B.L., Brady, E.C., Clauzet, G., Tomas, R., Levis, S., and Kothavala, Z., 2006, Last Glacial Maximum and Holocene Climate in CCSM3: Journal of Climate, v. 19, p. 2526–2544, doi: 10.1175/JCLI3748.1.

Otto-Bliesner, B.L., Brady, E.C., Shin, S.-I., Liu, Z., and Shields, C.A., 2003, Modeling El Niño and its tropical teleconnections during the last glacial-interglacial cycle: Geophysical Research Letters, v. 30, p. 2–5, doi: 10.1029/2003GL018553.

Otto-Bliesner, B.L., Tomas, R., Brady, E.C., Caspar, A., Kothavala, Z., and Clauzet, G., 2006, Climate Sensitivity of Moderate- and Low-Resolution Versions of CCSM3 to Preindustrial Forcings: Journal of Climate, v. 3, p. 2567–2583, doi: 10.1175/JCLI3754.1.

Power, S.B., and Kociuba, G., 2010, The impact of global warming on the Southern Oscillation Index: Climate Dynamics, v. 37, p. 1745–1754, doi: 10.1007/s00382-010-0951-7.

Rasmusson, E.M., and Wallace, J.M., 1983, Meteorological aspects of the el nino/southern oscillation.: Science (New York, N.Y.), v. 222, p. 1195–202, doi: 10.1126/science.222.4629.1195.

Rayner, P.J., Law, R.M., and Dargaville, R., 1999, The relationship between tropical CO 2 fluxes and the El Niño-Southern Oscillation: Geophysical Research Letters, v. 26, p. 493–496, doi: 10.1029/1999GL900008.

Roeckner, E., Oberhuber, J.M., Bacher, a., Christoph, M., and Kirchner, I., 1996, ENSO variability and atmospheric response in a global coupled atmosphere-ocean GCM: Climate Dynamics, v. 12, p. 737–754, doi: 10.1007/s003820050140.

Sarnthein, M., Winn, K., Jung, S.J.A., Duplessy, J.-C., Labeyrie, L., Erlenkeuser, H., and Ganssen, G., 1994, Changes in East Atlantic Deepwater Circulation over the last 30,000 years: Eight time slice reconstructions: Paleoceanography, v. 9, p. 209–267, doi: 10.1029/93PA03301.

Timmerman, a, Oberhuber, J., Bacher, a, Esch, M., Latif, M., and Roeckner, E., 1999, Increased El Niño frequency in a climate model forced by future greenhouse warming: Nature, v. 398, p. 694–697, doi: 10.1038/19505.

Toon, O.B., Pollack, J.B., Ackerman, T.P., Turco, R.P., McKay, C.P., and Liu, M.S., 1982, Evolution of an impact-generated dust cloud and its effects on the atmosphere: GSA Special Papers, v. 190, p. 187–200, doi: 10.1130/SPE190-p187.

Torrence, C., and Webster, P.J., 1999, Interdecadal Changes in the ENSO–Monsoon System: Journal of Climate, v. 12, p. 2679–2690, doi: 10.1175/1520-0442(1999)012<2679:ICITEM>2.0.CO;2.

Turney, C.S.M., Kershaw, A.P., Clemens, S.C., Branch, N., Moss, P.T., and Keith Fifield, L., 2004, Millennial and orbital variations of El Niño/Southern Oscillation and high-latitude climate in the last glacial period: Nature, v. 428, p. 306–310, doi: 10.1038/nature02386.

Tziperman, E., Zebiak, S.E., and Cane, M.A., 1997, Mechanisms of Seasonal – ENSO Interaction: Journal of the Atmospheric Sciences, v. 54, p. 61–71, doi: 10.1175/1520-0469(1997)054<0061:MOSEI>2.0.CO;2.

Wang, W., Saha, S., Pan, H.-L., Nadiga, S., and White, G., 2005, Simulation of ENSO in the New NCEP Coupled Forecast System Model (CFS03): Monthly Weather Review, v. 133, p. 1574–1593, doi: 10.1175/MWR2936.1.

Winguth, A.M.E., Heinmann, M., Kurz, K.D., Maier-Reimer, E., Mikolajewicz, U., and Segschneider, J., 1994, El Niño-Southern Oscillation related fluctuations of the marine carbon cycle: Global Biogeochemical Cycles, v. 8, p. 39–63, doi: 10.1029/93GB03134.

Xue, Y., Cane, M.A., and Zebiak, S.E., 1997, Predictability of a coupled model of ENSO using singular vector analysis .1. Optimal growth in seasonal background and ENSO cycles: Monthly Weather Review, v. 125, p. 2043–2056, doi: 10.1175/1520-0493(1997)125<2043:POACMO>2.0.CO;2.

Zebiak, S.E., and Cane, M.A., 1987, A Model El Nino–Southern Oscillation: Monthly Weather Review, v. 115, p. 2262–2278, doi: 10.1175/1520-0493(1987)115<2262:AMENO>2.0.CO;2.

Appedndix A

Preindustrial Control Simulation Results

A.1 Preindustrial Simulation with CCSM3

For the preindustrial simulation and in the northern North Atlantic Ocean, sea surface salinity is approximately 33-34 psu and the sea surface temperature is approximately 6°C -8 °C (Figure A-1 and A-2). Surface air temperature over Greenland is ~16 °C, and the precipitation for the same area is ~2 mm day^{-1}-3.5 mm day^{-1} (Figure A-3 and A-4). The surface air pressure is approximately 1007 hPa (Figure A-5). The AMOC strength at 30 °N and 1000 m depth is approximately 15 Sv, and the ideal age of water masses is approximately 200-300 years at 2000 m depth (Figure A-6 and A-7).

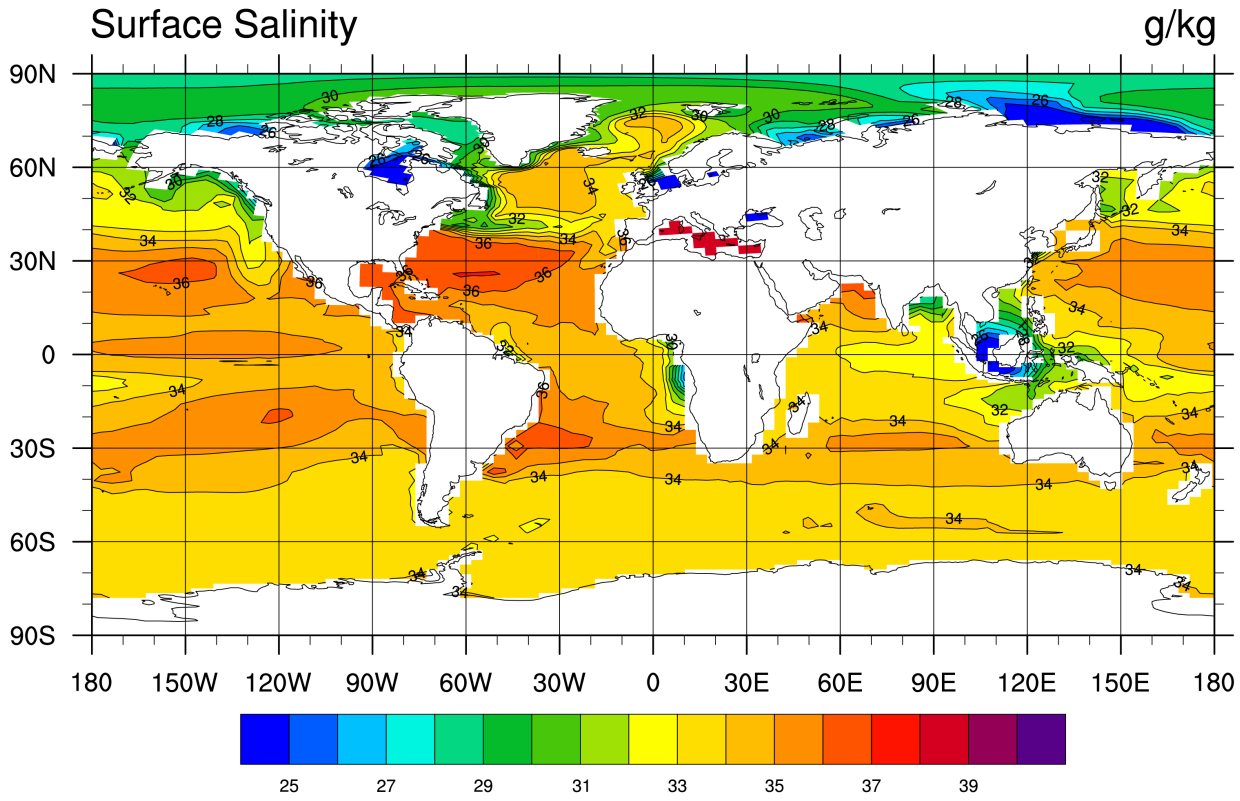

Figure A-1 Sea surface salinity in psu for the CCSM3 preindustrial control simulation.

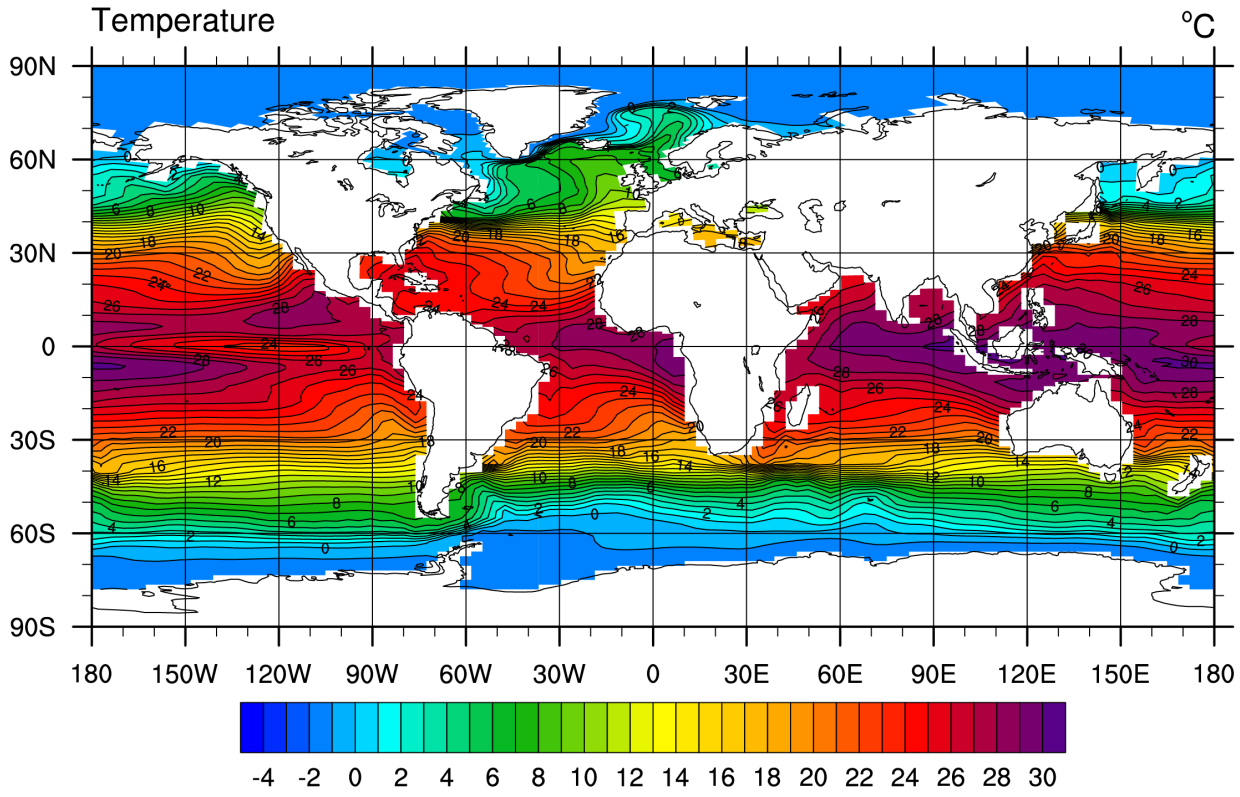

Figure A-2 Sea surface temperature in °C for the CCSM3 preindustrial control simulation.

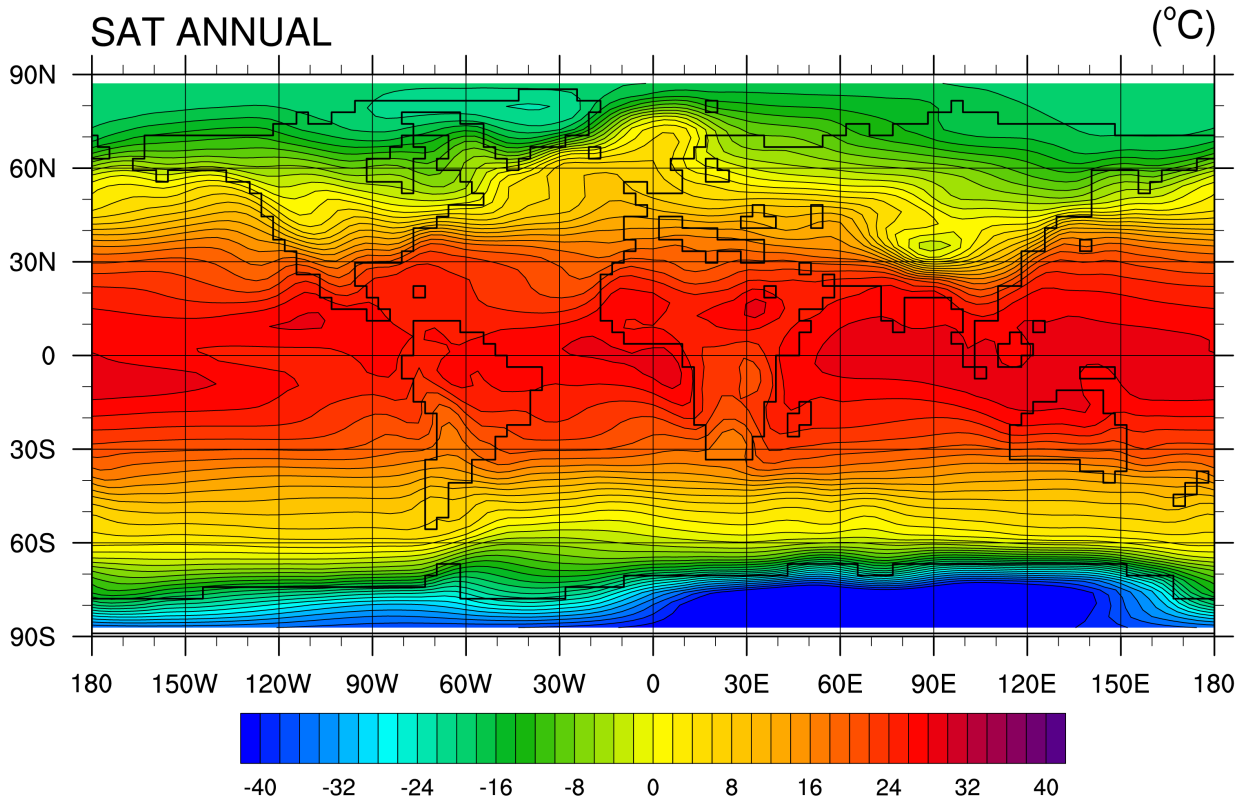

Figure A-3 Surface air temperature in °C for the CCSM3 preindustrial control simulation.

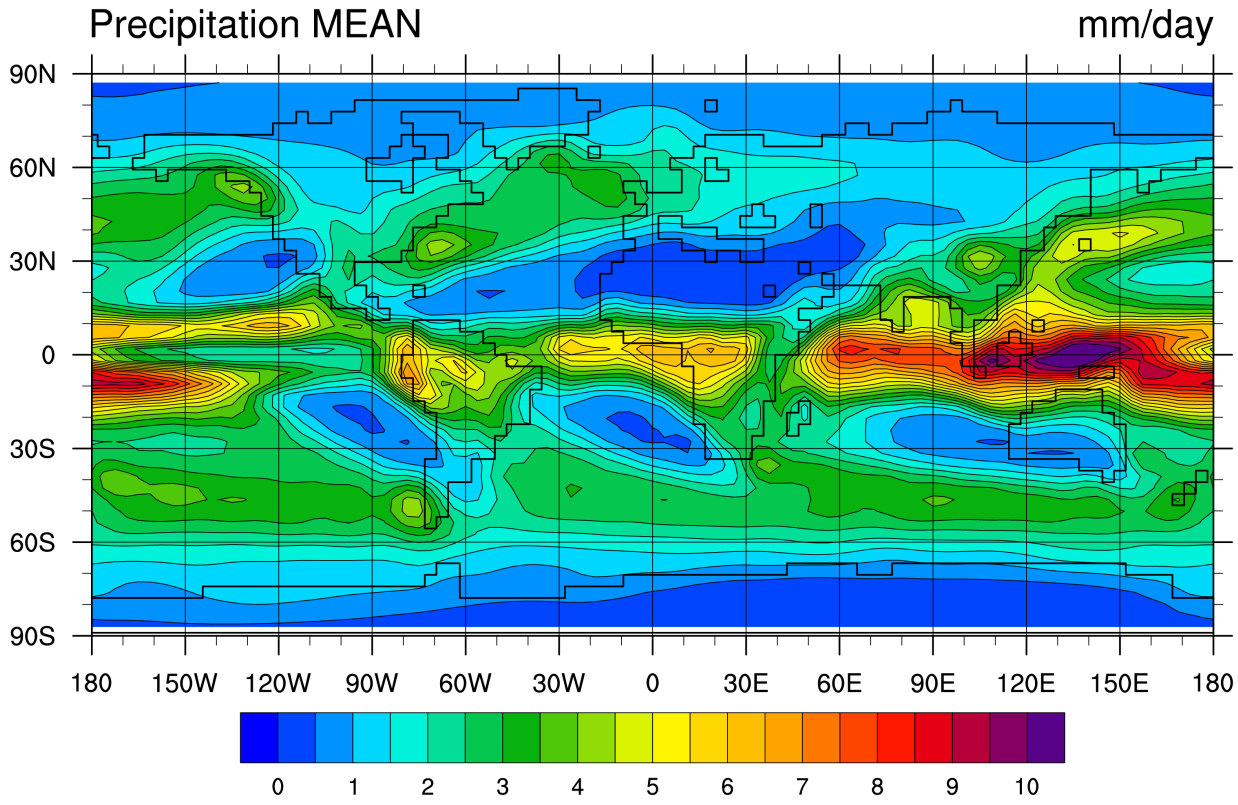

Figure A-4 Annual precipitation in mm day^{-1} for the CCSM3 preindustrial control simulation.

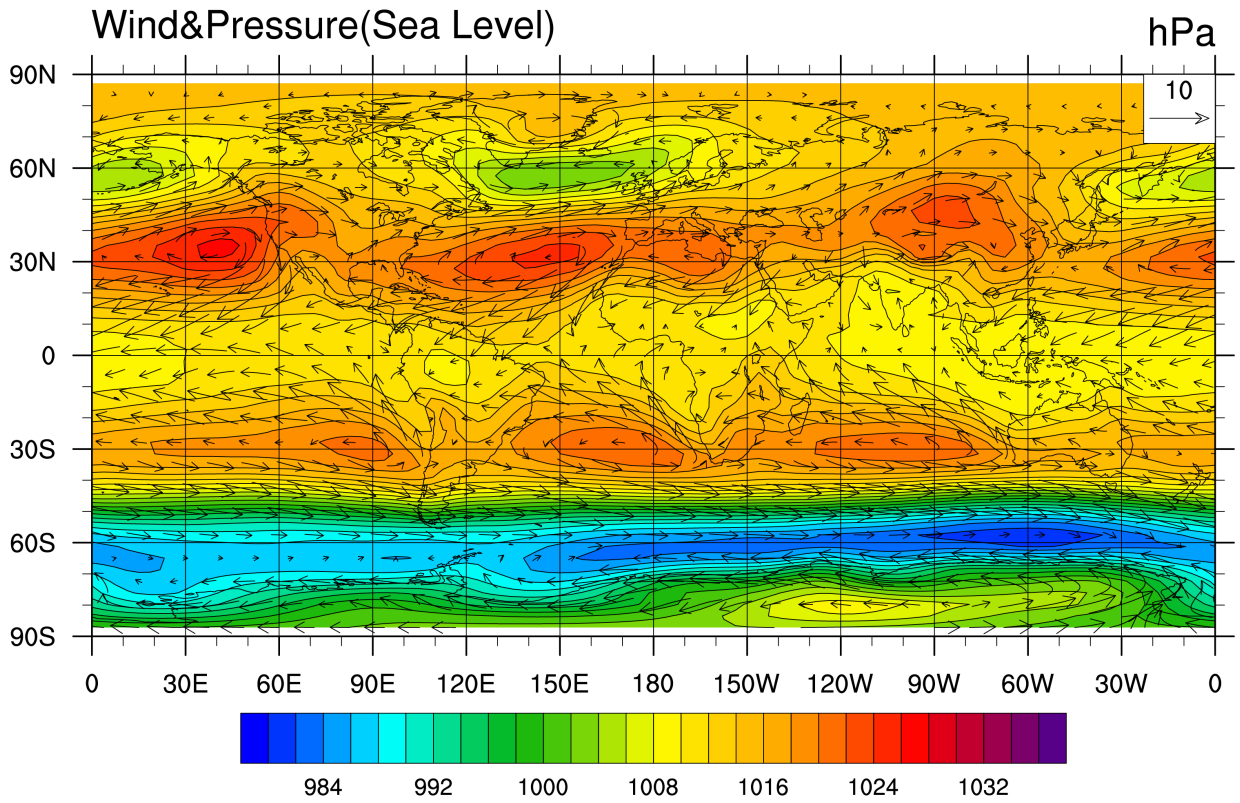

Figure A-5 Pressure at sea level in hPa and surface level winds in m s^{-1} for the CCSM3 preindustrial control simulation.

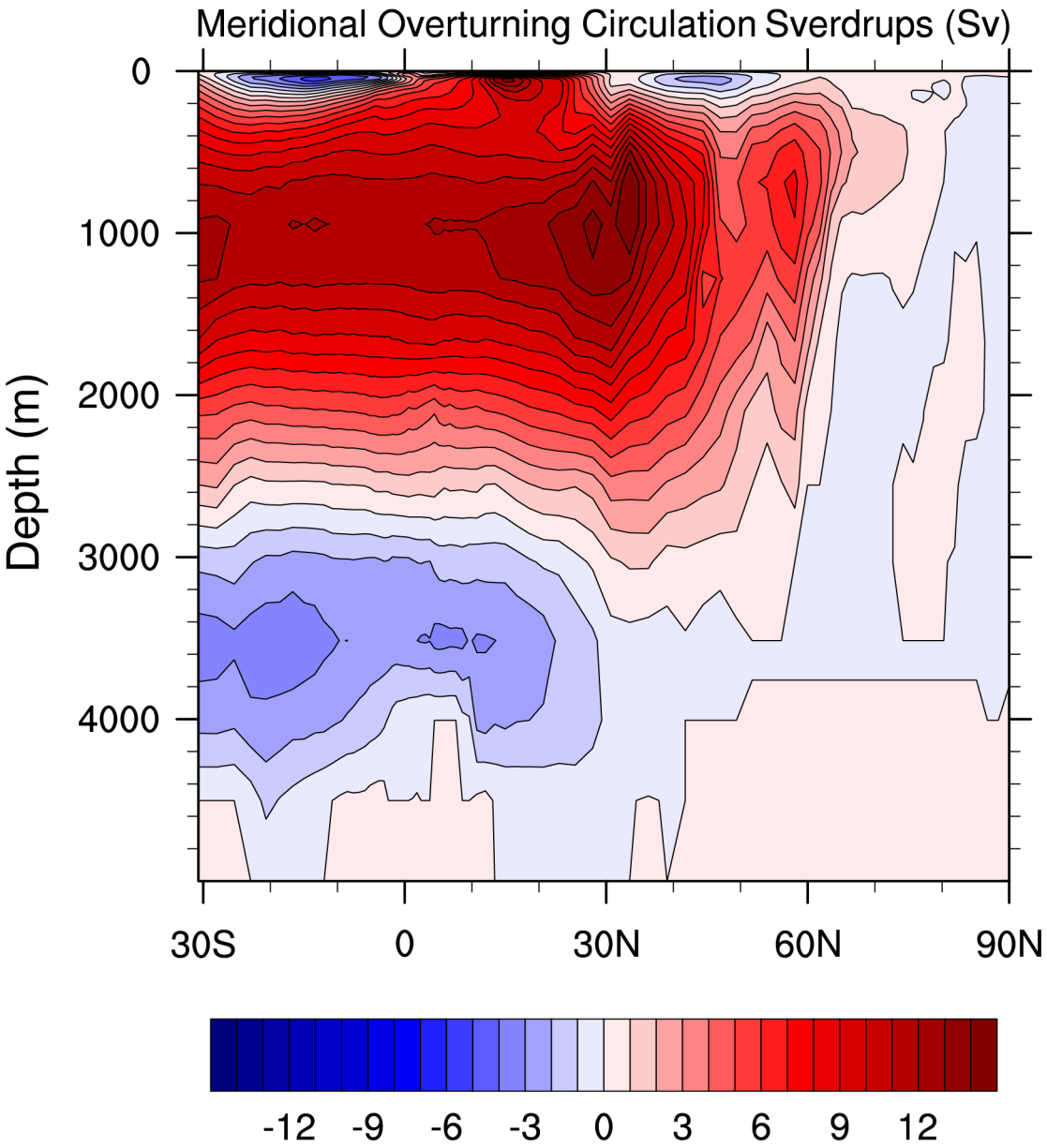

Figure A-6 Atlantic meridional overturning circulation in Sv for the CCSM3 preindustrial control simulation.

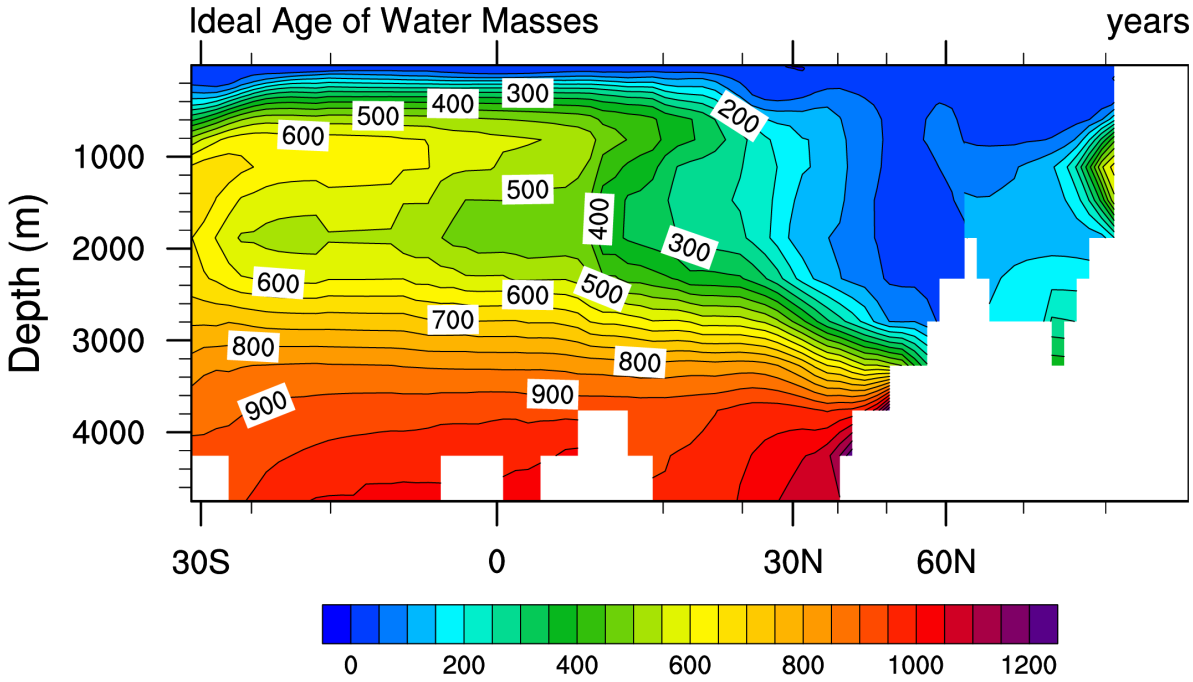

Figure A-7 Ideal age of water masses in years for the CCSM3 preindustrial control simulation.

A.2 Preindustrial Simulation Results with CESM1.0.5

The sea surface salinity for the near Greenland in the preindustrial simulation is approximately 35.5-36 psu, and the sea surface temperature for the same region is approxiamtely 10 °C (Figure A-8 and A-9). The surface air temperature over Greenland is approxiamtely -30 °C (Figure A-10). Annual precipitation over the Norwegian sea is approxiamtely 4 mm day^{-1} - 4.5 mm day^{-1}, and the annual surface air pressure is ~1000 hPa (Figure A-11 and A-12). AMOC strength at 30 °N and 1000 m is approxiamtely 28 Sv, and the ideal age of water masses is approximately 200-250 years at 2000 m depth (Figure A-13 and A-14).

Winter surface air temperature over the Mediterranean region is approximately 20 °C (Figure A-15 A). Maximum temperature over the continent is approximately 36 °C over the northern desert (Figure A-15 A). Temperatures decrease with decreasing latitude; the semi-arid region is 26 °C, the northern tropics is 23 °C, and the equatorial wet and southern tropical region are both 20 °C (Figure A-15 A). The summer temperatures are the same as the winter temperatures for each region (Figure A-15 B). Surface pressure in this region does not vary substantially during the season (Figure A-16 A and B). The lowest

surface pressure of 1008 hPa occurs over the northern desert region. All other regions have a sea level pressure of ~1014 hPa - 1016 hPa (Figure A-16 A and B). The convergence of the northern and southern equatorial trade winds is located at 5 °N (Figure A-16 A and B). Maximum precipitation for both the summer and winter averages occur over the northern tropics at 16 mm day^{-1} (Figure A-17 A and B). The precipitation for the remaining regions are 3 mm day^{-1}, 5 mm day^{-1}, and 2 mm day^{-1} for the semi-arid, equatorial wet, and southern tropics respectively (figure A-17 A and B).

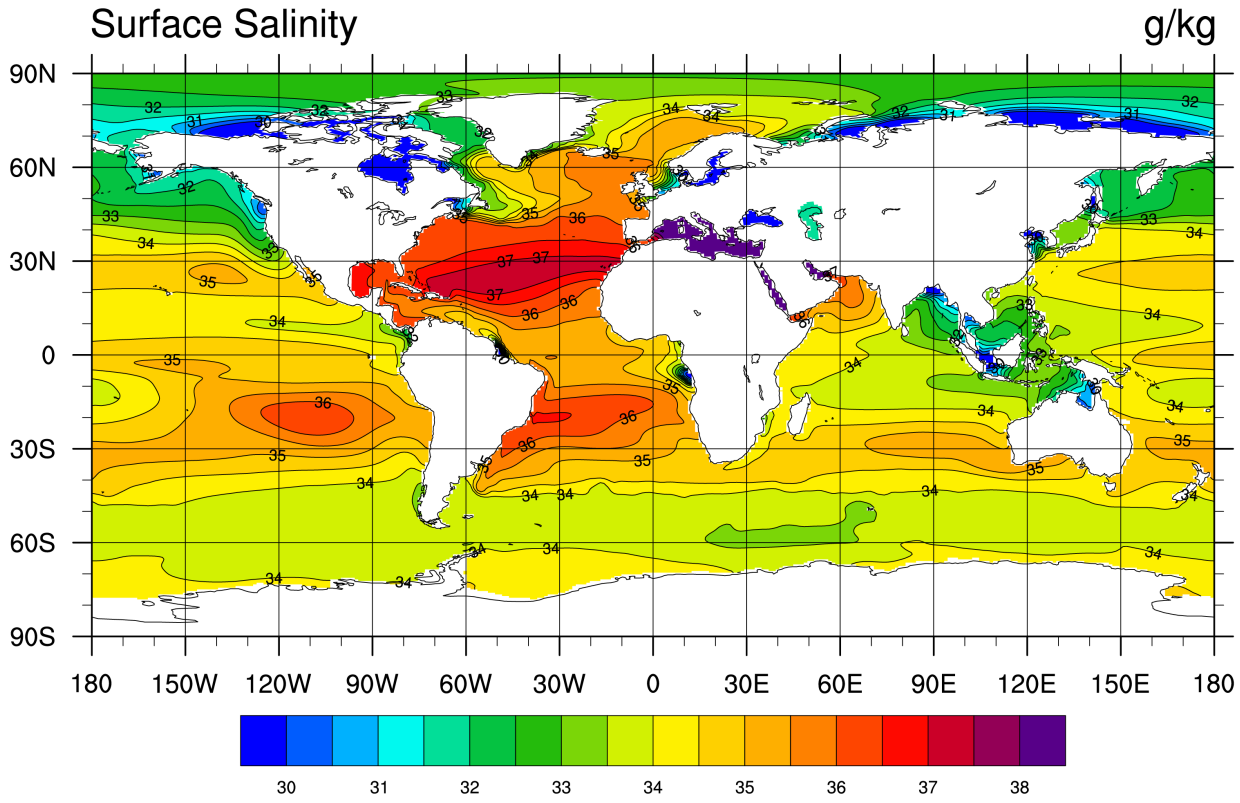

Figure A-8 Sea surface salinity in psu for the CESM1 preindustrial control simulation.

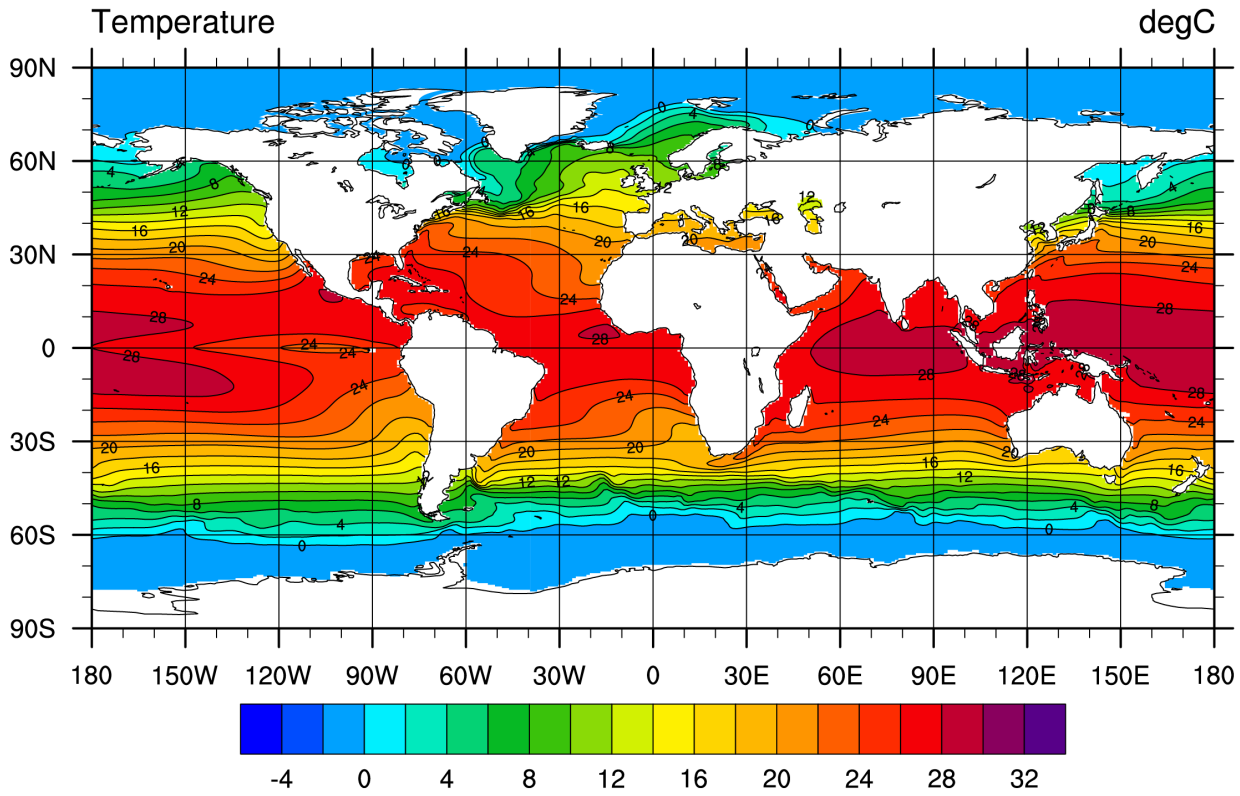

Figure A-9 Sea surface temperature in °C for the CESM1 preindustrial control simulation.

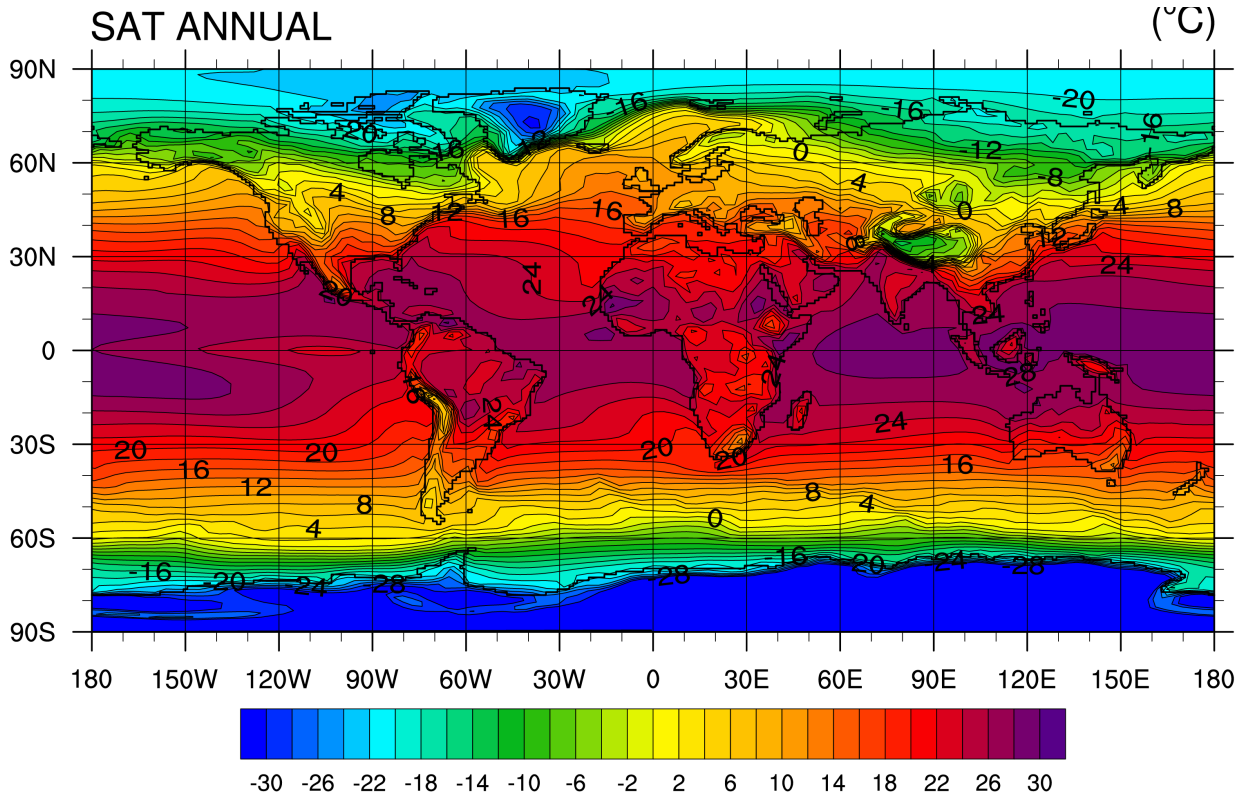

Figure A-10 Surface air temperature in °C for the CESM1 preindustrial control simulation.

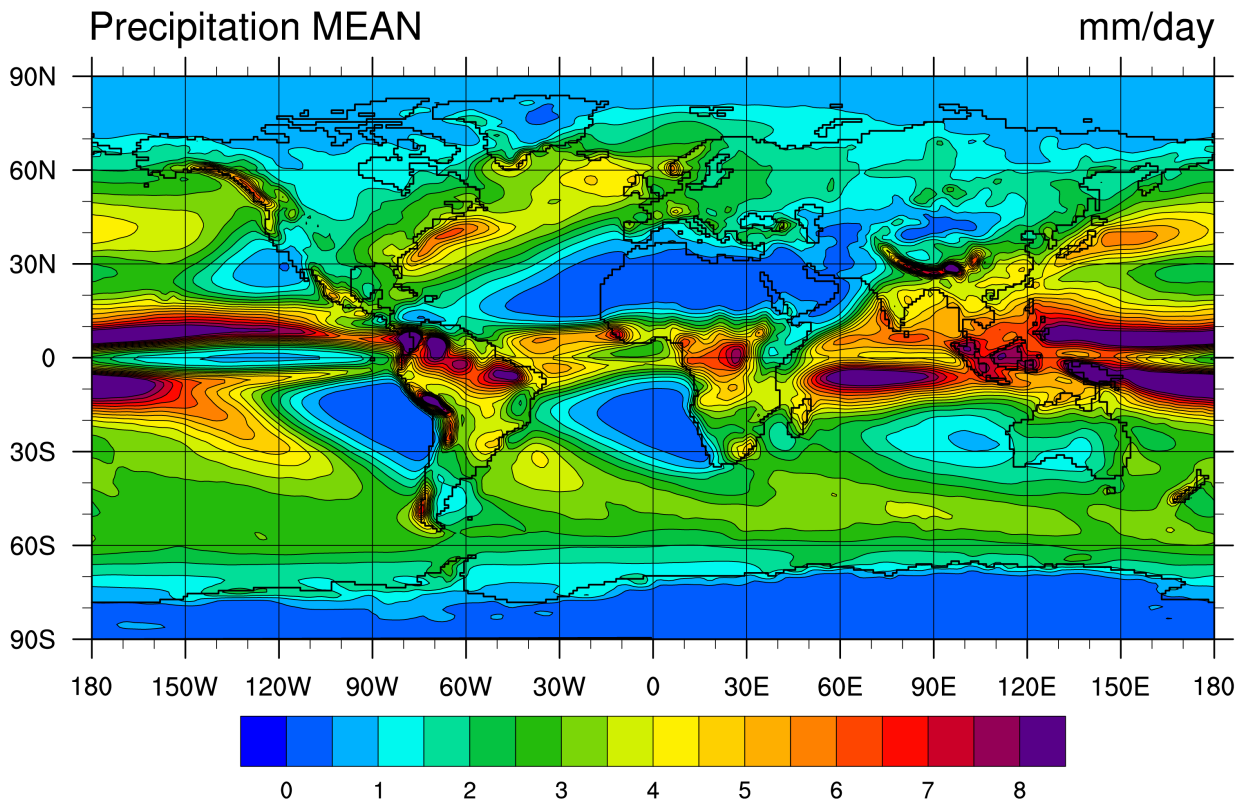

Figure A-11 Annual precipitation in mm day^{-1} for the CESM1 preindustrial control simulation.

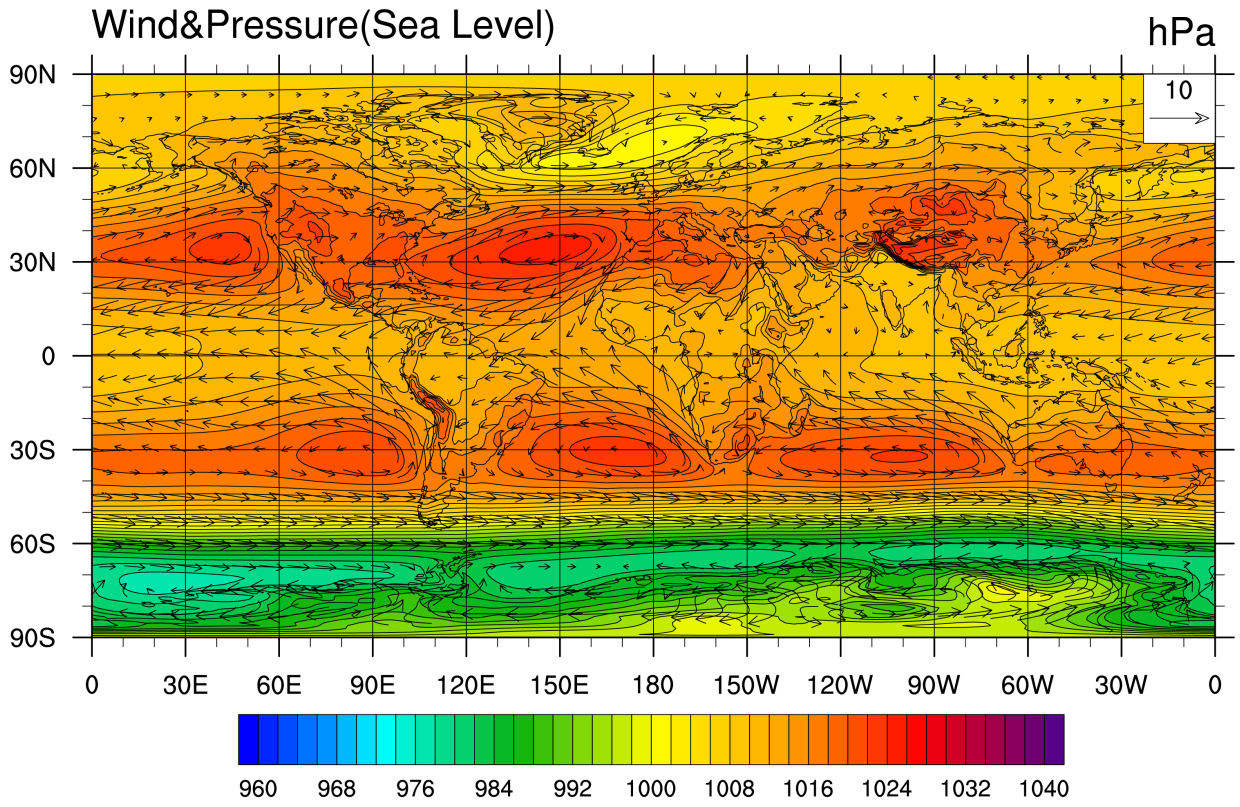

Figure A-12 Sea level pressure and surface level winds in hPa for the CESM1 preindustrial control simulation.

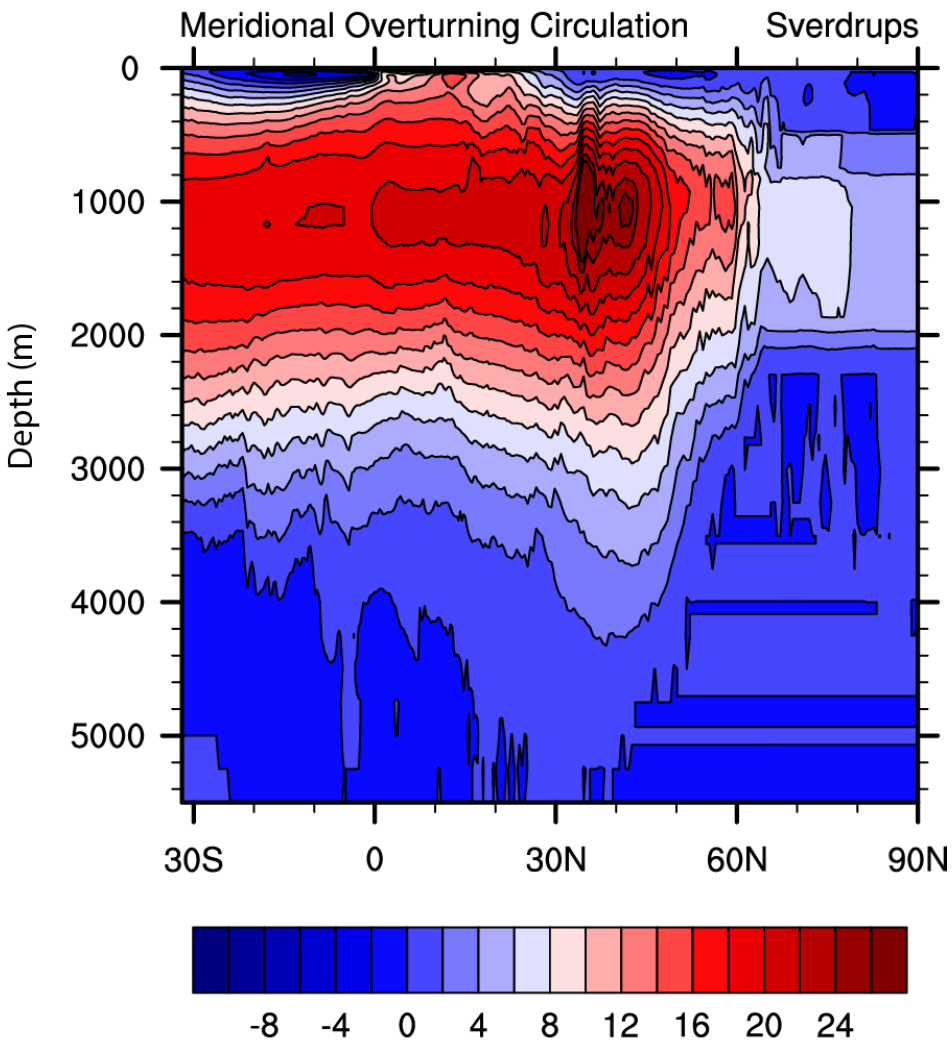

Figure A-13 Atlantic meridional overturning circulation in Sv for the CESM1 preindustrial control simulation.

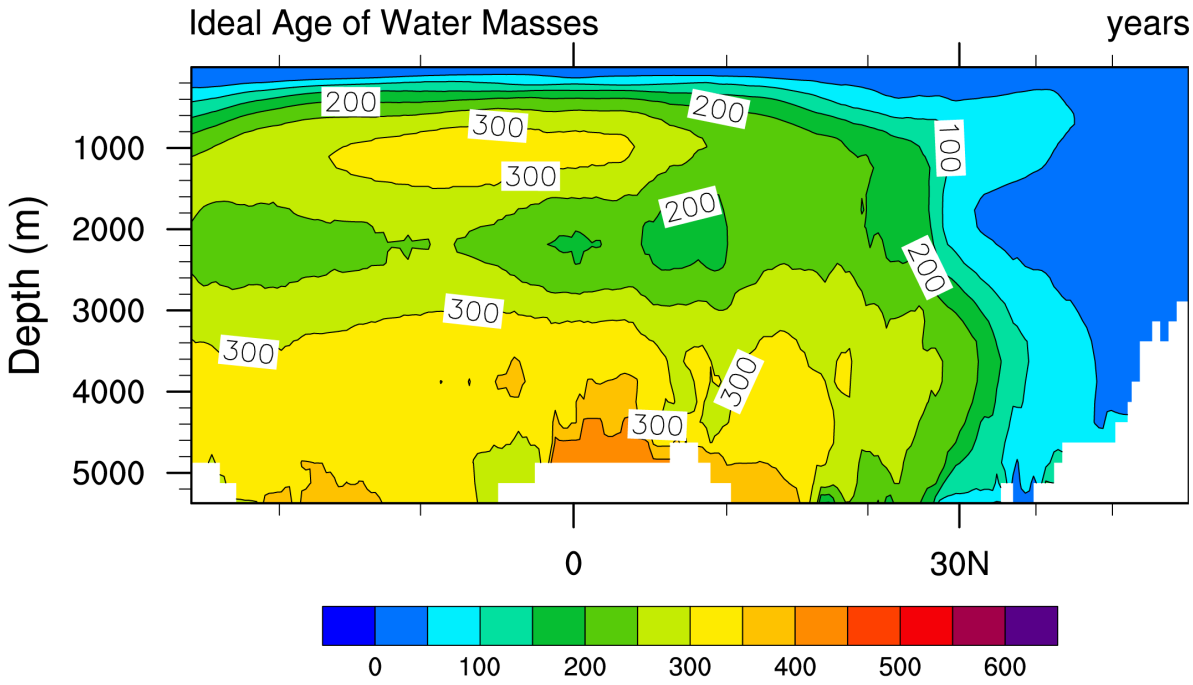

Figure A-14 Ideal age of water masses in years for the CESM1 preindustrial control simulation.

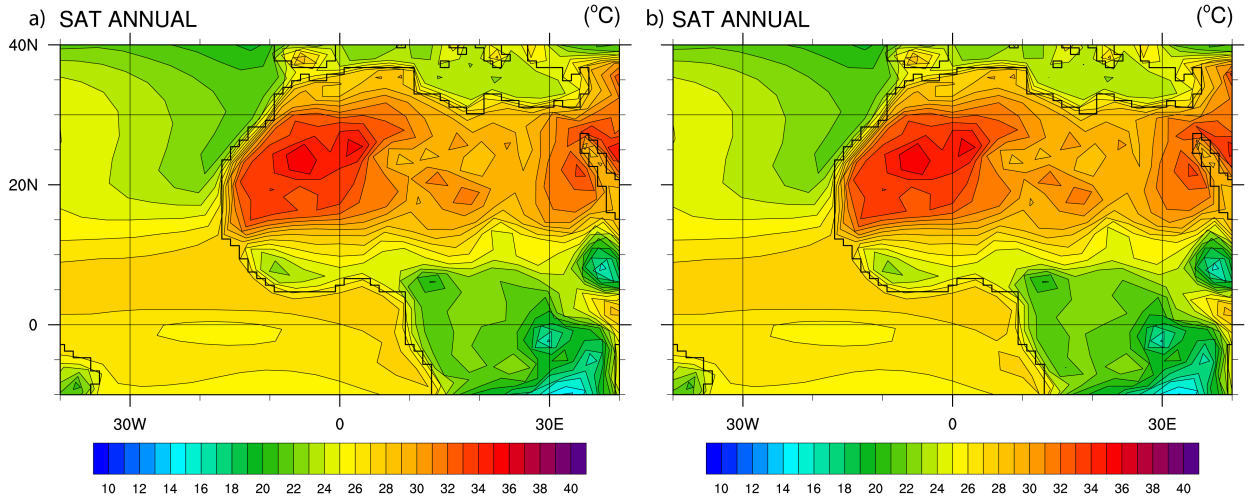

Figure A-15 Surface temperature in °C for the CESM1 preindustrial control simulation. A) winter (DJF) and B) summer(JJA).

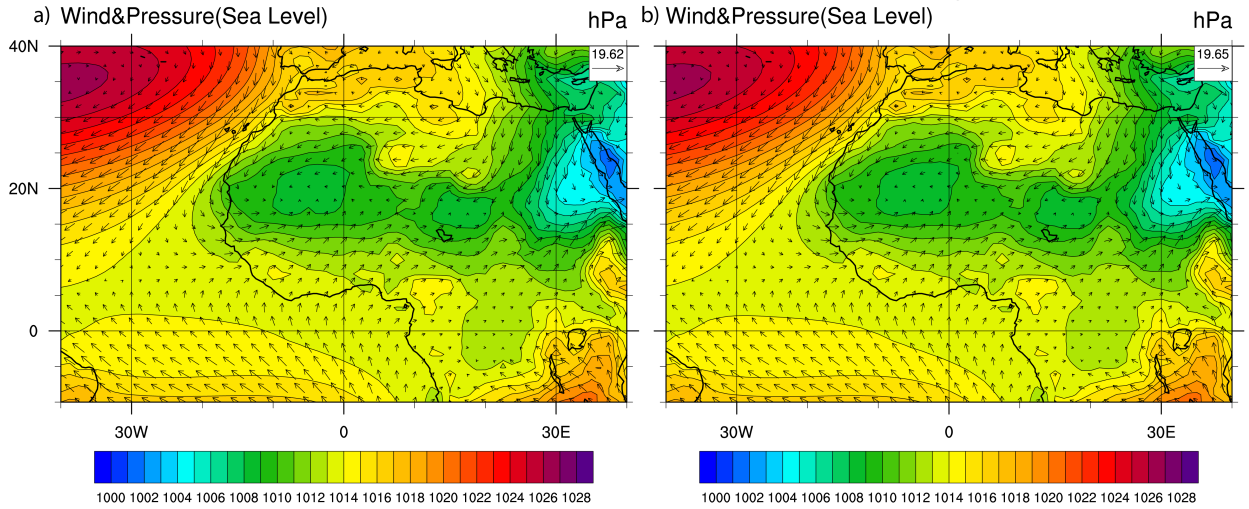

Figure A-16 Sea level pressure in hPa and surface level winds in m s^{-1} for the CESM1 preindustrial control simulation. A) winter (DJF) and B) summer (JJA).

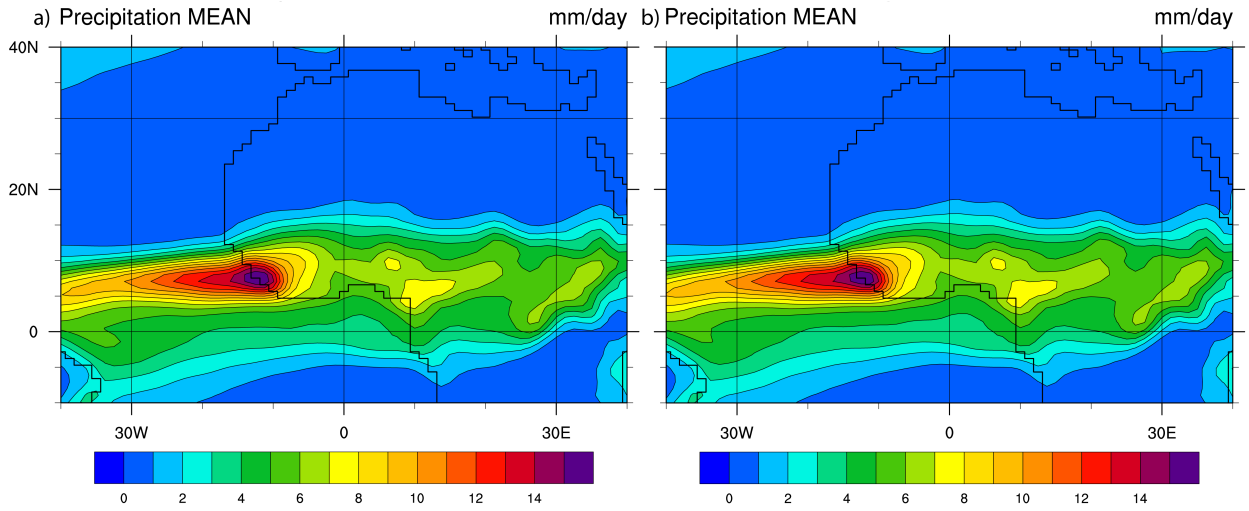

Figure A-17 Precipitation in mm day^{-1} for the CESM1 preindustrial control simulation. A) DJF. B) JJA.

A.3 Preindustrial Simulation with CESM1.2

In the northern North Atlantic Ocean, the sea surface salinity ranges between 35.5 psu to 36,psu and the sea surface temperature is ~10 °C (Figure A-18 and A-19). Surface air temperature over Greenland is approximately -34 °C, and the low pressure in the Greenland Sea is simulated with minimum values of ~1000 hPa (Figure A-20 and A-21). Precipitation over the Norwegian Sea is ~4-4.5 mm day^{-1} (Figure A-22). The AMOC strength is approximately 25 Sv at 30 °N and 1000 m, and the ideal age of water masses is approximately 200-250 years at 2000 m (Figure A-23 and A-24). The maximum amount of annual precipitation for the African continent occurs over the equatorial wet region at 9 mm day^{-1} (Figure A-25 A). For the winter averages, the maximum precipitation occurs over the southern tropics at 9 mm day^{-1}, and the maximum precipitation over the summer months is at the northern tropics (~15 mm day^{-1}; Figure A-25 B and C). For the winter averages, the high-pressure system is located over the Mediterranean and the northern desert regions, and the low-pressure region extends from the semi-arid region to the southern tropics (Figure A-26 B). The annual and summer high-pressure systems are located over the Mediterranean region, and the lowest pressure system is located over the northern desert and extends to the southern tropics (Figure A-26 A and C). The annual surface air temperature is maximum over the semi-arid region at 32 °C (Figure A-27 A). The maximum temperature is also located over the semi-arid region for the winter and summer averages, 24 °C and 32 °C respectively (Figure A-27 B and C).

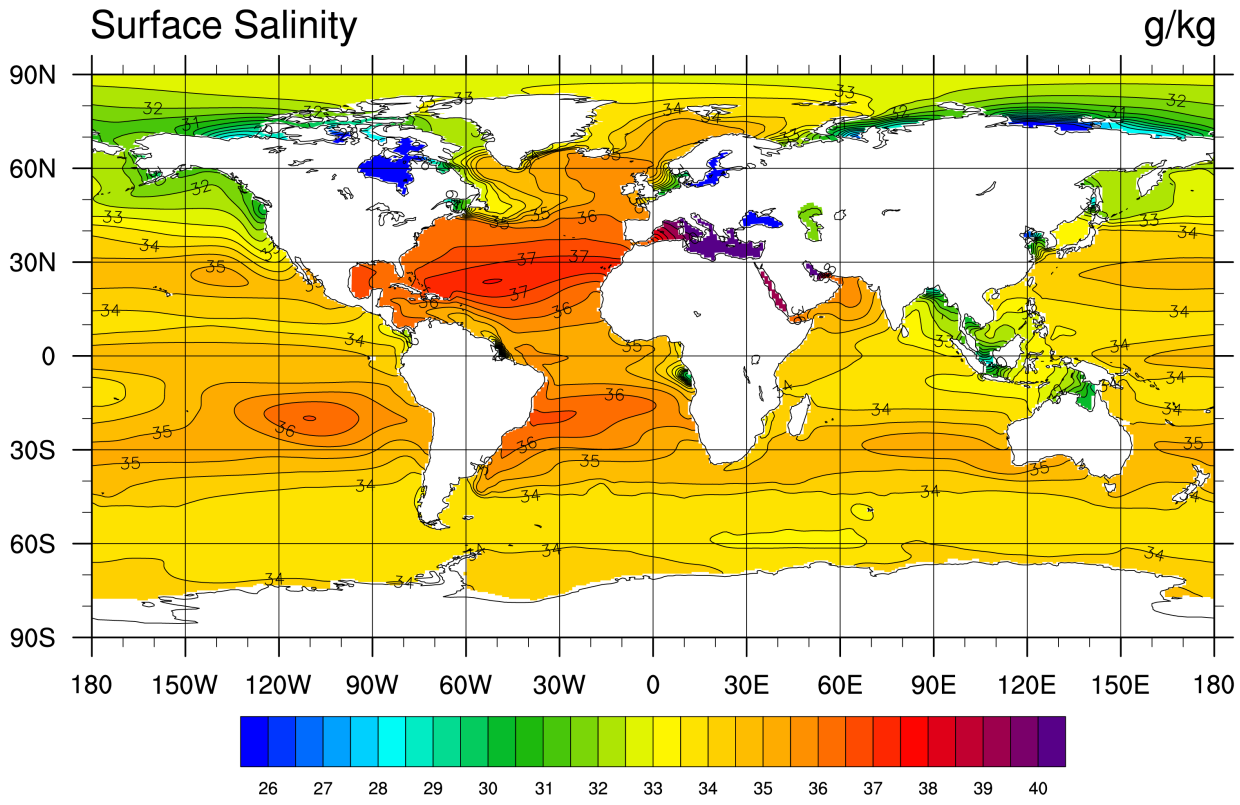

Figure A-18 Sea surface salinity in psu for the CESM1.2 preindustrial control simulation.

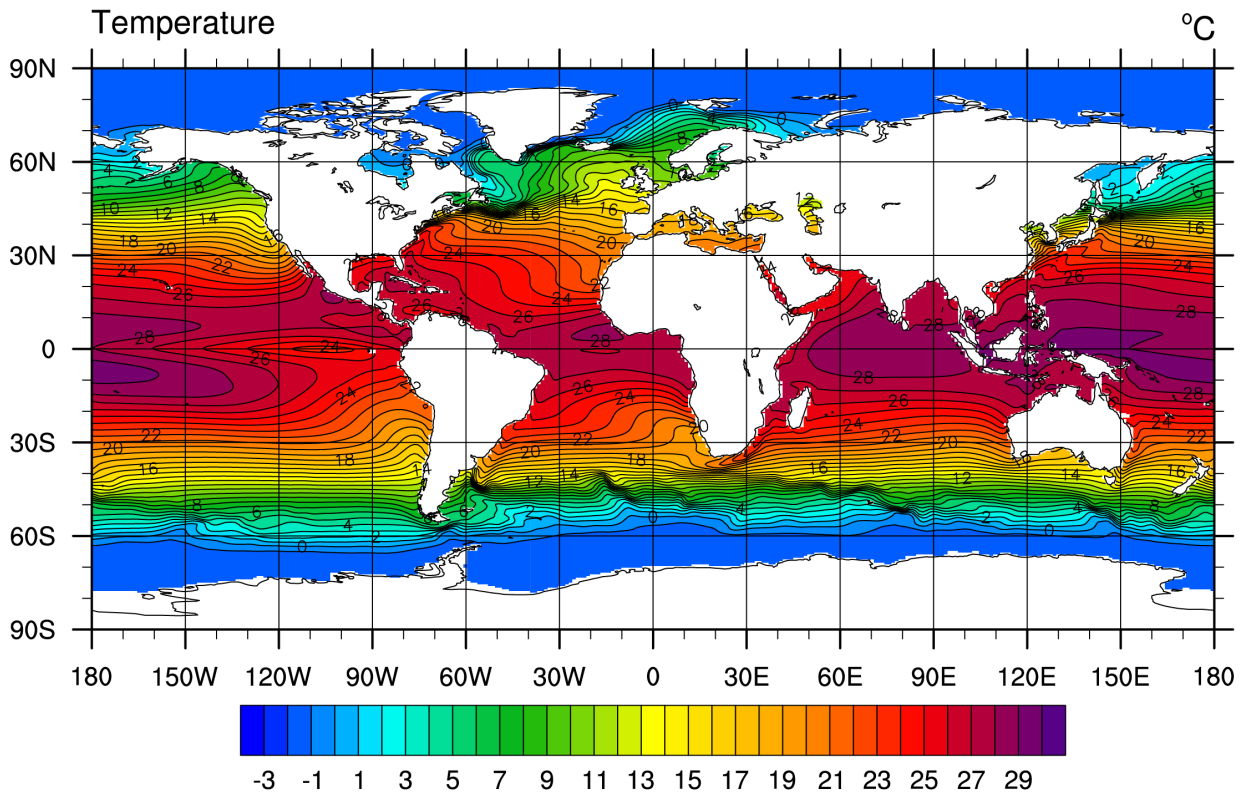

Figure A-19 Sea surface temperature in °C for the CESM1.2 preindustrial control simulation.

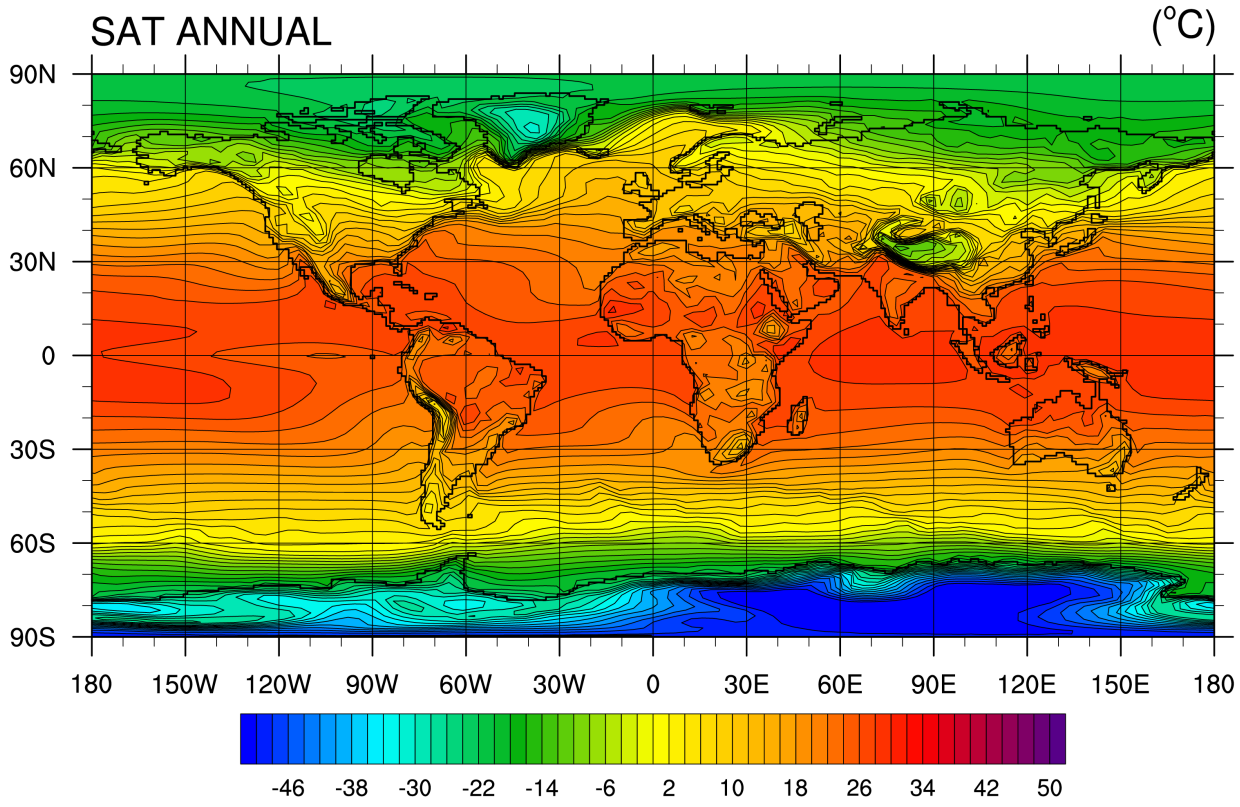

Figure A-20 Surface air temperature in °C for the CESM1.2 preindustrial control simulation.

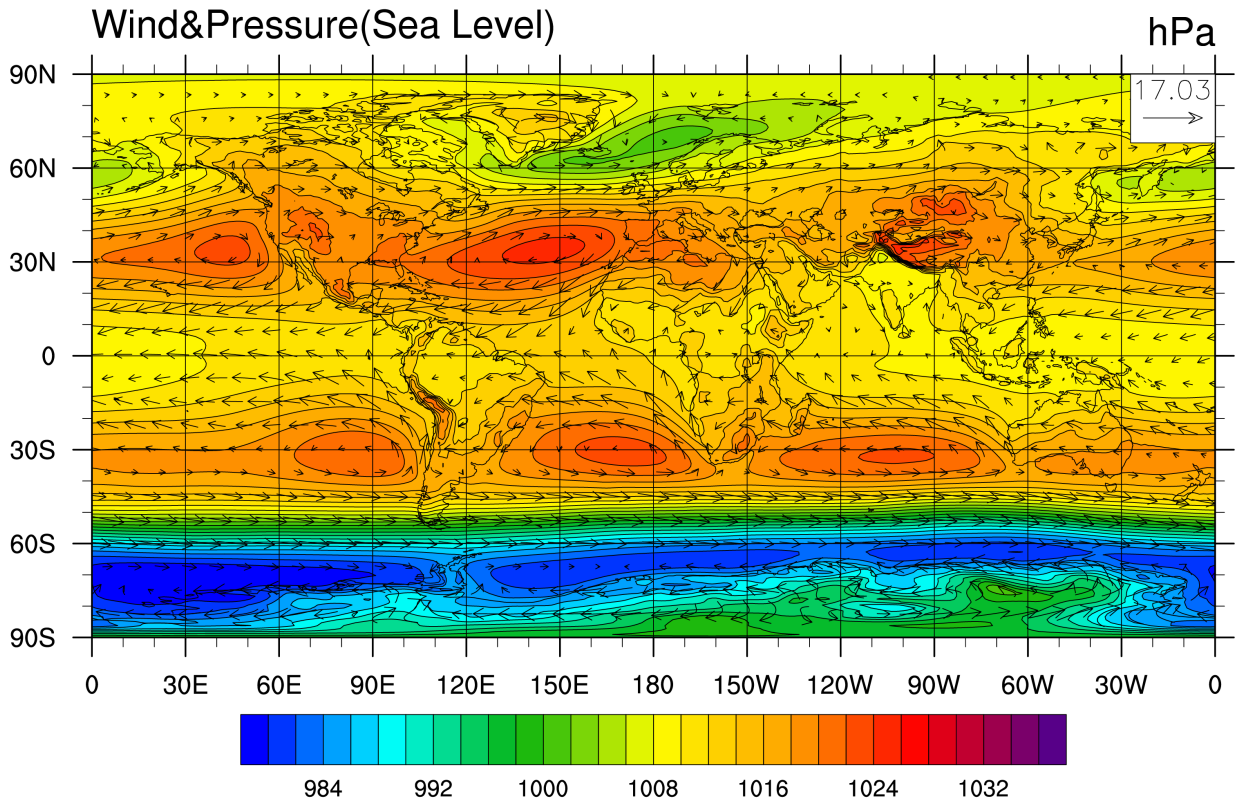

Figure A-21 Sea level pressure in hPa and surface level winds in m s^{-1} for the CESM1.2 preindustrial control simulation.

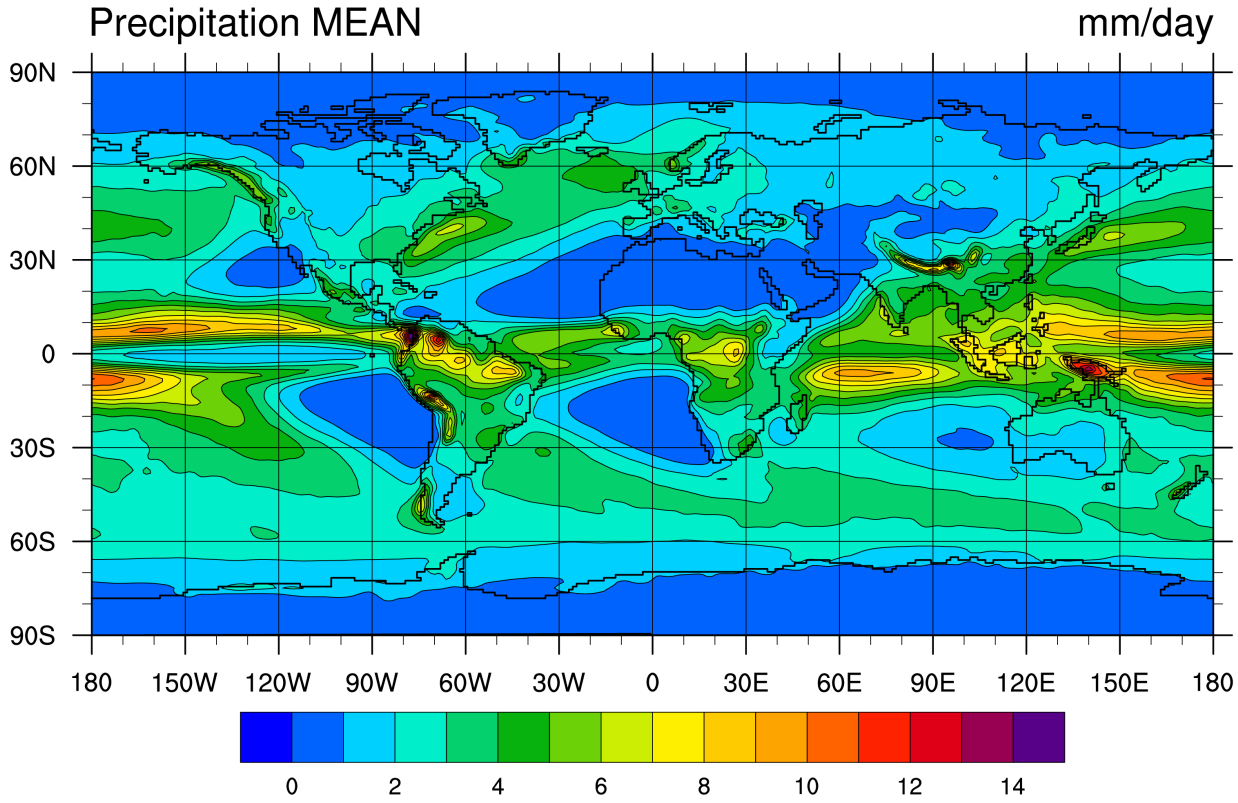

Figure A-22 Annual precipitation in mm day^{-1} for the CESM1.2 preindustrial control simulation.

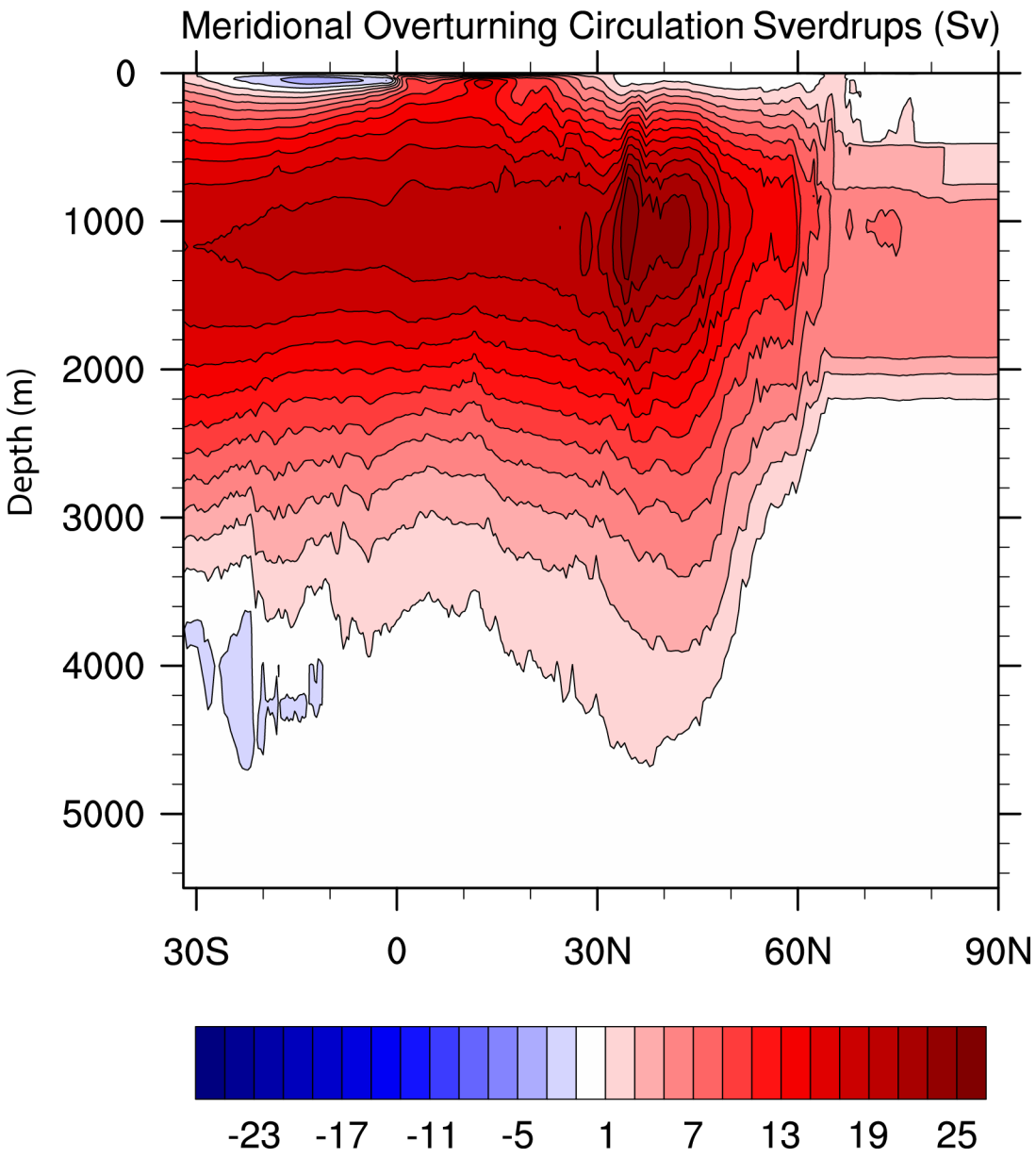

Figure A-23 Atlantic meridional overturning circulation in Sv for the CESM1.2 preindustrial control simulation.

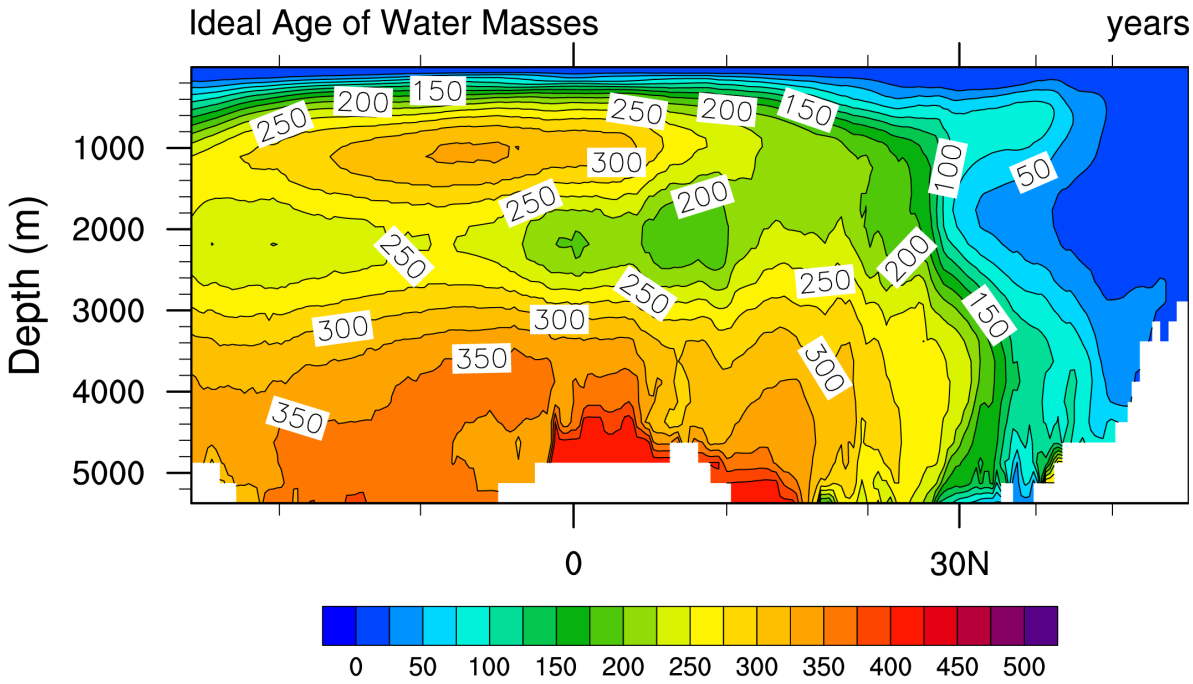

Figure A-24 Ideal age of water masses in years for the CESM1.2 preindustrial control simulation.

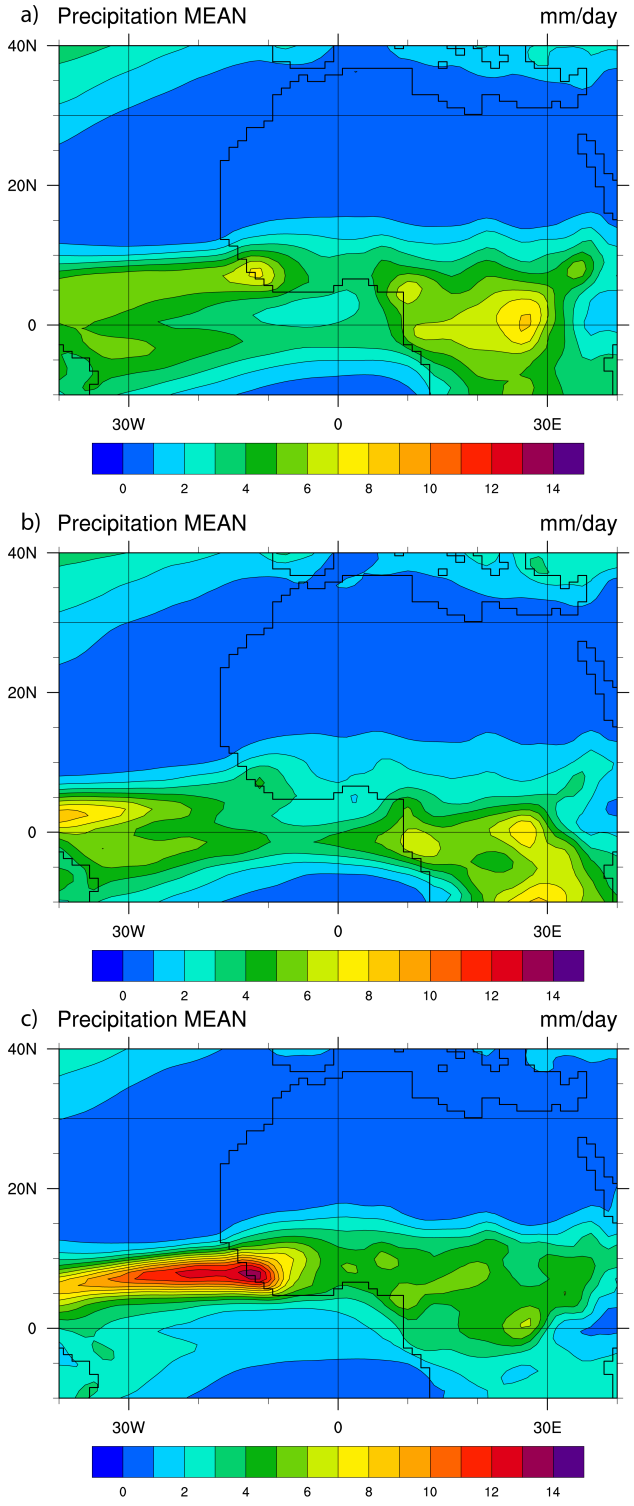

Figure A-25 Precipitation for Africa in mm day^{-1} for the CESM1.2 preindustrial control simulation for A) Annual, B) Winter (DJF), and C) Summer (JJA).

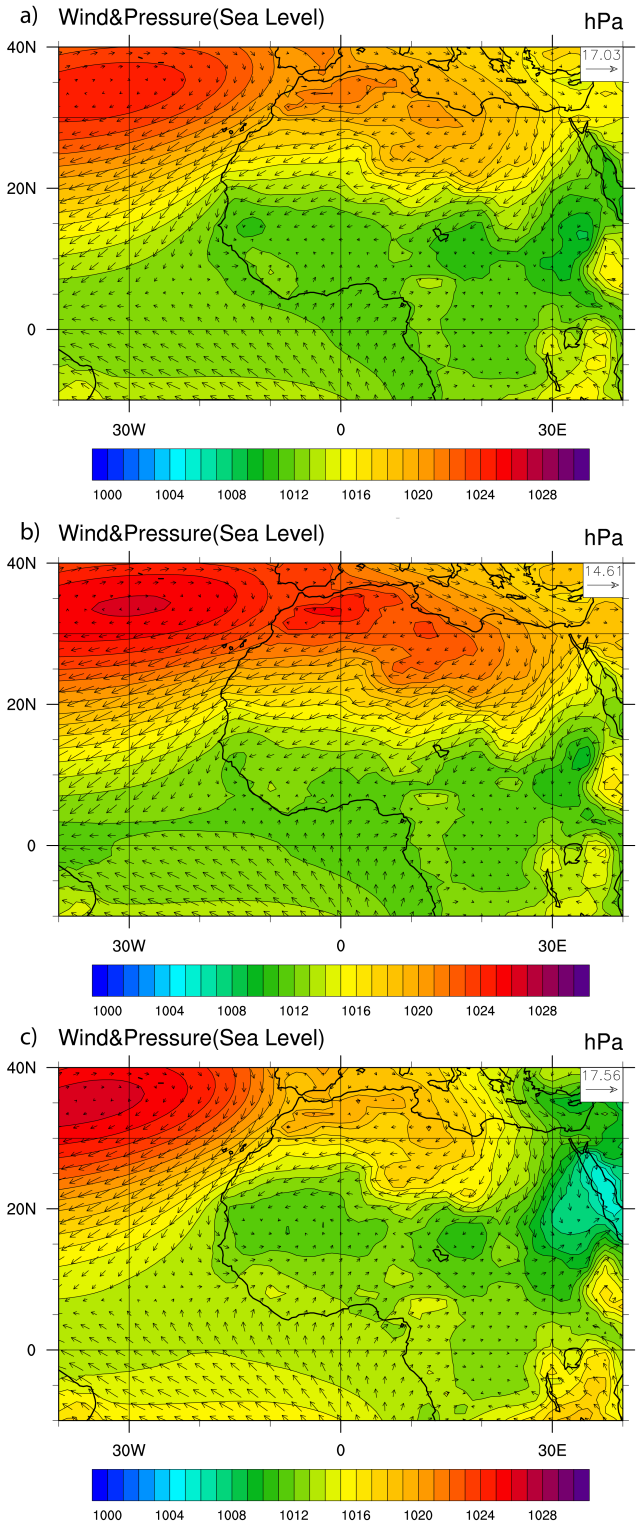

Figure A-26 Wind and pressure for Africa in hPa for the CESM1.2 preindustrial control simulation for A) Annual average, .B) winter (DJF), and C) summer (JJA).

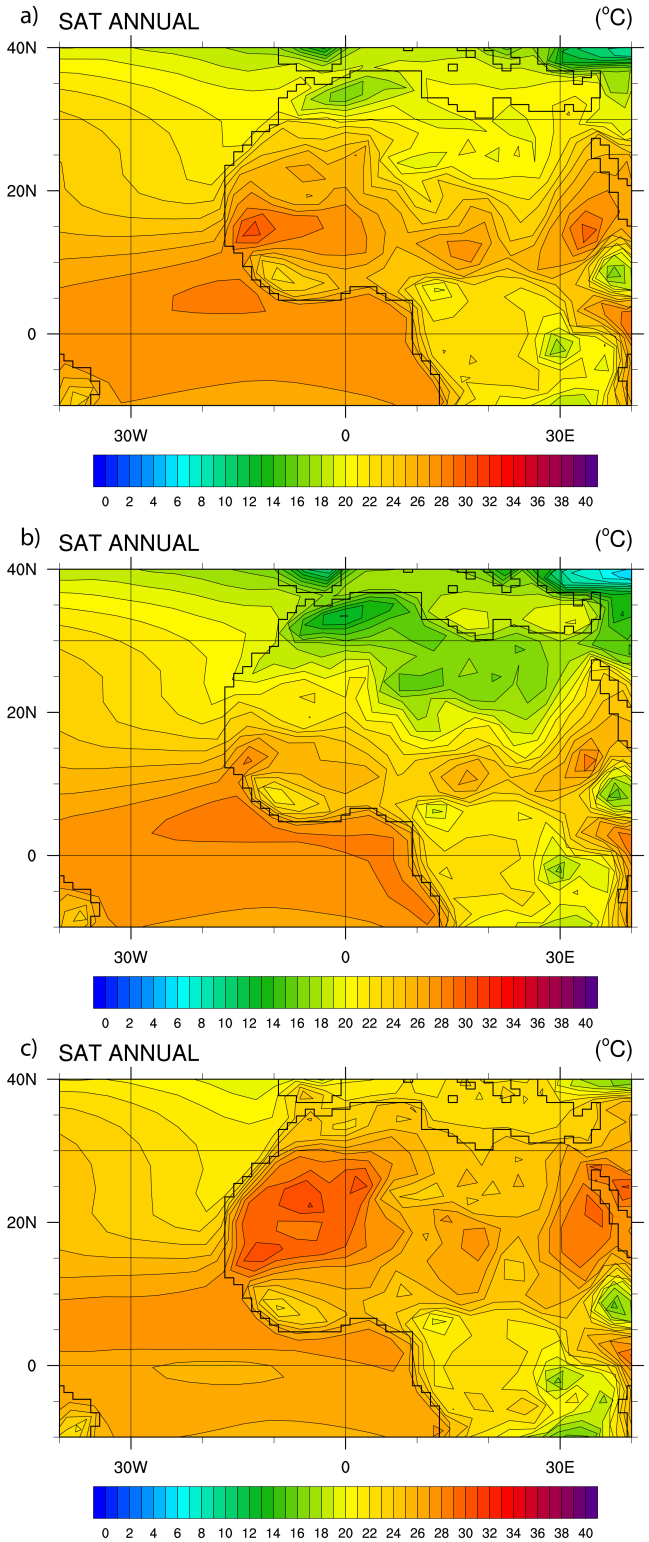

Figure A-27 Surface air temperature for Africa in °C for the CESM1.2 preindustrial control simulation. For A) Annual average, B) winter (DJF), and C) summer (JJA).

Biographical Information

Taylor Hughlett graduated from the University of Texas Arlington as a Geology major and Biology minor. In order to pursue her passion of meteorology and climatology, she joined Professor Arne Winguth to continue her Ph.D. studies in paleoclimate and climate modeling under NSF grants OCE 1536630 and EAR 0903071. Through the course of her undergraduate and graduate career at the University of Texas Arlington, Taylor has received numerous awards and honors including the Donald F. Reaser Field Camp Scholarship, the Enhanced Graduate Teaching Assistantship, the Graduate School Doctoral Dissertation Fellowship, and several travel grants. She is a member of many professional organizations including the Golden Key International Honor Society, the Association of Environmental and Engineering Geologists, the American Association of Petroleum Geologists, the American Meteorological Society, Geological Society of America, the American Geophysical Union, and Sigma Gamma Epsilon (Beta Omega Chapter). After the reciept of her Doctoral degree in May of 2016, Taylor plans to continue her path as a researcher and educator in a colligate setting.